# CHARACTERIZATION OF LANDSLIDE HAZARD IN THE SUB HIMALAYAN ZONE OF NEPAL


A THESIS SUBMITTED TO THE

**CENTRAL DEPARTMENT OF ENVIRONMENTAL SCIENCE**

**INSTITUTE OF SCIENCE AND TECHNOLOGY**

**TRIBHUVAN UNIVERSITY**

**NEPAL**

**FOR THE AWARD OF**

**DOCTOR OF PHYLOSOPHY**

**IN ENVIRONMENTAL SCIENCE**

BY

**BHARAT PRASAD BHANDARI**

**SEPTEMBER, 2023**

TRIBHUVAN UNIVERSITY

Institute of Science and Technology

# DEAN'S OFFICE

Kirtipur, Kathmandu, Nepal

Reference No.:

Institute of Science & Technology
Dean's Office
Kirtipur, 2023

## EXTERNAL EXAMINERS

**The Title of Ph.D. Thesis:** "Characterization of Landslide Hazard in the Sub Himalayan Zone of Nepal"

**Name of Candidate:** Bharat Prasad Bhandari

**External Examiners:**

(1) Prof. Dr. Danda Pani Adhikari
Department of Environmental Science
Tri-Chandra Multiple Campus
Tribhuvan University, NEPAL

(2) Dr. Prafulla Kumar Panda
Centurion University of Technology and Management
Odisha, INDIA

(3) Prof. Dr. Binod Tiwari
California State University
Fullerton, USA

September 27, 2023

(Dr. Surendra Kumar Gautam)
Asst. Dean

# DECLARATION

Thesis entitled "**Characterization of landslide hazard in the Sub Himalayan zone of Nepal**" which is being submitted to the Central department of Environmental Science, Institute of Science and Technology (IOST), Tribhuvan University, Nepal, for the award of the degree of Doctor of Philosophy (Ph.D.), is a research work carried out by me under the supervision of Associate Prof. Dr. Subodh Dhakal, faculty of the Department of Geology, Tri-Chandra College, Tribhuvan University.

This research is original and has not been submitted earlier in part or full in this or any other form to any university or institute, here or elsewhere, for the award of any degree.

Bharat Prasad Bhandari

September, 2023

# RECOMENDATION

This is to recommend that **Mr. Bharat Prasad Bhandari** has carried out research entitled **"Characterization of landslide hazard in the Sub Himalayan zone of Nepal"** for the award of Doctor of philosophy (Ph.D.) in **Environmental Science** under my supervision. To my knowledge, this work has not been submitted for any other degree.

He has fulfilled all the requirements laid down by the Institute of Science and Technology (IOST), Tribhuvan University, Kirtipur, for the submission of the thesis for the award of Ph.D. degree.

.....

**Subodh Dhakal, Ph.D.**

**Supervisor**

**Associate Professor**

Department of Geology, Tri-Chandra Campus

Tribhuvan University, Kathmandu, Nepal

September, 2023

# TRIBHUVAN UNIVERSITY

## CENTRAL DEPARTMENT OF ENVIRONMENTAL SCIENCE

Telephone : 4-332147
4-332711

Kirtipur
Kathmandu, Nepal


Ref:

Date: .....

## LETTER OF APPROVAL

On the recommendation of **Associate Prof. Dr. Subodh Dhakal**, this Ph.D. thesis submitted by **Mr. Bharat Prasad Bhandari,** entitled of "**Characterization of landslide hazard in the Sub Himalayan zone of Nepal"** is forwarded by Central Department Research Committee (CDRC) to the Dean, IOST, T.U..

.....

**Chhatra Mani Sharma, Ph.D.**

Professor

Head

Central Department of Environmental Science

Tribhuvan University

Kirtipur, Kathmandu

Nepal



Web: www.cdes.edu.np Email: info@cdes.edu.np

# ACKNOWLEDGEMENTS

First and foremost, I am incredibly grateful to my supervisor, Associate Prof. Dr. Subodh Dhakal, for his invaluable advice, continuous support, and patience during my Ph.D. study. His immense knowledge and ample experience have encouraged me throughout my academic research and daily life. My gratitude extends to the Ph.D. program coordinator of the department, Prof. Dr. Kedar Rijal, for his motivation and encouragement before and after joining the Ph.D.

I am very grateful to President Chure Tarai Madhesh Conservation Board, Nepal, for providing a research grant that was very important for logistics and laboratory work. This endeavor was only possible with the support of the Central Material Testing Laboratory, Pulchowk Engineering Campus, where I accomplished the laboratory test of 120 soil samples. Additionally, I would like to express gratitude to Prof. Dr. Rejina Maske Byanju and Prof. Dr. Kedar Rijal, former Head of the Department, and Prof. Dr. Chhatra Mani Sharma, head of the department, for their continuous official and documentation support during my Ph.D. period. I am also thankful to the professors and faculties of the Central Department of Environmental science, Tribhuvan University, for their continuous support and motivation. I am very thankful to Mr. Suman Pandey and Mr. Bishow Raj Silwal for their technical support in my study. I want to thank the Nepal Army of Bardia National Park, the Armed Polish Force, and the community polish of Dang and Salyan Districts for making my field visit and soil sampling easier and possible.

Finally, I would like to thank my wife, Mrs. Durga Bhetuwal, and my parents for their continuous support, motivation, and logistics management. Without their tremendous understanding and encouragement over the past few years, it would be impossible for me to complete my study.

Bharat Prasad Bhandari

September, 2023

# ABSTRACT

Landslides are a typical geological process in the Himalayan Mountains, causing yearly loss of life and property during the Monsoon period. Active tectonism, seismic activity, monsoon rainfall, complicated geology, and steep slopes are crucial markers of the Himalayan landslide process. The Siwalik is the world's youngest mountain range, comprising fragile sedimentary rocks. Landslides are a common natural disaster in the Sub Himalayan zone (Siwalik) during the Monsoon period, resulting in the loss of lives and property. Landslide mitigation and prevention are a significant challenge in the Siwalik region. The characterization is a new issue for this region to explore and comprehend the natural process of landslides. This study aims to characterize the landslide by using geological, topographical, hydrological, and geotechnical attributes along with landslide classification and susceptibility modeling in the Babai River watershed of the Siwalik region.

The procedure began with the spatial and temporal landslide inventory mapping by using Google Earth, Landsat, and Sentinel imageries. The spatial inventory map included all landslides in the study area, whereas the temporal inventory map included new landslides annually from 2010 to 2021. The size, length, area, and number of landslides in different geological units were investigated from the landslide inventory map. In addition, the mechanism of landslide beginning in geological units was studied. Total yearly and monsoon rainfall amounts, the geographical distribution of rainfall, and the distance to the drainage map were used as hydrological characteristics. Data from seven stations from 2010 to 2021 were used to create the rainfall distribution map. The slope, aspect, curvature, topographical wetness index, and “T” factors were used for topographical characterization. The shear behavior, phase relation, and index properties of 120 landslide soils were obtained for geotechnical characterization. A size, activity, and mechanism-based classification of the landslide were proposed. For the susceptibility analysis, 14 landslide-causing factors were chosen. Similarly, four bivariate models were used for landslide susceptibility analysis: the weight of evidence, frequency ratio, information value technique, and Shannon's entropy. The silt/clay ratio in Siwalik's soil is one of the leading causes of landslides in saturated conditions. The soils of the Middle Siwalik are stiff,

whereas those of the Lower and Upper Siwalik are soft. Lower and Upper Siwalik soils are similarly poorly graded. The average shear strength in the Lower and Upper Siwalik is also lower than in the Middle Siwalik. Minor and shallow landslides characterize the Lower and Upper Siwalik. Large-scale landslides are prevalent in the Middle Siwalik. The "T" factor and landslides have a positive association. There is a substantial positive relationship between total annual rainfall and yearly landslides. Similarly, hill slope and landslide incidents are strongly correlated. A size-based classification was created based on the landslide area's logarithmic scale. Size-based classification is proposed in five sizes: very small, small, medium, large, and very large. Landslides with less than 100 $m^2$ of surface area are considered very small, while those with more than 100,000 $m^2$ are considered very large. For activity-based classification, five activity states are recommended: new, active, inactive, stable, and reactivated. It describes the intended activity state conditions. Based on the landslide mechanism, five types of landslides have been proposed: Type 1, Type 2, Type 3, Type 4, and Type 5.

The percentage of very high susceptibility (21%) is obtained from the information value method, whereas the low susceptibility percentage (8%) is obtained from the Shannon entropy model. Medium susceptibility is obtained higher from the information value, weight of evidence, and frequency ratio models. The result shows that the susceptibility distribution is more or less similar between frequency ratio, the weight of evidence, and the information value model; however, the Shannon entropy model has a slightly different result. The weight of the evidence model has a higher accuracy and prediction rate, according to the results. The WoE model has a success rate of 85% and a prediction rate of 79.9%. The accuracy and prediction rate of the remaining three models are comparable. The prediction rate hierarchy is WoE (79.9%), FR (75.3%), IVM (74.4%), and SE (73.2%). The success rates of four different models (WoE, FR, IVM, and SE) are 85%, 78.75%, 78.57%, and 77.2%, respectively. Every model's accuracy and prediction rate are greater than 70%, indicating that all models can be used to predict landslide susceptibility in Nepal's Siwalik Hills.

**Key words: Landslide characterization, Sub Himalaya, landslide classification, bivariate models**

# नेपालको उप हिमालयन क्षेत्रमा पहिरो जोखिमको विशेषीकरण

## सोध सार

हिमालय क्षेत्रमा पहिरो खस्नु एउटा निरन्तर भौगर्भिक प्रक्रिया हो । नेपालको सवहिमालय (सिवालिक) क्षेत्रमा वर्षायाममा ठूलो मात्रमा पहिरो जाने गरेको छ जसले गर्दा हरेक बर्ष मान्छेको जिउ धनको क्षति हुने गरेको छ । सक्रिय टेक्टोनिक्स, भूकम्पीय गतिविधि, मनसुनी वर्षा, कमजोर भौगर्भिक अबस्था र ठाडो भिर युक्त जमिनहरु हिमालय भूस्खलन र पहिरो जाने प्रक्रियाका महत्वपूर्ण अवयवहरु हुन् । यस अध्ययनले नेपालको पश्चिम क्षेत्रको सवहिमालय (सिवालिक) भित्र पर्ने बबई नदीको जलाधार क्षेत्रमा पहिरोको वर्गीकरण र संवेदनशीलता मोडलिङका साथै भौगर्भिक, जलविज्ञान, भूसतहिक र भूप्राविधिक विशेषताहरु प्रयोग गरी पहिरोको विशेषता निर्धारण गर्ने लक्ष्य राखेको छ ।

अध्ययनको सुरुवात पहिरोको सूची नक्साङ्कनबाट गरियो । जसमा गुगल अर्थ, ल्याण्ड स्याट र सेन्टिनल इमेजरीहरुको प्रयोगबाट इस्वी सम्बत २०१० देखि २०२१ सम्मका नयाँ तथा पुराना पहिरोहरुको स्पेश र टाइमका फरक नक्साहरु तयार गरियो । डिजिटल एलिभेसन मोडलको प्रयोगबाट पहिरो जाने सम्भावित फ्याक्टरहरुको नक्सा तयार गरियो । भौगर्भिक नक्सा तयार गरी तीनवटा फर्मेशनहरु क्रमश लोयर सिवालिक, मिडल सिवालिक र अपर सिवालिक साथै चट्टान नबनेका तटीय सेडिमेन्टहरुलाई quaternary deposit मा छुट्याइयो । अध्ययन क्षेत्रको पुरै भाग समेटिने गरी प्रत्येक फर्मेसनबाट १०,००० वर्ग मिटर भन्दा बढि क्षेत्रफल भएका ४० वटा पहिरोहरु छुट्याई स्थलगत अध्ययन गरी माटोको नमुना सङ्कलन गरियो । सङ्कलित नमुनाहरुलाई भूप्रयोगशालामा ल्याई विभिन्न भूप्राविधिक परीक्षणहरु गरियो । पहिरो संवेदनशील नक्साङ्कनका लागि १४ वटा सम्बन्धित कारकहरुको नक्सा तयार गरियो र पहिरो प्रकोपको अवस्था थाहा पाउन ४ वटा bivariate model हरु छनोट गरियो । यस अध्ययनको नतिजाबाट समग्र बार्षिक वर्षा र समग्र बार्षिक पहिरो सङ्ख्या बिच पर्याप्त सकारात्मक सम्बन्ध देखियो । पहाडको पन्ध्र डिग्रीदेखि पैंतालिस डिग्रीको स्लोप बढी संवेदनशील देखिन्छ । दक्षिण aspect मा बढी पहिरो जाने गरेको भेटियो भने concave सतह भएको भिरालो जमिनमा बढी सङ्ख्यामा पहिरो जाने गरेको पाइयो । माटोमा पाइने सिल्ट/क्ले अनुपात वर्षाको पानीले पहिरो गराउने प्रमुख कारण रहेको पाइयो । Lower र Upper सिवालिकका माटोहरु नरम र कम घनत्वका भेटिए भने Middle सिवालिकका माटोहरु कडा र बढी घनत्वका भेटिए । समग्रमा Middle सिवालिकमा औसत shear strength parameter बढी देखियो जसले गर्दा चट्टानी पहिरो बढी तर माटोको कारणले जाने पहिरो न्यून सङ्ख्यामा देखियो । पहिरो जाने सम्यन्त्रका आधारमा सिवालिक क्षेत्रका पहिरोहरुलाई पाँच समूहमा बर्गीकरण गरियो । त्यसैगरी आकार र गतिशीलताका आधारमा पनि पाँच समूहमा बर्गीकरण गरियो । अध्ययन

क्षेत्रमा चारै ओटा मोडलका पहिरो संवेदनशील नक्साहरु तयार गरियो जसमा weight of evidence मोडलले frequency ratio, information value र entropy मोडल भन्दा उत्तम नतिजा दिएको छ भने चारैओटा मोडलहरु पहिरो जोखिम अध्ययनको लागी प्रयोग गर्न सकिने देखिएको छ। सबै मोडेलहरुले पहिरोको जोखिम बीस देखि तीस प्रतिशतको हाराहारीमा देखाएको छ। यो अध्ययनले नेपालको सिवालिक क्षेत्रको पहिरोको बहुआयामिक तवरले विशेषीकरण गरेको छ र उक्त क्षेत्रका पहिरो अध्ययन र अनुसन्धान तथा नियन्त्रणमा महत्वपूर्ण भूमिका खेल्न सक्ने छ।

**मुख्य शब्दहरु: पहिरो बर्गीकरण, पहिरोको विशेषता, सिवालिक, बाइ भेरीएट मोडेल**

# LIST OF ACCRONYMS AND ABBREVIATIONS

| | |
|---|---|
| AD | : Anno Domini |
| ASTM | : American Society for Testing and Materials |
| AUC | : Area under Curve |
| BhT | : Bheri Thrust |
| BS | : Bikram Sambat |
| BT | : Babai Thrust |
| CLR | : Centrer log ratio |
| Cp | : Conditional probability |
| CPT | : Cone penetration test |
| CV | : Coefficient of variance |
| DEM | : Digital elevation model |
| Df | : Degree of freedom |
| Dh | : Horizontal displacement |
| DHM | : Department of Hydrology and Meteorology |
| ERT | : Electrical Resistivity Tomogram |
| F | : Form factor |
| FR | : Frequency ratio |
| GIS | : Geographical information system |
| GPR | : Ground Penetrating Radar |
| IVM | : Information value method |
| J | : Average gradient of stream |

| | |
|---|---|
| KML | : Keyhole Markup Language |
| kPa | : Kilo Pascal |
| LL | : Liquid limit |
| LS | : Lower Siwalik |
| MBT | : Main Boundary Thrust |
| MFT | : Main Frontal Thrust |
| MoHA | : Ministry of Home Affaire |
| MS | : Middle Siwalik |
| NDVI | : Normalized difference vegetation index. |
| PI | : Plasticity index |
| PL | : Plastic limit |
| Pp | : Prior probability |
| PSI | : Persistent Scattered Interferometry |
| q-q | : quantile-quantile |
| ROC | : Receiver Operating Characteristics |
| S | : Ratio of catchment area and potential slope area. |
| SD | : Standard deviation |
| SE | : Shannon's entropy |
| SG | : Specific gravity |
| SPI | : Stream power Index |
| SPT | : Standard penetration test |
| Std | : Standard |
| T | : Topographical factor |
| TWI | : Topographical wetness index |

| | |
|---|---|
| US | : United States |
| US | : Upper Siwalik |
| USCS | : Unified Soil Classification System |
| WoE | : Weight of evidence |
| WP/WLI | : Working Party on World Landslide Inventory |

# LIST OF SYMBOLS

| | |
|---|---|
| $^{o}$ | : Degree |
| $\mu$ | : Micron |
| $\emptyset$ | : Angle of internal friction |
| c | : Cohesion |
| e | : Void ratio |
| Gs | : Specific gravity |
| Ln | : Natural Log |
| $\eta$ | : Porosity |
| $R^2$ | : Regression coefficient |
| Sr | : Degree of saturation. |
| Std | : Standard |
| w | : Moisture content |
| $\gamma_d$ | : Dry unit weight |
| $\gamma_s$ | : Unit weight of soil |
| $\gamma_w$ | : Unit weight of water |
| $\sigma$ | : Normal stress |
| $\tau$ | : Total shear strength |

# LIST OF TABLES

**Page No.**

# LIST OF FIGURES

# TABLE OF CONTENTS

**Page No.**

# CHAPTER 1

## INTRODUCTION

### 1.1 Introduction

The term “Landslide” is the movement of a mass of rock, debris, or earth down a slope under the influence of gravity (Cruden and Varnes, 1996). Various materials and downslope movements occur in the Nepal Himalayas, mainly in the rainy season. Geology, geomorphology, tectonics, stratigraphy, and the weathering condition of rocks are equally responsible for land sliding processes (Dahal et al., 2008; Dahal & Hasegawa, 2008; Dahal, 2012; Devkota et al., 2013; Dhakal, 2014; Regmi et al., 2014; Dhakal, 2015). The soil has typical geotechnical properties that play a vital role in the landslide initiation process (Yalcin, 2007; Yalcin, 2011; Tofani et al., 2017; Bicochhi et al., 2019). Continuous rainfall on adverse topography leads to the landslide process in the Himalayan region (Dahal & Hasegawa, 2008; Borga et al., 2002; Fernandes et al., 2004; Zhang et al., 2012; Ching et al., 2018; Hennrich & Crozier, 2004; Talebi et al., 2008). Landslides are widely distributed in the hills of Nepal. The land of Nepal is diversified into different geographical regions, namely the Mountain regions, Hilly regions, and the Terai region, based on geography and topography. The complex geology of the Nepal Himalaya, with major thrusts, numerous faults and folds, very low to high-grade metamorphic rock, weak sedimentary rocks, frequent rock and soil combination, adverse topography, and dynamic hydrological conditions, all contribute significantly to landslide occurrence. Every year, landslides in Nepal cause thousands of people to become homeless and lose their property. According to the Ministry of Home Affairs (MoHA, 2022), 92 people died, 80 people were injured, and 1968 houses were affected by landslides in the year 2020 alone, which caused 13,11,267 US dollar losses due to landslides in Nepal. Similarly, 15,866 landslides were marked from 2019 to 2021 in the Siwalik Hills of Nepal, causing the death of 30 people and destroying 142 houses. Within these years, 4,44,680 US dollars were lost by the country only in the Siwalik Hills of Nepal.

"Characterization of landslides" broadly means understanding or unraveling the mechanisms or interplay of all the determining factors that lead to any slope failure (Varnes, 1978). An adequate landslide characterization is necessary for slope instability, analysis, and mitigation planning. A single factor cannot adequately characterize landslides in complex geological and topographical conditions. A detailed landslide characterization consists of the geological, hydrological, topographical, geotechnical, and physical characteristics of landslides. For landslide characterization, a multidisciplinary approach has been used by various researchers for a long time (Ausilio & Zimmaro, 2017; Bhandari & Dhakal, 2021). The multidisciplinary approach involves the combination of different techniques that provide an adequate characterization of the landslide. The geological (Bhandari & Dhakal, 2018; Tsou et al., 2018a; Gerrard, 1994; Hasegawa et al., 2009), geotechnical (Yalcin 2007; Yalcin, 2011; Toffani, 2017), topographical (Tsou et al., 2018b; Zhang et al., 2016) and hydrological (Dahal et al., 2008a; Dahal et al., 2008b) conditions are crucial factors for landslide mechanism. Studying these factors is essential for a better understanding of the landslide process. Fragile geology is one of the significant reasons for landslide initiation in the Nepal Himalaya (Devkota et al., 2013; Regmi et al., 2014; Regmi et al., 2012a&b; Dahal et al., 2008; Bhandari & Dhakal, 2018; Gadtaula & Dhakal, 2019; Bhandari & Dhakal, 2020a). Continuous rainfall on adverse topography and geology leads to the landslide process in the mountainous areas of the Himalayan region (Weidinger, 1998; Borga et al., 2002; Fernandes et al., 2004; Zhang et al., 2012; Ching et al., 2018; Hennrich & Crozier, 2004; Talebi et al., 2008; Kayastha et al., 2012).

The most important events that play a role in hillslope instability are linked to the intricate hydrological shifts that occur below the surface. The hydrology of the hillslope's subsurface is determined by the amount of rainfall that is absorbed by the soil. Both internal and exterior characteristics have an impact on the amount of water that absorb by soil after rains. Internal parameters include soils' hydrological properties, like retaining moisture and hydraulic conductivity. External parameters include climatic conditions like rainfall intensity and duration, rainfall pattern, and evapotranspiration rate. Hydrological properties of soils, like moisture retention characteristics and hydraulic conductivity, are examples of internal parameters.

Various landslide classification methods have existed from the past to the present. Landslide classification aids in understanding the mechanism and behavior of landslides. The classification of a landslide ultimately gives information on movement types, materials present, and ways of initiation; however, more classifications are required to understand landslides. The landslide characterization provided by Varnes (1954, 1978) and Hutchinson (1968, 1988) is popular and widely accepted today. Cruden and Varnes (1996) modify the previous classification, including the multidimensional taxonomic system. Dana (1864) proposed three types of landslides based on the mechanism and initiation of a landslide. Only the types with detailed explanations are sufficient to understand the landslide. Baltzer (1875) differentiated the various movement models, e.g., fall, slide, and flow, but could not explain the other types of landslides. Several other landslide categorization systems have been developed, including those by Sharpe (1938), Hungr (2001, 2013), Zaruba, and Mencl (1969).

Cruden and Varnes (1996) defined a *landslide* as "complex" if it contains more than one type of landslide; however, this term is not straightforward and easy to apply because every single landslide may include more than two types. Most landslides appear to be of the complex type in complex geological terrain such as the Siwalik Hills. It creates confusion and difficulties for the mitigation process of a landslide, so mechanism- and initiation-based landslide classification based on the Siwalik zone is required for a general understanding of landslides. The possibility of a landslide occurring based on the surface condition of a specific location is referred to as landslide susceptibility (Brabb, 1984). The landslide susceptibility index provides information on where landslides are likely to occur. There are different approaches for assessing landslide susceptibility; nonetheless, a better prediction model is essential in landslide-prone areas. In Nepal, landslides and mass movements are significant challenges. The study of landslide susceptibility in Nepal's hills still needs to be expanded. Landslide susceptibility is commonly assessed using quantitative and qualitative methods (Yalcin et al., 2011). Quantitative tools assess the likelihood of sliding. It looks into the connection between causal variables and the occurrence of landslides. Bivariate and multivariate statistical techniques are used to estimate the susceptibility of landslides. Bivariate techniques include the weight of

evidence, frequency ratio, information value method, and entropy index, while multivariate techniques include logistic regression and support vector machines. The analytical hierarchy process (AHP) is an example of a qualitative technique in which the class and subclass are ordered and weighted based on expert judgment on a topic, making it semi-quantitative (Reis et al., 2012; Kayastha et al., 2013; Mansouri & Reza, 2014; Hung et al., 2015). Because qualitative procedures are more subjective and conventional, prediction accuracy may need to be more flawless and acceptable. In landslide-prone areas, better and more effective quantitative methodologies suggest producing a more accurate result, ultimately valuable for primary mitigation and other policy formulations for risk reduction.

### 1.2 Rationale of the study

The Sub Himalaya (Siwaliks) are the Himalayas' southernmost mountain range, and it is bounded by the Main Frontal Thrust (MFT) in the south and the Main Boundary Thrust (MBT) in the north (Dhital, 2015). The Siwalik region comprises young and brittle sandstones, mudstones, and conglomerates that are highly vulnerable to weathering, turning rock into soil relatively in a short time. The zone exhibits noticeable relief variation and significant slope steepness. After weathering, the rocks lose shear strength, increasing the likelihood of landslides and slope failure. Furthermore, increasing infiltration rate through accessible joints and fractures raises pore water pressure, which raises the driving force in the rock, creating slopes and causing slope failure (Dhakal, 2014). The annual rainfall in the Siwalik range is typically between 2,000 and 2,500 mm, and out of that, 1800 to 2100 mm rains occur in the Summer Monsoon only. As a result, geological factors and water availability make the Siwalik extremely vulnerable to landslide processes (Dahal, 2012). According to Dhakal (2014), the frequency of landslides in the Siwalik range is high. It varies by location due to underlying structural and neo-tectonic activity along the Main Boundary Thrust (MBT). The materials of Siwaliks are diverse, weak, and more fragile. Landslides are nearly complex, adding difficulty to the classification based on Varnes (1984) and Cruden and Varne’s (1996). Hence, a new technique for better landslide classification in the Siwalik Hills is necessary.

There are several methods for assessing the susceptibility of landslides. Every statistical method may need to be validated and appropriate for landslide hazard zonation at the catchment scale in the Siwalik. Only using geomorphological processes may not produce the desired results. The right approach for susceptibility evaluation is required to check the validity and appropriate prediction method. Landslide research in Nepal Himalaya has been dominated by GIS-based hazard and susceptibility mapping, and more focus has been given to earthquake-induced landslides (Regmi et al., 2014; Devkota et al., 2013; Kayastha et al., 2013; Pokharel & Bhandari, 2019; Tsou et al., 2018; Roback et al., 2018; Tomita et al., 2018; Tian et al., 2020; Ghimire, 2011; Gyawali & Tamrakar, 2018; Thapa & Bhandari, 2019). The Babai River is one of the high discharged River, originated from the Siwalik and have several landslides that occurred naturally. The river flows parallelly with Babai Thrust. Similarly, more than 75% of the area is covered by forest and vegetation. To interpret the natural characters of landslides, Babai River watershed is selected for present study.

The essential aspects of landslide research are the physical, geological, geotechnical, topographic, and hydrological approaches to landslide characterization. In Nepal's Siwalik Hills, shear strength parameters and their correlations with other soil index properties, topographical characteristics, geological control, and hydrological activities need to be enhanced. This study's findings can help with physical-based landslide prediction modeling, engineering design for landslide mitigation in the study area, and more extensive landslide analysis with numerical modeling.

### 1.3 Research questions

Following are the research questions for the proposed study.

- What are the geological, topographical, hydrological, and geotechnical characteristics of landslides in the study area?
- What are the dynamics of landslides (both past and present) prevalent in the study area?

- How can landslides of the Siwalik zone be classified based on landslide mechanisms and processes?
- Which quantitative modeling technique is suitable for landslide susceptibility study in the Siwalik Hills of Nepal?

## 1.4 Objectives

General objectives

- To characterize the landslides in the Babai River watershed of the Sub Himalayan zone and identify the potential landslide hazard zones with appropriate modeling techniques.

Specific objectives

- To map and characterize the existing landslides in terms of geological, topographical, hydrological, and geotechnical attributes.
- To examine the influence of triggering factors and other inherent processes of Sub Himalaya in the landslide classification system.
- To assess the appropriate techniques for landslide susceptibility mapping in the Sub Himalayas of Nepal.

# CHAPTER 2

## LITERATURE REVIEW

### 2.1 Landslide

Since the beginning, academics have provided many definitions of landslides. The Oxford English Dictionary has this definition of the word "landslide": "the sliding down of a mass of land on a mountain or a cliffside: the land which has so fallen" (Onion, 1993). Previously, some researchers used the term "landslip" without specifying "landslides" (Marr, 1916; Arber, 1941; Conway, 1974; Denness et al., 1975). According to Lyell (1833), a "landslip" is "a part of the land that has slid down as a result of disturbance by an earthquake or by being undercut by water washing away lower beds that supported it." Lyell used the term "landslip" to illustrate slope movement in his three-volume book "Principles of Geology," published in 1830–1833.

The term "landslide" was introduced in Niles' National Register on October 6, 1838, which noted, "an avalanche or sinking of the ground on the edge of the landing at Vicksburg" under the headline "Landslide in Vicksburg" (Craigie & Hulbert, 1942; Cruden, 1991). Terzaghi (1950) described a landslide as "the rapid movement of a mass of rock, residual soil, or sediment bordering a slope in which the moving mass's center of gravity advances in a downward and outward direction." Brunsden and Jones (1972, 1976) referred to the slope movement as a "landslide." According to Varnes (1978), a landslide is "a downward and outward movement of slope-forming materials under the effect of gravity." Crozier (1986) described the mass movement as "the outward and downward gravitational movement of earth material without the assistance of flowing water as a transportation agent." According to Cruden (1991), a landslide is the movement of a large amount of rock, debris, or earth down a slope. WLIWP (1990) defined a *landslide* as "the movement of a mass of rock, soil, or debris down a slope." Bates & Jackson (1987) described a landslide as "the downslope transport of soil and rock material masses under gravitational impact." Typically, the displaced material moves over a relatively limited zone or shear surface."

Similarly, the landslide is defined by Webster's Third International Dictionary as "the usually rapid downslope movement of a mass of rock, dirt, or artificial fill on a slope." Cruden and Varnes (1996) showed how landmasses are denuded by diverse agents such as wind, water, and ice mass, as well as a result of slides and other mass movements. Gravity allows these phenomena to transfer a large volume of slope materials downward. "The term 'landslide' describes a wide variety of processes that result in the downward and outward movement of slope-forming materials such as rock, soil, artificial fill, or a mix of these," according to a modified definition of Cruden and Varnes (1996). Materials can be moved by falling, toppling, sliding, spreading, or flowing. Numerous researchers widely recognize and use the definitions provided by Cruden & Varnes (1996).

### 2.2 Landslide characterization

The complex natural events known as landslides are brought on by the interaction of geological, geomorphological, hydrological, topographic, and geotechnical factors. Landslide characterization is one of the essential steps in understanding landslides in a given geological and geomorphological region. Identifying the characteristics of landslides and the roles played by the numerous elements that contribute to their occurrence is known as "landslide characterization." Several academics have carried out the characterization of landslides based on factors and methods throughout the years. Geological, geotechnical, topographical, and hydrological factors are crucial for landslide control, so these are essential for landslide characterization (Bhandari & Dhakal, 2018; Tsou et al., 2018; Gerrard, 1994; Hasegawa et al., 2009; Barton & Pearce, 2015; Yalcin, 2011; Yalcin, 2017; Tofani et al., 2017; Bicocchi et al., 2019; Tsou et al., 2018; Zhang et al., 2016; Dahal et al., 2008). Ausilio & Zimmaro (2016) used a multidisciplinary approach (geological, geotechnical, hydrological, and topographical) to characterize landslides. They used geotechnical and innovative geophysical and electromagnetic sensing techniques to investigate landslides. Irene et al. (2020) characterized landslides in Mexico by using techniques such as lithological and structural characterization, geomorphological mapping, persistent scattered interferometry (PSI) analysis, and electrical geophysical surveys. They have selected the major geomorphological features of a deep-seated landslide, such as a

counter-scarp, minor scarps, tension cracks, small landslides, avalanche breccia, toppling, and colluvial deposits. They have also estimated the rate of landslide movement from the deep-seated landslide.

### 2.2.1 Geological characterization

Amare et al. (2018) identified that soil's geotechnical properties determine a landslide's sliding mechanism. They obtained the shear strength behavior of landslide soil and concluded that the marl-shale layer is mainly responsible for sliding. Percolation in marl shale causes it to become saturated and exerts pore water pressure. Using geophysical landslide characterization, Kannaujiya et al. (2019) got subsurface information about a landslide in the Garhwal Himalaya of India. They used electrical resistivity tomography (ERT) and ground penetrating radar (GPR) and obtained the approximate depth of the slip surface by using four ERT profiles and one GPR radar gram profile.

Geological characteristics for the landslide mechanism provide geology and lithostratigraphy's fundamental natures. Fell et al. (2012) explored the landslide mechanisms in different rock types and identified the direct control of geology on landslides. The rock types, metamorphism, rock attitudes, joint status, and rock formation all have a significant role in landslide initiation (Bhandari & Dhakal, 2018). Landslides mainly occur because of the materials' strength, compactness, and cementing nature. The rock orientation on the slope is another major cause of landslides because the increased slope is no longer strong enough to resist the shear stress and gravity. The slope angle is an essential factor in landslide initiation. The increasing hill slope causes a reduction in the angle of internal friction. The rock and soil arrangement of the layer, the grain size of the rock, the hardness of the rock, its composition, and its weathering are critical factors for landslide occurrence. Various topographical factors, including the hill slope, slope curvature, slope aspect, elevation, relief, stream gradient, and landslide-catchment area ratio, are responsible for the initiation and distribution of landslides. Topography plays a vital role in landslides' occurrence. It causes severe problems in the hilly regions of the

world, like Nepal. The steep and highly concave slope is causing erosion-induced landslides in the Siwalik Hills (Bhandari & Dhakal, 2018).

### 2.2.2 Topographical characterization

According to Densmore et al. (1998), landslides are supposed to occur along the steep slope. The sliding threshold slope angle may depend on climate or lithology (Gabet et al., 2004b; Hurst et al., 2013). Acharya et al. (2015) stated that only three characteristics, slope inclination, soil depth, and slope length, can be considered principal topography parameters. These three parameters affect the initial subsurface zone moisture and instability before rainfall. The other parameters, such as plan shapes, profile curvatures, and slope width, are contained within the first three parameters along the slope profile. The other parameters' ability to play a role in the slope's instability is contingent on the local conditions of the first three parameters.

According to Dietrich et al. (1987, 2008), Iida (1999), Talebi et al. (2008), and Cha and Kim (2011), the topographic parameters slope inclination, slope shape, slope length, and slope width are the components that make up a topographical unit. As a result, these components can be thought of as topographic parameters. It has been widely acknowledged in a large number of studies, such as Montgomery and Dietrich (1994), Wu and Sidle (1995), Burton and Bathurst (1998), Pack et al. (1998), Borga et al. (2002), Dahal et al. (2008), and Harp et al. (2008). However, the slope's inclination is the only character that has been identified as being significant in these investigations from the slope stability perspective. The influence of slope inclination and soil depth on the stability analysis of infinite slopes has been explored in a few theoretical papers (Griffiths et al., 2011; Cha & Kim, 2011). This research looked at the influence of these factors. Many other studies (Troch et al., 2002; Dhakal & Sidle, 2003; Talebi et al., 2008) have shown that the geometric parameters of hillslopes (plan shapes and profile curvatures) also have a significant impact on the subsurface flow response and instability of complex hillslopes even though slope inclination and soil depth are two of the most critical factors.

According to the findings of Knapen et al. (2006), the segments of steep, flat, concave slopes that are located at a certain distance from the water divide and are oriented to the predominant rainfall direction (north to northeast) are the most sensitive to mass movement across the whole research region. Evaluation of the distribution and frequency of previous landslides is necessary for locating locations that provide a more significant threat of being affected by landslides (Silalahi et al., 2019). To better direct planning and risk management, topography, a significant land surface characteristic, and an essential precondition or factor in landslides must be researched further. Topography is a crucial precondition or element in landslide occurrence (Bhandari & Dhakal, 2019). According to Nugraha et al. (2015), the characteristics of the land surface, measured using geomorphometric techniques, show a strong link with the distribution of landslides. They noted that the occurrence of landslides coincides most of the time with an elevation of higher than 400 meters above sea level, a slope of 20 degrees, an east-to-west slope direction, and a flat curvature. According to Dahl et al. (2011), discriminant function analysis demonstrates that the primary factors responsible for the spatial distribution of debris slides are aspect, slope angle, stream density, plan curvature, and altitude.

Investigating topographic influence has been stressed by several researchers, including Fernandes et al. (2004) and Broothaerts et al. (2012), amongst others. According to Giuseppe et al. (2016), the factors that affect slope stability are a decrease in soil suction throughout the whole catchment during a rainfall event and (ii) higher water pressures that build up at concave locations, where water is topographically driven through saturated subsurface flows.

### 2.2.3 Hydrological characterization

The rainfall-induced landslide is very common in the entire Himalayan region. Because most landslides in Nepal occur during the monsoon season, heavy rainfall is regarded as the primary cause of landslides (Dahal, 2012; Dhakal, 2014; Bhandari & Dhakal, 2021). The hills near drainage have more landslide events in Nepal (Dahal et al., 2012; Devkota et al., 2013; Regmi et al., 2014a & b; Pokharel & Bhandari, 2019; Thapa & Bhandari, 2019). Toe cut and head erosion are major landslide-initiating factors in the Himalayas,

ultimately caused by hydrological activities. Long-term rainfall causes many landslides in the Himalayas (Dahal & Hasegawa, 2008; Dahal, 2012). Rainfall pattern, geology, and geomorphology determine a rainfall-induced landslide's characteristics. According to Chen et al. (2019), rainfall-induced landslides tended to occur on a dip slope rather than a windward slope. The authors concluded that geological settings were a more effective control of the mass wasting processes on a hill slope scale than the rainfall condition. Chigira (2011) studied Japan's geological and geomorphological characteristics of rain and earthquake-induced landslides. According to Chigira (2011), the responses of various geological materials to rain and ground shaking differ. The trigger of a landslide depends on material strength loss, precipitation through pore pressure, and water table height (Larsen et al., 2010; Guzzetti et al., 2008; Dahal et al., 2012).

### 2.2.4 Geotechnical characterization

Many researchers have studied the soil classification and phase relationship of the soil in recent years for the geotechnical study of landslides (Cencetti & Conversini, 2003; Bicocchi et al., 2019; Zhao et al., 2013; Mugagga et al., 2011; Tofani et al., 2017; Yalcin, 2011; Riemer et al., 2015). The soil classification provides information on the compositional structure of the soil. Landslide initiation is greatly influenced by the proportions of the soil's constituents (gravel, sand, silt, and clay). The clay fraction with higher moisture content is highly responsible for shallow landslides (Yalcin, 2007; Yalcin, 2011). By categorizing landslides under the grain size distribution, one can gain a deeper comprehension of the characteristics of the soil in several different ways. When varying levels of water and shear stress are present, the classification of the soil can be related to the composition of the soil. According to the Unified Soil Classification System, soils are typically categorized based on the range of particle sizes from fine to coarse. The soil mass that passes through a 0.075 mm sieve is considered fine soil, while the soil mass that remains in the same sized sieve is considered coarse soil. In addition, the fine-grained soils are tested using a hydrometer to categorize them further as either clay or silt. More than soil component identification and classification, it is needed to understand soil behavior. Analyzing the soil's composition reveals each component's function in the onset of

landslides. It will be simple to determine the sources of the particles present in the soil (Bicocchi et al., 2019).

In recent years, the geotechnical characteristics of soil have been studied worldwide for physical-based landslide modeling, landslide mitigation, slope stability analysis, and a better understanding of landslides (Yalcin, 2011; Iwashita et al., 2012; Zhao et al., 2013; Tofani et al., 2017; Salvatici et al., 2018; Bicochhi et al., 2019). Numerous studies were carried out to identify the spatial variation of the geotechnical properties of the landslides (Duffera et al., 2007; Shoaei & Sidle, 2009). The study of the shear strength of soil is significant for various engineering structures and slope stability. The shear strength analysis of soils from the slip surface of the existing landslides is one of the most important parameters to evaluate the landslide mechanism (Li et al., 2017; Wen & Ji, 2019). The drained residual strength controls the further movement of the existing slip surface of the past failure plane (Skempton, 1985). Some past researchers studied the residual shear strength of the preexisting shear surface of a landslide. They concluded that the shear surfaces of old landslides exhibit higher shear strength than the drained residual value, and the slope becomes stable (D'Appolonia et al., 1967; Ramiah et al., 1973; Gibo et al., 2002; Carrubba & Fabbro, 2008). In the case of active landslides, the shear strength value is lower, and the slip surface is unstable. The shear strength of soil is affected by many other factors, such as soil types, index properties, pore pressure, groundwater level changes, chemical reactions, occurrence states, and environmental conditions (Cernica, 1995; Morrow et al., 1982; Skempton, 1985; Wen & Aydin, 2004; Mugagga et al., 2010; Benac et al., 2014; Zhou et al., 2016). The soil saturation causes many slope failures through seepage (Rahardjo et al., 2010). Soil's shear deformation and strength parameters should be studied to understand landslides better.

The geotechnical characteristics of landslides provide profound information about soil engineering properties like shear strength, phase relationship, composition, and gradation. Higher moisture content causes a loss of both cohesion and internal friction, resulting in a decrease in the shear strength of the soil (Yalcin, 2011; Chen et al., 2021). The failure probability increases with decreasing soil shear strength. Furthermore, once the complex

shear behaviors and geotechnical properties of slope materials are studied in depth, the study of rainfall-induced landslides is complete. Grain size distribution and soil classification are necessary for engineering and geotechnical fields to depict the properties and behavior of soil, which helps to separate the soils into the same group or class having similar properties (Casagrande, 1932; Howard, 1984; Das, 2009; Dundulis et al., 2010; Das & Sobhan, 2013). Because the engineering characteristics of soil are influenced by the shape, size, and arrangement of soil particles, the soil must be classified before designing and constructing any project. The interrelationship of different soil phases' mass, volume, and weight is known as the "phase relationship." The three phases of soil are gas, liquid, and solid. The phase relation is expressed either in terms of mass-volume or weight-volume relationships. The phase relationship defines the soil's condition or physical make-up, so it is essential to identify the interrelationships of different soil phases. Dry unit weight, bulk unit weight, porosity, void ratio, specific gravity, moisture content, and degree of saturation are soil phase relationships (Bicochhi et al., 2019).

### 2.3 Landslide classification

Numerous ways to classify landslides have been developed based on the types of movement, materials, movement velocity, morphometry, amount of water, and rate of unset.

#### 2.3.1 Dana’s classification

Dana (1864) grouped landslides into three types based on the mechanics of the landslide.

Type 1: A mound of soil on a side hill, possibly with the growth of forest trees on its surface and beds of gravel and stones below, may get so weighted with the waters of heavy rain and so loosened below by the same means as to slide down the slope by gravity.

Type 2: Water from springs or rain could make a clay layer on top of other horizontal layers so soft that the mass above it pushes it out to the side, if it can, and sinks to take its place.

Type 3: When the rocks tilt and create a mountain slope, the softening of a clayey layer or another layer beneath in the way just described may result in a slide of the superincumbent layers down the hill.

### 2.3.2 Baltzer classification

Baltzer (1875) recognized three fundamental forms of motion: fall, slide, and flow. That classification was incomplete because spreading and toppling were not covered. Many additional researchers adopted Baltzer's nomenclature. Stiny (1910) and Sharpe (1938) developed another classification system based on movement type, substance, and velocity. They distinguished between debris flows (channeled), debris avalanches (open-slope), and earth flow. Slip and flow are examples of movement, while earth or rock are examples of substance. In the Sharpe classification, movement speed is a secondary criterion. The classification specifically mentions slope movement and transportation by water or ice. Heim (1932) and Zaruba and Mencl (1969) concentrated on landslide types defined by specific materials. The materials on the facies were characterized using geological nomenclature.

### 2.3.3 Sharpe classification

In the late 1930s, Sharpe (1938) attempted to compile a significant portion of the earlier landslide research into a singular, all-encompassing classification scheme. That was the first book written in the United States of America on landslides. He utilized the type of movement and material as the primary designators. In contrast, the velocity, amount, and phase of the $H_2O$ system (water and ice) were utilized as additional elements.

### 2.3.4 Nemcok classification

Nemcok (1972) proposed four types of slope processes: creep, sliding, flow, and fall. The term “creep” refers to movements that occur over geologically long periods and have a constant velocity without clearly defined sliding surfaces. Deep-seated flow, often known as viscous flow, can describe most situations. These movements are called creeping movements, and the phenomenon that results from them is known as rock creep, talus

creep, or soil creep. When it reaches a certain point of critical acceleration, the creep transforms into a sliding, flow, or falling motion. In this situation, creeping is a stage before sliding, flowing, or falling. Sliding is the movement of coherent masses down a slope along one or more well-defined shear surfaces. This movement is referred to as a landslide by us. The movement of slopes in rocks and soils that is equivalent to the movement of liquids is called flow. Rock streams are also sometimes referred to as mudflows or earthflows. A fall is a quick movement down a slope, during which the moving masses lose their coherence and, for a little time, their contact with the rock underneath.

### 2.3.5 Varnes classification

Varnes (1954, 1978) expanded Sharpe's approach and incorporated it into the Transportation Research Board of the National Research Council of Washington. Varnes classified landslides according to the forms of movement and the elements included in the sliding mass. The movement kinds were fall, slide, topple, lateral spread, and flow. He had named it “complex” for combining more than one movement type. Likewise, he proposed two materials: bedrock and engineering soil (Table 1). He further divided the engineering soil into two types: predominantly fine and predominantly coarse.

### 2.3.6 Cruden and Varnes classification

Cruden and Varnes (1996) modified the Varnes classification. They offered the direct name of a landslide by employing movement and rate of flow (Fig. 1). The categorization is completed by a velocity scale, which was later modified by the International Geotechnical Society's UNESCO Working Party on World Landslide Inventory (WP/WLI) (1995) and Cruden and Varnes (1996).

Hutchinson (1968, 1988) classified landslides based on numerous dimensions, including material, morphology, water content, rate, kinematics, and failure and propagation processes. (Casagrande, 1940) defined "flow slide" as an exceptionally rapid failure caused by the liquefaction of saturated sand or the remolding of sensitive clay (Meyerhof, 1957; Hungr et al., 2013.

**Table 1:** Landslide classification system proposed by Varnes (1978).

| Types of movement | | Types of materials | | |
|---|---|---|---|---|
| | | | Engineering soil | |
| | | Bedrock | Predominantly coarse | Predominantly fine |
| Fall | | Rock fall | Debris fall | Earth fall |
| Topples | | Rock topples | Debris topples | Earth topples |
| Slides | Rotational | Rock slides | Debris slides | Earth slides |
| | Translational | | | |
| Lateral spreads | | Rock spreads | Debris spreads | Earth spread |
| Flows | | Rock flow | Debris flow | Earth flow |
| Complex: Combination of two or more principal types of movements | | | | |

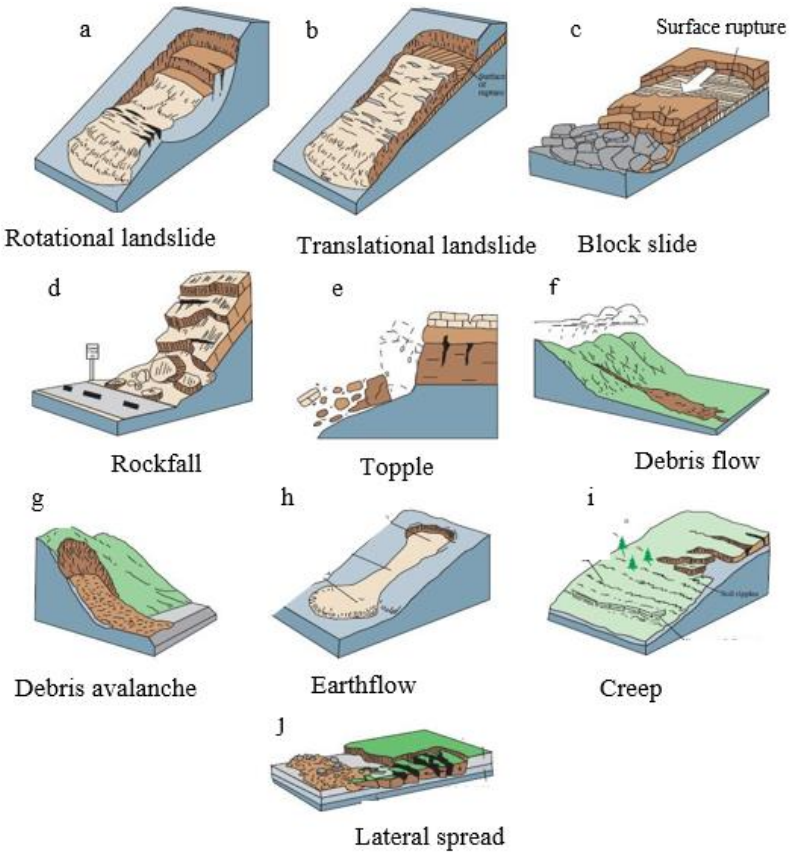


**Figure 1:** Major types of landslide classification by Cruden and Varnes (1996).

The phrase "flow slide" has grown in popularity and utility in the geotechnical discipline. Rock engineers then used the names "wedge slide," flexural topple," and "block topple" (Goodman & Bray, 1976; Londe, 1965; Hoek & Bray, 1981). Because the engineers and engineering geologists needed to provide the correct name of the landslide, their classifications were limited to the engineering field only.

### 2.3.7 Hungr classification

Classification may be taxonomic, non-taxonomic, and typological. The classification proposed by Hutchinson's is non taxonomic. He used the basic kinematic patterns as the principal attributes (Hungr et al., 2001). Hungr et al. (2001) classified the flow-type landslides into ten classes (Table 2).

**Table 2:** Classification of flow types materials (Hungr et al., 2001).

| Materials | Water content | Velocity | Name |
|---|---|---|---|
| Silt, sand, gravel, and debris(talus) | Dry, moist, or saturated | Various | None liquefied sand (Silt, gravel, debris) flow. |
| Silt, sand, debris, and weak rock. | Saturated at rupture surface. | Extremely rapid. | Sand (silt, debris, rock) flow slide |
| Sensitive clay | At or above the liquid limit | Extremely rapid | Clay, flow, slide |
| Peat | Saturated | Slow to very rapid | Peat flow |
| Clay or earth | Near plastic limit | Less than rapid | Earth flow |
| Debris | Saturated | Extremely rapid | Debris flow |
| Mud | At or above the liquid limit | Greater than very rapid | Mudflow |
| Debris | Free water present | Extremely rapid | Debris flood |
| Debris | Partly or fully saturated | Extremely rapid | Debris avalanche |
| Fragmented rock | Various, mainly dry | Extremely rapid | Rock avalanche |

### 2.3.8 Other classifications

Ladd (1935), Zairuba, and Mencl (1969) recognized that similar failure patterns occur in a wide range of lithologies. They used this discovery to classify landslides according to the lithology of the shear plane. Terzaghi (1950), Terzaghi (1958), and Yatsu (1967) categorized landslides in a manner analogous to the mechanics of slope failure. The

geometry of the failure plane is determined by the thickness of the moving mass (Skempton, 1953). In order to correctly classify the landslide, it must be investigated in great detail. The essential criteria for landslide classification are the type of movement, the reason for the movement, the lithology, the soil's engineering characteristics, and the landslide's physical qualities.

Similarly, landslide classifications based on failure reasons are only useful with detailed studies, typically and predominantly carried out by soil engineering laboratories (Blong, 1973). According to Skempton and Hutchinson (1969) and Hutchinson (1968), the sheer variety of mass movements makes it challenging to describe them accurately. The classification devised by Sharpe and Varne is solely predicated on geomorphic features and uses comprehensive terminology. The difficulty that these categories have in responding to certain motions has been brought to light by many scholars (Ward, 1948; Irwin-Hunt, 1960; Bailey & Rice, 1969; Rice et al., 1969; Blong, 1973). Blong (1973) proposed a method that uses numbers to classify landslides into three categories: debris flow, debris slide, and debris avalanche. He suggested classification by making use of many different classification variables.

Different landslide failure processes can be utilized to categorize different types of landslides. Similarly, the amount of activity, the proportional mobility, and the method one slide are all crucial classifiers. Landslides were classified by Cruden and Varnes (1996) as being either progressive, increasing, retrogressive, numerous, or sequential, depending on their level of activity at the time. These words are used to describe the mechanical status of a landslide. Many experts in the field of academia were cautious about using the word "progressive" when referring to the landslide and instead suggested using the phrase "progressive failure," which is commonly found in studies on slope stability (Morgenstern, 1992; Leroueil et al., 2012). Additional adjectives like "re-activated," "dormant," and "relict" are proposed by Cruden and Varnes (1996) to characterize the behaviors of the landslide after it has failed. Single-rotating slides, multiple retrogressive slides (also known as earth flows), progressive translational landslides, and spreads are the four primary types of sensitive clay identified and classified in Canada by Tavenas and

colleagues (1984). The use of the Varnes (1996) classification for the categorization of landslides is currently producing challenges on a global scale. Varnes (1978) and Cruden & Varnes (1979) used the binomial system for their naming. Classifying the landslide under the circumstances and the process involved is necessary to comprehend it.

### 2.4 Landslide analysis

Many scholars have questioned the relationship between the phrases "landslide susceptibility" and "landslide hazard" because there is still some ambiguity in this area (Chacón et al., 2006; Guzzetti, 2006). Even though the two names communicate different concepts, many scholars have nonetheless used them as synonyms for each other (Fell et al., 2008a; Reichenbach et al., 2018). According to Brabb (1984), landslide susceptibility is the possibility of a landslide occurring in a particular region due to the local terrain and environmental factors. According to Reichenbach et al. (2018), susceptibility measures how much future slope movements would affect the landscape and calculates the potential surface area for landslides. In mathematics, the term "susceptibility" refers to the likelihood that a landslide or other slope failure may occur, given the current situation (Guzzetti et al., 2005).

Susceptibility indicates the likely location of a landslide, not its size or volume, but it is still possible to do a susceptibility analysis on a variety of size-based landslides (Carrara et al., 1995). Up until recently, a variety of techniques and models were used all around the world to determine landslide risk. The old and new landslides can be identified in the field or by satellite imagery. Similarly, the identified landslide can be classified and precisely mapped using remote sensing techniques (Rib & Liang, 1978; Varnes, 1978; Hansen, 1984; Hutchinson, 1988; Cruden & Varnes, 1996; Dikau et al., 1996; Griffiths, 1999; Mondini et al., 2011; Guzzetti et al., 2012). For landslide prediction, the physical characteristics of landslides can be statistically, probabilistically, or deterministically evaluated (Crozier, 1986; Hutchinson, 1988; Dietrich et al., 1995; Dahal et al., 2012). According to Hutchinson (1995), previous and present landslides are crucial to the future, making it crucial to analyze them when determining landslide vulnerability (Varnes, 1984; Carrara et al.,

1991). Analyzing the susceptibility of landslides can be done using qualitative, quantitative, or indirect methods. In any susceptibility zone, quantitative methodologies generate numerical estimates or probabilities of the occurrence of landslides (Guzzetti et al., 1999). Overall, there are five different types of landslide susceptibility studies: (i) geomorphological mapping; (ii) landslide inventory analysis; (iii) heuristic or index-based approaches; (iv) process-based methods; and (v) statistically-based modeling methods (Reichenbach et al., 2018).

The expert judgment approach for assessing landslides is heuristic. Experts rate the landslide-causing causes under their contribution to the landslide's occurrence and assign a weight to each element (Hansen, 1984; Hansen et al., 1995). The researcher's judgment and experience determine the validity and quality of a heuristic assessment (Nilsen & Brabb, 1977; Abella & Westen, 2008; Ruff & Czurda, 2008). In the accuracy of the heuristic evaluation, the researcher's bias may be present. The stability criteria are examined using "limit equilibrium models" in the physical-based approach (Baum et al., 2008; Anagnostopoulos et al., 2015; Alvioli & Baum, 2016). Statistical methods for landslide susceptibility studies are based on the functional relationship between the response variable and the predictor variable (Carrara, 1983; Guzzetti et al., 1999; Huabin et al., 2005; Chacón et al., 2006; van Westen et al., 2008). Landslide susceptibility is a response variable, while other related variables that directly or indirectly contribute to the incidence of landslides are predictor variables. The predictor factors assist in simulating and forecasting the potential area for landslide occurrence.

Beginning in the middle of 1970, researchers began to analyze and map landslides' susceptibility, and at that period, numerous publications with the heading "landslide hazards" were made (Carara, 1983). At first, statistical models based on published research predominated (Guzzetti, 2006). Bivariate discriminant analysis was employed by Neuland (1976) to create a model for predicting landslides. Carrara (1983) used discriminant and multiple regression analysis to estimate landslide susceptibility based on a significant amount of landslide with geological and geomorphological information (Reichenbach et

al., 2018). The spatial investigation of the landslide was assessed using GIS and automated cartography applications.

### 2.5 Previous reviews on statistical approaches for landslide susceptibility

Since 1970, research has been conducted on landslide susceptibility using statistical analysis. Extensive research began after 1980 and peaked in 2000. Several works of literature have been published on landslide susceptibility models. Some of the researchers critically reviewed the different landslide susceptibility models, types of data, and types of analysis (Aleotti & Chowdhury, 1999; Guzzetti et al., 1999; Guzzetti et al., 2000; Huabin et al., 2005; Chacón et al., 2006; Fell et al., 2008a, 2008b; Galli et al., 2008; van Westen et al., 2008; Kanungo et al., 2009; Pardeshi et al., 2013; Reichenbach et al., 2018). Similarly, Aleotti and Chowdhury (1999) and Guzzetti et al. (1999) explored the existing literature on landslide susceptibility assessment. Aleotti and Chowdhury (1999) pointed out the importance of landslide susceptibility for landslide risk analysis. Guzzetti et al. (1999), Carrara et al. (1982), Carrara (1983), and Carrara et al. (1991, 1995) focused on the need for high-quality landslide and geo-environmental data for landslide susceptibility zonation, as well as statistically-based susceptibility modeling approaches. Many researchers have shown the importance of GIS technology for landslide susceptibility analysis (Huabin et al., 2005; Chacón et al., 2006; Fell et al., 2008a, 2008b; Galli et al., 2008; van Westen et al., 2008; Kanungo et al., 2009; Goodchild, 2010; Dahal et al., 2012; Thapa & Bhandari, 2019; Pokharel & Bhandari, 2019).

### 2.6 Quantitative assessment of landslide susceptibility

Data analysis and value determination are necessary for a quantitative assessment to be successful. Quantitative approaches are data-based and based on numerical calculations to provide results with a specific value. The historical landslide data and landslide causative elements provide numerical approximations in the quantitative landslide evaluation (Van Westen et al., 2006). This evaluation assumes that the landslides and their contributing causes are dispersed evenly over the region. For landslide susceptibility mapping, the quantitative assessment determines the pixel-based weightage of each causative element

and produces the final rating value. Calculating the weight and final rating values requires mathematical equations and statistical significance tests.

For the analysis of landslide susceptibility, several earlier scholars argued that statistical methods are highly reliable and predict quantitative methodologies (Aleotti & Chowdhury, 1999; Guzzetti et al., 2002; Bui et al., 2012; Yalcin et al., 2011; Raichenbach et al., 2014; Yu et al., 2019; Farooq & Akram, 2021). Landslide susceptibility evaluation can be assessed statistically using either a bivariate or multivariate technique. Landslide factor maps and landslide inventory maps are merged in the bivariate technique to determine the weights for each parameter. The weight of evidence, frequency ratio, information value, and entropy models are a few examples of the popular bivariate techniques used to determine landslide susceptibility. The association between landslide occurrence and a controlling factor is examined using the multivariate technique. However, bivariate methods are among the most popular global techniques for mapping landslide vulnerability. Combining all of the criteria for the final score is necessary because there are many different causal factors in the Siwalik zone of Nepal.

### 2.6.1 Information value (IV) method

The information value method is a quantitative bivariate technique to find a relationship between causal and response factors. In the landslide study, the information value method is used to identify the relationship between landslides and their response variables (Yin & Yan, 1988; Chen et al., 2016; Achour et al., 2017; Afungang et al., 2017; Banshtu et al., 2020). This method was used in various sectors to identify the likelihood of certain factors. Jade and Sarkar (1993) and van Westen (1997) proposed this method for the likelihood of landslide occurrence, which was further elaborated by Zazere (2002) for landslide susceptibility assessment. This method was compared to the Nominal Susceptibility Factor (NSF) and the Analytical Hierarchy Method (AHP) by Saha et al. (2005) and Singh and Kumar (2018). They have reported that the information value method performs better for landslide prediction than the AHP and NSF methods. Yin and Yan (1988), Jade and Sarkar (1993), Atkinson and Massari (1998), Wang and Sassa (2005), Pradhan et al. (2012), Sarkar et al. (2012, 2013), Wang et al. (2014), and Sarda and Pandey (2019) adopted the

information value method for better prediction of landslide susceptibility. Wubalem and Meten (2020) compared this method with the logistic regression method for landslide susceptibility analysis. They obtained higher predictions from the information value method than the logistic regression model. Chen et al. (2016) also reported that the IVM model has higher prediction accuracy than other statistical models (Wubalem & Meten, 2020).

### 2.6.2 Frequency ratio

The frequency ratio is a quantitative method for assessing landslide susceptibility that may be evaluated using GIS tools and spatial data (Bonham-Carter, 1994; Lee & Talib, 2005; Chen et al., 2016; Ding et al., 2017; Thapa & Bhandari, 2019). It is a bivariate statistical technique for analyzing landslide susceptibility based on the relationship between prior landslides and causal elements. The frequency ratio (FR) is computed by dividing the chance of a landslide occurrence by the probability of a non-occurrence for a particular cause. The frequency ratio (FR) method is the most commonly used and most reliable method for mapping landslide susceptibility (Audisio et al., 2009; Choi et al., 2012; Ehret et al., 2010; Lee et al., 2004; Lee & Pradhan, 2006; Lepore et al., 2011; Mandal & Mondal, 2019; Mezughi et al., 2011; Mohammady et al., 2012; Oh et al., 2009; Pal & Chowdhuri, 2019; Pradhan & Youssef, 2010; Rossi & Reichenbach, 2016; Yalcin, 2008; Yalcin et al., 2011; Yilmaz, 2009; Yilmaz, 2009; Reis et al., 2012; Umar et al., 2014; Chen et al., 2016; Wu et al., 2016; Wang & Li, 2017). It is based on the probabilistic relationship between the landslide inventory and the causes of landslides.

The frequency ratio approach is a systematic and reliable bivariate method for mapping landslide risk, according to Korup and Stolle (2014) and Tehrany et al. (2019). The susceptibility evaluation is easier to conduct in a GIS environment, making it user-friendly, effective, and fundamentally straightforward (Lee & Pradhan, 2006; Yilmaz, 2009; Oh et al., 2011). This method also evaluates the sensitivity of landslide failure to specific landslide-related variables (Guo et al., 2015; Vakhshoori & Zare, 2016; Aghdam et al., 2017; Oh et al., 2017; Razavizadeh et al., 2017). According to numerous experts, the frequency ratio method can be more precise than other landslide susceptibility methods

(Ozdemir & Altural, 2013; Ramesh & Anbazhagan, 2015; Guo et al., 2015; Vakhshoori & Zare, 2016; Ding et al., 2017; Huang et al., 2018; Sharma & Mahajan, 2018). Some researchers obtained contradictory results against frequency ratio and demonstrated that machine learning generally outperforms the frequency ratio technique (Pradhan & Lee, 2009; Park et al., 2013; Chen et al., 2015; Youssef, 2015; Youssef et al.,2015; Aditian et al., 2018). Nonetheless, the FR is a straightforward and uncomplicated method that is highly valid and suitable for landslide susceptibility study.

Numerous other researchers have also discovered the superior accuracy of the frequency ratio method (Pradhan, 2010; Mohammady et al.,2012; Ozdemir & Altural, 2013; Regmi et al., 2014; Chen et al., 2016; Ding et al., 2016; Vakhshoori & Zare, 2016). It is user-friendly since its ideas are straightforward and straightforward. Similarly, the data entry, calculation, and output methods, as well as the GIS's working steps and processes, are transparent and straightforward. Due to these factors, this method is a highly acceptable, essential instrument for assessing landslide vulnerability; however, further data is required for greater precision. Süzen and Doyuran (2004 a, b) used frequency ratio analysis to determine the vulnerability to landslides. A landslide inventory map and multiple landslide causative factor maps were utilized for landslide susceptibility. They determined the weight value by dividing the landslide's size by the theme class's area. The ratio of the landslide-affected area to the unaffected area was calculated. The rating or weight value for the landslide susceptibility map was determined using the final ratio values (Lee & Talib, 2005; Lee & Pradhan, 2007; Vijith & Madhu, 2008; Bourenane et al., 2016; Chimidi et al.,2017; Hamza & Raghuvanshi, 2017; Pirasteh & Li, 2017; Maheshwari, 2019).

Some researchers compared the frequency ratio method with other techniques, such as logistic regression (Lee & Sambath, 2006; Devkota et al., 2013), artificial neural network (Yilmaz, 2009), analytical hierarchy (Demir et al., 2013; Kumar et al., 2019), and weight of evidence (Ozdemir, 2020; Arifianti et al., 2020), and found that the FR method has better prediction rate.

### 2.6.3 Weight of evidence

The weight of evidence is a prominent Bayesian probability-based, data-driven method for landslide susceptibility assessments. Prior and conditional probabilities are used in this approach. Initially, the weight of evidence model was established to evaluate potential mineral regions (Bonham-Carter et al., 1988, 1989; Agterberg et al., 1993). It has since been prevalent in landslide susceptibility assessment (Van Westen et al., 2003; Lee et al., 2004; Lee & Talib, 2005; Lee & Sambath, 2006; Pradhan et al., 2010; Dahal et al., 2012). This model uses landslide distribution data to predict favorable and unfavorable landslide susceptibility conditions (Lee et al., 2002; Lee & Choi, 2004; Thiery et al., 2004, 2007; Sharma & Kumar, 2008). The likelihood ratios are generated to calculate positive and negative weight values and the possibility of a landslide. Negative weight is subtracted from positive weight to determine the contrast value C (Ilia et al., 2010; Sterlacchini et al., 2011; Armas, 2012; Kayastha et al., 2012; Neuhauser et al., 2012; Piacentini et al., 2012). Positive contrast values imply favorable spatial relationships, while negative contrast values suggest unfavorable spatial relationships. Using historical landslide data, Blahut et al. (2010) and Martha et al. (2013) utilized the weight of evidence technique for LSM and found positive sensitivity test results. Ilia and Tsangaratos (2016) conducted landslide susceptibility mapping in Greece using the weight of evidence approach. They determined that the sensitivity of the results depends on the causes selected for the study.

### 2.6.4 Shannon’s entropy

The degree of uncertainty in a continuous probability distribution has been represented as entropy (Shannon, 1948; Yufeng and Fengxiang, 2009). Entropy is often applied in the science of thermodynamics to quantify the chaos and dispersion of natural processes. Shannon initially quantified the theory of entropy (Shannon, 1948). The theory of entropy was subsequently utilized for landslide susceptibility evaluation. Entropy relates the development of a landslide to its underlying causal causes (Pourghasemi et al., 2012b). The index system's entropy increases owing to a number of significant reasons. "Shannon's entropy was initially created in landslide susceptibility to balance the influence of variation

and predominant factors based on the knowledge-driven weights assigned to the many sub-categories" (Sharma et al., 2012a, 2015).

The Shannon entropy model is superior to the frequency ratio model (Panchal and Shrivastava, 2021). The frequency ratio model does not account for the weighting of causal factors; only the weighting of sub-factors is considered (Roodposhti et al., 2016). Shannon's entropy measures the unpredictability or instability of a system. With landslide susceptibility mapping, it is possible to estimate the extent to which a specific factor influences the chance of a landslide (Sharma et al., 2014).

### 2.6.5 Other adopted methods

Both geo-environmental factors and quantitative prediction models are required for landslide susceptibility mapping. Geo-environmental factors are those that are related to the occurrence of landslides. As a result of recent developments in computer resources, geographic information systems, also known as GIS, have become increasingly prevalent in preparing for and managing those factors. Many quantitative models have been proposed to integrate the causal factors and apply these models to landslide susceptibility mapping. Logistic regression has been applied widely to map landslide susceptibility (Lee & Sambath, 2006; Greco et al., 2007; Akgun, 2012; Atkinson and Massari, 1998; Dai and Lee, 2002). Other models include evidential belief functions (Park, 2011; Althuwaynee et al., 2012; Lee et al., 2013), fuzzy set theory (Pradhan, 2010; Park et al., 2017; Cengiz & Ercanoglu, 2022).), artificial neural networks (Lee et al., 2004; Lee, 2007; Choi et al., 2010 Dou et al., 2015), and support vector machines (Yao et al., 2008; Ballabio & Sterlacchini, 2012; Huang & Zhao, 2018).

Such models for landslide susceptibility mapping have also been employed for various other geological predictive modeling tasks, such as mineral potential mapping (Carranza & Hale, 2008; Porwal et al., 2004) and ground subsidence mapping (Kim et al., 2006). In addition to these fields, species distribution modeling in ecology is another active research field of predictive models. To make predictions regarding the distributions of species, several statistical and machine-learning models have been applied. The generalized linear

and additive models are two types of multivariate statistical models frequently used in modeling species distribution. Machine learning algorithms are another essential method for landslide susceptibility where boosted regression trees and random forests are mainly used. Both landslide susceptibility mapping and species distribution modeling share many similarities. In both cases, known occurrences are used to model the target distribution, and multiple environmental variables are considered during the modeling process. The models mentioned above that have been used in modeling landslide distribution require both presence and absence of a landslide.

# CHAPTER 3

## MATERIALS AND METHODS

### 3.1 Study Area

The Babai River watershed was approached for the present study. The Babai River originated from the Siwalik Hills and extended up to the flat land of the Tarai. The Babai River watershed in the Siwalik zone is proposed for the present study. Babai River has some typical characteristics such as east-west trending, parallels with rock strikes, less interruption of humans, and more than 80% of the area is covered by forest. The total area is between 27º57'59.03''N, 82º33'42.80" E in the East, 28º28'30.14''N, 81º28'30.14''E in the West, 28º12'47.90''N, 82º15'46.08'' in the North and 28º01'03.89''N, 82º12'39.61''E in the South. After its development, it enters the flat Dun Valley and reenters the Siwalik (Fig.2). The total catchment area of the Babai watershed is 1952 $km^2$, but for the present study, only 1157 $km^2$ is included because the rest of the area is either Dun valley or Terai plain.

#### 3.1.1 Climate of the study area

The climate of the research area is subtropical, and Soria Robusta is the predominant plant species. It has a spectacular hilly topography, and the height ranges from 109 meters to 1550 meters above the mean sea level. The region's climate is divided into a dry and a rainy season. The dry and wet seasons are much longer than they should be. The extended wet seasons are divided into three monsoon periods: pre-monsoon, monsoon, and post-monsoon. June, July, and August are referred to as the monsoon period, whereas April and May are considered the pre-monsoon period. June to September is typically referred to as the long-term rainy season. The months of September and October are referred to as the post-monsoon periods. In contrast, rainfall during the dry season tends to be moderate to low intensity, making it far less frequent than during the wet season (Bhandari & Dhakal, 2019). The temperature can drop below zero in the winter and rise well above forty degrees in the summer. During the monsoon season, the rainfall is typically substantial and can be

relatively strong. The yearly precipitation ranges between 1750 and 3250 millimeters from 1990 to 2021. Only during the monsoon season does the average annual rainfall range from 1550 to 2470 millimeters. More than 85 percent of annual precipitation occurs in the Monsoon period.

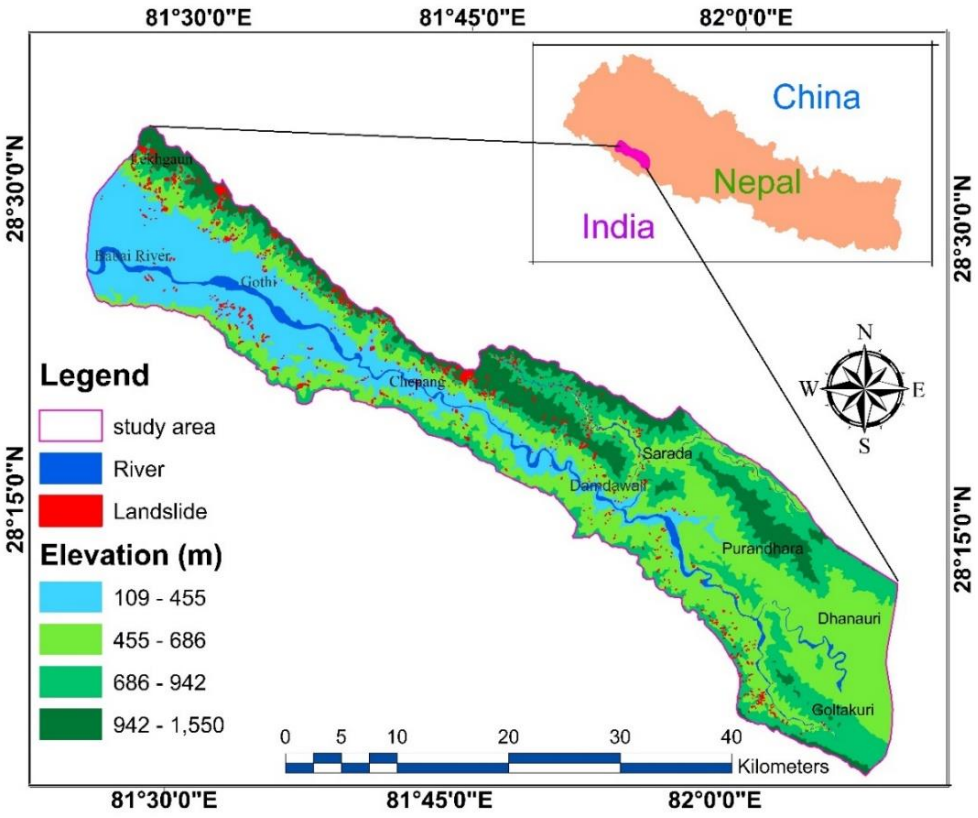


**Figure 2:** Location map of the Babai River watershed, Nepal.

### 3.1.2 Geomorphology

The Babai River flows in a direction parallel to the strike of the rocks and the hills and rills. The landforms are dynamic, constantly shifting, and evolving with time. Various processes, including the weathering of rocks, the continual erosion of weathered materials, landslides, and other mass movements, and the deposition of large masses of sediments, cause changes in landforms. In the area under investigation, tectonism is also responsible for the evolution of the landforms and the mass movement. The study area is characterized mainly by landforms that were formed by erosion and deposition. The rough landscape, steep slopes,

cliffs, and narrow ridges all contribute to the rapid erosion rate and the creation of gullies. Rock canons and George were formed due to a continual water discharge that occurred on a steep slope composed of weak sedimentary rocks. The debris flow fan, the talus cone, the bank deposits, and the river terraces are all common depositional landforms in the study region. Because of the several strata of rock masses, the region contains characteristics that are usually identical and distinct. The weathering pattern and the mechanism of rock fall may be seen clearly because weak rocks' erosional layers alternate with strong ones (Bhandari & Dhakal, 2019). Interesting geomorphological features of the studied area include the various summits of the hill, sequential saddles, parallel hill ranges, and the several river valleys that may be found between the narrow hills.

### 3.1.3 Geology

The rocks of the study region were previously categorized into three geological units based on lithology and rock composition: Lower Siwalik, Middle Siwalik, and Upper Siwalik (Bhandari & Dhakal, 2018), from bottom to top, respectively. The top of the stratigraphy is covered by a recent deposit called the Quaternary deposit.

#### 3.1.3.1 Lower Siwalik

The Lower Siwalik comprises sandstone, mudstone, and a small amount of limestone in the study area. The sandstone is medium- to thickly bedded and fine- to medium-grained. The sandstones are interbedded with reddish-purple and greenish-grey shale (variegated mudstone). The shale is thinly bedded, predominately red, and laminated in the lower part of the Lower Siwalik. Some concretionary layers are also observed in the Lower Siwalik. The Lower Siwalik is well exposed in the Babai Valley—Salyantari section of the Surkhet and Salyan Districts. In this section, the massive and hard sandstone beds are observed. The medium- to thickly bedded, fine- to medium-grained, greenish-grey sandstone is interbedded with greyish-brown mudstone and purple shale. Along the Tulsipur-Nepalgung road, greenish-gray, medium-bedded, fine-grained sandstone is interbedded with light brown mudstone. In this section, some of the beds are weathered. The red-purple shale, variegated mudstone, and occasional thin bands of limestone are typical features of

this geological unit. The continuous interbedding of weak mudstone and sandstone is extended throughout the study area.

#### 3.1.3.2 Middle Siwalik

The Middle Siwalik is well exposed in the study area. The Middle Siwalik in the study area comprises thickly bedded (>5 m), medium- to fine-grained sandstone interbedded with thickly bedded (>3 m) brownish-gray mudstone. The sandstones are greenish-gray in color, medium to fine-grained, massive, and well-jointed along the Babai Valley–Harrey Road section, pepper and salt sandstone alternate with a thin layer of yellowish-brown mudstone. There is transitional contact between Lower and Middle Siwalik and sharp contact between Middle and Upper Siwalik; however, the contact cannot be observed distinctly due to eroded boulders and pebbly conglomeratic beds. The upper part of the Middle Siwalik is mainly covered by plants and debris deposited from the Upper Siwalik. The width of the Middle Siwalik varies from place to place, and due to thrusts, the Middle Siwalik is observed in three sequences. The weak mudstone between thick sandstone layers is highly weathered and easily erodible in the continuous rainy season. Due to weathering and erosion of mudstone or shale, there seems to be a gap between thick sandstone beds.

#### 3.1.3.3 Upper Siwalik

The Upper Siwalik of Babai section comprises cobble and pebble-bearing conglomerate beds. Most conglomerates are cemented by clay components, whereas some beds are cemented by calcite. The boulder conglomerate beds are well exposed in the Babai Valley-Salyantari Road section. A thin layer of brown mudstone and grey sandstone transitionally overlies the conglomerate beds. The boulders, cobbles, pebbles, and other sediments are derived from the Lesser and Higher Himalayas. The pebbles are well-rounded to sub-rounded and made of quartzite, slate, and marble. The boulders present on the conglomerate beds are sub-rounded to rounded. The boulders are made of gneiss, quartzite, and granite. Sand-gravel mixed, non-compacted fluvial deposits cover the study area's flat terrain-numerous fluvial deposits in and around the river terraces and lower valley. Debris flow and other slope debris and landslide deposits are typical in hilly terrain colluviums

(Bhandari & Dhakal, 2019b). The colluvium derived from erosion and landslides typically consists of sub-angular cobbles and boulders of sandstone and mudstone with some conglomeratic fragments.

### 3.2 Data collection and interpretation

The overall method of the study is divided into four phases: desk study, field study, lab test, and data analysis. Desk study includes literature review, preparation of spatial and temporal landslide inventory map, geological map in GIS, extraction of DEM, and preparation of landslide causative factor map. Literature on landslides, classification, susceptibility, and characterization was reviewed for research preparation. The research gaps were identified after conducting the literature review. The methodological framework for data collection and processing is shown in Figure 3.

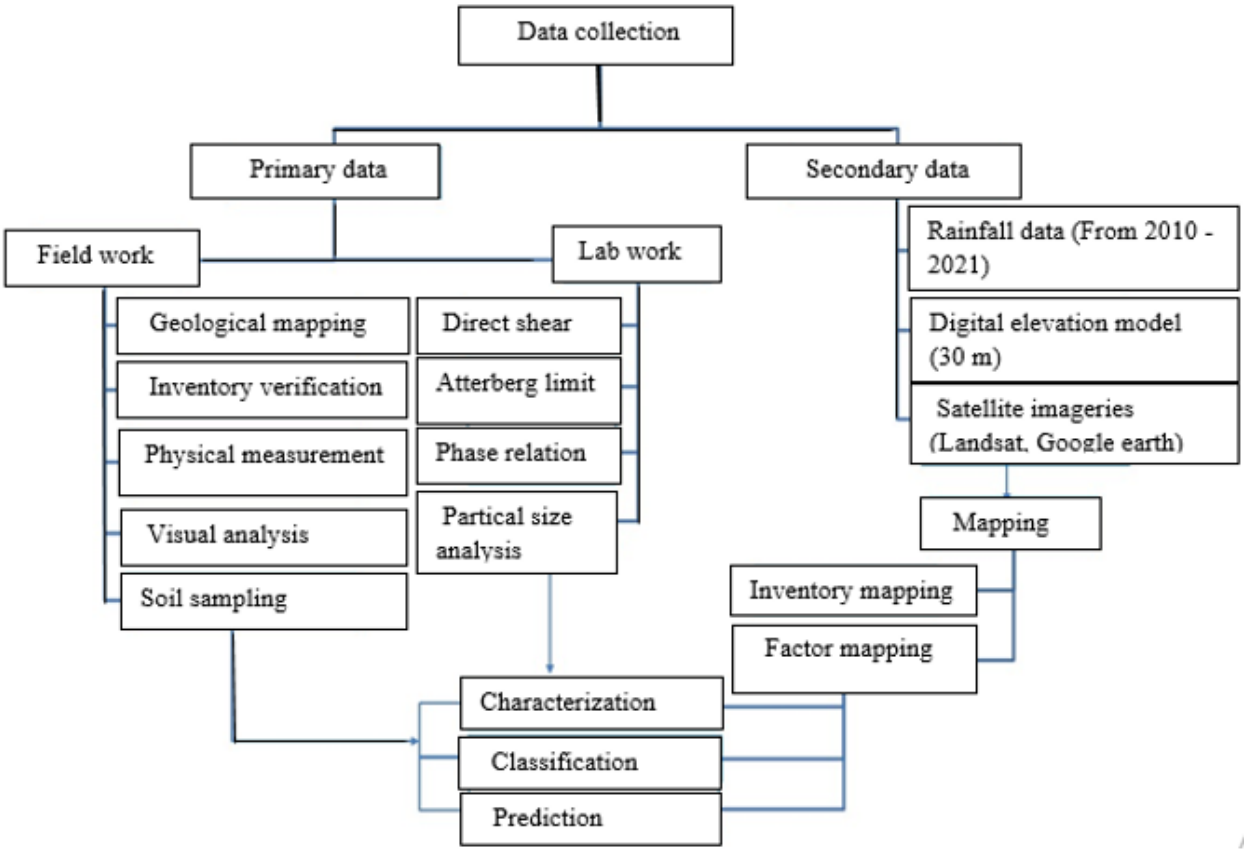


**Figure 3:** Methodological framework of data collection and processing.

More than 200 literatures related to the objectives were reviewed from the index journals. The field study includes soil sampling, physical measurement of landslides, landslide inventory map verification, geological map preparation, and causative factor verification. Significant geotechnical properties of soil samples were tested in the lab following standard protocol. The detailed laboratory analysis is given in the next section. Finally, both the lab and field data were used for analysis. The study included the Casagrande plasticity index, compositional analysis, multiple regression analysis, Karl Pearson correlation, and sieve data analysis. Similarly, the four statistical models were used: weight of evidence, frequency ratio, Shannon's entropy, and information value models for landslide susceptibility.

### 3.2.1 Preparation of landslide inventory map

The research work has begun with landslide characterization. Various primary and secondary datasets are used in this research for landslide characterization and susceptibility analysis. Various procedures for data collection and analysis were used. The work began with the identification of the landslide. The landslides can be spotted and plotted using satellite imagery or aerial photography (Guzzetti et al., 2012). However, in the hilly region of Nepal, it is rather challenging to capture explicit imagery using either technique due to dense vegetation and frequent cloud cover (Bhandari & Dhakal, 2020). The spatial and temporal landslide inventory map was created using the following steps: (a) Every landslide was recognized and identified using images from Google Earth Pro, Landsat, and Sentinel-2,3; (b) The polygon tool was used to outline the landslide on the images, and the resulting KML file was saved; (c) The KML file was retrieved from the GIS layer, and the 1:10,000 scale map was prepared; (d) the prepared spatial and temporal inventory maps were validated on-site; (e) Some landslides missing from the image were recorded with GPS data and then digitalized on the map.

The inventory of landslides from 2010 to 2021 has been compiled based on activity level, space, and time. Three different inventory maps were prepared: spatial, temporal, and activity state. The imagery used to map landslides was acquired between August and December of each year. Some images are severely cloud-affected; however, the many sets

of images from various dates helped to avoid difficulties (Bhandari & Dhakal, 2020). After field verification, the map has been updated to represent a region severely impacted by cloud cover and steep terrain. In the photograph, the scar of the landslides was determined by color variation and topographical characteristics. The landslide boundaries in the satellite photos were recognized based on headwall scarps, chutes, vegetation differences, and landforms.

### 3.2.2 Preparation of geological map

The study area's geological map was prepared using the Topo-sheet of 1: 25,000 developed by the Department of Survey, Government of Nepal (Fig.4). The geological traverse was conducted throughout the study area. The strike and dip amount of the bedrock was measured in the various rock units. The contact between two rock sequences was identified and plotted on the map. As mentioned in the geology section above, the geological formations were identified and named accordingly. The lithology and stratigraphy were the main focus of the mapping. The rock types, composition, and combination were considered for the geological mapping. The strike and dip amount of the bedrock outcrop were plotted in the topo map of the respective area. The draft map prepared in the field was digitized in the GIS layer and obtained the final map of a 1:10,000 scale.

### 3.2.3 Physical measurement

After preparing the inventory map, the traced landslides were checked for accuracy in the field. For the field investigation, a random sample of 120 landslides with an area greater than 1000 square meters was chosen from 1140 landslides. Manual measurements of landslides were taken, such as length of landslides, slip surfaces, tow length, distance traveled by slide materials, slope, aspect, and elevation. The area of the landslides that were measured in the polygon, as well as their length, were compared with the field data. The geological features and formations, in addition to their influences on the occurrence of landslides, were also investigated in the field. In addition, the physical aspects of landslides, such as the descriptions of landslides and the physical elements that contributed

to the beginning of landslides, were investigated and evaluated. Field observations were the basis for researching and analyzing the mechanisms that initiate landslides.

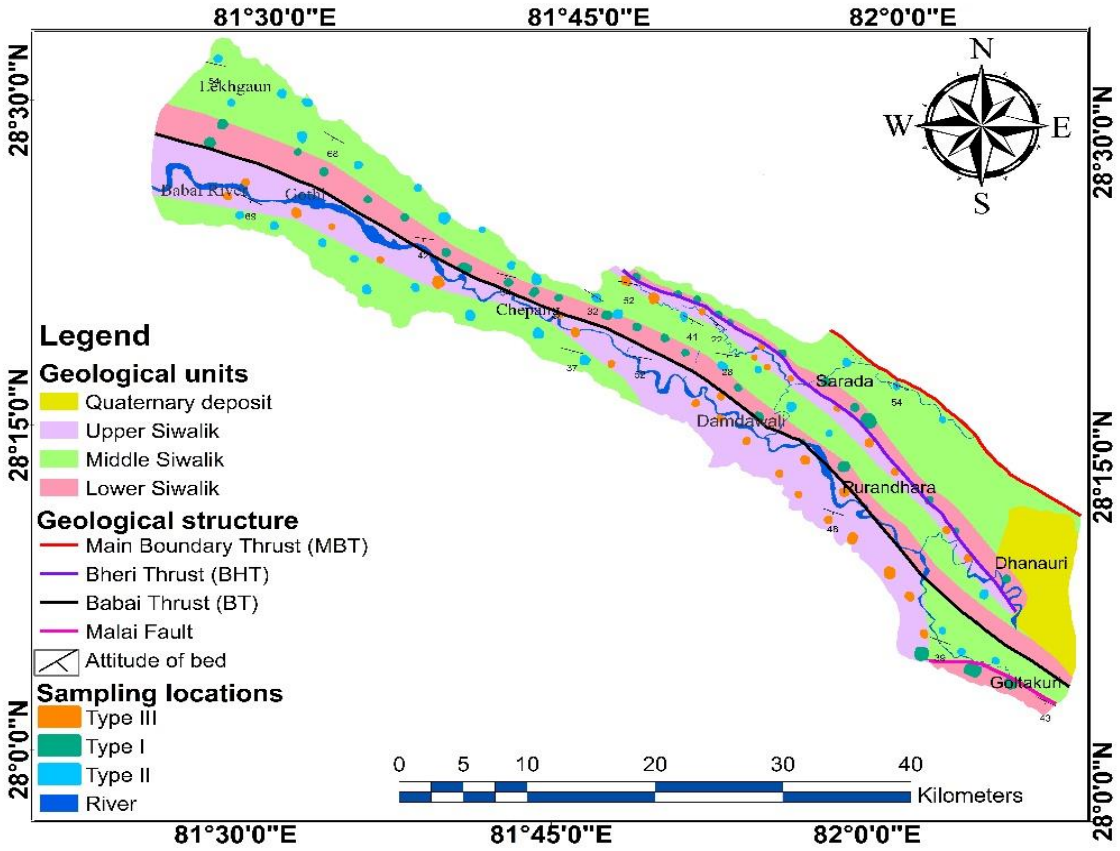


**Figure 4:** Geological map showing the location of the Babai River catchment along with the sampling landslide.

### 3.2.4 Landslide characterization

The methodological framework of landslide characterization using four attributes is shown in Figure 5. Landslides were characterized in terms of geological, topographical, hydrological, and geotechnical attributes. In geology, three factors are used: geological formation, stratigraphy, and lithology. Similarly, five different factors were used for topography: slope distribution, curvature, aspect, TWI, and "T" factors.

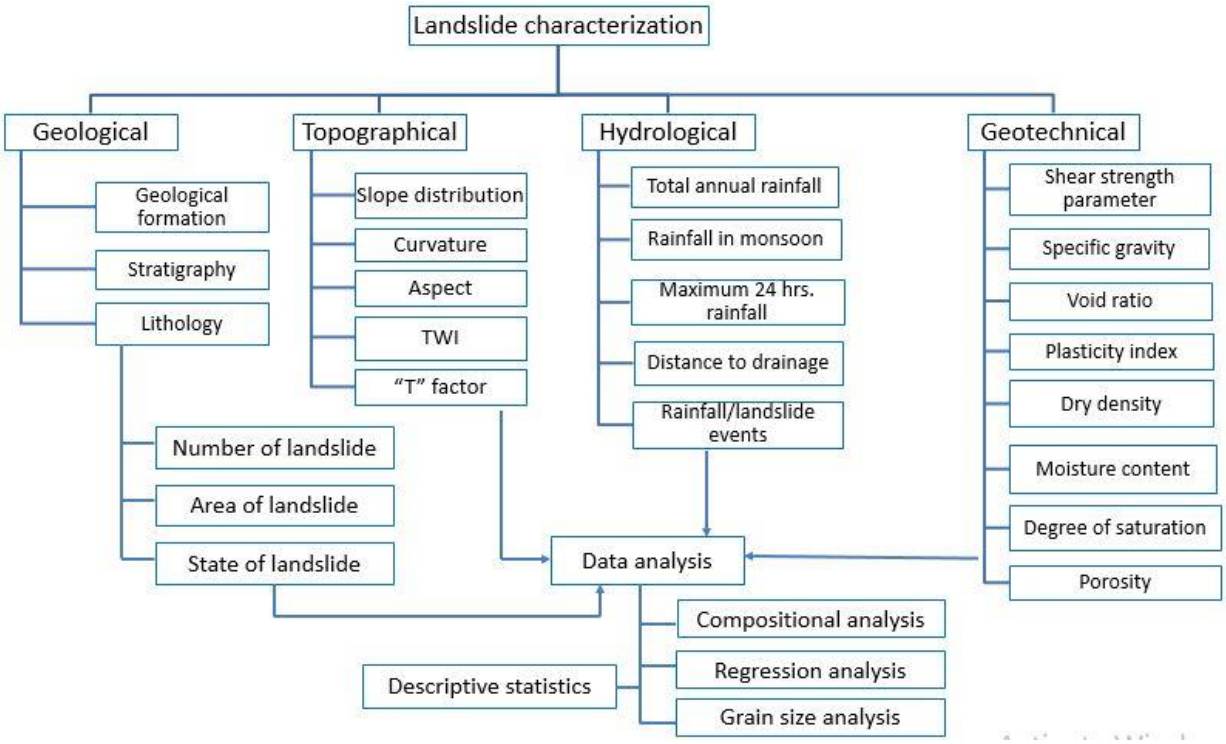


**Figure 5:** Methodological framework of landslide characterization.

### 3.2.4.1 Geological characterization

Geological characterization means identifying and assessing the geological nature and character of landslides in the study area. Moreover, it gives geological control over landslides. The landslide inventory and geological map are converted into a raster format. The size of the landslide and each geological unit are obtained by cross-tabulating the inventory map and geological map in the raster format. Similarly, the temporal area distribution of landslides from 2010 to 2021 was obtained after cross-tabulating the temporal inventory map with the geological map. The size distribution of the landslide was obtained in the geological units.

Similarly, the geological units' temporal and activity state distribution of landslides were obtained. Likewise, the landslide mechanism and causes in the three geological units were also assessed. The area and length-based landslide distribution was obtained in the geological units. The distance-to-thrust analysis was also conducted based on the landslide

inventory map. The landslide distribution in the geological units is compared, and landslide-susceptible geological units are estimated.

### 3.2.4.2 Topographical characterization

The landslide inventory map created using satellite imagery was downloaded to the GIS layer and converted into a shape file. The length and size of each landslide were determined using a GIS open attribute table. Topographical analysis can use a variety of elements; however, only five topographical factors are used: slope, aspect, curvature, T factor, and topographical wetness index. A digital elevation model (DEM) with a resolution of 30 m was employed to obtain topographical maps freely available at the USGS Alaska Satellite Facility. The GIS's spatial analyst tool was applied for topographical analysis. The slope angle is classified into four classes based on landslide potential (Bhandari & Dhakal, 2020) : (a) $<15^{o}$ (b) $15^{o}$-$30^{o}$ (c) $30^{o}$- $45^{o}$ (d) $>45^{o}$. The aspect class is divided into four sub-classes: a) NE, b) SE, c) SW, and d) NW. The curvature is classified into three categories based on low to high value: (a) convex, (b) planar, and (c) concave. The concave slope accelerates the mass movement rate more than the convex slope. The topographical wetness index is classified into four classes based on equal interval division from low to high pixel numbers. The vector polygon-based inventory was obtained on the raster map, and the raster's pixel-based area was calculated using cell size and pixel number. The landslide area in each topographical factor was obtained from the cross-tabulation tool of GIS.

The landslide-prone and potential slope was identified and justified by logical description. This characterization mainly analyzed the topographical control of the landslide activities. Landslide distribution in the aspect, plan curvature, and profile curvature was obtained, and potential spaces were identified. The topographical wetness index and landslide distribution relation were obtained.

**Topographical “T” factor**

The polygons of each of the gullies, including those with and without landslides, were outlined. The catchment area of the landslide was determined from the area of the landslide. The total area of the gullies in the given catchment was determined. On the field, the

sensitive gullies in the landslide were highlighted. To conduct a topographic factor analysis, specific topographical criteria, such as watershed area, stream length, elevation difference, an average gradient of stream, form factor, and percentage of basin area with slope angle, were chosen (Li et al., 2015; Bhandari & Dhakal, 2019b).

**Form factors (*F*)**

The form factor (*F)* was calculated by taking the ratio of catchment area and square of the length of a stream. The equation was adopted from After (Li et al., 2015; Bhandari & Dhakal, 2019).

$$F = A / L^2 \quad (1)$$

Where, *A* is the catchment size of each landslide, and *L* is the stream length in the particular catchment. According to Chang (2007), a watershed with a large form factor is more likely to generate landslides under the same conditions. The larger the form factor, the larger the discharge and flow velocity (Bhandari & Dhakal, 2019b).

**Average gradient of a stream (*J*)**

The average gradient of a stream, denoted by the letter J, is determined by taking the elevation difference between the slope at the stream's point of origin and the slope at the catchment's point of exit and dividing that value by the square of the stream's length (Bhandari & Dhakal, 2019b). To determine the gradient, the stream was segmented into several different portions. The equation proposed by Li et al. (2015) and Bhandari & Dhakal (2019) determines the average gradient of the stream that runs through the area where the landslide occurred.

$$\text{Average gradient of stream } (J) = [\sum (h_{i-1} + h_i) Li - 2h_o L] / 1000\, L^2 \quad (2)$$

Where $h_i$ is the elevation of the upper part of each section and $h_0$ is the elevation of the lowest part of each section. $L_i$ is the stream length of each section, and *L* is the total length of the stream.

**Ratio of catchment area with terrain gradient (*S*)**

The area of the catchment and the potential slope area was obtained using a digital elevation model of 30 m resolution. The ratio of each slope class's area and the catchment's area is denoted as"

$$S = \frac{Catchment\ area\ (A1)}{Potential\ slope\ area\ (A2)} \quad (3)$$

Landslides and rock falls are ubiquitous, with slopes greater than thirty degrees (Bhandari & Dhakal, 2021). The gradient or slope of the catchment plays a vital role in forming landslides. In general, the flow velocity of water is higher on the steep slope.

**"T" factor**

*T* factor is obtained from the combination of form factor, catchment size, an average gradient of stream, and the ratio of slope class area and catchment area (Bhandari & Dhakal 2019).

Topographical factor ($T$) = $FJS\ (A_1/A_2)^{0.2}$ (4)

**3.2.4.3 Hydrological characterization**

Within the scope of this study, there are a total of seven rain gauge stations available. The data on the amount of rainfall recorded at each of the stations that were accessible were collected by the Department of Hydrology and Meteorology (DHM) of the Government of Nepal. From 2010 to 2021, the twelve-year raw data was collected, and the average rainfall was computed using the total station. It was determined how much rain might fall in 24 hours, how much rain in an entire year, and how much during the monsoon season (June–September). The landslide analysis using a pixel-based system was carried out. The distance from the drainage map was developed to determine whether there was a significant association between the landslide occurrence and the drainage.

### 3.2.4.4 Geotechnical characterization

#### 3.2.4.3.1 Sampling area selection

The landslide inventory map was overlaid on the geological map to determine the general distribution pattern of landslides based on geology. Forty landslides having a size greater than 10,000 $m^2$ were selected randomly from each geological formation. The sample locations covered east to west of the study area. The geological map and sampling locations are shown in Figure 5. Based on geological heterogeneity, a total of 120 sampling sites was selected, and one sample was obtained from each sampling site (Fig. 4), where the sampled landslides have an area greater than 10,000 $m^2$. The sampling locations were chosen to provide a spatial distribution of a representative sample of landslides. Forty sampling locations with an average gradient greater than 30 degrees were chosen from each geological unit. The average distance between sites is 2 - 3 km (Bhandari & Dhakal, 2020b). The sampled landslides ranged from 10,000 to 2,23,456 square meters. The landslide type and mechanisms of the three geological formations differ. For a better analysis with suitable terminology, the landslides of Lower Siwalik have been termed the name type I. Similarly, landslides of Middle and Upper Siwalik are named type II and type III, respectively.

#### 3.2.4.3.2 Sampling techniques

The study area is located in the Siwalik zone of Nepal. As discussed earlier, the region is fragile and vulnerable. Field study and soil sampling in the monsoon period are challenging and risky, so soil samples were collected from September 2017 to May 2020, the dry season. The soil samples of new and active landslides were obtained from the sliding surface, whereas the soil samples of historical landslides were collected from the scar. There are several methods for obtaining undisturbed soil samples from the field. Long split-spoon, piston, and pitcher barrel samplers are frequent sampling instruments for undisturbed soil. Piston samplers are thin-walled tube samplers that capture samples of soft soil without disturbance. The piston samples perform poorly in gravel, sand, or lithified sediments. In addition to hand augers and core drillers, hand augers and core drillers are

often used to sample undisturbed soil. After removing the disturbed surface soil, hand augers and soil drillers were used to collect undisturbed soil samples from the scar area 60-100 cm below the ground surface. This soil sampling depth is essential for identifying the soil components implicated in landslides (Tofani et al., 2017). Similarly, a pitcher-barrel sampler was used to collect the sample without disturbance. To preserve the samples' natural wetness, they were packed in a plastic bag and wrapped in paper. The wrapped samples were placed in the paper box within three weeks and transported to Kathmandu for laboratory analysis.

#### 3.2.4.3.2 Sample preparation and laboratory test

The bulk soil samples were processed in the laboratory without altering the soil's preexisting structure. To determine the soil failure mechanism, shear strength parameters (cohesion and angle of internal friction) are required. The soil samples were subjected to a widely used consolidated drained direct shear test to evaluate the shear strength parameters.

#### Direct shear test

It is possible to measure soil shear strength by tests carried out in the field or the laboratory. In-situ testing primarily includes

- Cone penetration test (also known as the CPT),
- Standard penetration test (also known as the SPT),
- The pressure meter test, and
- The Vane shear test.

The most popular tests for shear strength behavior analysis are the direct shear test and the tri-axial test. Both of these tests have been in use for a very long time. This research used the multi-reversal direct shear test. The partially saturated bulk soil samples acquired from the landslide scars were dimensionally reduced until they fit into the shear box. A wet cotton cloth was put on the top of sample to make the dry sample to provide moisture for partially developing partially saturated condition. The shear box had dimensions of 5.1 centimeters by 5.1 centimeters by 2.5 centimeters. The horizontal displacement of each

sample was measured after an initial loading of 20 kPa, and the results were acquired by gradually increasing the shear stress. The horizontal displacement resulting from shear stress can be measured using the direct shear test to determine post-peak shear strength. The normal stress of 40 kPa and 60 kPa were applied during the second and third phases of the experiment, respectively. The method was carried out until the shear strength value experienced a significant decline after reaching its highest value.

The Mohr-Coulomb failure envelope was derived by graphing the normal and peak shear stress. It was possible to determine whether the soil was generally dense/loose or stiff/soft by examining the curves that showed the relationship between shear stress and horizontal displacement. The shear strength parameters (angle of internal friction and cohesion) were obtained from the Mohr-Coulomb failure criterion, and shear strength was obtained from equation 5 (Terzaghi, 1943). The pore water pressure cannot be obtained from the direct shear test, so the effective stress is equal to the total stress that was considered in this test.

$$\tau = \quad c + \sigma_n \tan\emptyset \qquad (5)$$

Where $\tau$ is the shear strength of soil, $c$ is cohesion, $\sigma_n$ is normal stress and $\emptyset$ is the angle of internal friction.

**Moisture content test**

The moisture content is a crucial property utilized in establishing a correlation between the behavior of the soil and its index properties. Additionally, the moisture content is essential to express the phase relationships of air, water, and solids in a particular volume of material. The moisture content of each soil sample was calculated by ASTM D4643-17 using microwave oven heating. The mass of water was obtained by subtracting the dry mass from the bulk mass of the soil. The moisture content value was determined by taking the water and solid soil ratio in a specific volume (Lee et al., 1983).

$$\text{Moisture content } (w) \quad = \frac{Ww}{Ws} \times 100\% \qquad (6)$$

Where, *Ww* is the weight of water and *Ws* is the weight of solid.

**Soil density test**

ASTM D7263 - 09 standards were adopted to determine the soil's dry and bulk density. After weighing the oven-dried soil sample, the dry density was calculated. The ratio of dry soil mass to total volume is known as dry density, whereas the ratio of wet sample bulk mass to total volume is known as bulk density. Bulk and dry densities are used to convert soil's water fraction from mass to volume and vice versa. Dry density can be used to evaluate porosity and void ratio and assess soil compaction. The dry unit weight was calculated using dry density (Eq. 3) **(**Lee et al., 1983; Das, 2009**)**

$$\text{Dry unit weight } (\gamma_d) = \frac{Wd}{V} \quad (7)$$

Where $V$ is volume and $Wd$ is the weight of soil.

**Atterberg limit test**

Another essential aspect of soil analysis is the Atterberg limit. The Atterberg limit describes the expansion potential of soil at various moisture and clay content levels (Selby, 1993; Mugagga et al., 2012). The ASTM D4318 standard was used to calculate the Plastic Limit (PL) and Liquid Limit (LL). The plasticity index (PI) was calculated by subtracting the plastic limit (PL) from the liquid limit (LL). For further USCS classification of fine soil, the plasticity index and liquid limit were plotted on the Casagrande plasticity chart (Casagrande, 1932).

**Specific gravity test**

The Pycnometer test was conducted under the ASTM D854-00 standard for soil solids based on the phase relationship between air, water, and soil solids in a given soil volume. The specific gravity of soil is simply the ratio of the mass of soil to the mass of 4$^{o}$C water equivalent. The specific gravity of soil is primarily used to determine phase relationships such as void ratio, porosity, and degree of saturation (Eq.8).

$$Gs = \frac{\gamma s}{\gamma w} \quad (8)$$

Where *Gs* is specific gravity, $\gamma s$ is the unit weight of soil, and $\gamma w$ is the unit weight of water (Lee et al., 1983; Das & Sobhan, 2009).

**Void ratio**

The numerical relation proposed by Sivakugan & Das (2009) was adopted to obtain the void ratio (Eq. 9).

$$\text{Void ratio } (e) = \frac{Gs\,\gamma w}{\gamma d} - 1 \qquad (9)$$

Where *Gs* is the specific gravity of the soil sample, $\gamma$w is the unit weight of water, and $\gamma$d is the dry unit weight of soil.

**Porosity**

Porosity was determined by using the special relation of the void ratio (Lee et al., 1983; Das, 2009)

$$\text{Porosity } (\eta) = \frac{e}{1+e} \qquad (10)$$

Where $\eta$ is porosity and *e* is the void ratio.

**Degree of saturation**

The degree of saturation is the volume of water content in the total pore volume of soil. The degree of saturation was calculated by the special relation of water content, specific gravity, and void ratio (Lee et al., 1983; Das, 2009).

$$\text{Degree of saturation } (Sr) = \frac{wGs}{e} \qquad (11)$$

Where w is moisture content, *Gs* is specific gravity, and *e* is the void ratio.

**Particle size distribution**

The soil particle size distribution was conducted according to the ASTM (American Society for Testing and Materials) standard (ASTM D422). For grain size distribution, both sieve analysis and hydrometer analysis were conducted. Sieve analysis was conducted for the soil with a grain size greater than 75 μ, and hydrometer analysis was conducted for the fine soil with a grain size less than 75 μ. The sample was prepared for hydrometer analysis by passing the soil through a U.S. No. 200 sieve (ASTM D422-63 2007).

### 3.2.5 Soil classification

The particle size distribution curve, ternary diagram of clay, silt, and sand (Davis & Bennett, 1927), and Casagrande plasticity chart (Casagrande, 1932) were adopted for soil classification. The obtained information was compared with the unified soil classification table, and a final soil classification was made.

### 3.2.6 Data analysis

#### 3.2.6.1 Compositional analysis

The compositional statistics (Aitchison, 1982) have been carried out to comprehensively examine soil composition (sand, silt, and clay). The compositional data for the mass of the soil have been utilized in the past by a variety of other studies (Eynatten, 2004; Thomas & Aitchison, 2005; Buccianti, 2013; Bicocchi et al., 2019).

The "geometrical mean" (often abbreviated as "$g_c$") can be used as a suitable measure of the central tendency of compositional data (Bicocchi et al., 2019). The compositional dataset, which includes sand, silt, and clay, is broken into a few different components, each representing the "*n*" variable. Each compositional data point can be represented by a real vector "*x*" with positive components ($x_1$, $x_2$,.....$x_n$). "Composed data" is the term used to refer to the sample space for compositional data (Simplex). The abundance of a part of the composition (percentage of the total weight) is referred to as the "center" of compositional

data and is represented by a closed geometric mean "$g_c$" (Aitchison, 1982; Bicocchi et al., 2019). The center "$g_c$" is defined as,

$$g_c = C(g_1, g_2, \ldots . g_n) \qquad (12)$$

where "C" stands for closer operation for any vector of real positive component (Aitchison, 1982). And *C* with the positive vector component (*x*) is defined as,

$$C(x) = \left[ \frac{x1}{\sum_{i=1}^{n} zi}, \frac{x2}{\sum_{i=1}^{n} zi} \ldots\ldots\ldots \frac{xn}{\sum_{i=1}^{n} zi} \right] \qquad (13)$$

And the geometrical mean "$g_i$" is calculated by

$$g_i = \sqrt[n]{\prod_{i=1}^{n} xi} \qquad (14)$$

In addition, because the single center value cannot provide information on the variability of the evaluated dataset, we have investigated the link between the various components that make up entirely (Bicocchi et al., 2019). The variation array of the log-ratio mean value between the centroid of the data and the variance of the same log-ratio was constructed so that more information could be gleaned from it. One can measure the values' dispersion around the centroid by calculating the same log ratio's variance. After everything was said and done, the centered log-ratio (clr) transformation was acquired. Similarly, the clr (centered log-ratio) variance for each component was also acquired to evaluate each grain size fraction following the change of center log-ratio (Aitchison, 2003; Egozcue, 2005; Bicocchi et al., 2019).

$$clr(x) = y = [y_1, y_2, y_3 \ldots\ldots . y_n] \qquad (15)$$

Where $y_i = \left[ \ln \frac{x1}{g(x)}, \ln \frac{x2}{g(x)} \ldots\ldots\ldots \ln \frac{xn}{g(x)} \right]$ (16)

Where, *g(x)* is the geometric mean of the components of the compositional vector *x*.

The relationship between the composition's sections was then examined in the following stage. The variation array determined the relationship between a log ratio's mean value and

variance. The variation array has been generated using CoDapack v.2.02.21, a freely available program developed by the University of Girona's research group in statistics and compositional data analysis. Other researchers have used CoDapack v.2.01.15 for similar purposes (Bicocchi et al., 2019; Bhandari & Dhakal, 2020). Finally, the centered log-ratio variance (clr) has been calculated. Similarly, descriptive statistics were applied to the acquired data via MS Excel and CoDapack v.2.02.21. The minimum, maximum, arithmetic means, standard deviation and coefficient of variation of each data were acquired to identify landslide initiation range and data variation. The distribution of each parameter was shown on the histogram, and the highest frequency class was noted.

#### 3.2.6.2 Correlation and Regression

Karl Pearson Correlation (Pearson, 1895) was calculated for each variable and plotted on the correlation matrix. Karl Pearson's coefficient of correlation is a widely used mathematical tool that uses numerical representation to assess the degree of relationship between linearly related variables. The relationship between each variable (shear strength parameters and index properties) is obtained in this study to understand the association and control of one variable towards another. The relevant covariates of soil shear strength were investigated using multiple regression analysis. We can see how the response variable changes as the predictors or independent variables are altered using multiple linear regression. The response variable (shear strength) was compared to the eight predictor variables (moisture content, specific gravity, dry unit weight, cohesion, angle of internal friction, void ratio, degree of saturation, and plasticity index). The data were checked for normality of the response variable using the quantile-quantile (q-q) plot and the Shapiro test before running multiple regression models. The quantile-quantile (q-q) plot is a graphical tool to determine a dataset's theoretical distribution. Some examples of theoretical distributions include the normal distribution, the exponential distribution, and the uniform distribution.

The predictor variables were fitted into the model, beginning with the most complex model, which included all available variables. After running it once, we simplified the model with manual updates to get the bare minimum of an appropriate model. The link between shear

strength and the slope angle of the sliding surface was determined using linear regression. Similarly, the shear strength values of new, active, and reactivated landslides were compared and investigated.

### 3.2.7 Landslide classification

The landslide classification proposed by Cruden and Varnes (1996) was adopted in this study. However, the mechanism-based landslide classification was proposed. The initiation mechanism of landslides was studied in detail in the field. After detailed analysis and investigation, types of landslides were proposed with their descriptive characteristics. Mainly, five types of landslides were investigated and proposed as mechanism-based landslide classification—a detailed description is given in the result section. The five types of size-based classification were also proposed where landslide size is named qualitatively: very small, small, medium, high, and very high based on area. The activity states are categorized into five categories: new, active, inactive, stabilized, and reactivated. The sketch of five mechanisms was also developed.

### 3.2.8 Susceptibility analysis

For the landslide susceptibility analysis, four different bivariate models have been used: the weight of evidence (WoE), the frequency ratio (FR), Shannon's entropy (SE), and the information value method (IVM). The susceptibility analysis started with a map of the landslide inventory. The past landslides were used as a guide for what might happen in the future. Landslides will happen in the future under the same factors, location, geology, slope, etc., that caused them in the past (Lee & Talib, 2005). As already said, in this study, all old and new landslides were tracked and mapped. Over the study area, 1154 landslides were found and put on a map. Seventy percent of the landslides were used for training, and thirty percent for testing. After making the landslide inventory map with training and testing data, the vector landslide data (polygons) were turned into a raster in the GIS without changing the coordinates or the size of the pixels. The methodological framework of landslide susceptibility is shown in Figure 6.

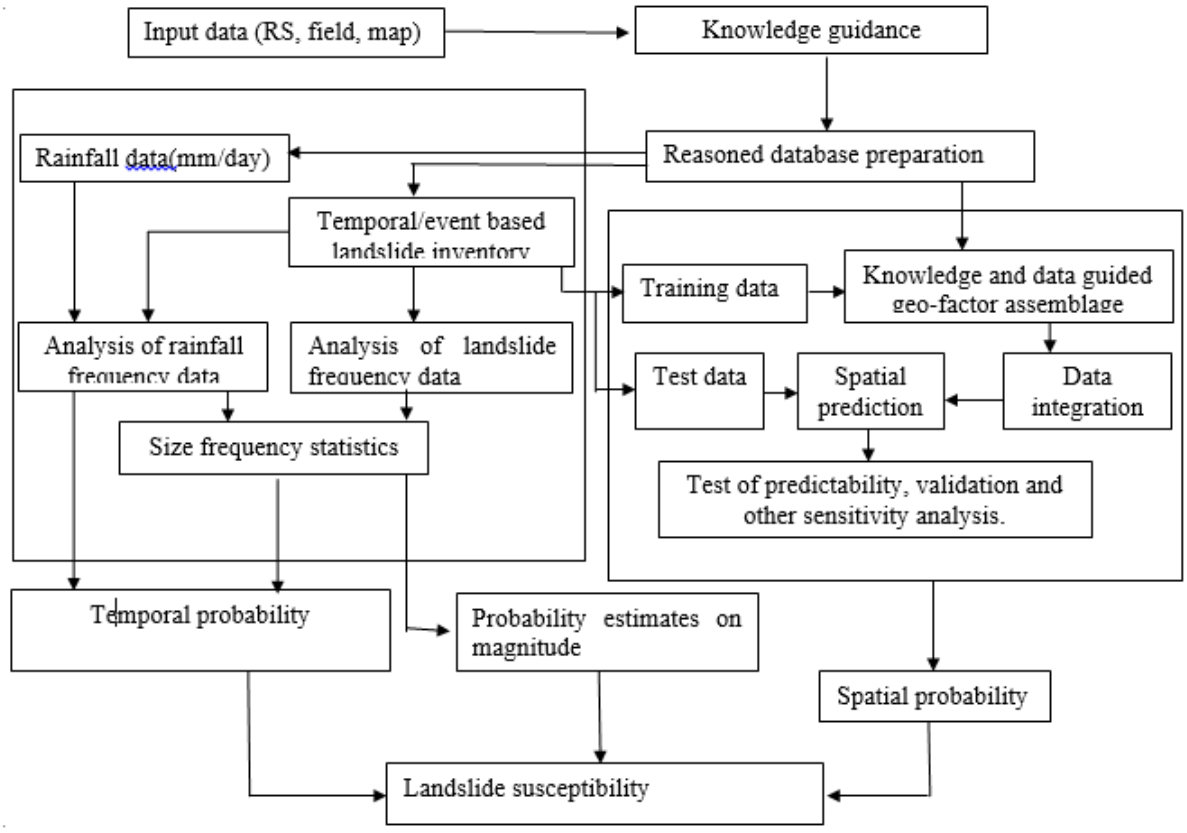


**Figure 6:** Methodological framework of landslide susceptibility analysis.

### 3.2.8.1 Landslide conditioning factors

The conditioning factors are selected based on the literature and field observations. The effects of landslide causative factors were observed and estimated in the field after detailed observation. A landslide, for example, clearly shows the impact of a hill slope. The role of water, geology, curvature, and aspect are commonly identified factors. Every mapped landslide was observed in the field. The causes and triggering factors of landslides were studied in the field. A total of 14 conditioning factors were selected after a rigorous field study and several literature reviews. The causal factors considered in the present study are slope, aspect, plan curvature, profile curvature, topographical wetness index (TWI), stream power index (SPI), geology, land use, distance from the river, distance from the fault, NDVI, and rainfall. The digital elevation model (DEM) of 30 m resolution downloaded from the Alaska satellite facility was used to obtain slope, aspect, curvature, stream power index, topographical wetness index, and an elevation map. Land use and NDVI were

obtained from the images downloaded from the Earth Explorer (Landsat-8). The geological map was prepared in the field. The description of each thematic map used in the present study is explained below. The causative factor maps are presented in annex 5.

**Slope angle**

The angle of internal friction, cohesion, and materials on it determines the slope's stability. Increasing the percentage of water in the higher slope may result in mass movement due to reduced friction. The slope gradient also increases the flow velocity and rate of movement. The slope angle values vary between 0° and 78° in the study area. A slope map of a 1:10,000 scale was obtained using a 30 m digital elevation model from a spatial analyst in a GIS environment. The slope angle values were classified into 0-15$^{o}$, 15-30$^{o}$, 30-45$^{o}$, and >45$^{o}$. Many researchers categorized the slope angle into five classes: 0-15$^{o}$, 15-25$^{o}$, 25-35$^{o}$, 35-45$^{o}$, and > 45$^{o}$ (Pradhan & Lee, 2010a; Devkota et al., 2013; Thapa & Bhandari, 2019; Pokharel & Bhandari, 2019). The hill slope angle determines landslides' distribution pattern and strength (Shafique et al., 2016).

**Slope aspect**

The slope aspect is the direction of the slopes of the land surface. The slope aspect gives the direction of the maximum slope of the land surface regarding the north (Xu et al., 2012). Although no universally proven or standard relationship exists between landslides and the slope aspect (Ercanoglu et al., 2004), many researchers have used the slope aspect to identify landslide causative factors. The amount of sunlight exposure and rainfall distribution may vary depending on the slope aspect. The aspect map was prepared using DEM data of 30 m resolution in the GIS environment. This study divides the slope aspect into eight classes: N, NE, E, SE, S, SW, W, and NW. The terrain aspect is the slope direction, which controls vegetation covers, soil moisture, and shear strength so that the aspect may influence landslide initiation (García-Rodríguez et al., 2008; Basharat et al., 2016).

**Lithology**

In the Siwalik Hills of Nepal, lithology is vital in causing landslides (Bhandari & Dhakal, 2018). The land surface's lithological characteristics control the slope materials' strength

and permeability, due to which the landslide initiates (Kamp et al., 2008). Lithology and the slope of the surface determine the nature and intensity of a landslide (Chen et al., 2018; Sabokbar et al., 2014). The rock composition, soil composition, and stratigraphy also impact the causes of landslides. The geological map was prepared in the field after several field visits. The topo-sheet of 1:25,000, developed by the Department of Survey, Government of Nepal, was used for field preparation of the map. The draft map prepared in the field was digitized in the GIS and used to create the final map.

**Land use/ land cover**

The mechanism and distribution of landslides are heavily influenced by land cover. The global data shows that the landslide distribution is higher in barren land. The root systems of the plants provide strong mechanical support, which plays a significant role in slope stabilization (García-Rodríguez et al., 2008). The land cover map of the study area was extracted from the Landsat images, and the extracted images were processed in the GIS layer. The land cover of the area was classified as water bodies, dense forests, sparse forests, and sediment deposits. Because barren land and agricultural lands are limited and have little correlation with landslide occurrence, they were excluded from the map.

**Distance to the fault**

The fault planes were identified in the field after rigorous geological study. The fault lines were traced out on the map. The polygon shapefile was converted into a raster. Using a spatial analysis tool in a GIS, distances to the fault were divided into six buffer zones at 500-meter intervals. The effects of the fault can be seen from a far distance, so the distance to the fault was taken at an interval of 500 m.

**Distance to drainage**

Streams make the slope unstable when it has a high-water discharge. A stream may have a higher slope and cause toe cuts, side erosion, and deposition. Similarly, the stream increases the infiltration rate and makes the ground saturated. The area nearby the river and streams are mostly wet and water-saturated, which increases landslide susceptibility (Gorum et al., 2011). For the evaluation of a stream's potential to cause a landslide, the distance to the drainage map was prepared using a digital elevation model. GIS software

divided the distance to the stream into five buffer zones with an interval of 50 m. The location of landslides from the river was discovered using multiple-ring buffering.

**Distance from road**

The development of roads, railways, and trails in mountainous terrain mostly leads to slope instability and landslides (Shafique et al., 2016). In the mountains of Nepal, haphazard road construction leads to landslide mechanisms. The rocks of the Siwalik are weak, fragile, highly ruptured, and naturally unstable. Constructing the road on such terrain ultimately causes several mass movements, primarily landslides. A road network map was created using Google Earth imagery and extracted into a GIS layer to assess the impact of roads on landslides. The prepared map was verified in the field. The road map was buffered into five intervals of 100 m, and the distance to the road map was finalized.

**Rainfall**

Rainfall is one of the most important extrinsic factors that can start a landslide, so Dahal et al. (2012) used mean annual rainfall to measure landslide susceptibility. Thirty years (1991–2021) of rainfall data from the seven rainfall stations were taken from the Department of Hydrology and Meteorology and used for the preparation of the mean annual rainfall map. The rainfall amount was divided into seven classes.

**Curvature**

Curvature describes the morphological characteristics of the slope shape, which reflects the formation of surface erosion and surface runoff. The slope's shape provides spaces for slope sliding. Landslides are more likely on a concave slope than a convex or planar slope. Generally, curvature maps are divided into plan curvature and profile curvature. The plan and profile curvature measures are extracted from the digital elevation model.

**Topographic wetness index (*TWI*)**

The topographical wetness index gives the flow accumulation at a particular point. The TWI shows topographical control on hydrological processes. Somehow it represents the soil moisture distribution. The *TWI* reflects the amount of flow accumulation at any point in the study area. To some extent, the TWI represents the distribution of soil moisture. For the calculation of *TWI*, equation 17 was used.

$$TWI = ln\ (AS \div tan\beta) \quad (17)$$

In the above equation, *AS* represents the slope contributing area, and $\beta$ represents the slope angle.

The *TWI* is also categorized into four classes.

**Stream power index (*SPI*)**

The SPI measures the flowing water's erosive capacity at the topographic surface's given point. The flow velocity of the water increases with an increasing slope gradient. As a result, the stream power index and rate of erosion increase. Like other variables, the stream power index is also derived from a digital elevation model.

The SPI can be calculated by using the given equation

$$SPI = AS \times tan\beta \quad (18)$$

In equation 18, *AS* is the slope contributing area, and $\beta$ is the slope angle.

**Relative relief**

Relief is the difference between a particular surface's highest and lowest altitudes. The relative relief is derived from the digital elevation model. It was extracted by using Neighborhood and Raster Calculator in the GIS software. Elevation data were derived from the DEM with a resolution of 30 m obtained from the Alaska satellite facility.

**Normalize difference vegetation index**

Vegetation indices are a linear combination of the reflectance measurement of the visible and near-infrared bands. The vegetation indices were used to separate vegetation-covered areas from non-covered areas for image classification. We can use various indices, from simplest to complex band combinations, to determine the vegetation cover. The Normalized Differences Vegetation Index (NDVI) is a numeral indicator used to analyze remote sensing data and determine the vegetation cover on a particular land surface. It uses the visible and near-infrared bands of the electromagnetic spectrum.

The processing of Landsat-8 images in the GIS software obtained an NDVI map. A higher NDVI indicates more vegetation cover and a stable slope; however, a higher NDVI may lead to more landslides on the rocky slope covered with thick vegetation. The NDVI can be obtained from Equation 19.

$$NDVI = \frac{B5-B4}{B5+B4} \quad (19)$$

where, *B5* is near infra-red (NIR) and *B4* is a red band.

### 3.2.9 Susceptibility model

Four bivariate statistical models were selected for the landslide susceptibility mapping based on field experience and previous literature.

#### 3.2.9.1 Weight of evidence model

This model was initially created to examine mineral potential (Bonham-carter et al., 1988). The weights of evidence method is a bivariate statistical technique that employs a log-linear Bayesian approach. This model calculates the likelihood of a landslide based on the contribution of evidence for slope instability (Mathew et al., 2007). This approach uses historical data to determine factors that affect, precipitate, and occur in landslides.

The terminology and mathematical derivations are taken from Bonham-Carter et al. (1989). Bonham-Carter (1994) and Bonham-Carter et al. (1989) comprehensively describe vocabulary and mathematical derivations. The weight of evidence model assigns a weight to each landslide predicting factor (B) based on the existence or absence of the landslide (L), as stated by Bonham-Carter et al. (1994) and Dahal et al. (2012).

$$W^{+} = \ln \frac{P\{\frac{B}{L}\}}{P\{\frac{B}{L'}\}} \quad (20)$$

$$W_i = \ln \frac{P\{\frac{B'}{L}\}}{P\{\frac{B'}{L'}\}} \quad (21)$$

where,

*ln* is the natural log, and *P* is probability.

*B* is the presence of a potential landslide factor

*B*' is the absence of a potential landslide factor

*L* and *L'* are the presence and absence of landslide.

$W^+$ and $W^-$ indicate the presence and absence of predictive variables, respectively. Similarly, $W^+$ shows a positive correlation between a predictive variable and the landslide, whereas $W^-$ shows a negative correlation between a predictive variable and the landslide.

After obtaining the *W*+ and *W*- value, the weight contrast (*C*) was calculated by subtracting $W^-$ from $W^+$. The weight contrast (*C*) gives the association between landslides and predictive variables.

The presence and absence of landslide in each predictive variable and their sub-class were obtained on a pixel basis. The formula was obtained in the modified form to calculate the pixel number (Pokharel and Bhandari, 2019).

$$W^+ = \ln\left\{\frac{\frac{A1}{A1+A2}}{\frac{A3}{A3+A4}}\right\} \quad (22)$$

$$W^- = \ln\left\{\frac{\frac{A2}{A1+A2}}{\frac{A4}{A3+A4}}\right\} \quad (23)$$

where,

*A1* is the landslide pixels present on a given factor class.

*A2* is the landslide pixels absent in the given factor class.

*A3* is the pixels in the given factor class in which no landslide pixels are present;

*A4* is the number of pixels in which neither landslide nor the given factors are present.

The obtained weight is further used to produce a contrast value for the particular susceptible variable, which is given by;

$$C = W^+ - W^- \quad (24)$$

The obtained difference between weights (*C*) measures the strength of the correlation between the analyzed variable and landslides.

#### 3.2.9.2 Frequency ratio model

The frequency ratio bivariate methodology is frequently used when assessing landslide susceptibility using GIS and spatial data (Bonham-Carter, 1994; Lee & Talib, 2005; Chen et al., 2016; Ding et al., 2017). It is often and successfully utilized for mapping landslide susceptibility (Yilmaz, 2009; Reis et al., 2012; Umar et al., 2014; Chen et al., 2016; Wu et al., 2016; Wang & Li, 2017). The landslide inventory map and factor map have been combined using the standard equation to determine the frequency ratio (FR) for each class of the causative components (Mondal & Maiti, 2013).

Numerous researchers have adopted this approach to study landslide susceptibility in the past, and they have asserted that the FR model is a commonly used, highly accepted model with a high prediction rate (Choi et al., 2012; Ehret et al., 2010; Lee, 2014; Lee & Pradhan, 2006; Mezughi et al., 2011; Mohammady et al., 2012; Torizin, 2011; Yalcin et al., 2011; Yilmaz, 2009; Thapa & Bhandari, 2019). In this study, frequency ratio is utilized to calculate the ratio of the number of pixels in the class to the entire number of pixels present in the study region, as well as the ratio of the pixels in the class to the total number of landslide pixels. The FR is the ratio of the area of the class as a percentage of the overall map to the number of landslides in the targeted class as a percentage of all landslides (Ehret et al., 2010). Total FR was determined for each factor after computing the FR value for each subclass. Each factor's final weighted value was determined. The final susceptibility map was created by overlaying the total weighted values with each factor in the GIS. Total FR values above one is thought to indicate high susceptibility, whereas values below 1 indicate low susceptibility. The frequency ratio computation process is illustrated below.

$$FR = \frac{\frac{A}{B}}{\frac{C}{D}} \tag{25}$$

Where,

*A* is the number of landslide pixels for each factor.

*B* is the number of total landslide pixels in the study area.

*C* is the pixel number in the class area of each factor.

*D* is the total pixel in the study area, and FR is the frequency ratio of a class for the factor.

### 3.2.9.3 Information value method

The information value model is a standard bivariate statistical method. This technique frequently forecasts the geographic link between landslides and factor classes (Sarkar et al., 2006). Yin and Yan (1988) created and adopted this model for the slope instability study. Sarkar et al. (2013) improved the model further and attempted to make it more valid and precise.

The information value of each factor was determined using conditional and prior probability. First, the conditional probability was calculated by dividing the landslide pixel of each subclass by a single component of the pixel of this subclass. Similarly, the prior probability was calculated by dividing the total number of landslide pixels in the study region by the total number of pixels in the study area. The mathematical derivations and relations are available in Yin and Yan (1988). The following ways simplify the relation provided by Yin and Yan (1988).

$$\text{Conditional probability } (Pc) = \frac{Si}{S} \quad (26)$$

$$\text{Prior probability } (Pp) = \frac{Ni}{N} \quad (27)$$

$$\text{Information Value } (IV) = \frac{Pc}{Pp} \quad (28)$$

Where,

*Si* is the number of landslide pixels present in the subclass

*S* is the pixel of the subclass

*Ni* is the landslide pixel of the total area

*N* is the pixel of the whole area.

### 3.2.9.4 Shannon's entropy method

Shannon's entropy model is derived from the frequency ratio model. The frequency ratio model does not consider the weightage of the causative factor (Panchal & Srivastava, 2021). The term entropy was adopted from the Boltzmann principle, which measures the disorder or uncertainty of a system (Yufeng & Fengxiang, 2009; Sharma et al., 2014). In the present day, the entropy value is used to analyze natural hazards. In the case of a landslide, the entropy value gives the environment dissimilarity, which indicates the potential factors that cause a landslide. The index of entropy consists of the following procedures to calculate the weightage of causative factors.

$$Pab = FR / \sum_{a=1}^{m} \mathrm{FR} \tag{29}$$

$$\sum_{a=1}^{m} \mathrm{Eab} = \sum_{k=0}^{n} (Pab) * (lnPab) \tag{30}$$

$$Hab = 1 + \sum_{a=1}^{m} \mathrm{Eab} \tag{31}$$

$$Wb = Hab / \sum_{a=1}^{m} Hab \tag{32}$$

*Pab* is the probability density, and *FR* is the frequency ratio of sub-factors. *Wb* is the weightage of causative factors obtained from Shannon's entropy technique.

### 3.2.10 Validation of susceptibility

We validated the results by using the receiver operating characteristic (ROC) curve. It is a tried-and-true approach for determining how accurately different algorithms are used to create landslide susceptibility maps (Shirzadi et al., 2018; Dam et al., 2022). The validation was carried out with the assistance of thirty percent of the testing data that was generated while preparing the landslide inventory map. The ROC curve is constructed with the help of a two-axis graph. On the Y axis, we could determine the true positive rate (sensitivity); on the X axis, we could evaluate the false positive rate (1-specificity). The AUC value is somewhere in the range of 0.5 and 1. The accuracy of the models determines by examining the curve. The model with full accuracy for forecasting landslide susceptibility has an AUC value of 1, whereas the weak model without useful information has an AUC value of 0.

# CHAPTER 4

## RESULTS AND DISCUSSION

### 4.1 Results

#### 4.1.1 Landslide characterization

A total of 1140 landslides (old and new) are noted in the images and from field verification (Fig.7). The size-based inventory showed that the area of landslides is log-normally distributed (Fig.8). For size-based classification, five sizes were adopted based on area. The size of landslides was chosen from <100 $m^2$ to >1000000 $m^2$. The landslides with areas from 1000 $m^2$ to 10000 $m^2$ covered 67.7% of the total landslide area. The result indicates that the landslides having an area between 1000 $m^2$ to 10000 $m^2$ (medium-sized) are dominant in the study area (Bhandari & Dhakal, 2018; 2019).

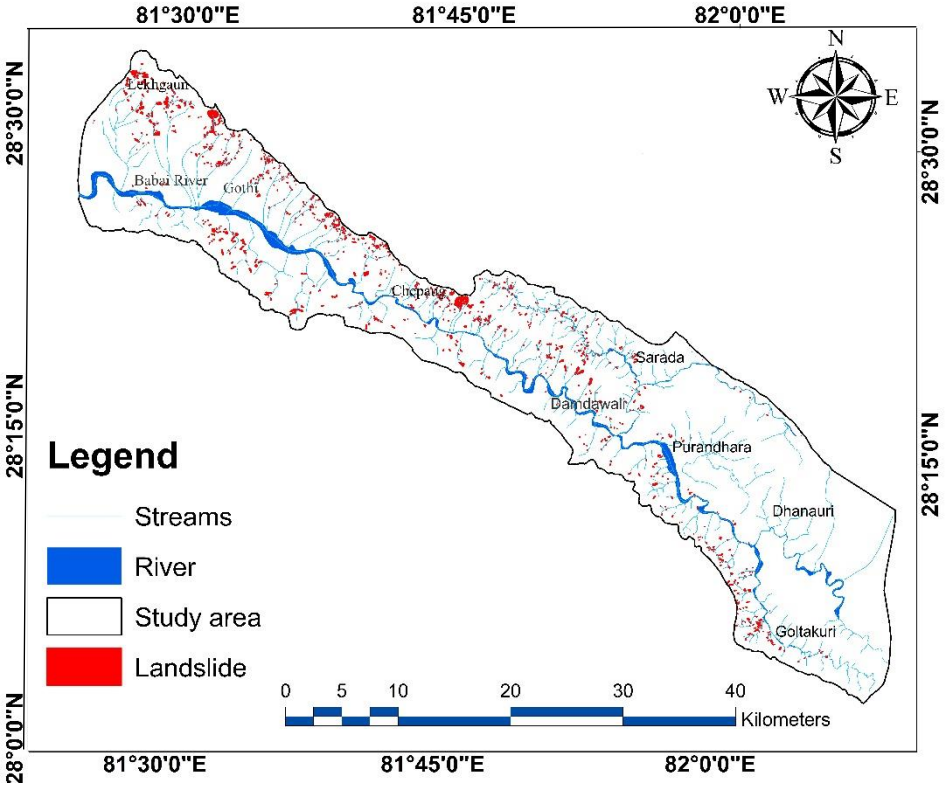


**Figure 7:** Spatial landslide inventory map of Babai River watershed, Nepal.

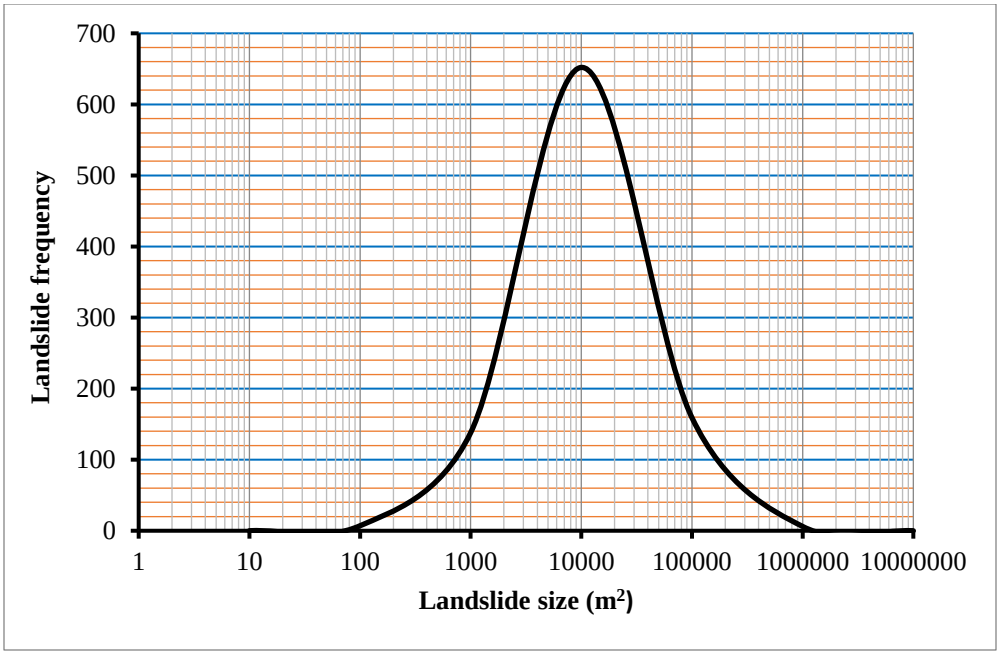


**Figure 8:** The curve shows the landslide size and frequency relationship.

#### 4.1.1.1 Geological characterization

Based on the stratigraphic unit, the geological distribution of landslides was determined. Figure 9 depicts the distribution of landslides in the stratigraphy-based geological units. There are 589 small to large landslides in the Middle Siwalik, whereas 302 and 249 in the Lower and Upper Siwalik, respectively. Table 3 illustrates the distribution of landslides in the geological units based on size. In each geological unit, the number of landslides with an area of 1000–10,000 $m^2$ is higher. Very small to very large landslides are rare in the entire geological unit. Each geological unit has a considerably different average length of the landslides. In the Upper Siwalik, shallow and small landslides with sliding lengths less than 100 m are frequently seen, but landslides with lengths between 100 and 200 m predominate in the Lower and Middle Siwalik. The Babai Thrust, Bheri Thrust, and Main Boundary Thrusts are three geological Thrusts in the research region. Table 3 depicts the distribution of landslides along the thrust zone. The Babai Thrust is the longest thrust that runs parallel to the Babai River from east to west and contains many landslides. Because there have been more landslides on the hanging wall than on the footwall, which eventually

indicates higher susceptibility, the hanging wall appears more susceptible to landslides. The majority of the landslides occur within 1 km of the Thrust.

**Table 3:** Landslide distribution in the geological units and the thrust structures.

| Size of landslide ($m^2$) | Number of landslides in the Geological units | | |
|---|---|---|---|
| | Lower Siwalik | Middle Siwalik | Upper Siwalik |
| <100 | 4 | 0 | 3 |
| $10^2$ -$10^3$ | 116 | 118 | 76 |
| $10^3$ -$10^4$ | 133 | 398 | 141 |
| $10^4$ -$10^5$ | 49 | 69 | 28 |
| >$10^5$ | 0 | 4 | 0 |
| Length (m) | Lower Siwalik | Middle Siwalik | Upper Siwalik |
| <100 | 75 | 98 | 122 |
| 100-200 | 202 | 148 | 84 |
| 200-300 | 102 | 63 | 9 |
| 300-400 | 24 | 6 | 2 |
| 400-500 | 8 | 3 | 0 |
| >500 | 4 | 2 | 0 |
| Thrust | Number of landslides in the Fault structure | | |
| | Hanging wall | Foot wall | Fault plain |
| Babai Thrust | 272 | 77 | 96 |
| Bheri Thrust | 122 | 53 | 26 |
| Malai Thrust | 72 | 42 | 21 |

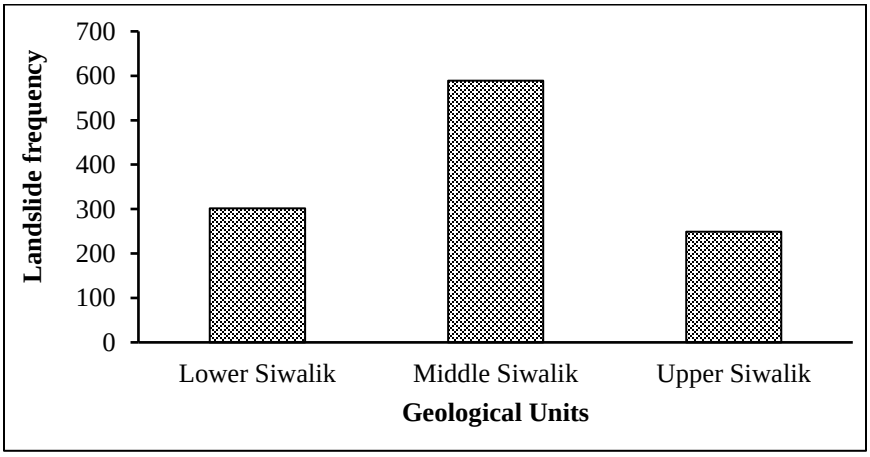


**Figure 9:** Distribution of landslides in the geological units.

#### 4.1.1.2 Landslide description

The landslides are first classified according to their materials and movement types (Cruden & Varnes, 1996), and then a new classification model is proposed. Many landslides in the study area are flow and fall types; however, sliding types are also commonly distributed. The landslides are spatially and temporally dynamic. The landslide initiation, development, advancement, mitigation, and reactivation processes can be seen in large-sized landslides. About 25% of the landslides recorded were less than 100 m long, whereas only six were recorded with lengths greater than 500 m. Different modes of sliding and failure are noticed in three geological units.

##### 4.1.1.2.1 Landslide in Lower Siwalik

Medium to massive beds with several jointed mudstones characterized the Lower Siwalik. The observed mudstones are very weak, physically weathered, and have residual soil on the surface in many places. The thick colluvium on the bedrock revealed evidence of many old and naturally mitigated landslides. As a result, most failures were observed along the colluvium and colluvium bedrock contacts. Multiple weathering of the weak, crumble, and concretion mudstone results in the flow type of landslide.

Similarly, the variegated mudstones of Lower Siwalik are highly weathered and easily erodible. Several gullies with shallow landslides were observed during the field visit. Translational slides are predominant along the colluvium covered with successive vegetation and primary forest. Similarly, rotational slides have been observed on thick colluvium beds with thicknesses greater than 3 m. Erosion-induced landslides, mudflows, and mudslides were noted in Lower Siwalik (Fig. 10 a, b). Many landslides started as slides and later converted to flows because of excessive water on the steep terrain. The type distribution of landslides in the Lower Siwalik is shown in Figure 11. Erosion-induced landslides are dominant in the Lower Siwalik.

a

b

**Figure 10:** Erosion-induced landslides on the variegated mudstone at (a) Tui Khola section and (b) Upper Babai section, Dang**.**

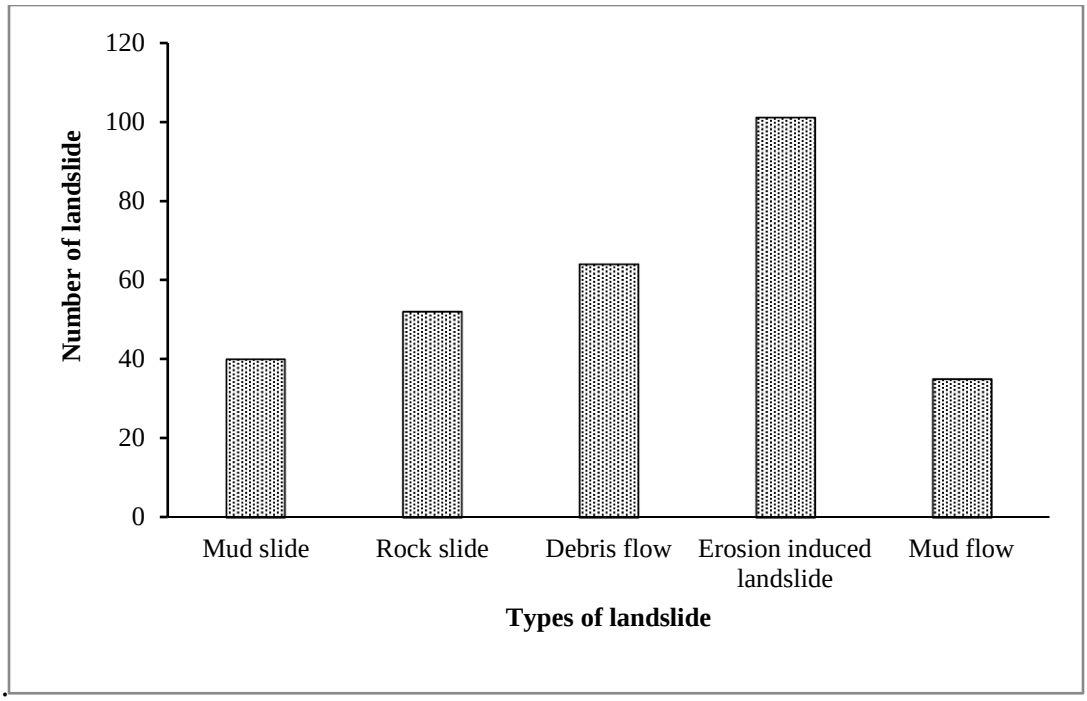


**Figure 11:** Landslide type distribution in Lower Siwalik.

#### 4.1.1.2.2 Landslide in Middle Siwalik

Coarse-grained, less compacted, and massive sandstone beds are observed in the Middle Siwalik. There is very weak intergranular bonding in sandstone beds. Thinly layered mudstone and shale are present between thick and massive Sandstone beds. The thinly layered shale is weathered and easily erodible. Seasonal drying and wetting made the shale fragile, so thin shale layers eroded out. The weathered and eroded shale caused the development of gaps between thick sandstone beds because the sandstone beds could not bear their load and slide down. Because of this reason, rock falls, and rock slides were very common. The major landslide types of the Middle Siwalik are rock fall, debris fall, debris slide, and fall-induced debris flow (complex). Figure 12 (a, b, c, d) depicts the Middle Siwalik landslides. The landslide-type distribution of Middle Siwalik is shown in Figure 13. Number of rock fall is significantly greater in the Middle Siwalik than other landslide type.

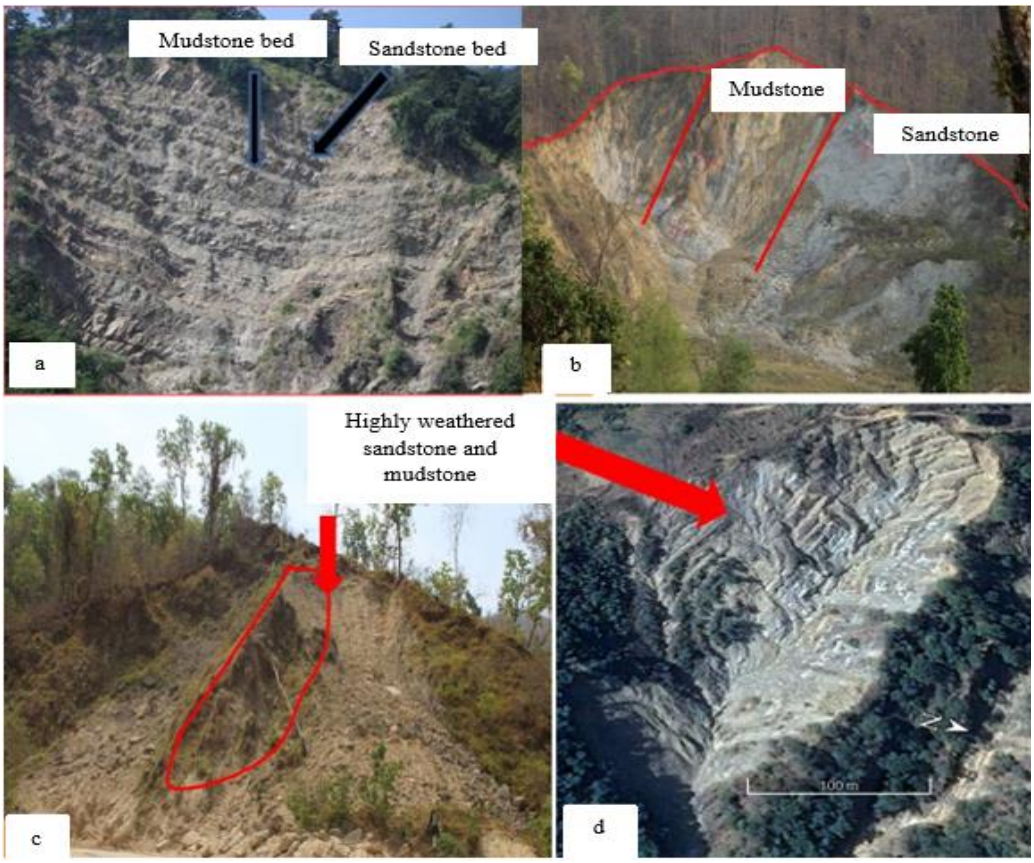


**Figure 12**: Landslides in the various parts of Middle Siwalik a) near of Salyantari b) Bangaun of Bardiya District c) Nearby Babai valley of Bardiya District d) Nearby Lekhparajul.

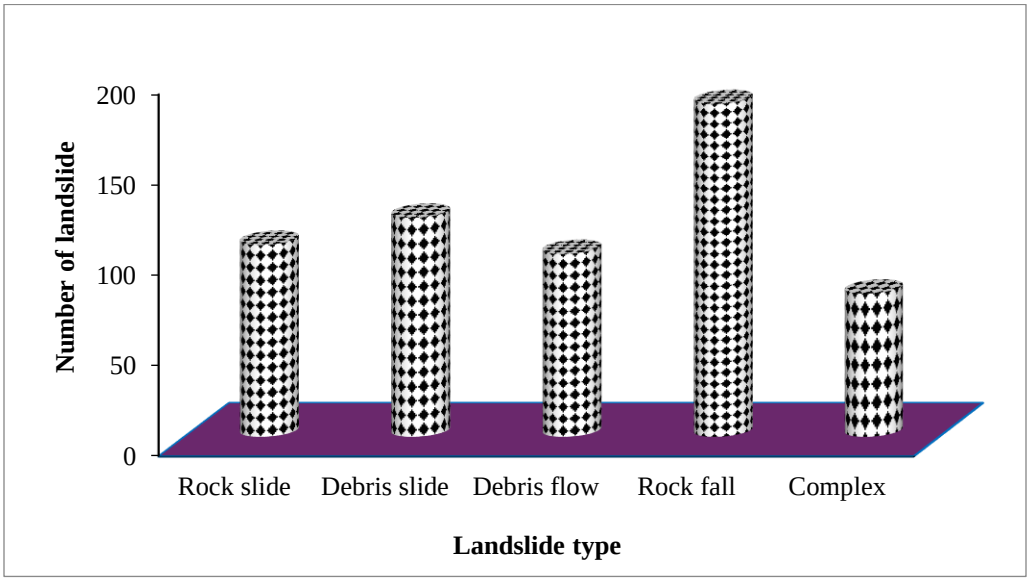


**Figure 13**: Landslide type distribution in the Middle Siwalik**.**

#### 4.1.1.2.3 Landslide in Upper Siwalik

The conglomerate observed in the Upper Siwalik is mainly clay-bonded. Pebbles and clasts are able to become separated from conglomerates as a result of the softening and eroding of the clay that takes place during the wet season (Fig.14). In Upper Siwalik, there is a thin layer of weak and loose mudstone that can be observed in between the conglomerate beds. During the monsoon season, the fragile mudstone is subjected to weathering and repeated erosion. After the mudstone has been eroded, the conglomerate beds will begin to separate and slide down, resulting in a block slide, a block fall, and a debris fall. After combining with the rains, the landslide mass turned into a debris flow. Figure 15 depicts the distribution of different landslides in the Upper Siwalik.

**Figure 14**: Landslide on the clay-bonded conglomerate beds present in the Upper Siwalik of Babai Valley, Bangaun section**.**

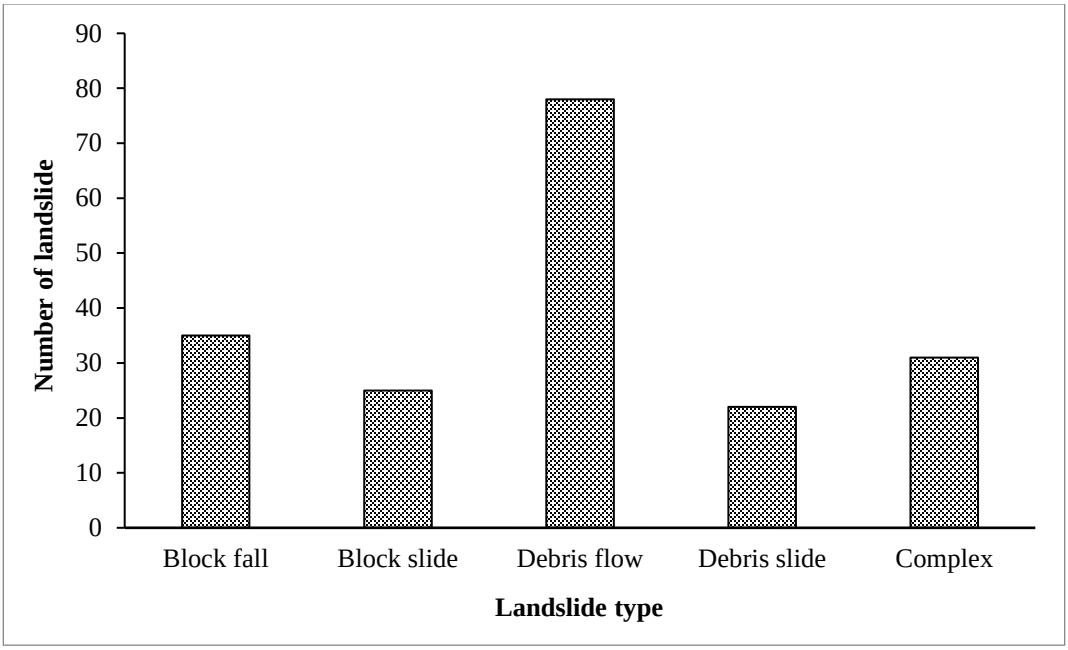


**Figure 15:** Landslide-type distribution in the Upper Siwalik

#### 4.1.1.2 Topographical characterization

The correlation between slope and the occurrence of landslides needs to move in a positive direction. On the steeper slope, there are fewer landslides, and they occupy less area. The moderate slope has a more significant landslide than the steeper slope. Most landslides can be found on the slope at angles ranging from 15 to 45 degrees. It was determined that the slope does not have a positive significance on landslides; the study area is somewhat affected by sliding due to the combination of numerous elements. The distribution of landslides is highest on the southwest aspect, followed by the southeast aspect, and then the northern aspect has a relatively low number of landslides. The topographic distribution of landslides is presented in Table 4. The planner surface contains the largest quantity of land affected by landslides. The landslides cover an area of 2.35 $km^2$ on the concave surface, whereas no landslides have been observed on the convex slope. There is an inverse relationship between the topographical wetness index and the area of landslides. As the topographical wetness index has increased, the landslide area has decreased.

**Table 4**: Landslide area distribution into the various topographic factors.

| Slope angle | Area of landslide ($km^2$) | Aspect | Area of landslide ($km^2$) | Curvature | Area of landslide ($km^2$) | Topographical wetness index | Area of landslide ($km^2$) |
|---|---|---|---|---|---|---|---|
| <15 | 0.8 | NE | 0.66 | Convex | 0 | 2.79-6.79 | 5.42 |
| 15-30 | 3.01 | SE | 2.23 | Planar | 4.32 | 6.70-10-79 | 1.15 |
| 30-45 | 2.41 | SW | 2.93 | | | 10.79-14.7 | 0.09 |
| >45 | 0.66 | NW | 0.84 | Concave | 2.35 | 14.79-19.11 | 0.0008 |

In the research area, the T value ranges from 0.023 to 0.098. The "T" value is highest in the Middle Siwalik and lowest in the Lower Siwalik. In Upper Siwalik, the standard deviation of the T value is 8.6, which indicates that the difference between the minimum and highest values is not as great. There is a more significant disparity between the minimum and maximum values in the Middle Siwalik. The highest T value is in Middle Siwalik (0.098), and the lowest is in Lower Siwalik (0.023). In the Middle Siwalik, the average T value is substantially greater.

The topographical factor "T" and the size of the landslide have a positive relationship (Fig.16). Similarly, the regression line of Figure 17 shows positive association between the number of landslides and the topographical factor "T" value. It implies that the likelihood of a landslide will increase in the specific location if the T value is higher than in other areas.

**Table 5:** Descriptive statistics of T value in the geological units.

| Formation | Minimum "T" value | Maximum "T" value | M ± SD | Coefficient of variance (%) |
|---|---|---|---|---|
| Lower Siwalik | 0.023 | 0.036 | 0.028± 10.2 | 9.2 |
| Middle Siwalik | 0.042 | 0.098 | 0.049± 12 | 10.8 |
| Upper Siwalik | 0.033 | 0.042 | 0.034± 8.6 | 7.9 |

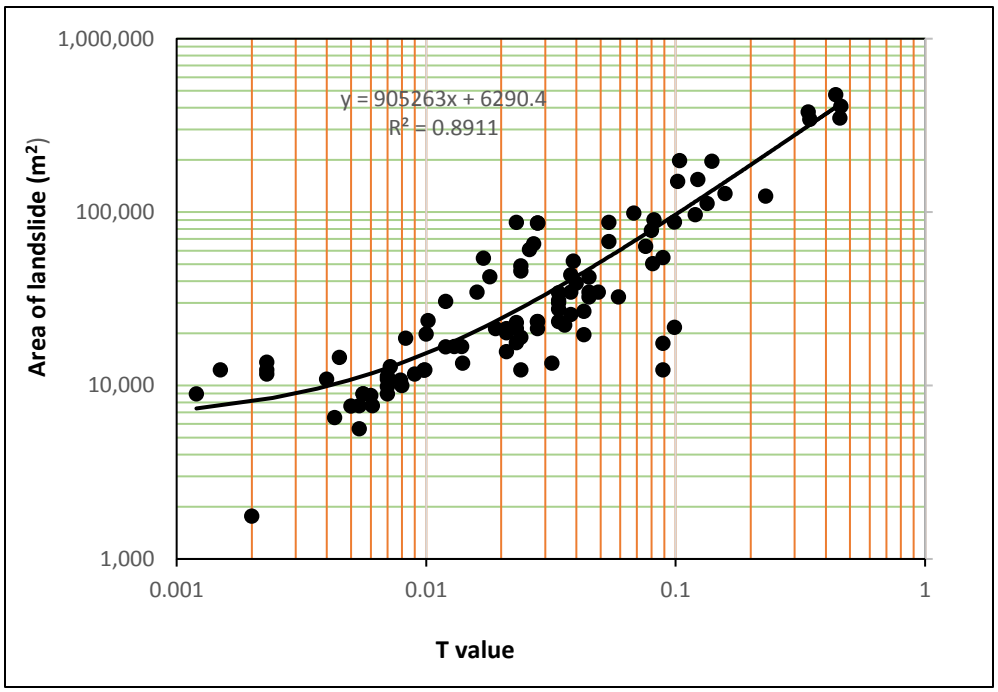


**Figure 16:** The relationship between T value and the landslide area.

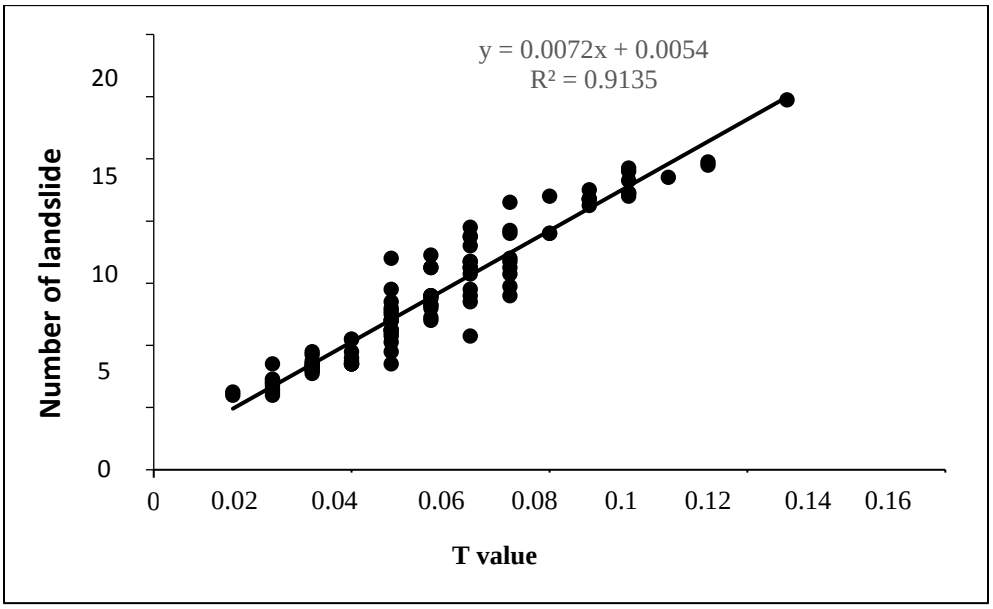


**Figure 17:** The relationship between T value and the number of landslides.

#### 4.1.1.3 Hydrological characterization

##### 4.1.1.3.1 Rainfall and landslide

The hydrological parameters demonstrate a clear relationship between hydraulic activity and landslide activity. The hydraulic properties are analyzed using stream power index, drainage, and rainfall data. Table 6 displays the different amounts of rainfall and the frequency of landslides. Figure 18 displays the rainfall amounts and the landslide incidents. A low ($R^2$ = 0.29) association exists between the maximum 24-hour rainfall and the occurrence of landslides (Fig.18a). The $R^2$ value shows that the data are poorly fit in the regression. The P value (0.07) in Table 7 shows that the outcome is not significant. The monsoon rainfall significantly correlated with the number of landslide events (p = 0.0004). The linear line between landslides and rainfall only in the monsoon period is shown in Figure 18b. With a $R^2$ of 0.975, the total annual rainfall and total annual landslides have the best fit for the regression model (Fig.18c). The total annual rainfall and total annual landslide have a significant positive association with negligible p-value (2.19E-09) (Table 7). The outcome demonstrates a significant positive relationship between the landslide event and rainfall. Similarly, the time series monthly data of rainfall and landslide from 2010 to 2021 shows a significant positive relation (p=0.00008) between rainfall and landslide (Fig.18d).

**Table 6:** The total annual landslide distribution and rainfall pattern from 2010 to 2021.

| Year | Maximum 24 hrs rain (mm) | Rain in Monsoon period (mm) | Total annual rain fall (mm) | Total annual landslides (mm) |
|---|---|---|---|---|
| 2020 | 112.5 | 892.4 | 1666 | 398 |
| 2011 | 124.4 | 1424.1 | 2089 | 556 |
| 2012 | 138.2 | 985 | 1700 | 422 |
| 2013 | 187.5 | 1957.7 | 2151 | 575 |
| 2014 | 215.6 | 1609.5 | 1978 | 464 |
| 2015 | 198.4 | 1481 | 1750 | 428 |
| 2016 | 212.3 | 1633.8 | 2270 | 600 |
| 2017 | 215.1 | 1841.41 | 2380 | 622 |
| 2018 | 220.7 | 1887.76 | 2416 | 698 |
| 2019 | 186.4 | 1914.8 | 2584 | 716 |
| 2020 | 210.2 | 1966.6 | 2646 | 742 |

| | | | | |
|---|---|---|---|---|
| 2021 | 198.46 | 1934.46 | 2608 | 724 |

**Table 7**: Significant level of regression between A) maximum 24 hrs. rainfall and landslide, B) rainfall in the monsoon period and total landslide, C) total annual rainfall and landslide

| A | Coefficients | Standard Error | t –Stat | P-value |
|---|---|---|---|---|
| Intercept | 246.8798 | 166.9595 | 1.47868 | 0.17002 |
| X Variable 1 | 1.794087 | 0.88551 | 2.02605 | 0.070267 |
| B | | | | |
| Intercept | 109.9701 | 95.01876 | 1.157352 | 0.274025 |
| X Variable 1 | 0.288058 | 0.05703 | 5.050962 | 0.000499 |
| C | | | | |
| Intercept | -189.702 | 38.96221 | -4.86888 | 0.000653 |
| X Variable 1 | 0.351453 | 0.017606 | 19.96159 | 2.19E-09 |

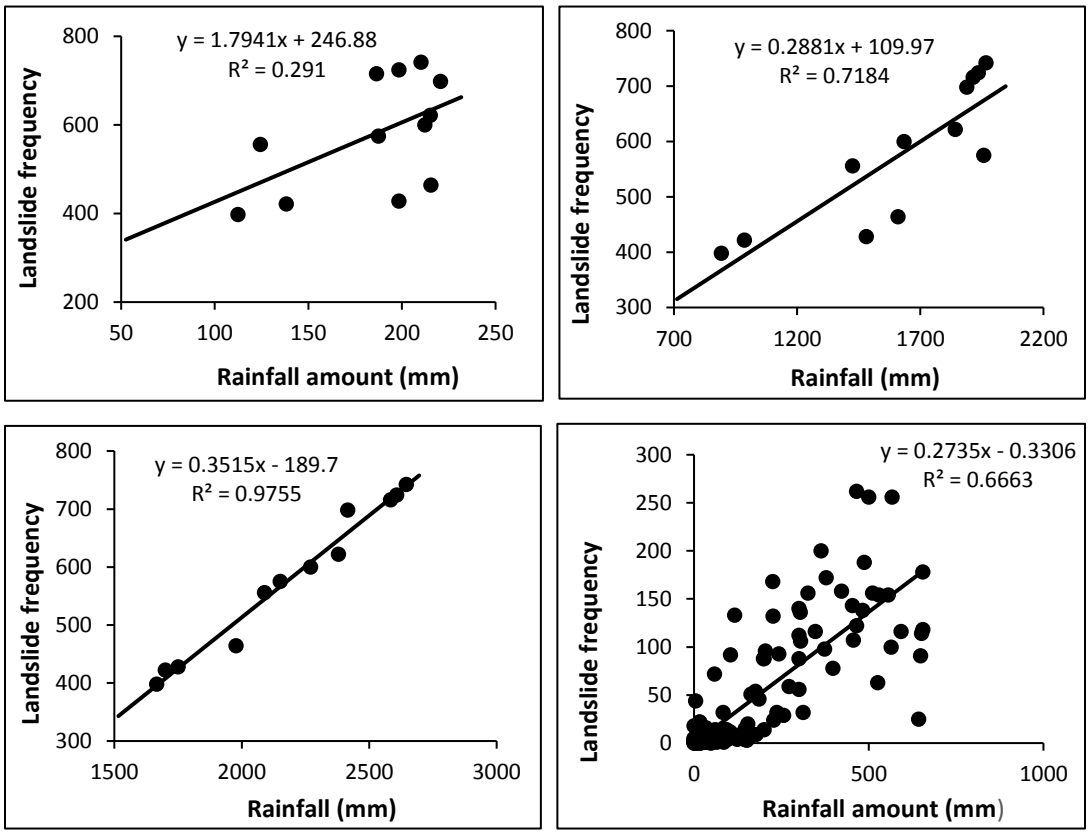


**Figure 18:** The linear relation between rainfall and landslide events, a) maximum 24 hrs. rainfall and total annual landslide, b) total rainfall in the monsoon period and total annual landslide, c) total annual rainfall and total annual landslide events, d) monthly rainfall and monthly landslide from 2010 to 2021.

The magnitude of rainfall, duration of rain, events of landslides with the date, and landslide size are summarized in Table 8. The various data from 2020 to 2021 are presented with landslide location and landslide date so that the rainfall and landslide date can relate. The real-time data shows that rainfall time, short-term rainfall amount, and landslide size are not exactly related.

#### 4.1.1.3.2 Rainfall map and landslide

The rainfall map was prepared by using the average annual precipitation from 7 stations (Fig.19). The rainfall class was divided into seven subclasses. The frequency ratio was obtained from class percent and percentage of landslides in each class. The landslide percentage and class percentage were obtained from the spatial analyst of GIS. The frequency ratio of each class shows that rainfall and landslides are positively correlated (Table 9).

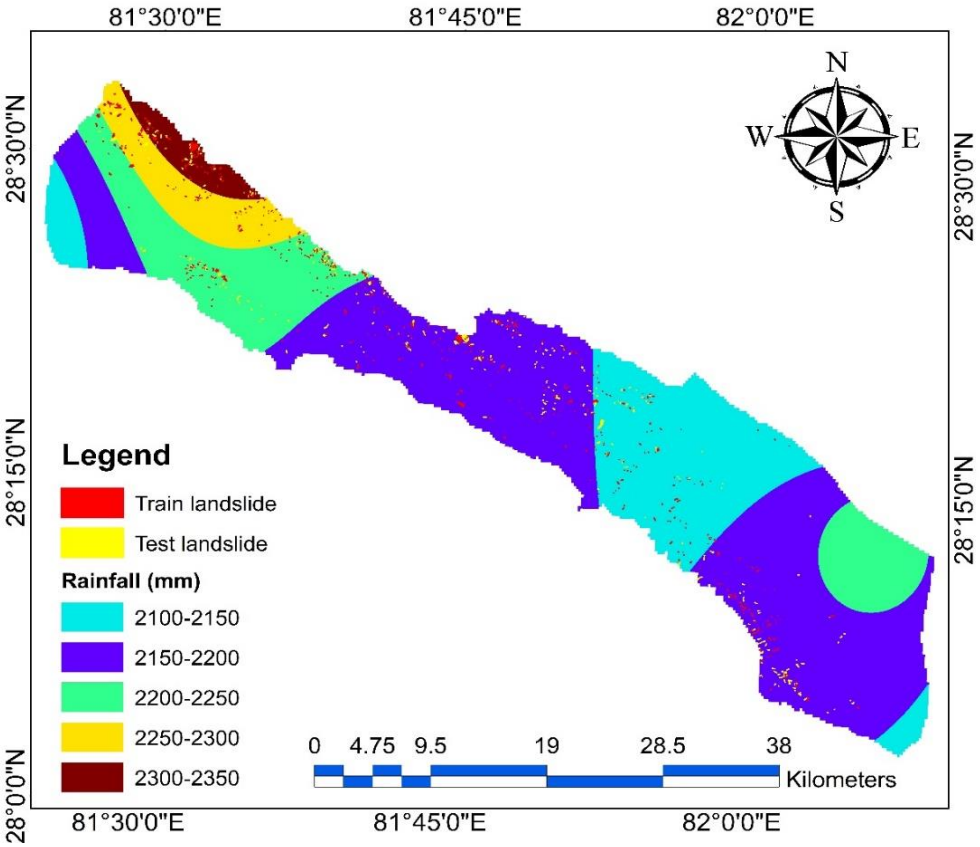


**Figure 19:** Rainfall map of the study area

**Table 8:** Rainfall amount, intensity and landslide events in temporal series of representative landslides

| SN | Rainfall date | Rainfall (mm) | Rainfall Duration (Hrs) | Landslide Date | Size ($m^2$) | Location |
|---|---|---|---|---|---|---|
| 1 | 7-2-2010 | 100.6 | 3.0 | 7-6-2010 | 14,678 | Babai village |
| 2 | 8-30-2010 | 39.4 | 1.5 | 9-06-2010 | 1,34,342 | Ban gaun |
| 3 | 7-23-2011 | 96.6 | 6.0 | 7-26-2011 | 45,231 | Mulkharka |
| 4 | 8-23-2011 | 120.2 | 4.3 | 8-23-2011 | 53,125 | Khahare |
| 5 | 7-02-2012 | 77.5 | 3.2 | 7-04-2012 | 45,567 | Purandanda |
| 6 | 9-04-2012 | 40.6 | 1.2 | 9-04-2012 | 1,23,187 | Guhiyachaur |
| 7 | 7-02-1013 | 56.78 | 1.2 | 7-05-2013 | 24,156 | Sarada Khola |
| 8 | 8-09-2013 | 86.21 | 1.6 | 8-09-2013 | 9,786 | Damdawali |
| 9 | 6-28-2014 | 116.5 | 1.4 | 7-04-2014 | 96,176 | Gidde Khola |
| 10 | 7-16-2014 | 154.0 | 6.0 | 7-17-2014 | 1,56,342 | Gidde Khola |
| 11 | 7-17-2014 | 215.0 | 8.0 | 7-17-2014 | 2,77,879 | Gidde Khola |
| 12 | 6-02-2015 | 175.2 | 2.5 | 6-04-2015 | 1,34,456 | Harre |
| 13 | 6-21-2015 | 263.3 | 5.0 | 6-26-2015 | 39,213 | Lekhparajul |
| 15 | 7-06-2016 | 95.6 | 1.5 | 7-11-2016 | 6,22,362 | Lekhparajul |
| 16 | 7-28-2016 | 120.5 | 2.5 | 8-06-2016 | 9,62,409 | Babai Village |
| 17 | 8-09-2017 | 157.5 | 4.3 | 8-09-2017 | 4,34,980 | Bardia National park |
| 18 | 8-18-2017 | 125.0 | 3.2 | 8-19-2017 | 2,13,435 | Bardia |
| 19 | 7-22-2018 | 122.5 | 1.2 | 7-22-2018 | 99,876 | Salyantari |
| 20 | 8-17-2019 | 178.5 | 3.5 | 8-22-2019 | 3,66,178 | Bardia |
| 21 | 7-22-2020 | 154.27 | 8.2 | 7-22-2020 | 4,22,317 | Salyantari |
| 22 | 7-28-2021 | 162.6 | 6.4 | 7-29-2020 | 2.34.567 | Chepang |

Source: *Department of Hydrology and Meteorology, Nepal government, and field study*

**Table 9:** Average annual rainfall and frequency ratio of landslides.

| Rainfall (mm) | Pixel of class | Area ($m^2$) | (FR) |
|---|---|---|---|
| 2148-2182 | 109128 | 76500 | 0.29 |
| 2183-2218 | 380072 | 585900 | 0.64 |
| 2218-2253 | 346537 | 773100 | 0.92 |
| 2253-2288 | 155242 | 261000 | 0.69 |
| 2288-2323 | 61297 | 303300 | 2.05 |
| 2323-2357 | 40284 | 313200 | 2.46 |
| 2357-2392 | 17881 | 365400 | 8.47 |

#### 4.1.1.3.3 Drainage to Distance Analysis

The drainage-to-distance analysis was carried out by calculating the landslide pixel of drainage to distance from <100 m to >500 m by using drainage to distance map (Fig.20). The landslides near the drainage signify the effect of runoff for landslide initiation. The area of landslide, distance from drainage, and frequency ratio are shown in Table 10. The distribution of landslides is greater at the near distance from drainage. Similarly, the value of the frequency ratio is also highest at the near distance from the stream. The result showed that the number of landslides increases with decreasing distance from drainage.

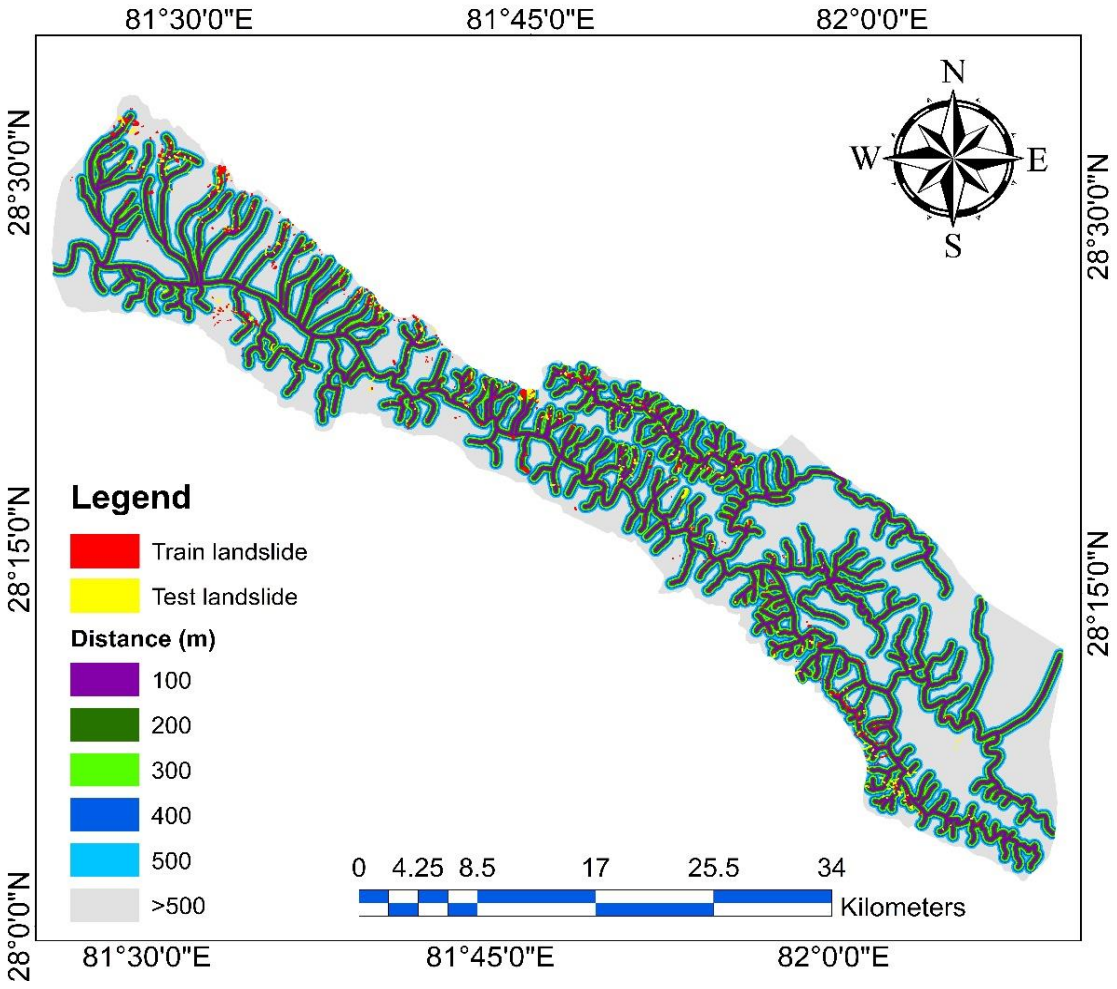


**Figure 20:** Drainage to distance map of study area.

**Table 10:** Area distribution of landslides in the various distances from drainage

| Distance (m) | Pixel | Area ($m^2$) | (FR) |
|---|---|---|---|
| <100 | 19645 | 619200 | 2.363379 |
| 100-200 | 19061 | 557100 | 2.191502 |
| 200-300 | 18589 | 447300 | 1.804252 |
| 300-400 | 17989 | 349200 | 1.455532 |
| 400-500 | 17448 | 277200 | 1.191247 |
| >500 | 108436 | 432900 | 0.299343 |

#### 4.1.1.4 Geotechnical Characteristics

##### 4.1.1.4.1 Soil classification and compositional statistics

One hundred twenty soil samples contain mainly four types of soil: CL, ML, CL-ML, and SC. The results demonstrated that 52 soil samples have more than 15% clay. Based on the ternary diagram of sand, silt, and clay, the dominant soil type in the landslide is CL (Fig. 21). With a mean value of 25.49%, the range of liquid limit values was between 16.4% and 48.64%. The lowest and highest plastic content limits are 6.39% and 29.52%, respectively. The average value of the plastic limit was 14.78%. The plasticity index values varied from 7.56 to 17.78, with a mean value of 13.13, indicating that the soil types were medium plastic.

However, based on the data shown on the plasticity chart, the soil was classified as clay-rich with moderate plastic behavior (Fig. 22). Out of the 120 samples, 61 were of type CL (Fig.23).

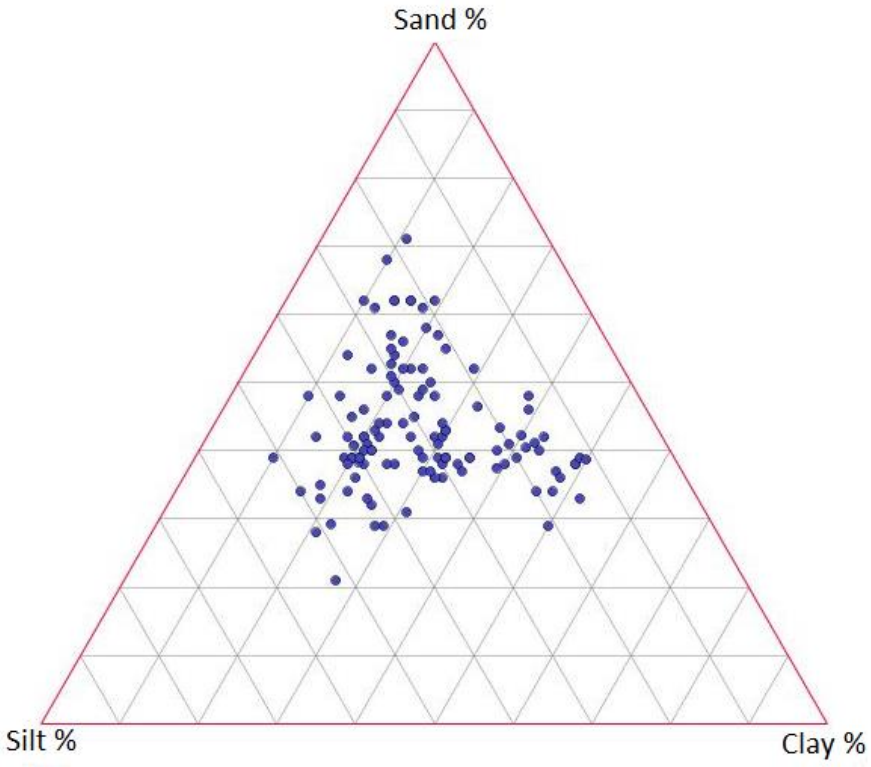


**Figure 21:** Ternary diagram showing the soil type based on particle distribution.

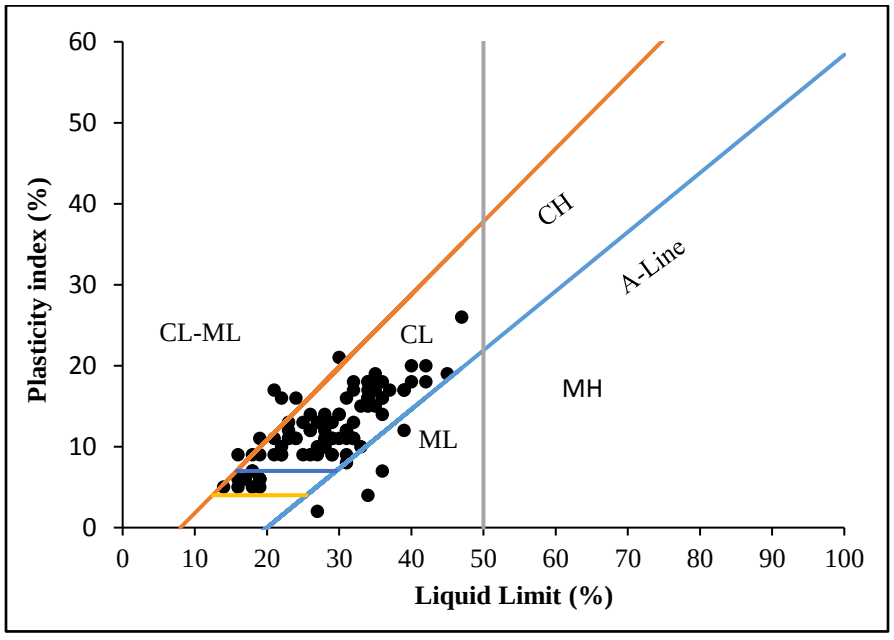


**Figure 22:** Casagrande plasticity chart showing the liquid limit/ plasticity index chart and soil classification.

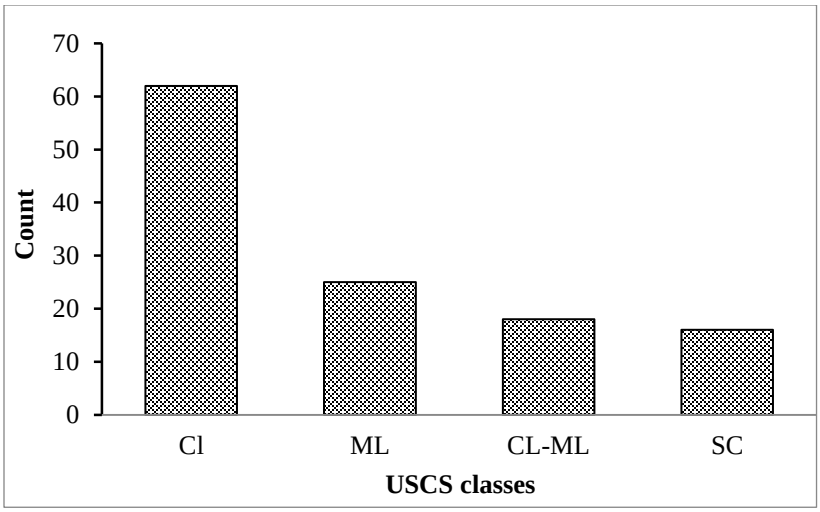


**Figure 23:** The distribution of the soil type according to USCS classes.

#### 4.1.1.4.2 Soil gradation

The sieve analysis reveals that 64 samples were well-graded while 56 were poorly graded. In the landslides of Lower Siwalik, poorly graded soils predominate. Similarly, in the Middle Siwalik landslides, well-graded soils predominate. In Upper Siwalik, the distribution of soil types is relatively uniform. Rich in coarse particles and dominated mainly by gravelly clay, the Upper Siwalik is characterized by a preponderance of gravelly clay. The distribution of sandy clay to gravelly clay is uniform in Middle Siwalik (Table 11).

**Table 11:** Gradation of soil into different geological units.

| Geological units | Gradation | Number of landslides |
|---|---|---|
| Lower Siwalik | Well graded | 7 |
| | Poorly graded | 33 |
| Middle Siwalik | Well graded | 31 |
| | Poorly graded | 9 |
| Upper Siwalik | Well graded | 18 |
| | Poorly graded | 22 |

#### 4.1.1.4.3 Compositional statistics

The center of the three compositions was obtained (Sand = 40.9%, Silt =36.67%, and Clay =22.36%). The obtained values are consistent with the USCS classification. The predictive region of the center (gi) is shown in Figure 24. The ternary diagram of the center plot shows that the center (gi) value lies in the maximum point concentrated location (Fig.25).

According to the variation array's findings between the log ratio's mean value and the variance of the same log ratio (Table 12), the variance of the silt-clay log ratio is the highest (0.4258). In contrast, the variances of the sand-clay log-ratio and the sand-silt log-ratio are both lower. The sand-silt log ratio has the least amount of variation. According to the centered log-ratio value of a single component, the silt and clay fraction has the highest fractional variation (> 79%). Similarly, the clr values of the sand-silt fraction and the sand-clay fraction are, respectively, 56% and 64%.

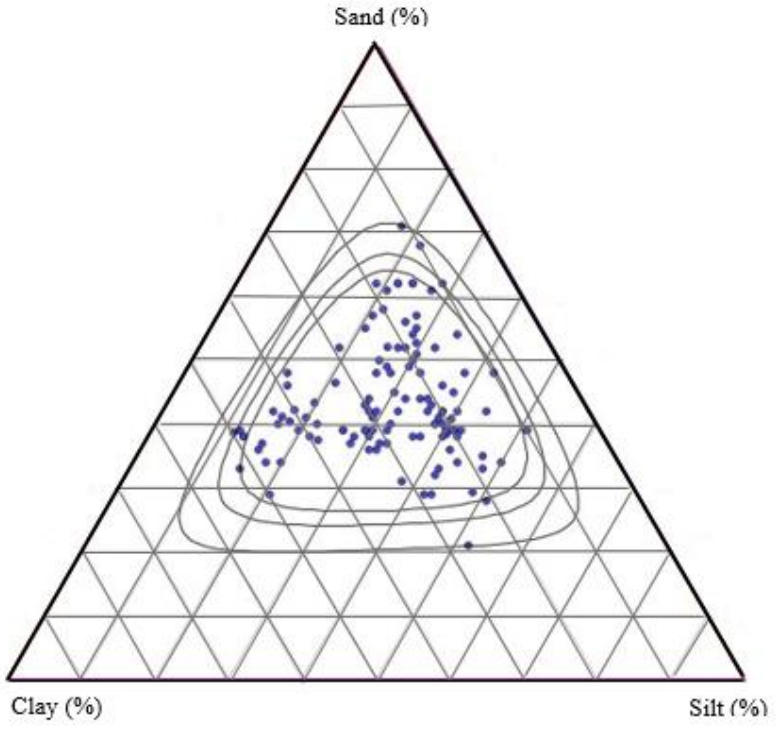


**Figure 24:** The predictive region of the center.

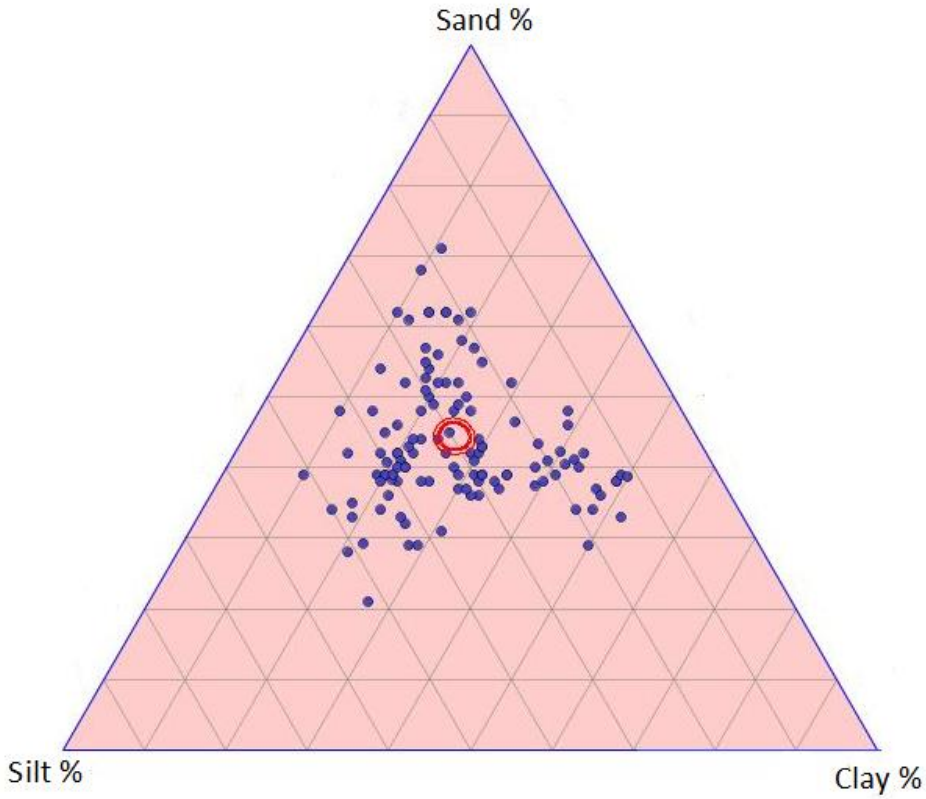


**Figure 25:** The centered confidence region of the center (gi).

**Table 12:** Variation array of soil grain size distribution.

| | | Variance ln ($X_i/X_j$) | | |
|---|---|---|---|---|
| $X_i/X_j$ | Sand | Silt | Clay | clr variance |
| Sand | - | 0.2086 | 0.2800 | 0.0613 |
| Silt | -0.4025 | - | 0.4258 | 0.1099 |
| Clay | -0.5439 | -0.1413 | - | 0.1337 |
| | Mean ln ($X_i/X_j$) | | | 0.3048 |

#### 4.1.1.4.4 Shear behavior of soil

The shear stress vs. horizontal displacement (dh) curve was obtained during the direct shear test. The shear stress fluctuation and horizontal displacement curves for normal stresses of 20 kPa, 40 kPa, and 60 kPa from three types of landslides dispersed in three different geological units are depicted in Figures 26, 27, and 28.

Shear stress initially rose gradually until it peaked, coinciding with the compaction and linear stages of the soil. The soil samples mobilized their peak and reached their stable state in type I landslides (which occurred in Lower Siwalik) at about 3.7– 4 mm shear displacement and 32–36 kPa shear strength at 60 kPa normal stress. The identical samples also achieved their highest shear strengths at 20 kPa normal stress and 15–18 kPa at 3-3.5 mm shear displacement. In type I landslides, the shear stress increased quickly with small horizontal displacement increments, while the displacement accelerated quickly with increasing shear stress. Figure 26 depicts the relationship between horizontal displacement and shear stress for the four largest type I landslides. The stress/dh curve for normal stress and achieved residual strength in type I soils does not have a pronounced peak, indicating that the soils are loose. The loose soils gradually develop residual shear strength but never peak strength (Skempton, 1985; Zhang et al., 2016; Zhao et al., 2013a; Zhao et al., 2013b). Type II landslides (Landslide occurred in the Middle Siwalik) showed shear stress and horizontal displacement on the sliding surface that showed a well-defined peak for normal stresses of 20 kPa, 40 kPa, and 60 kPa, respectively, and decreased resistance after reaching the maximum peak. As the horizontal displacement was similar, the shear stress increased quickly. After peaking, shear stress then started to decline and stabilize. It shows that the residual condition is obtained during the last stage when the shear displacement changes quickly, but the shear stress remains constant (Fig. 26). The residual condition is not the residual shear strength because residual shear strength cannot be obtained from the direct shear test.

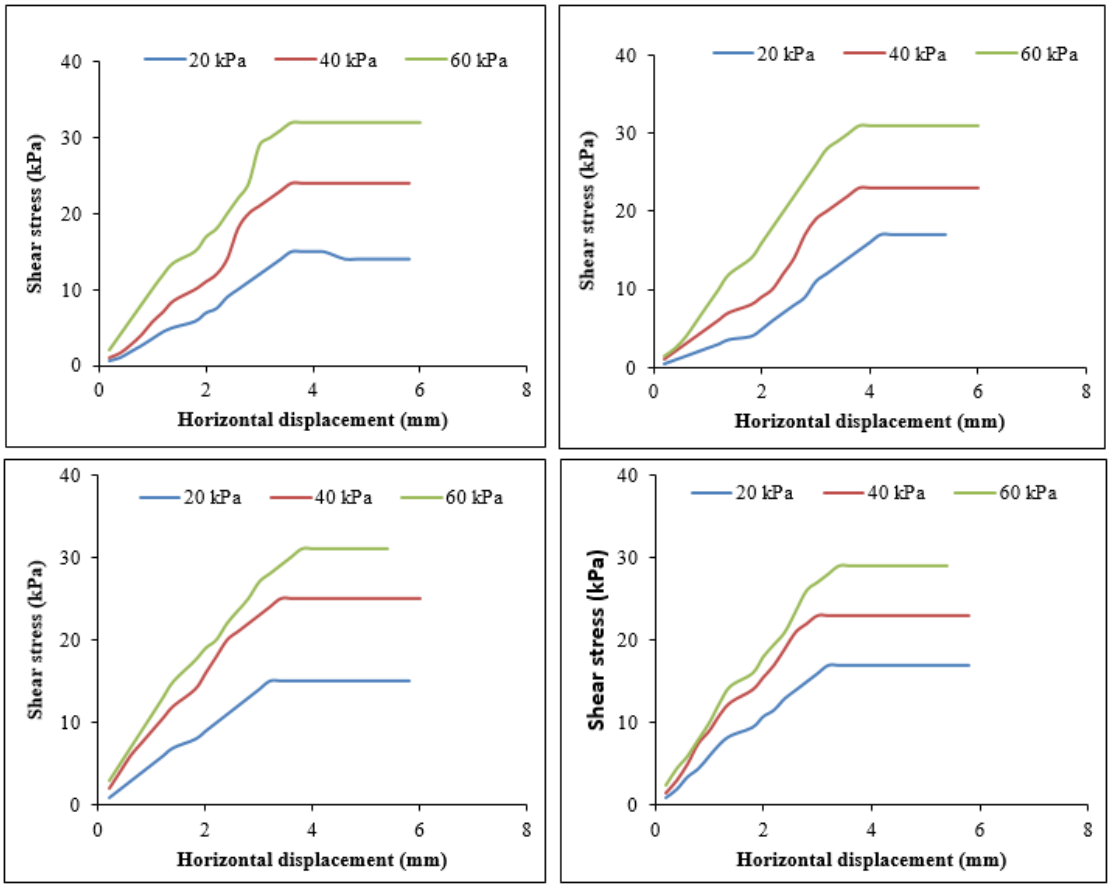


**Figure 26:** The shear stress versus horizontal displacement of the four largest landslide soil of type I landslide

The soils are dense and compact, as seen by the curves in Figure 27. Similarly, the shear stress in the sliding surface of type III landslides (landslides occurred in Upper Siwalik), reached a maximum and remained constant as the displacement increased (Fig.28). The peak is not noticeable in any major way. In type II landslides, the increased ratio of shear stress is higher but lower in type I and type III landslides. However, the increased shear stress and horizontal displacement ratio is somewhat higher in type I landslides. There is a more significant variation in shear stress in type II landslides when subjected to various normal loads. Compared to the shear stresses of normal stress 40 kPa and 60 kPa, the ratio of shear stress to 'dh' is much lower in the shear stress of normal stress 20 kPa.

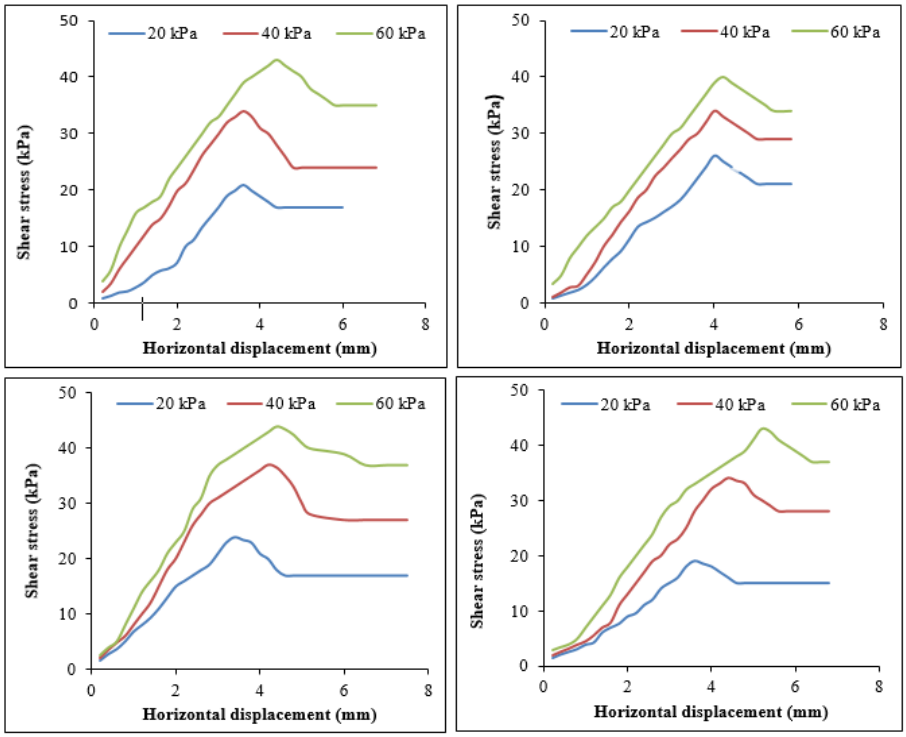


**Figure 27:** The shear stress versus horizontal displacement of the four largest landslide soil of type II landslide.

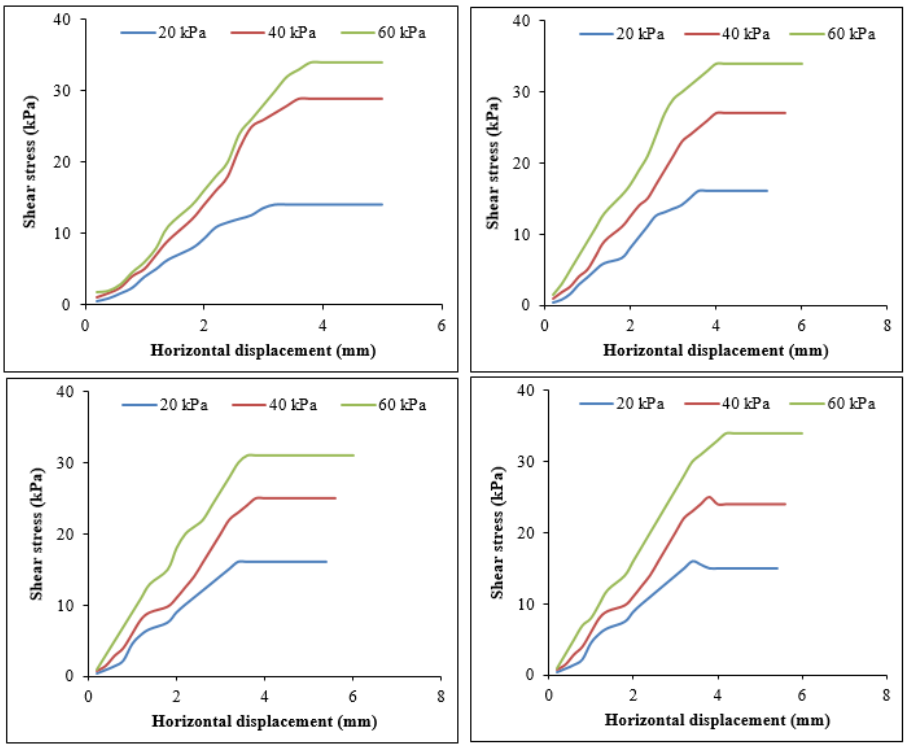


**Figure 28:** The shear stress versus horizontal displacement of the four largest landslide soil of type III landslide

#### 4.1.1.4.5 Shear strength parameters and index properties

Laboratory analysis provided the shear strength data of the soil from 120 landslides. Figure 29 depicts the value distribution of shear strength parameters and index properties of landslide soils, while Table 13 displays descriptive data. The specific gravity ranges from 2.03 to 2.62, with an average of 2.37. The range and average value of the Atterberg limit/plasticity index show that the soils are medium plastic. The average values for the liquid limit and plasticity index are 25.49 and 13.13, respectively. With an average of 11.79 percent, moisture content ranges from 8.38 to 18.60 percent. There is a significant data gap with a coefficient of variance of 36.95 and a void ratio range from 19.23 to 56.44. The local soil compaction and geological and lithological control over it could bring on a vast data gap.

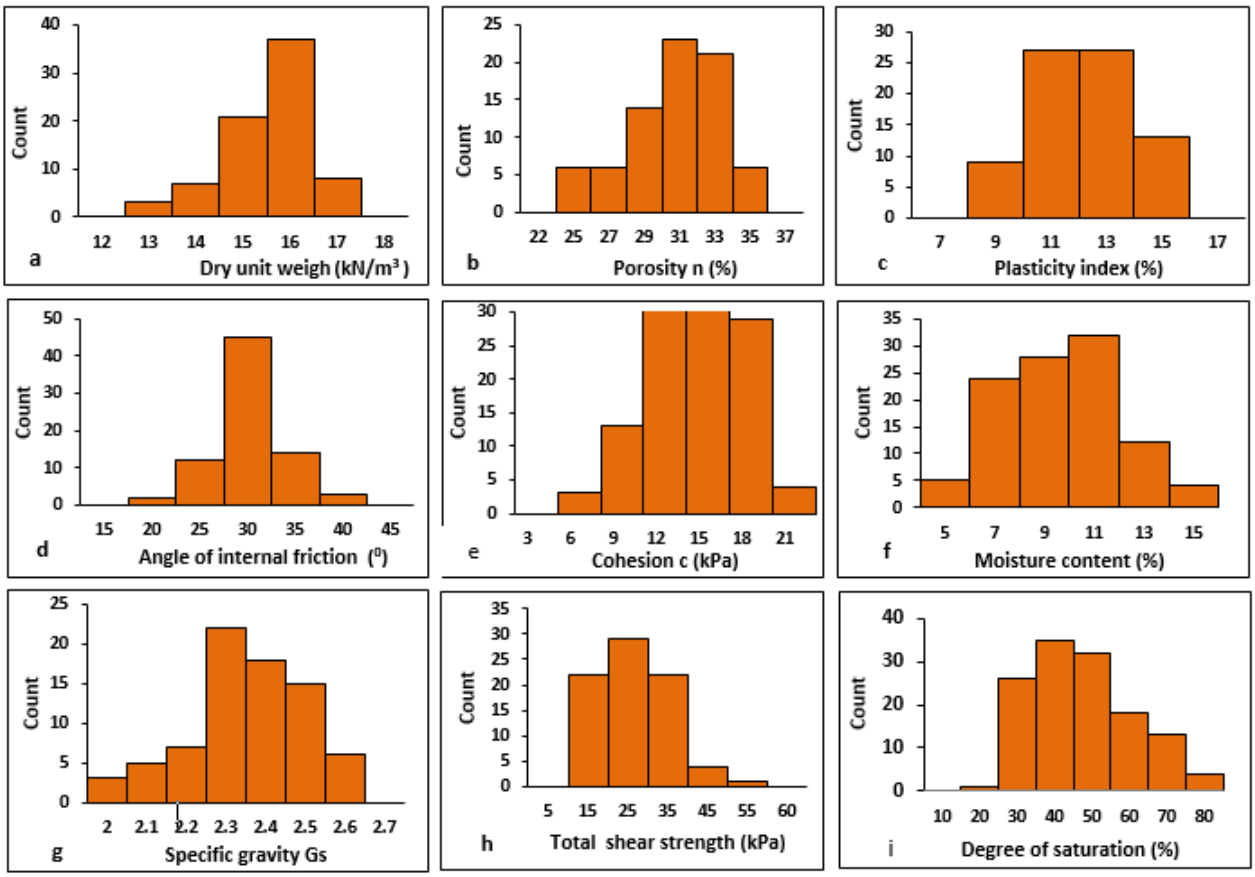


**Figure 29:** The frequency distribution of index properties and shear strength parameters.

#### 4.1.1.4.6 Shear strength parameters and stratigraphy

The coefficient of variance of cohesion and angle of internal friction is higher in type I (Lower Siwalik) landslides. Mudstone, sandstone, and a thin shale layer alternately comprise the Lower Siwalik. Clay, silt, and sand exhibit a variety of consolidation characteristics. The ratio of silt to sand and silt to clay may impact cohesion and internal friction. The different geological compositions of the Lower Siwalik may explain the huge difference between the minimum and maximum value of cohesion. Type II landslides have a higher coefficient of variance in shear strength than the other two categories. Table 14 displays the shear strength characteristics for the three forms of failure in terms of their minimum, maximum, mean, standard deviation, and coefficient of variance.

The mean value, the coefficient of variance, and the shear strength characteristics were all examined based on how they differed between the three types of geology and failure zones. There is a significant disparity in the mean shear strengths across the three types of failure. It is common for landslides of type II to have greater shear strengths than landslides of type I and type III. The mean and the coefficient of variation of shear strength are both greater in type II landslides when compared to type I landslides at the 0.05 level of significance. Likewise, the total and mean cohesion are higher in type II landslides than in type I landslides. In addition, the mean value of the angle of internal friction was compared between the three different types of landslides. When comparing the three different types of landslides, there was a substantial difference in both the mean value and the coefficient of variance of the angle of internal friction. In the Middle Siwalik, the value of the angle of internal friction is noticeably larger than in other geological units.

**Table 13:** Shear strength parameters and index properties of 120 soil samples obtained from the laboratory analysis. Am is the arithmetic mean, SD is the standard deviation, and CV is the coefficient of variation.

| Geotechnical properties | Min. value | Max. value | M ± SD | CV % |
|---|---|---|---|---|
| Cohesion (kPa) | 4.06 | 36.49 | 17.24 ± 6.97 | 39.96 |
| Internal friction (º) | 14.00 | 42 | 24.70 ± 4.52 | 12.05 |
| Sp. Gravity ($kN/m^3$) | 2.03 | 2.62 | 2.37 ± 0.13 | 5.48 |
| Liquid limit (%) | 16.40 | 48.67 | 25.49± 6.80 | 26.67 |

| | | | | |
|---|---|---|---|---|
| Plastic limit (%) | 6.39 | 29.52 | 14.78 ± 6.98 | 47.22 |
| Plasticity index (%) | 7.56 | 17.78 | 13.13 ± 2.04 | 15.53 |
| Moisture content (%) | 8.38 | 18.60 | 11.79 ± 1.63 | 16.64 |
| Dry unit weight (kN/m$^3$) | 13.14 | 17.46 | 15.91 ± 0.94 | 5.90 |
| Wet unit weight (kN/m$^3$) | 14.25 | 18.86 | 17.13 ± 0.99 | 5.77 |
| Shear strength (kPa) | 19.03 | 48.21 | 29.70 ± 3.58 | 12.05 |
| Void ratio (%) | 19.23 | 56.44 | 38.72 ± 6.07 | 36.95 |
| Degree of saturation (%) | 19.8 | 72.2 | 46 ± 8.3 | 16.23 |

**Table 14:** Comparison of the descriptive statistics of cohesion, angle of internal friction, and shear strength in the three types of landslides.

| Landslides | Parameters | Min. value | Max. value | Mean ± SD | CV% |
|---|---|---|---|---|---|
| Type I | Cohesion (kPa) | 4.06 | 18.6 | 9.08 ± 3.065 | 9.4 |
| | Angle of internal friction (º) | 19 | 32 | 27.43 ± 3.87 | 15.03 |
| | Shear strength (kPa) | 15 | 34.62 | 22.69 ± 6.2 | 28.6 |
| Type II | Cohesion (kPa) | 12.56 | 36.49 | 14.9 ± 2.52 | 6.4 |
| | Angle of Internal Friction (º) | 25.23 | 42 | 31.35 ± 2.72 | 7.40 |
| | Shear strength (kPa) | 26.43 | 48.21 | 35.26 ± 6.5 | 35.62 |
| Type III | Cohesion (kPa) | 5.49 | 16.5 | 11.53 ± 2.551 | 6.51 |
| | Angle of internal friction (º) | 20.77 | 32 | 29.72 ± 3.24 | 10.48 |
| | Shear strength (kPa) | 16.6 | 39.91 | 29.35 ± 5.05 | 25.54 |

### 4.1.1.4.7 Covariates of shear strength

Eight variables (plasticity index, void ratio, moisture content, dry unit weight, specific gravity, degree of saturation, cohesion, and angle of internal friction) were used to predict shear strength. Only five variables were significantly related to shear strength (p= <0.05, standard error=1.452, degree of freedom=5). Shear strength was found to have a substantial positive relationship with cohesion, angle of internal friction (p=0.000) and dry unit weight (p=0.002) but a negative relationship with plasticity index (p=0.007) and degree of saturation (p=0.007). The relation of shear strength is not significant with void ratio, specific gravity, and moisture content. Table 15 shows the significant covariates of shear

strength and their significance level. The relation of shear strength and significant covariates is shown in Figure 30.

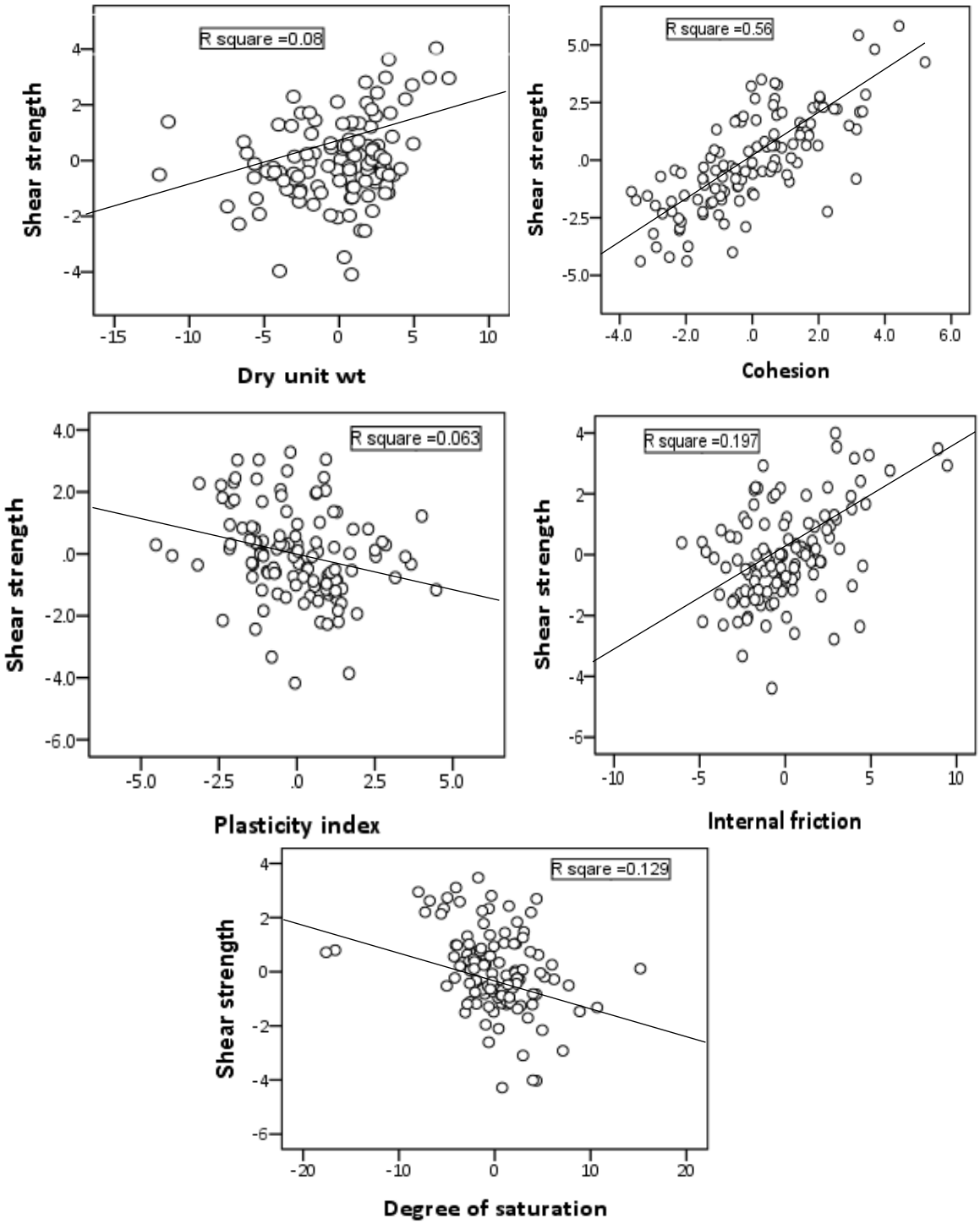


**Figure 30:** Significant covariates of shear strength

**Table 15:** Covariates of shear strength and their significant level.

| Coefficients | Estimate | Std. Error | t- value | p-value |
|---|---|---|---|---|
| Intercept | 17.643 | 3.971 | 4.443 | 0.000 |
| Dry unit weight | 0.390 | 1.480 | 3.095 | 0.002 |
| Cohesion | 0.862 | 0.073 | 11.879 | 0.000 |
| Internal Friction | 0.258 | 0.50 | 5.200 | 0.000 |
| Plasticity Index | -0.242 | 0.082 | -2.724 | 0.007 |
| Moisture content | 0.012 | 0.111 | 0.111 | 0.912 |
| Void ratio | 1.510 | 1.480 | 1.020 | 0.310 |
| Degree of saturation | -0.125 | 0.032 | -3.956 | 0.000 |
| Specific gavity | -1.945 | 1.103 | -1.764 | 0.081 |
| $R = 0.96$, $R^2 = 0.934$, St. Error =1.44, df=8, F=193.47, P =000 | | | | |

#### 4.1.1.4.8 Correlation matrix

The correlation matrix for each variable is displayed in Table 16. This outcome led to a better understanding of the relationship between each variable. Cohesion and shear strength are positively correlated (correlation coefficient 0.918 with a significance level of less than 0.01). Shear strength and plasticity index negatively correlate with a correlation coefficient of -0.676. The association shear strength and dry unit weight is positive and has a significance level of less than 0.01 (correlation coefficient 0.789). The results imply some degree of substantial correlation between the variables. Cohesion and internal friction have a strong positive correlation with shear strength, but plasticity index, moisture content, and degree of saturation have a strong negative correlation. The slope will be supported by soil with a higher shear strength, which is considered stable (Yalcin, 2011).

#### 4.1.1.4.9 Relation of shear strength with landslide state

Only new, active, and reactivated landslides were used to determine the distribution of shear strength values. The shear strength value of a reactivated landslide is higher than that of an active or new landslide. Below the 30 kPa, the shear strength distribution is stronger in the active landslide. The result shows that the shear strength value of reactivated

landslides is significantly greater than that of new or active landslides; however, the reactivation could cause unstable colluvium in the old landslide.

**Table 16:** The correlation matrix of nine major geotechnical properties.

| | T | e | Yd | C | PI | Φ | Gs | W | Sr |
|---|---|---|---|---|---|---|---|---|---|
| τ | 1 | | | | | | | | |
| e | 0.196 | 1 | | | | | | | |
| Yd | 0.789* | 0.157** | 1 | | | | | | |
| c | 0.918** | 0.163 | 0.724 | 1 | | | | | |
| PI | -0.676** | -0.052 | -0.541 | -0.623 | 1 | | | | |
| ϕ | 0.698** | 0.111 | 0.550 | 0.544 | -0.460 | 1 | | | |
| Gs | 0.139* | 0.210 | 0.203 | 0.185 | -0.120 | 0.116 | 1 | | |
| W | -0.722 | 0.058 | -0.708 | -0.751** | 0.586 | -0.434 | -0.317 | 1 | |
| Sr | -0.839** | -0.244** | -0.712 | -0.741** | 0.566** | -0.656 | -0.136 | 0.66** | 1 |

** Correlation is significant at 0.01 level (one-tailed)

* Correlation is significant at 0.05 level (one-tailed)

### 4.1.2 Landslide classification

#### 4.1.2.1 Mechanism-based classification

The surface failures were noted mainly along the old colluviums. Similarly, the colluvium-bedrock contact has a significant number of landslides. Several landslides were noted on the geological contact and around the fault zone. Based on the landslide mechanism and process, five types of landslides are mainly noted, and the types are proposed as a new classification system.

**Type 1**: The landslide occurred on the massive sandstone beds when a thin layer of shale or mudstone between the sandstone beds eroded out (Fig. 31 a). The eroded shale layers develop the gap between massive beds and cause rock mass failure. The permeable and weak shale weathers and erodes easily.

**Type 2:** This type of landslide begins with erosion on the soil surface and a small channel or rill. Slope erosion causes the landslide to leave a short scar (Fig. 31 b). Such landslides resulted in an alluvial fan at the bottom after transporting huge amounts of landslide mass (debris) during heavy rain. The slope has been vital in transporting such massive landslide debris toward the bottom of the hill through the channel.

**Type 3**: Conglomerate beds of study areas are two types. One is calcite binding, and another is clay binding (Bhandari & Dhakal, 2018). The loose binding of cementing material weakens as a result of environmental changes. The detached rock fragments and clay-rich soil layer flow with water during heavy rains. Similarly, the mud/clay vein on conglomerate beds weathers and forms the joints with the rock bed. The large block broke away from the intact rock (Fig. 31 c).

**Type 4**: The rocks and soils of the fault zone are crumbly and fragile. A seismic wave or any active stress applied to the area causes the rock/soil to slide or fall. Tension cracks and joints are common in the fault zone. When the water enters the cracks and joints, it creates pore water pressure, reduces friction, and ultimately causes a landslide (Fig. 31 d).

**Type 5**: The colluvium deposit of an old landslide has been covered by a thin layer of soil, causing the development of a forest. During the rainy season, the density of the soil increases in its saturated state. The colluviums loosen the bedrock when the colluviums make contact. The trees and forest increased the soil density, causing a landslide (Fig. 31 e).

The field photograph of all the 5 types landslides are shown in the Figure 32. The schematic diagrams shown in the Figure 31 are based on the real ground scenario of the landslides in the field.

#### 4.1.2.2 Activity of state

Five activity classes are proposed and established for this study namely: new, active, inactive, reactivated and stabilized. The basis of classification of landslides based on activities is as given in Table 17. The field photographs of the landslides based on activity state are shown in the Figure 33.

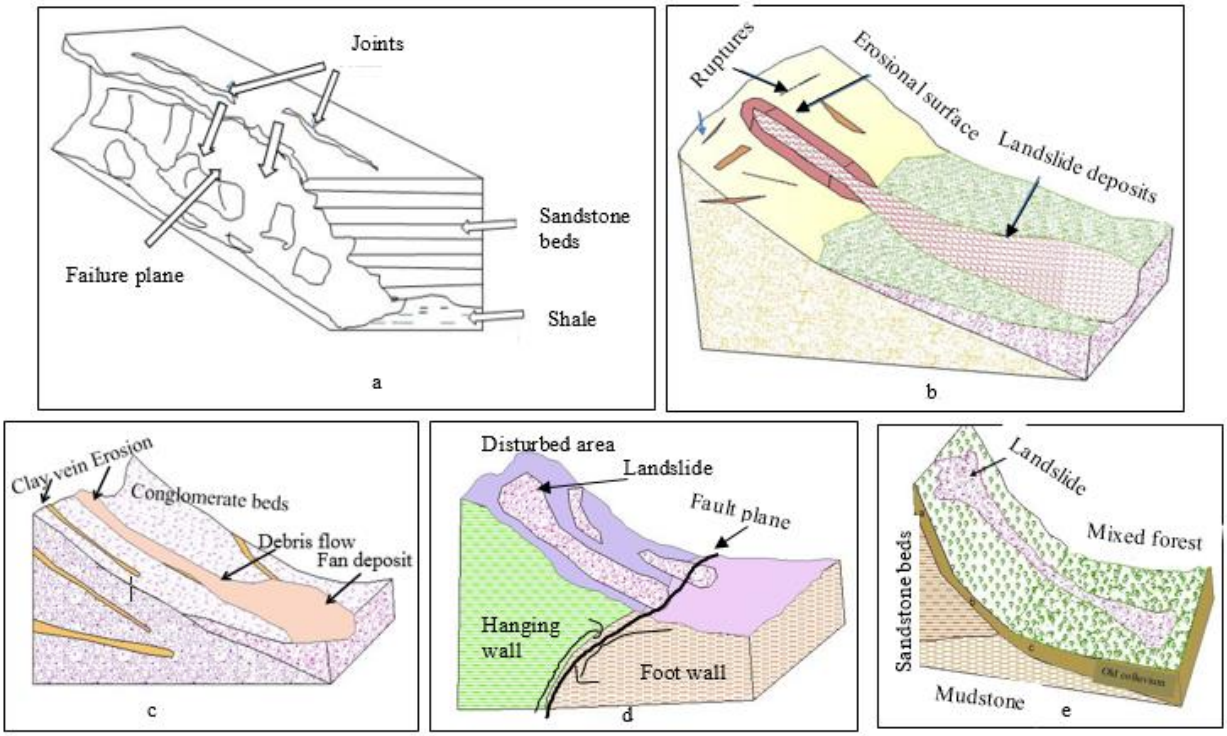


**Figure 31:** Schematic sketch of (a) Type 1 (b) Type 2 (c) Type 3 (d) Type 4 (e) Type 5 landslide.

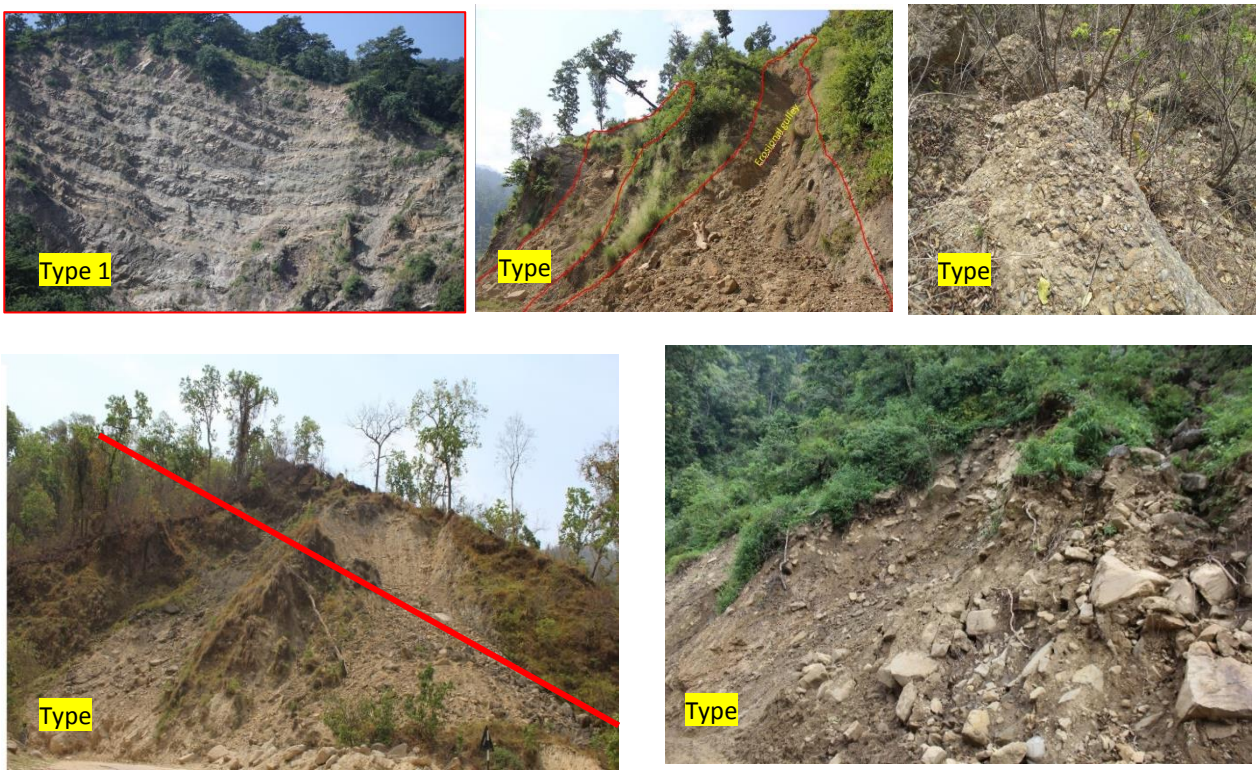


**Figure 32:** Field photograph of type 1 to type 5 landslides.

**Table 17:** Landslide classification based on its activities of states.

| Activity state | Description |
|---|---|
| New (N) | : Landslides that have occurred in the last 24 months |
| Active (A) | : Landslides that have been moving every year/ Movement re-occurred over the previous 12 months |
| Inactive (I) | : No movement has occurred for 36 months, and having no the prior probability of reactivating soon |
| Reactivated (R) | : Landslide reoccurred in the inactive or stabilized landslide |
| Stabilized (S) | : The landslide mitigated naturally or structurally and seems stable for the present. |

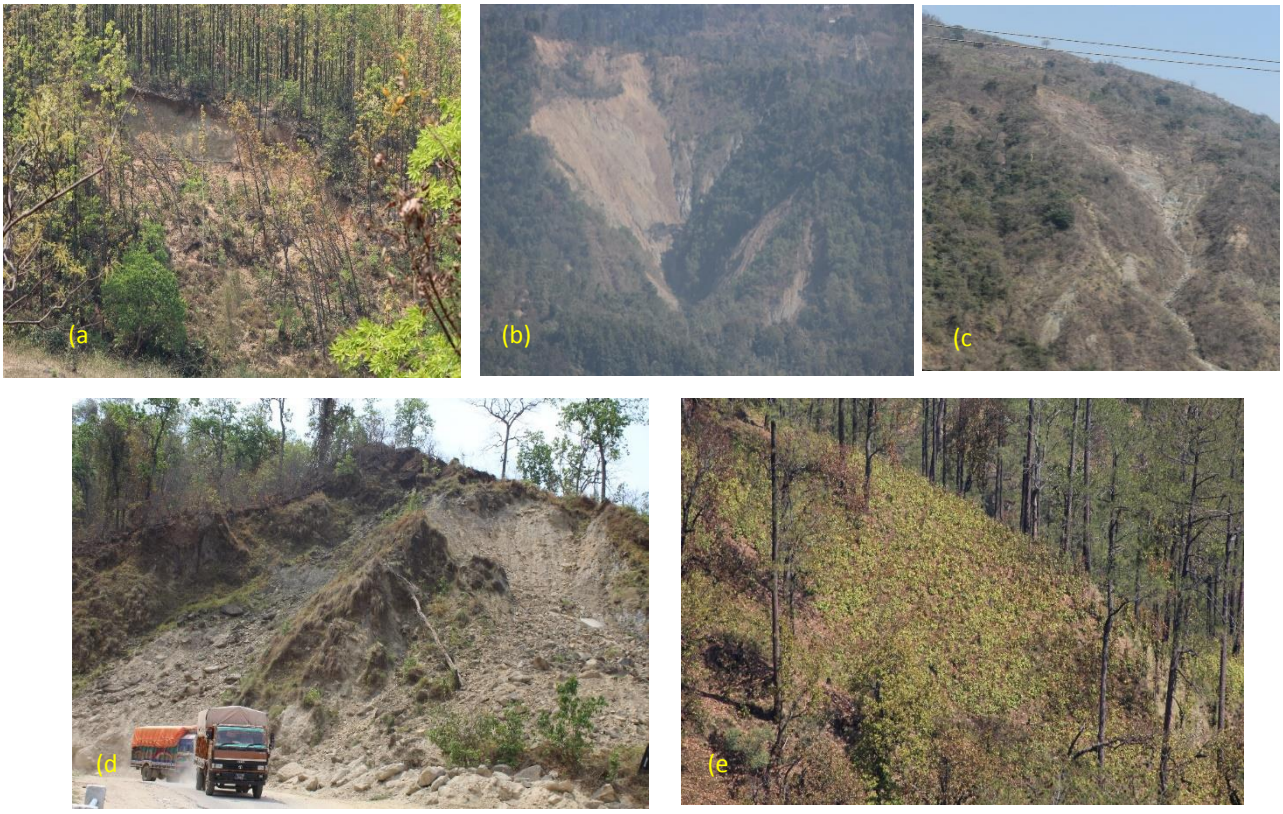


**Figure 33**: Landslide pictures of activity state a) New b) Active c) Inactive d) Reactivated e) Stabilized

The total area of different states of landslides is given in Figure 34. The result showed that most landslides have been active for a decade. The occurrence of new landslides is less than an active landslide. Similarly, the rate of reactivation of landslides is 26%, the second highest rate of landslide occurrence.

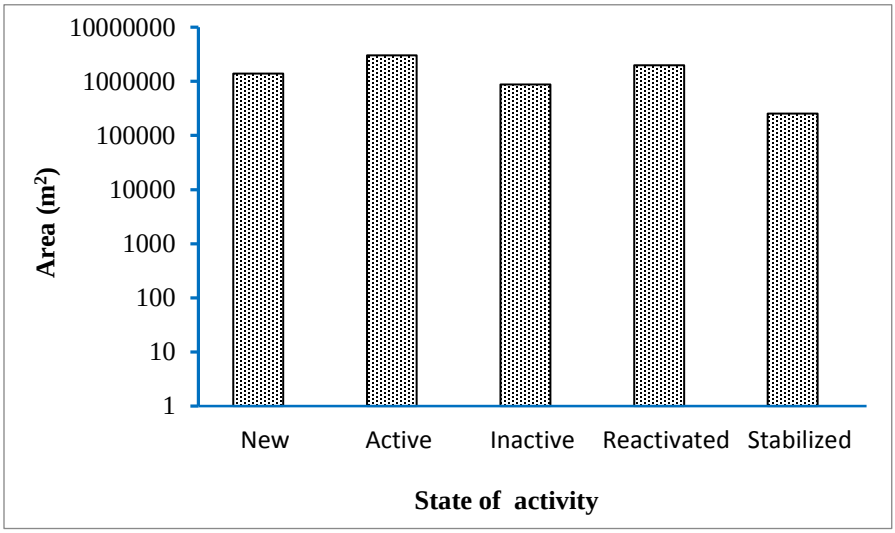


**Figure 34:** Area distribution of activity states of landslides.

### 4.1.2.3 Geological distribution

According to the geological formation, the geological distribution of landslides was determined. There are three regional formations: Lower Siwalik, Middle Siwalik, and Upper Siwalik. All types of landslides are prevalent in Middle Siwalik, whereas in Lower Siwalik, only new landslides are prevalent. The entire length of a landslide varies considerably among geological formations. In each formation, landslides having a length of less than 200 meters predominate (Fig. 35). The Babai thrust has the highest potential for landslides of the three major thrusts in the research area. In the thrust zone, landslides are more common near hanging walls. Most of the landslides are either hanging walls or foot walls of the fault zone. Compared to the footwall, the hanging wall is comprised of a large number of landslides due to the crumbling, strongly jointed, and crushed nature of the hanging wall's rocks.

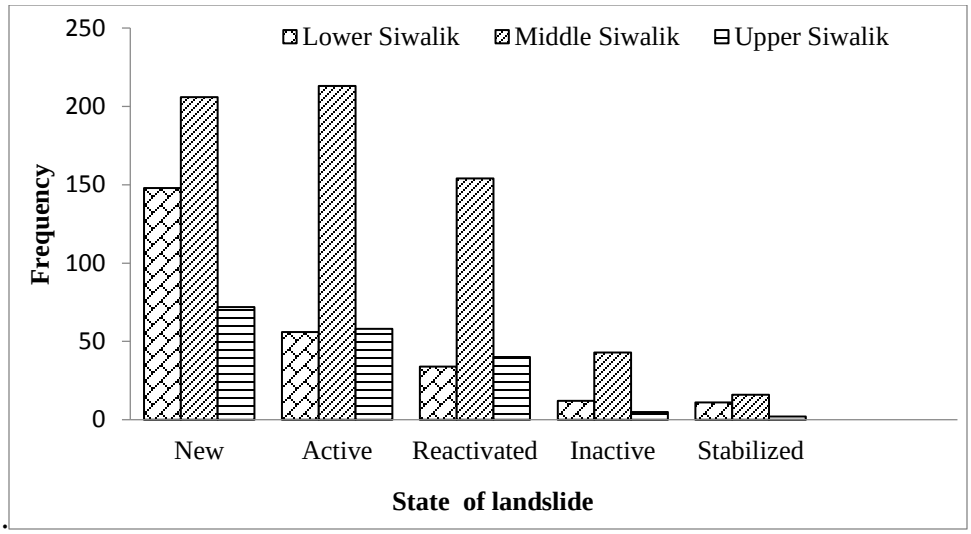


**Figure 35:** Figure showing frequency of state of landslide activity in the different geological formations

### 4.1.2.4 Size based classification

Five landslide size classes are proposed on the basis of log- arrhythmic scale. The proposed landslide size classes are adopted on the basis of area for the size-based classification (Table 18).

**Table 18:** Landslide size on the basis of area

| SN | Area($m^2$) | Size class |
|---|---|---|
| 1 | <100 | Very small |
| 2 | 100-1000 | Small |
| 3 | 1000-10000 | Medium |
| 4 | 10000-100000 | Large |
| 5 | > 100000 | Very large |

The medium sized landslide dominates all geological formations (Fig.36). There is no major difference between geological formations regarding the size-frequency of landslides.

In all geological formations of the research area, the size distribution of landslides follows a normal distribution. The data indicate that the distribution of landslide sizes across all geological formations is identical.

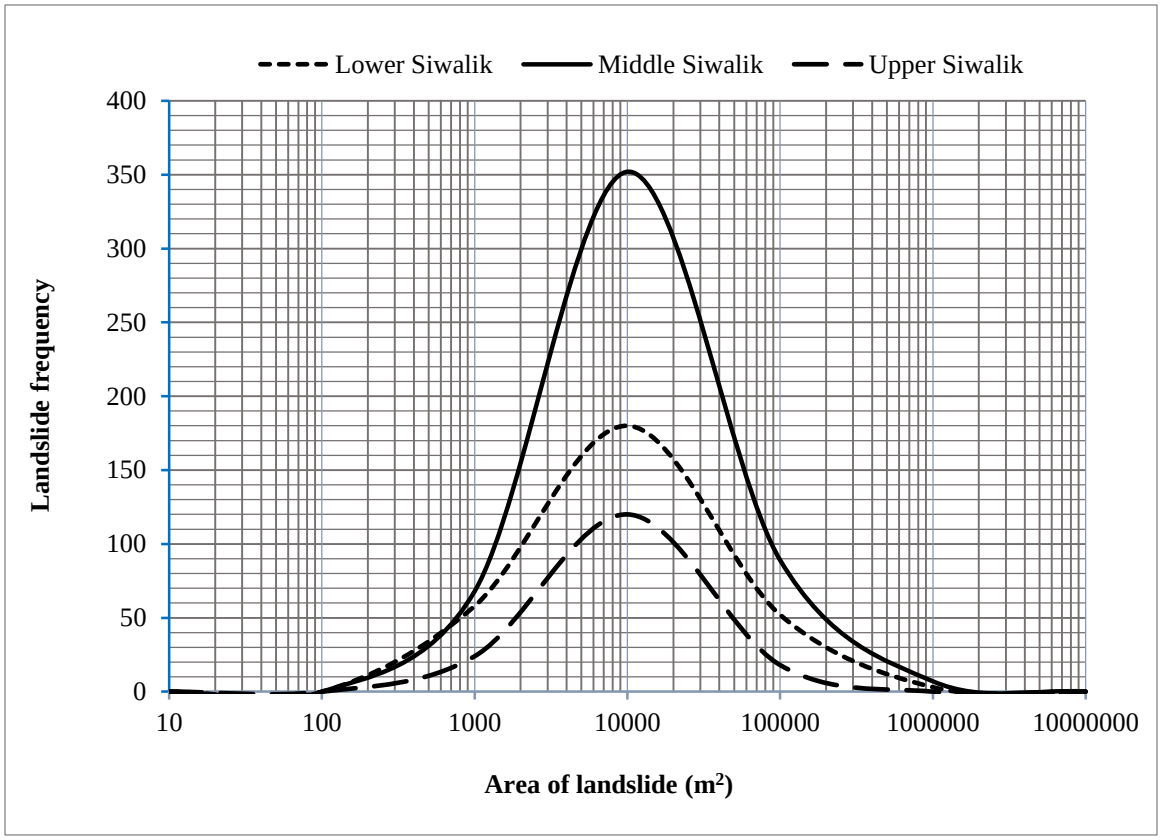


**Figure 36:** Landslide size distribution in the geological units**.**

### 4.1.2.5 Temporal dynamics of landslide

A study of landslides' spatial and temporal distribution from 2010 to 2021 was carried out (Fig. 37). During 2010–2021; there was considerable variation in the annual landslide frequency. In 2010, there were only 398 landslide incidents, which considerably increased to 556 in 2011. In 2012, there were fewer landslides than in any previous year. After that, there was a significant upward trend in the frequency of landslides from 2013 to 2021. The overall pattern of landslides dynamic may be separated into three distinct ways:

1. The number of landslides increased in 2011 and reduced in 2012.

2. The number of landslides increased continuously from 2013 to 2018.
3. Increased continuously from 2018 to 2021

The pattern repeats itself across all of the geological formations. The region's size affected by the landslide has varied yearly. In 2011, a larger land area was affected by the landslide than in previous years, although this trend reversed by 2013. From 2010 to 2011, the total landslide area of Lower Siwalik grew; however, it went down in 2012. Between 2013 and 2017, the area of landslides increased. In 2018, the area declined, but it increased in 2019, 2020, and 2021. 2019 has been the year with the largest recorded number of landslides across all geological formations. Both the number of landslide incidents and their total area are much higher in the Middle Siwalik (Fig. 38). The result shows that the Middle Siwalik is more potential for landslides.

The area of new landslides decreased in 2011, whereas it increased in 2012 and 2013. In 2014, the area went through a further decline, although it increased again between 2016 and 2021. The rate of active landslides has shown an upward trend from 2010 to 2016, with a slight decline in 2017, followed by an increase in 2018 and 2019, respectively. 2011 and 2012 saw a decrease in the reactivation rate, whereas 2013 through 2019 saw a rise. The findings indicate that the number of landslides and their total area was significantly lower in 2012 and 2018. In previous years, the area affected and the number of landslides that occurred increased. Since the beginning of this decade, the relationship between the area and the number has followed a normal distribution. Every year, the average size of the landslide that occurs is between 10,000 and 100,000 square meters. Since 2010 and continuing through 2021, the pattern of landslide area and number curves has remained consistent. It indicates that the landslides possess a dynamic nature in the study area.

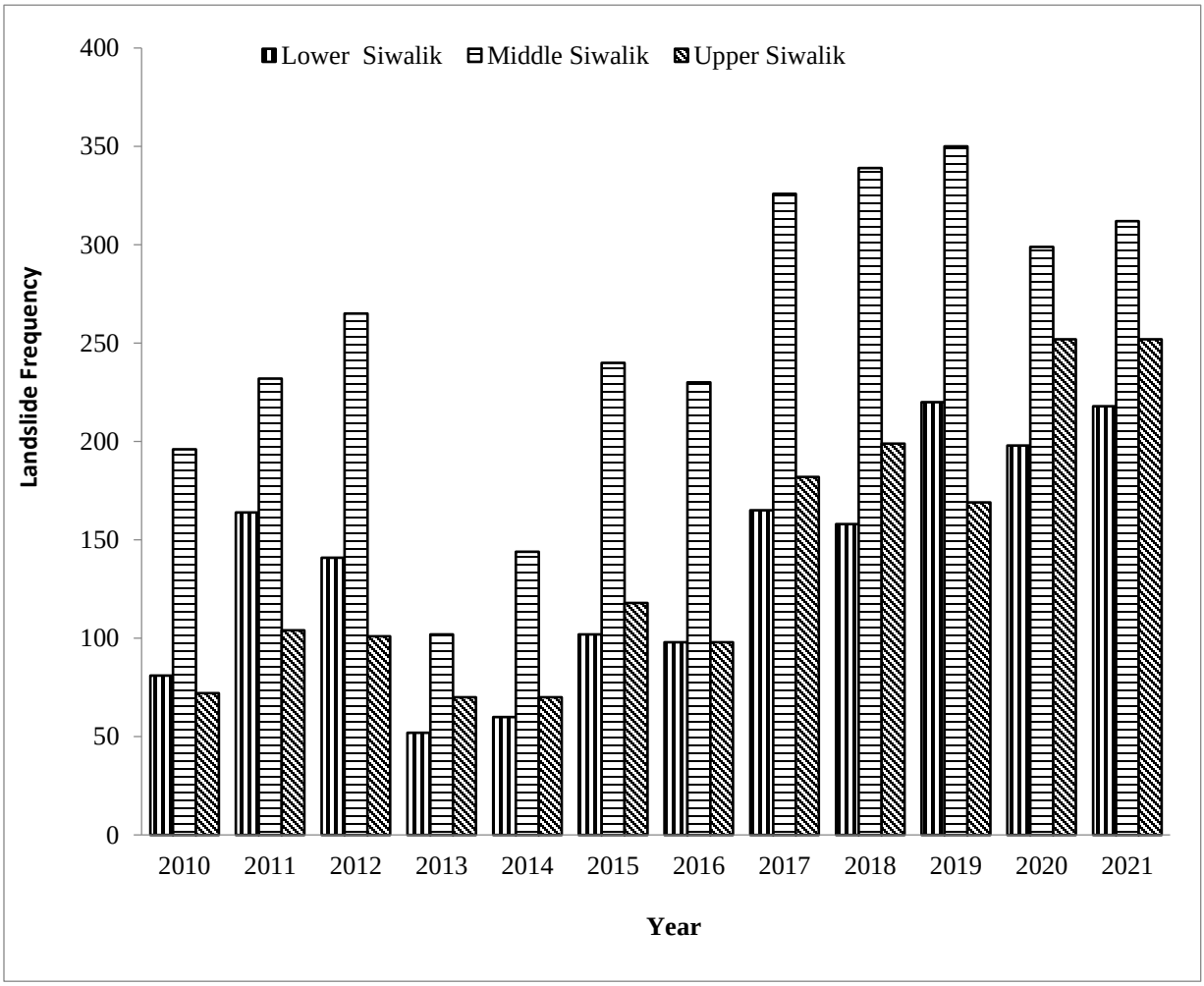


**Figure 37:** Temporal distribution of landslide from the year 2010 to 2021.

The temporal distribution of the state of activity is given in Figure 39. The result shows that the number and area of landslides mainly decreased in two years; that is, 2012 and 2018. In other years, the landslide area and frequency have increased. Since the decade, the area frequency relation has been in a normal distribution. The medium-sized landslide (having an area of 10000-100000 $m^2$) is dominant yearly. The trend of the landslide area frequency curve has been the same every year from 2010-2021 (Fig.40). It indicates that the landslide size is not significantly different every year. The landslide event has been increasing every year since 2010.

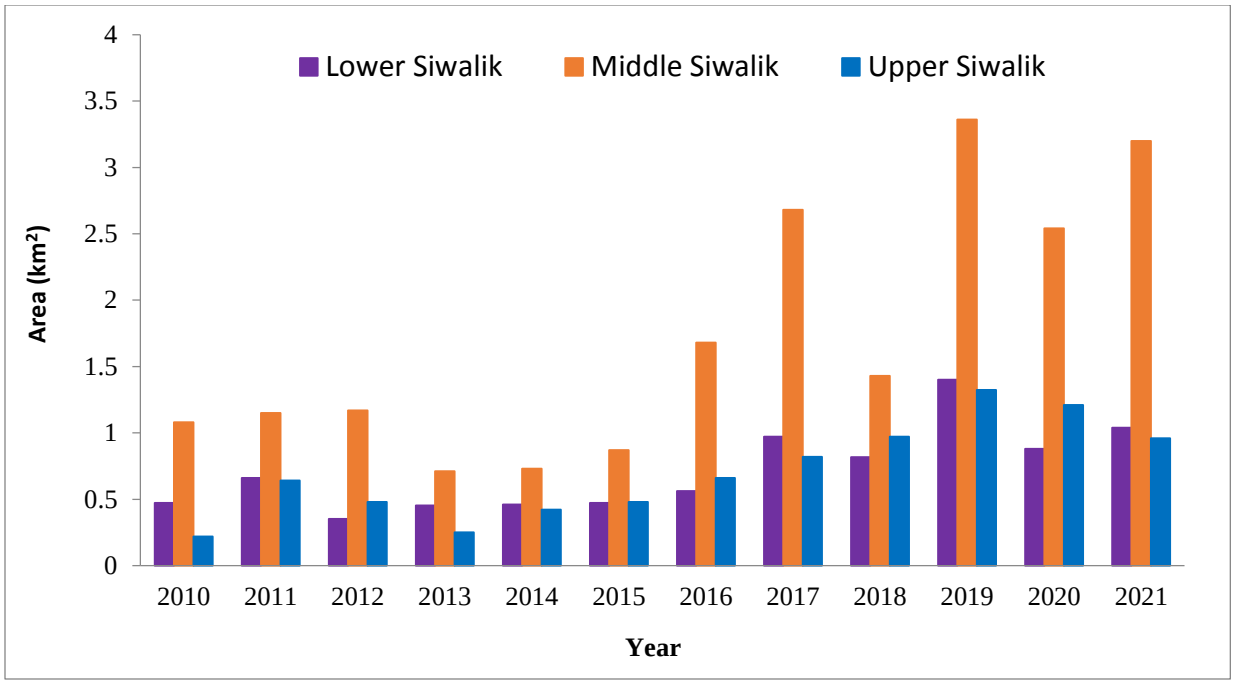


**Figure 38:** Temporal distribution of landslide area in the geological units from the year 2010 to 2021.

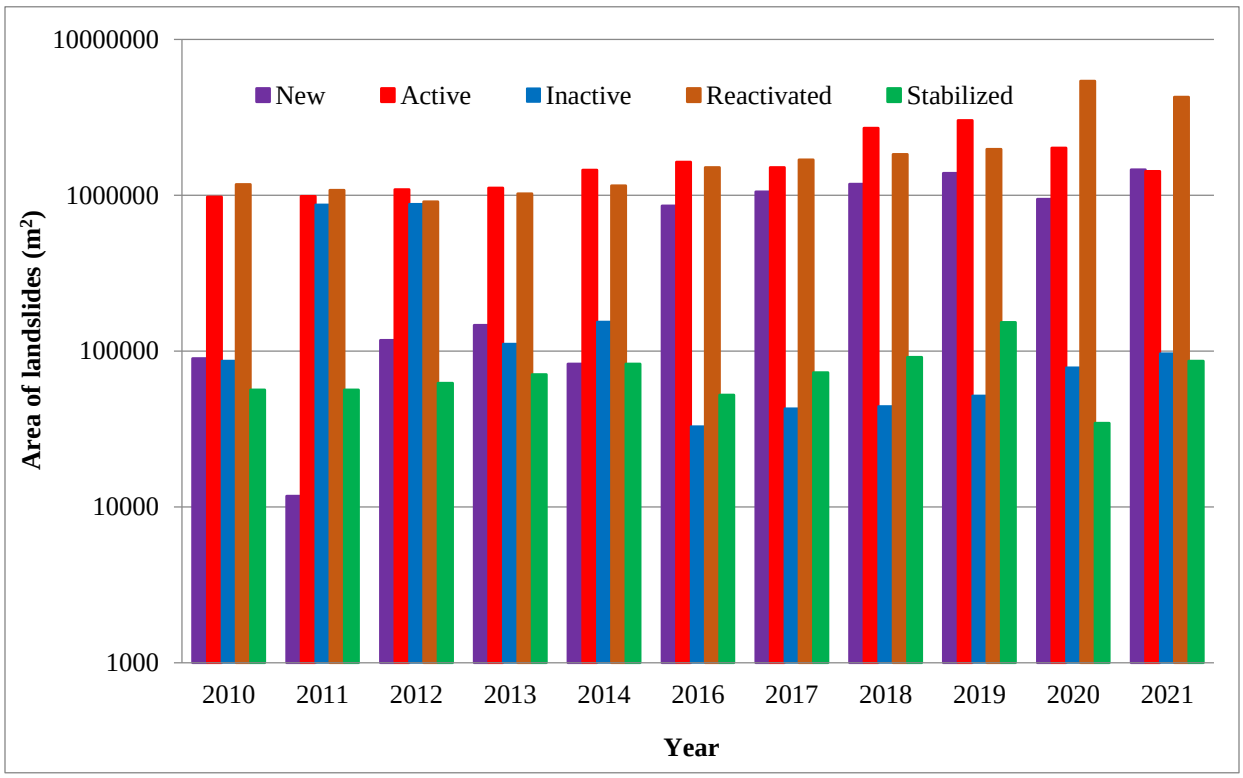


**Figure 39:** The temporal distribution of landslide area with state of activity.

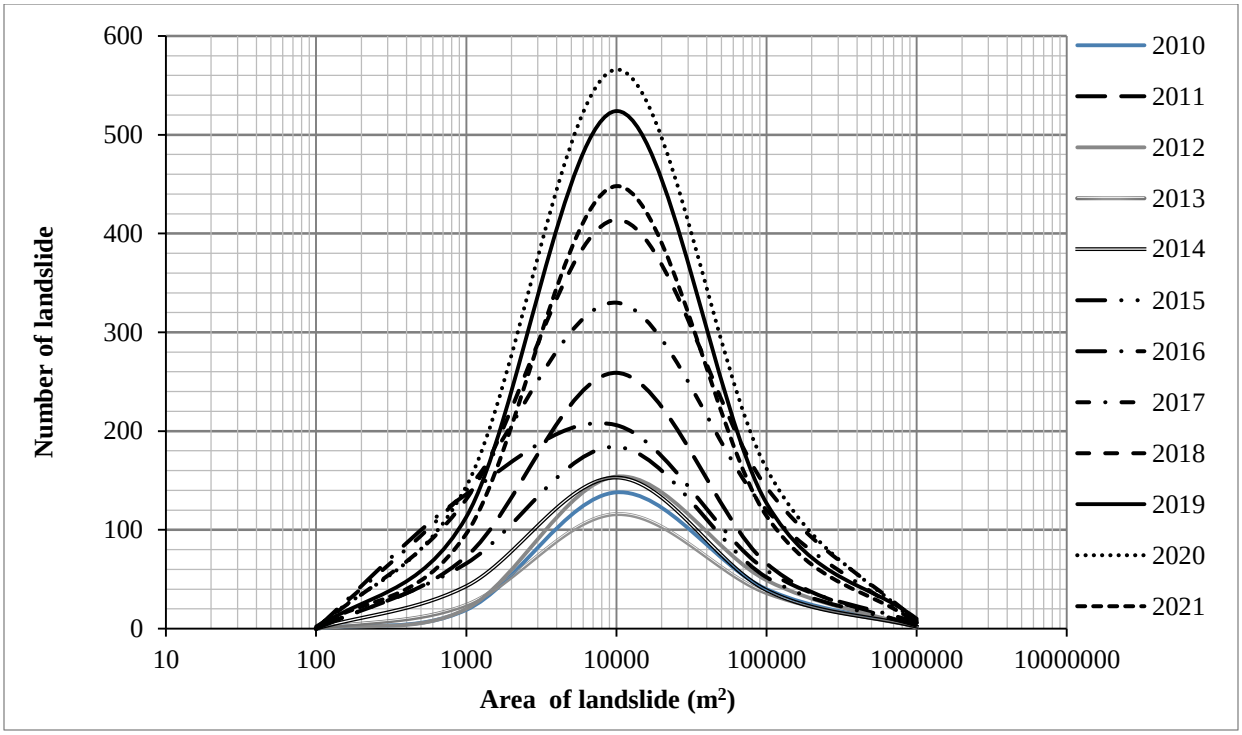


**Figure 40:** The area frequency relationship of landslides from 2010 to 2021.

### 4.1.3 Landslide susceptibility analysis

The susceptibility analysis of four bivariate models is presented below.

#### 4.1.3.1 Frequency ratio model

The frequency ratios of the sub-factors are represented in Table 18, and the susceptibility map for landslides that were derived using the frequency ratio model is displayed in Figure 41. As a result, if the weight is positive and the value is high, the landslide condition is favorable, whereas if the weight is negative. The value is low, indicating that the landslide condition is unfavorable. There is a considerable positive correlation between the total amount of rainfall and the area affected by landslides. The FR value increased to a higher level as the total amount of rain increased. The FR value of the water body and the areas of sparse vegetation is higher. The FR value of the southern aspect is greater than that of the northern aspect. The southwest aspect provides the most potential FR value. FR value

is at its peak when the NDVI is the lowest and when it is the highest. The FR value of a concave or convergent slope is much larger than that of a planar slope.

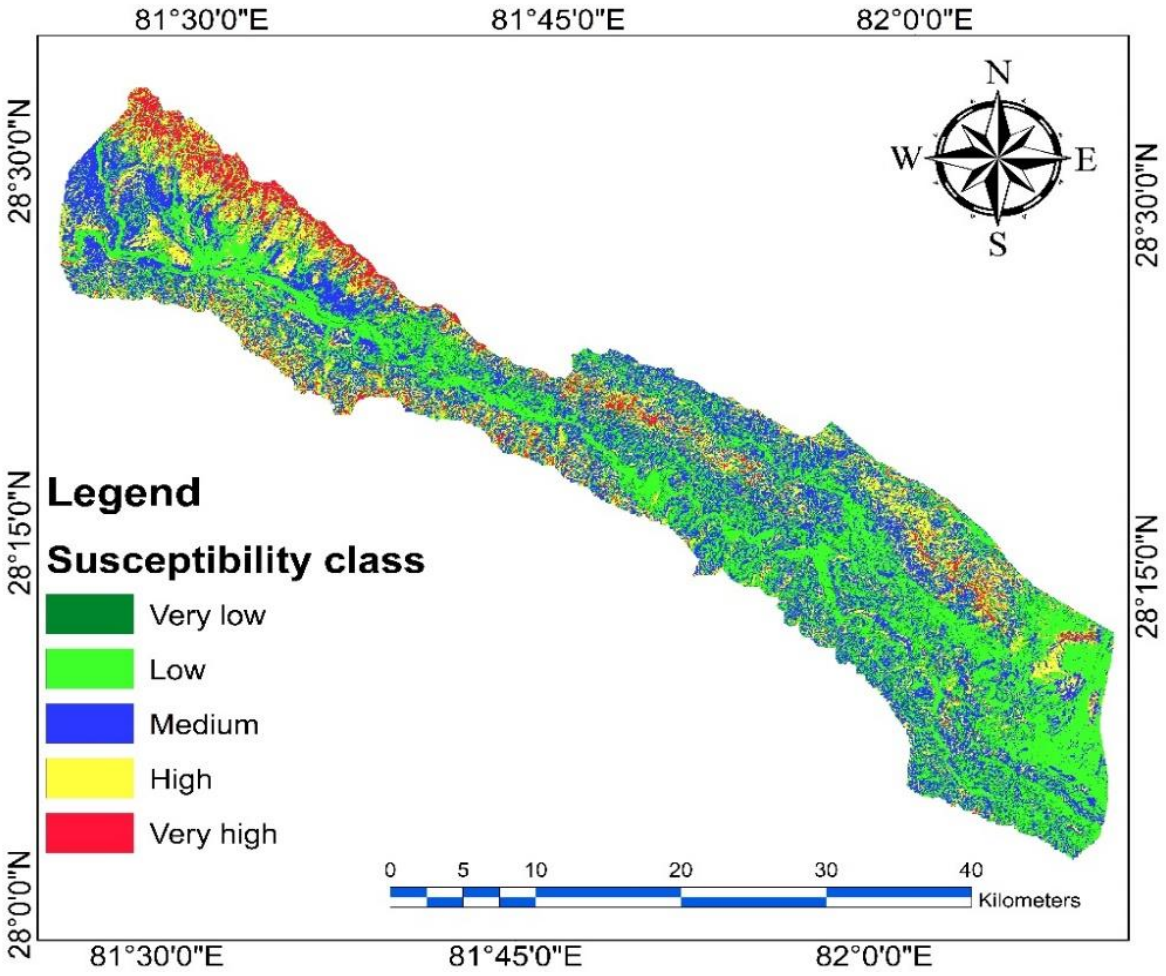


**Figure 41:** The landslide susceptibility distribution of the study area using the frequency ratio method.

Regarding its geology, the Middle Siwalik has an FR value noticeably higher than the Lower and Upper Siwalik. There is a statistically significant positive link between the hill slope and the FR value. The FR value rose higher as the hill's slope became steeper. When the topographical wetness index is at its lowest, the FR value is at its highest. There is a negative relationship between the distance to the road and the FR value, which states that the FR value will grow when there is less distance between the road and the landslide. There was a substantial positive correlation between the stream power index and the FR value. Similarly, there is an inverse relationship between the distance to the River and the

FR value. The value of the FR increased as the distance to the River decreased. Near the fault plane, the FR value has increased. The equation of final weighted value and secondary reclassified factors is shown in equation 33.

$$Y = Rainfall \times 15.54 + Landuse \times 7.38 + Aspect \times 7.46 + NDVI \times 324.04 + Profile\ curvature \times 3.92 + Plan\ curvature \times 4.08 + Geology \times 2.81 + Slope \times 332.14 + TWI \times 2.62 + Distance\ to\ road \times 2.37 + Relief \times 3.5 + Distance\ to\ river \times 9.3 + Distance\ to\ fault \times 5.5 + SPI \times 637.7. \quad (33)$$

The terrace, alluvium deposits, and plain lands are less susceptible, whereas forest areas are highly susceptible. Altogether, 21% area falls under a very high susceptible area, whereas 28% and 32% fall under high to medium susceptible areas.

#### 4.1.3.2 Weight of evidence model

The final landslide susceptibility map obtained using the weight of evidence model is shown in Figure 42. The result of the spatial relationship between landslides and conditioning factors is shown in Table 18. The WoE value is highest in the area with the highest rainfall. The old colluvium and alluvium have the highest WoE value. In the case of the slope, the WoE value is greatest at slopes greater than 60 degrees and decreases as the slope decreases. The results show that the occurrence of landslides increases as the slope increases. The WoE value is highest at the SE and SW aspects.

Landslides are more likely to occur in areas with a low topographical wetness index. Similarly, southern aspects are more susceptible to landslides. Landslides are very likely to occur in Middle Siwalik. The equation of the final weighted value and secondary reclassified factors is shown in equation 34.

$$Y = Rainfall \times 0.95 + Landuse \times 0.099 + Aspect \times 4.89 + NDVI \times -3.93 + Profile\ curvature \times 0.73 + Plan\ curvature \times 0.23 + Geology \times 0.006 + Slope \times 4.69 + TWI \times -5.33 + Distance\ to\ road \times -8.68 + Relief \times -3.64 + Distance\ to\ river \times -4.32 + Distance\ to\ fault \times -4.79 + SPI \times -4.36. \quad (34)$$

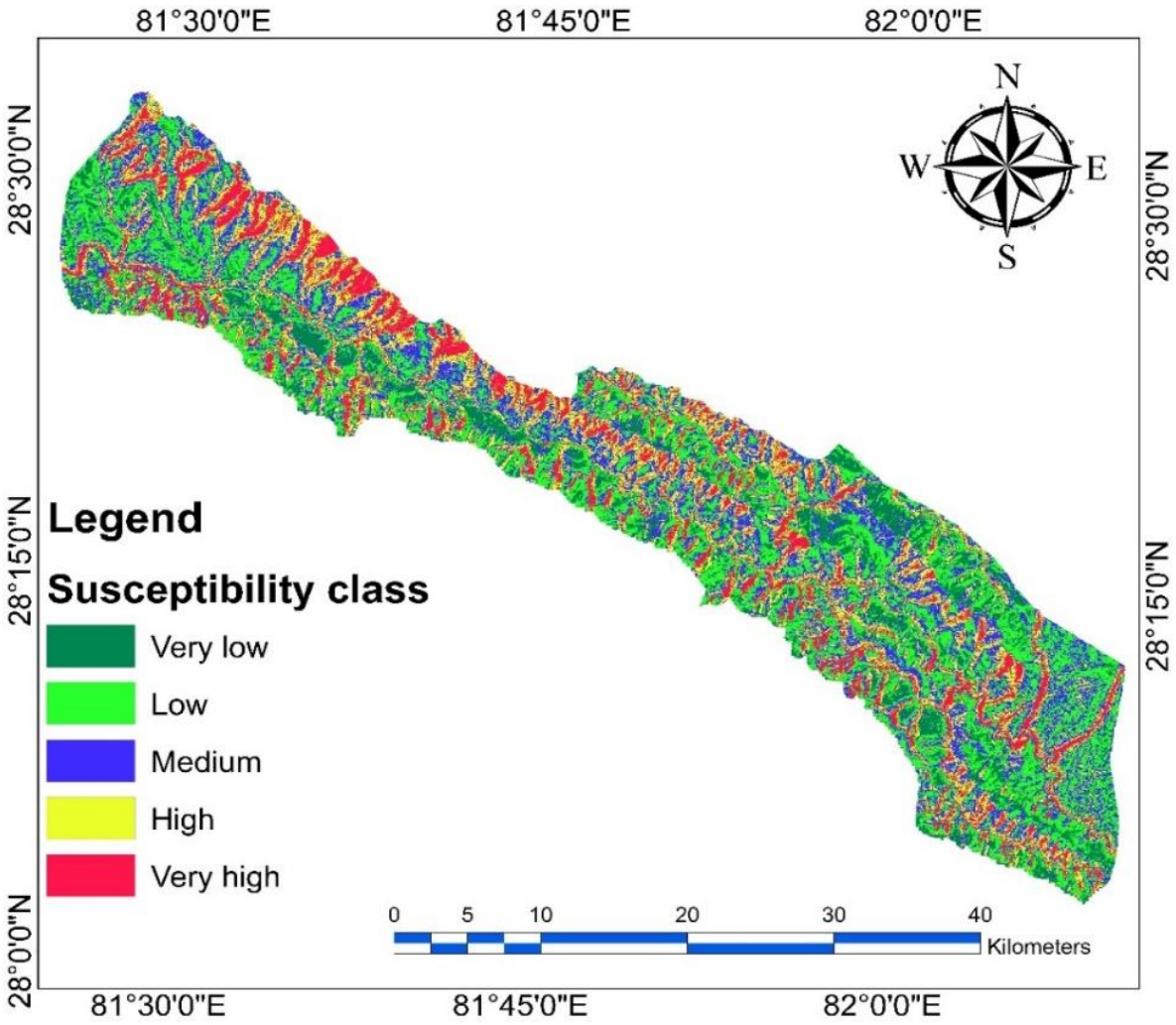


**Figure 42:** The map showing landslide susceptibility distribution using the weight of evidence method.

#### 4.1.3.3 Information value model

The final landslide susceptibility map obtained by using the information value method is shown in Figure 43. The information value analysis results show that landslide occurrence and rainfall amount are positively associated. The information value is higher in areas with higher rainfall. This model also showed that the southern aspect is more susceptible to landslides. Both convex and convergence slopes have a higher information value. The Middle Siwalik has a higher information value.

Similarly, slope gradient and information value showed significant positive relationships. The lower topographical wetness index has a higher information value. Likewise, the information value increases as the stream power index decreases. The distance from rivers shows that the information value increased with decreasing distance from the river. The final equation containing the weighted value and secondary reclassified factors obtained using the information value model is shown in equation 35.

$$Y = Rainfall \times 0.826 + Landuse \times 0.087 + Aspect \times -0.99 + NDVI \times 1.65 + Profile\ curvature \times 0.189 + Plan\ curvature \times 0.278 + Geology \times -0.181 + Slope \times 4.09 + TWI \times -0.94 + Distance\ to\ road \times -4.45 + Relief \times 0.005 + Distance\ to\ river \times 0.68 + Distance\ to\ fault \times -0.50 + SPI \times 2.98. \quad (35)$$

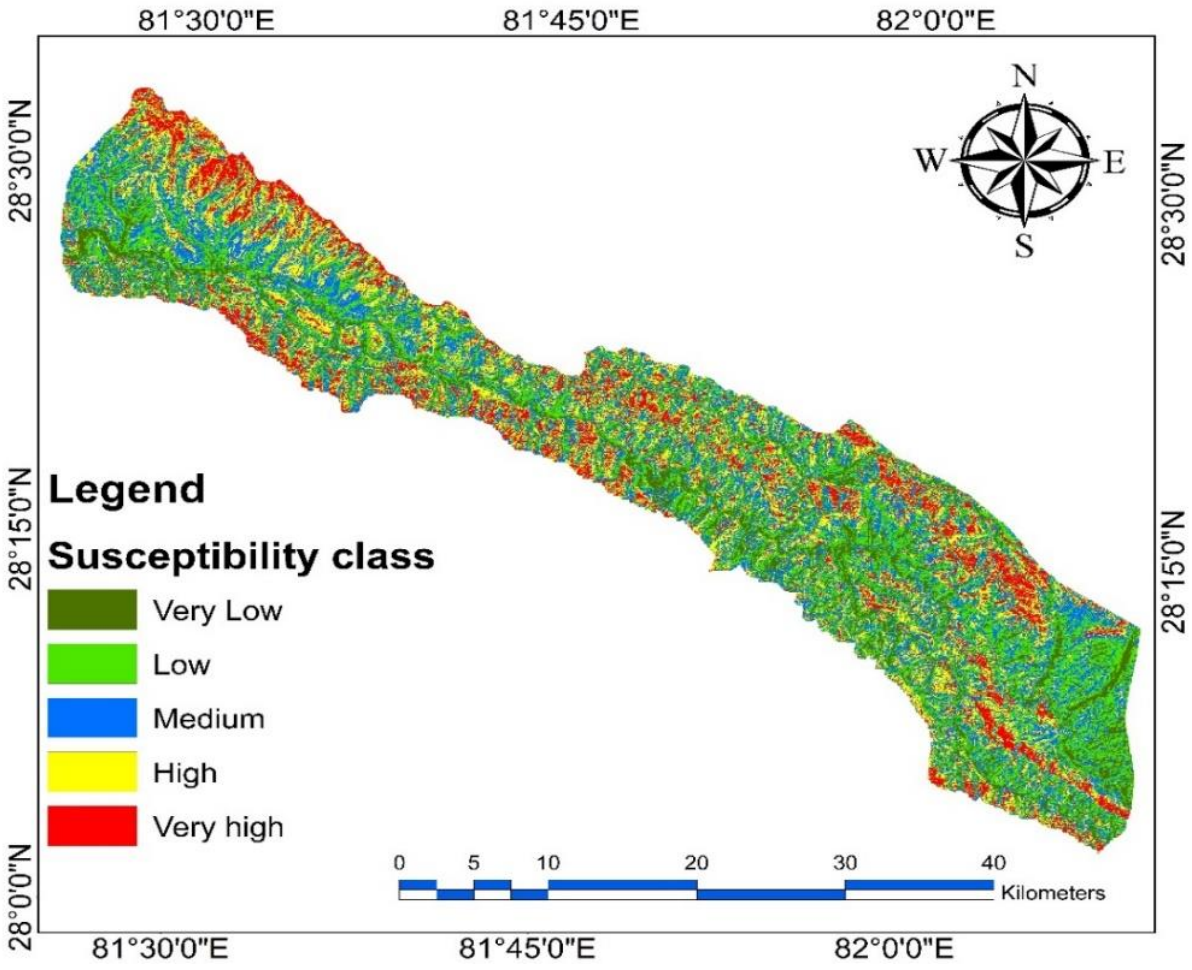


**Figure 43:** Figure shows the landslide susceptibility distribution by using information value method.

#### 4.1.3.4 Shannon entropy model

Table 18 displays the relationship between landslide and conditioning factors according to the Shannon Entropy model. The resulting map of landslide susceptibility is depicted in Figure 44. As seen in the preceding section, the Pab value for Shannon entropy grows as rainfall quantity increases. For land use, colluvium, and alluvium, Pab has a greater value. Land use has the greatest entropy. It indicates land use has the most significant influence on landslide occurrence, followed by precipitation, geology, profile curvature, and topographic wetness index. In terms of geology, the likelihood of a landslide is greatest in the Lower Siwalik, followed by the Middle and Upper Siwalik. In terms of slope curvature, concave slopes are more susceptible to landslides. The hill slope between 30 and 45 degrees is more prone to landslides. In locations with a lower topographic moisture index, the Pab value is greater. Similarly, the Pab value is greatest (0.15 at 0-100 m and 1.048 at greater than 500 m) at a distance of 0-100 m. In terms of distance to fault, the Pab value is greatest at a distance greater than 2,000 meters. The conclusion indicates that the hanging wall of the thrust is susceptible to developing a landslide.

Equation 36 depicts the final equation of weighted value and secondary classed components derived from the Shannon entropy model.

$$Y = Rainfall \times 0.066 + Landuse \times 0.260 + Aspect \times 0.051 + NDVI \times 0.053 + Profile\ curvature \times 0.056 + Plan\ curvature \times 0.055 + Geology \times 0.0559 + Slope \times 0.048 + TWI \times 0.0556 + Distance\ to\ road \times 0.053 + Relief \times 0.05 + Distance\ to\ river \times 0.055 + Distance\ to\ fault \times 0.052 + SPI \times 0.048. \quad (36)$$

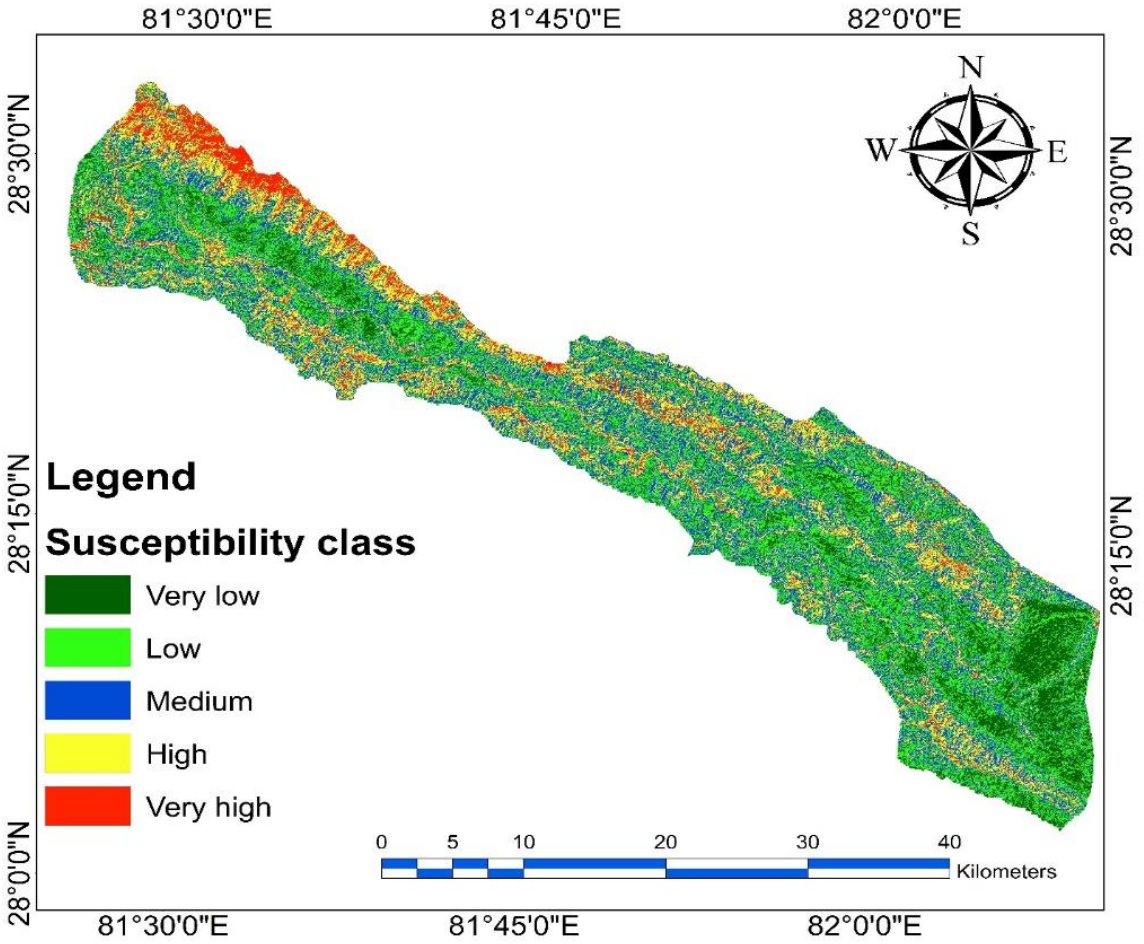


**Figure 44:** Landslide susceptibility distribution by using Shannon Entropy method.

### 4.1.3.5 Validation of the susceptibility

The results of the susceptibility class were compared and presented in Figure 45. The percentage of very high susceptibility is obtained from the information value method, whereas the low susceptibility percentage is obtained from the Shannon entropy model. Medium susceptibility is obtained higher from the information value model, weight of evidence model, and frequency ratio model, whereas low susceptibility is obtained higher from the Shannon entropy method. The result shows that the susceptibility distribution is more or less similar between frequency ratio, the weight of evidence, and the information value model however, the Shannon entropy model has a slightly different result.

The success and prediction rate of all four models are shown in Fig.46 (a, b, c, and d). The success and prediction rate of the weight of evidence is greater than the other three models. The success and prediction rate curves show that the weight of the evidence model has better prediction with the higher area under the curve (79.9%) followed by frequency ratio (75.3%). The prediction of the frequency ratio model was followed by the information value (74.4%) method, and Shannon entropy has the least prediction (73.2). However, the accuracy and prediction of the three models, frequency ratio, information value, and Shannon's entropy, are more or less equal.

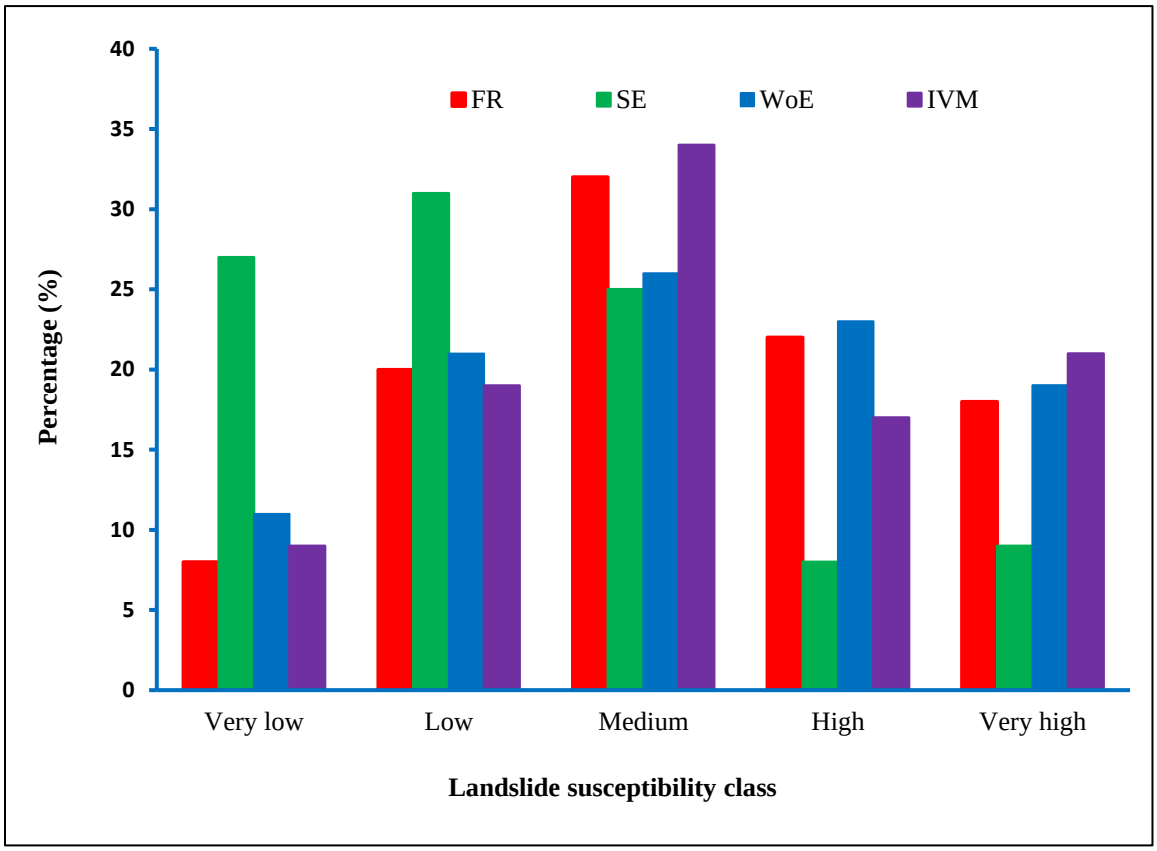


**Figure 45:** Landslide susceptibility class distribution of four different models.

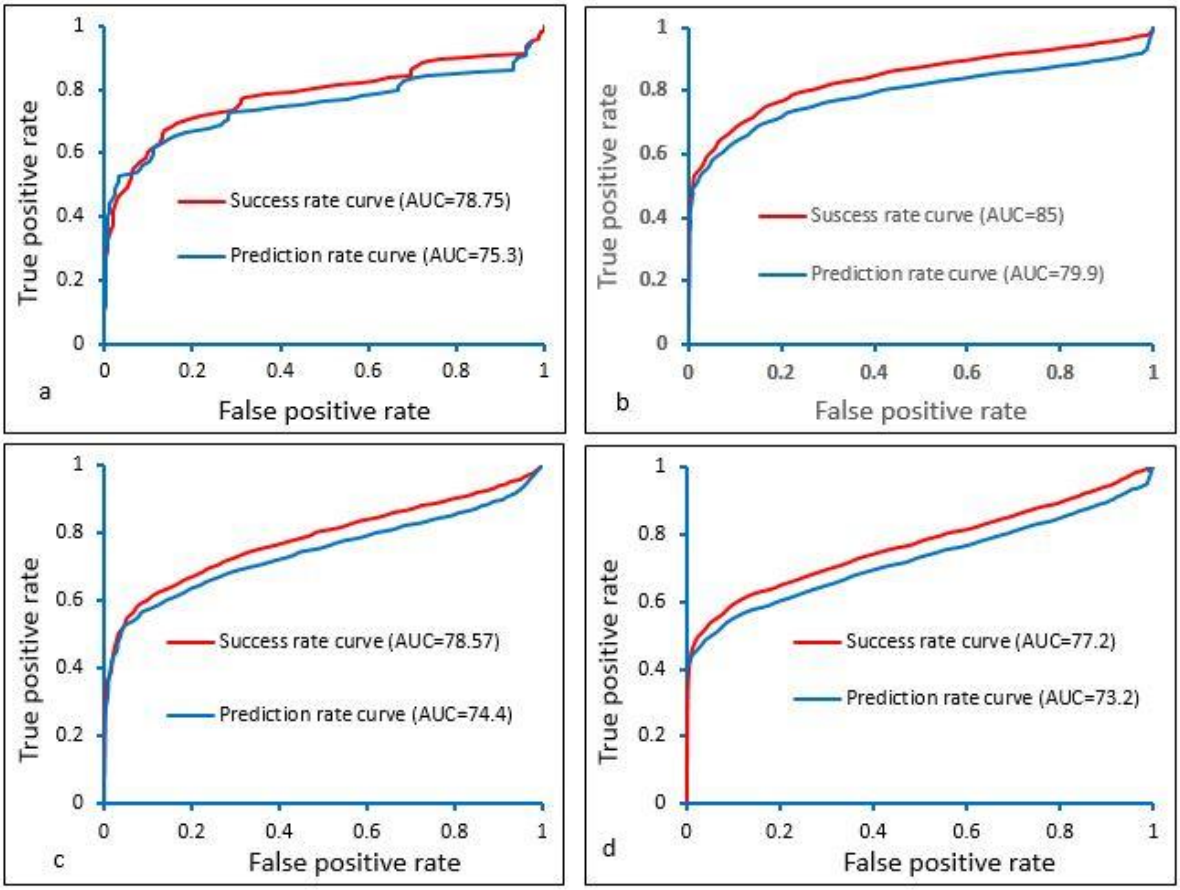


**Figure 46:** The area under curves shows the prediction rate of the susceptibility map produced by a) FR b) WoE, c) IVM d) SE models.

## 4.2 Discussions

### 4.2.1 Landslide characterization

Landslide characterization, hazard determination, susceptibility analysis, and landslide classification are essential for landslide management, mitigation, and risk reduction. Landslide characterization provides a general understanding of landslides of surface conditions, the role of surface materials, water, and other hydraulic activities. Similarly, landslide classification is another broad task for landslide study because the classification provides the ongoing status of landslides. The classification consists of size-based, state-based, material-based, movement-based, and mechanism-based classifications, ultimately essential for landslide management. Securing landslide susceptibility is another crucial

practical approach for landslide management (preparedness and mitigation). Landslide susceptibility provides information about the probable area and level of susceptibility, whether the area has high or low susceptibility to occur landslides.

There are various ways for landslide characterization. The study of the spatial distribution of landslides on topography is called topographical characterization. Studying the geological nature and distribution of landslides is called geological characterization. The hydrological, engineering and geotechnical, sub-surface and temporal characterization, and rock-soil-water interaction (chemical characterization) are crucial for landslide understanding. All characterizations are essential for landslide study; however, topographical, hydrological, geological, and geotechnical are the mostly applied and adopted characterizations (Ausilio & Zimmaro, 2017; Bhandari & Dhakal, 2021). The study area is divided into three geological units based on lithology and stratigraphy: Lower Siwalik, Middle Siwalik, and Upper Siwalik from bottom to top, respectively as shown in the Figure 4. This classification is also called the three-fold classification of Siwalik and has been proposed by various other researchers in the past (Medlocott, 1875; Medlicott & Blanford, 1879; Middlemiss, 1890; Blanford, 1883; Pilgrim, 1910; Gansser, 1964a; Auden, 1935; Hagen, 1951,1959,1969; Chaudhri, 1982). There are other various geological classifications of Siwalik; however, a three-fold classification is easier for the general people, planners, policymakers, and other concerned people associated with landslide management in the Siwalik hill of Nepal. Moreover, three-fold classification has a wide area of stratigraphy and lithology that can be recognized easily in the field. So, a three-fold classification is adopted in this study. The recent fluvial deposit of plain land is also included in our geological map and named the "Quaternary deposit."

The landslide distribution, initiation mechanism, and state of the landslide were studied in terms of geology. Comparing the number of landslides in the geological units, the Middle Siwalik has 589 landslides among 1140 landslides (Fig.9). In total, 51.6 % of landslides are present in the Middle Siwalik. The result is significant because composed of sandstone, mainly medium to coarse-grained, and a thin layer of mudstone or shale is present between the thick layers of sandstone. Due to various environmental assemblages, the weak shale

physically disintegrates or chemically decays, mainly in the monsoon period. Within the long-term monsoon period, the shale or mudstone undergoes weathering and erodes. The layer between thick sandstone beds became open and caused to increase in infiltration rate. Interaction of heat and water, increasing gravity due to steep slope and losing the support of shale between the thick beds cause physical weathering on the rock mass. More than 22% area of Middle Siwalik lies on a slope greater than 30 degrees, so the rate of erosion increases.

Similarly, the newly formed soil reduces the cohesion and angle of internal friction in the saturation state so that the landslide process begins. Due to this mechanism, small to large landslides occurred in the Middle Siwalik. Comparing the total area of geological units, the Middle Siwalik occupies 61.33 % of the study area. It also might be the cause of a large number of landslides in the Middle Siwalik. The thick forest on the rocky slope also may cause landslides in it. The number of medium-sized (1000-10000 $m^2$) landslides is significantly higher in each geological unit. Massive landslides are limited in the study area because the length of the hillslope is less in the Siwalik Hills. The elevation of Siwalik ranges from 109 m to 1550 m. The maximum relative relief of the hill slope is only 427.16 m. It indicates that the maximum distance that a landslide can travel is less than 427 m. So massive size landslides are rare. Similarly, in the low relief area, landslide does not occur. The highest relief and slope angle are higher in the Middle Siwalik. Due to these reasons, the Middle Siwalik has many large landslides. The lower Siwalik comprises variegated mudstone, brown shale, and greenish-grey sandstone. Lower Siwalik's rocks are weak, fragile, and easily breakable. The concretion and spheroidically weathered rocks are present in the Lower Siwalik. Most rocks are weathered, decomposed, and developed as residual soil. Head erosion is the main problem of Lower Siwalik. Mudslides, mudflow, and erosion-induced landslides are mainly distributed in the Lower Siwalik. Most landslides begin from soil erosion and later on converts into landslide (Fig.10 a & b).

The highest number of landslides are on the slope between 15-45 degrees. Some previous researchers noted that the number of landslides increases with increasing hill slope. However, in this study, we noted that landslides are less on the slope, less than 15 degrees,

and greater than 45 degrees (Table 4). The vegetation cover is very thick at the slope, with 15–45 degrees. As the slope increases, the thickness of the soil decreases. Additionally, there is less of a cover of plants on the steep hill. As the slope increases, more water will run off the land, which will cause less water to percolate into the ground. The majority of erosion and gully formation is caused by runoff from the surface. On the steep slope, rock fall and rock slide are mainly distributed. The highest number and area of landslides are noted in the southern aspect. The sunlight exposes more time to the southern aspect than the northern aspect. Various researchers pointed out that the southern aspect of Nepal is highly susceptible to landslides than the northern aspect (Dahal et al., 2012; Regmi et al., 2014; Devkota et al., 2013; Pokharel & Bhandari, 2019; Thapa & Bhandari, 2019). Similarly, the rainfall pattern is higher on the southern aspect of Nepalese hills. Continuous shrinkage and swelling of ground materials may lead to a landslide on the southern aspect.

Curvature is considered one of the most responsible topographical factors for landslide occurrence. Plan and profile curvature were taken for topographical characterization. In the case of profile curvature, the concave slope has the highest (53.43%) landslide, whereas, in plan curvature, the planar surface has the highest landslide. The field observation shows that the result is valid and acceptable. Very few landslides were noted on the convex slope. Topographical wetness index and landslide events have a negative relation to each other. The area of landslides decreased with an increasing topographical wetness index. The index value is a function of the slope and the upstream area per unit width perpendicular to the flow direction. Similar results were obtained by previous researchers in the Hills of Nepal (Devkota et al., 2013; Dahal et al., 2013; Dahal, 2012; Ghimire, 2017). TWI is commonly used for quantifying topographic control on hydrological processes.

The topographical factor "T," which is utilized for determining the topographical control on landslides, has been the subject of contemporary research and discussion. Analysis of landslides, forests, debris flows, and erosion modeling can make use of this relations and calculation approach for the T factor. The findings indicate that the T factor has a substantial positive link with the number and the area of landslides. There is a correlation

between the T value and the number of landslides (Fig.17). When looking at the T factor in the various geological units, the Middle Siwalik has a value that is noticeably higher than the others. The prior result demonstrates that the Middle Siwalik has the most significant number of landslides (Table 5).

The Himalayas have a significant relationship between hydrological activities and landslides. The result shows that long-term rainfall substantially affects the formation of landslides. There is a considerable positive relation between the total annual rainfall and the total annual landslide. According to the data collected in real-time, the landslide occurred after a few days of intense rainfall, and it occurred most frequently in July and August. In Nepal, the monsoon season typically begins at the end of May. According to previous research findings, the frequency of landslide incidents peaks toward the end of the monsoon season. Compared to the number of landslides that occurred during the early monsoon period, the number of landslides that occurred during the late monsoon period was significantly higher. After analyzing the soil's geotechnical properties, the outcome will become more evident.

Similarly, the spatial study of rainfall and landslides reveals that the area of landslides is more significant in the areas with higher rainfall. The twenty-year annual average rainfall at seven different locations ranged from 2148 to 2392 millimeters. For the cross-tabulation, the minimum-maximum range was divided into seven various subclasses. According to the findings of the frequency ratio study, the highest rainfall class (2357-2392 mm) has the highest FR value (Table 9). This interval has a deficient pixel class but a higher landslide area than the preceding and following intervals. Overall results show a positive correlation between rainfall and landslide occurrence. The drainage to distance map was divided into six subclasses, with a distance interval of one hundred meters between each class. It was determined that the closest distance was less than 100 meters, and the farthest distance was greater than 500 meters. According to the distribution of landslides, the frequency and area of landslides are much larger in the areas closer to drainage. Similarly, the frequency ratio is highest for the near distance. Because the concave slope has a substantially higher FR

value, and the drainage is obviously on the concave slope. The curvature result and the drainage result are very identical to one another.

Some of the most critical soil properties were found for the geotechnical characterization of landslides. Soil characterization and classification are both essential for understanding landslide soil. The Casagrande plasticity chart, composition analysis, and particle size analysis were used for soil classification. The phase relationships, as well as its shear strength parameters, were obtained from the laboratory test. The results from a ternary diagram, a Casagrande plasticity chart, and a sieve analysis are all similar. Three tests show that the area primarily has CL-type soil, meaning fine soil (Fig. 21, 22 & 23). Based on sieve analysis, 64 of the samples are poorly graded, and the soils are mostly made up of fine particles.

Compositional statistics and soil classification show that the soils are predominately fine (Fig. 24 & 25). In the same way, the compositional statistics show that the silt-clay log ratio has the highest variation. The highest variance of the log ratio is responsible for landslide occurrence. Silt-clay has a log ratio variance of 0.425 (79%), while sand-clay only has a log ratio variance of 0.28 (Table 12). Also, the clr variance for silt-clay is 64% and 56% for sand-clay. Most of the landslide mass is made up of the disturbed soil at the surface of the slide. By analyzing these materials in a lab, it may not be possible to understand the landslide's index properties and shear behaviors fully. In this study, the soil samples were taken from the undisturbed area after removing the surface soil from the landslide scars. However, the study area is disrupted and fragile because of three main geological thrusts. A widely used direct shear test was conducted to analyze the shear behavior of soil. Since many of the landslides occurred on steep slopes, it is hard to get soil samples from the scar of the landslide. Soil samples were taken during the dry season to avoid these problems. To understand the behavior of landslide soil, the knowledge of shear strength parameters and the deformation nature of the soil is necessary. Therefore, the traditional consolidated drained direct shear test was conducted for shear behavior analysis of landslide soil. The shear stress versus horizontal displacement curve was obtained at the natural moisture content. The curves and significant peaks were compared

between three geological formations (Fig. 26, 27 & 28). The landslides of Lower, Middle, and Upper Siwalik were named type I, type II, and type III, respectively, for easier understanding and analysis. The shear stress versus horizontal displacement curve of three types shows that the type I and type III landslides have no significant peak. The result indicates that Lower and Upper Siwalik soils are soft and not stiff. The shear stress versus horizontal displacement curve of Middle Siwalik soils shows a significant peak at 20, 40, and 60 kPa normal stress. The soils of Middle Siwalik are stiff.

As per the previous discussion, the number of erosion-induced landslides in the Lower and Upper Siwalik is more significant, whereas erosion-induced landslide is negligible in the Middle Siwalik. The Upper Siwalik is composed of several layers of red color soil between the conglomerate beds, and these layers of soil are soft and cause frequent erosion in the long-term rainy season. The erosion rate is low in stiff soil and high in soft soil.

Derbyshire et al. (1994) and Chen et al. (2021) investigated the shear behavior of a slip surface on Chinese loess soils and concluded that a reduction in shear strength from the peak could imply a loss of structural strength in undisturbed loess soil. The reorientation of clay particles during shearing could cause a considerable decrease in shear strength from peak to residual conditions, as noted in prior studies (Skempton, 1985; Li et al., 2017; Tika et al., 1996). The decrease in soil cementing capacity is responsible for the considerable changes in cohesiveness between peak and steady-state (Chen et al., 2021). Zydron and Zawisza (2011) researched soil shear strength in the landslide area of southern Poland. They discovered that moisture content in the soil causes a drop in cohesiveness and angle of internal friction, resulting in a reduction in peak shear strength. The moisture content is also affected by the presence of clay or silt.

Similarly, the clay minerals in the soil, and the kinds of clay minerals, determine the soil's residual shear strength (Dimitriova and Yanful, 2012: Skemton, 1985; Michell, 1993; Tiwari et al., 2005; Chen et al., 2021; Morrow et al., 2000). The plasticity chart of Figure 22 shows that the clay-rich soil is dominant in the study area. As discussed earlier, the Siwalik soils have a larger clay and silt component. The identification of the types of clay minerals present in the soil was not included in this study. Fine soil particles (clay and silt)

predominate in the soils of the study area, which could be the reason for residual shear strength in type II landslide soil. Igwe et al. (2006) discovered a link between the coefficient of uniformity and sand shear strength, finding that raising the uniformity coefficient enhanced the peak and steady-state strength of the sandy soil.

The mean shear strength is higher in type II landslides associated with the Middle Siwalik (Table 13). As mentioned in the geology section, the Middle Siwalik comprises an alternate layer of thickly bedded sandstone and a thin layer of clay-bearing shale. The soils of Middle Siwalik are comparatively compacted and tightly packed, due to which the peak to residual shear strength is obtained in the type II landslides. In the case of Upper and Lower Siwalik, the soils are loose, less compacted, and easily erodible in the Monsoon period due to the continuous action of rainwater. Because of these reasons, the residual shear strength could not be achieved in these geological units. The Middle Siwalik soils are, therefore, more compact than the Lower and Upper Siwalik soils. Table 1 shows that the shear strength parameter (cohesion and angle of internal friction) has a wide range of variation, with coefficients of variance of 42.96 and 12.05, respectively.

We investigated the relationship between shear strength parameters and the types of landslides in this work. The relationship between shear strength and potential variables was discovered. The difference in the mean values of shear strength, cohesion, and angle of internal friction in the three types of landslides was shown to be substantial. The Middle Siwalik has a much greater mean shear strength. Because the Middle Siwalik's soils are compacted with a low void ratio, the average shear strength value is higher. The soil moisture content in a type II landslide is lower than in a type I landslide (Table 14). The average cohesion and internal friction angle are higher in the Middle Siwalik. The study shows an inverse relationship between the moisture content and cohesion; however, the $R^2$ value is a low and low degree of significance.

Dijkstra et al. (1994) researched the loess soil of North-Central China about the geotechnical properties of slope soil. They depicted that the cohesion of soil slightly increases with increasing moisture content. However, the cohesion decreases after a certain

threshold of moisture content. Chen et al. (2021) also discovered that the fine soil's cohesion reduces when the moisture content rises. However, in this study, the direct relation between moisture content and cohesion of overall soil samples was obtained and showed positive relation. Analyzing the cohesion into different moisture levels of the same soil sample is beyond the scope of this study. Also, the internal friction angle has an inverse relationship with moisture content. Middle Siwalik is primarily located on the Babai and Bheri thrust's hanging wall. Due to its unique tectonism, the Siwalik zone's hanging wall of thrust is more sensitive than the footwall (Bhandari & Dhakal, 2020a). The cause of active landslides in the Middle Siwalik is the activeness of thrusts along the study area. The plasticity index has a greater mean value in type I landslides but a lower mean value in type II landslides. Because the mudstones of Lower Siwalik are made up of fine-grained silt and clay, the mean plasticity index in Type I landslides is higher. The research is centered on the shear behavior of landslide soils. A variety of other geotechnical factors influence landslide initiation.

Shear strength is one of the most fundamental and crucial geotechnical metrics for describing the mechanical characteristics of soil that determine the slope's stability. The laboratory examination yielded the shear strength parameters, the void ratio, plasticity index, moisture content, specific gravity, and dry unit weight of soil. As a result, the relationship between shear strength and other geotechnical parameters was shown. The multiple regression model for shear strength was initially set up with eight predictor variables. The non-significant factors were eliminated, leaving just the highly significant variables for the final model with the greatest fit. Borecka et al. (2006), and Yalcin (2011), Zydron & Zawiswa (2011) found that increasing shear strength was associated with an increase in cohesiveness. The results reveal that as the cohesiveness and angle of internal friction rise, the shear strength increases dramatically. There are a few more factors that may have an impact on shear strength. The penetration and strengthening of the activity of tree roots can significantly boost shear strength, especially in the case of shallow slip surfaces (Fleming & Johnson, 1994; Turner, 1996; Schmidt et al., 2001; Sidle & Ochiai, 2006). Because larger clay fraction soil expands faster, it is more susceptible to landslides (Mugagga et al., 2010; Yang et al., 2007; Kitutu et al., 2009; Wati et al., 2010; Ohlmacher,

2000; Yalcin, 2011; Bhandari & Dhakal, 2020b). In clayey soil, the voids allow water to travel slowly, while clay traps and stores the water for longer. The fine clay blocks the drain at the bedrock's base, which causes the clay to retain and store water. This mechanism resulted in increased pore pressure, which led to causes landslides (Wati et al., 2010; Yalcin, 2011; Mugagga et al., 2019). Because of their strong water-holding and blocking capacity, clayey soils with fine texture have numerous microscopic holes and gradually release water, making them more susceptible to landslides on the soil slope. The soil from landslides in the Babai River basin includes clays and silts of medium plasticity, according to Bhandari & Dhakal (2020b). Due to the drop in shear resistance, highly flexible soils are prone to sliding during rainstorm events, according to Dai et al. (2002). A large number of landslides were encountered in the forest area.

The value of the specific gravity of some soil is nearly 2, indicating that the soils are organic or mixed. The soil of the forest area could be organic soil. However, even if the soils are of medium plasticity, the shear strength of the soils reduces during the wet season. The study's main finding is that in the soils of type II (Middle Siwalik) landslides, mean shear strength and shear strength parameters are much higher. The main source of landslides in the Lower and Upper Siwalik is soft soil that erodes from rainfall. The regression analysis further supported the relationship between shear strength and other geotechnical features. The findings were based on partially or unsaturated (dry soil) samples gathered during the dry season. During the monsoon season, increased moisture content directly impacts soil cohesiveness and the angle of internal friction, resulting in a decrease in shear strength. The regression analysis showed that as the void ratio and plasticity index increase, the shear strength drops down. Long-term rainfall (total yearly rainfall) is more effective than the maximum 24-hour rainfall for the incidence of landslides in Siwalik hill, according to Bhandari & Dhakal (2020a). According to the result, clay-rich soil loses cohesiveness and shear strength at saturation levels with prolonged rainfall during the monsoon season, leading to landslide processes.

Many researchers studied the preexisting shear surface's residual shear strength and found that the shear surfaces of old landslides have a higher shear strength than the drained

residual value, and the slope becomes stable (D'Appolonia et al., 1967; Ramiah et al., 1973; Gibo et al., 2002; Carrubba & Fabbro, 2008). The shear strength value is lower in active landslides, and the sliding surface is unstable. The current study's findings are comparable to those of the previous research. Many other elements, such as soil types, index characteristics, pore pressure, groundwater level variations, chemical reaction, occurrence state, and environmental circumstances, affect soil shear strength (Cernica, 1995; Morrow et al., 1982; Skempton, 1985; Wen & Aydin, 2004; Mugagga et al., 2010; Benac et al., 2014; Zhou et al., 2016). This study shows that the shear strength is controlled by dry density, cohesion, plasticity index, degree of saturation and angle of internal friction. Many slope failures occur due to soil saturation caused by seepage (Rahardjo et al., 2010). Furthermore, the relationship between the shear strength and coefficient of uniformity (Cu) of 120 soil samples was obtained. The result shows that the strength increases with an increased coefficient of uniformity. Shear strength showed negative relation with void ratio. The void ratio is less in the type II landslide, indicating that the soils are well-graded. Igwe et al. (2007) also identified the positive relationship between shear strength and uniformity coefficient of landslide soil.

### 4.2.2 Landslide classification

Previously, many researchers proposed a landslide classification system. The classification of Baltzer (1875) was based on the body's motion, like fall, slide, and flow. Heim (1933) proposed the landslide classification based on the type of materials. Stini (1910) identified the various debris movements in the Hills. Bull (1964) termed the name "mudflow" in the arid region of southwestern USA. As mentioned in the literature section, various classification systems have developed worldwide for a long time. The classification based on the materials and movement is the best. However, the types of materials and movement may not provide detailed information on the landslide mechanism. Landslide mitigation is challenging in the Siwalik Hills without understanding the landslide mechanism. Rockfall is a type of landslide, but the mechanisms of rockfall are different. Rockfall may be structural control, tectonic control, or topographical control. The classification of Varnes (1964) and Cruden & Varnes (1996) has to be clarified. Complex is a confusing word, and

it has no limitations. The landslide movements and materials may have different origins and ends; for example, the mudslide may convert into mud flow.

Similarly, rockslides may convert into a debris flow. Providing the name complex is not perfect for landslide classification. So, in this study, the mechanism-based landslide classification is developed. The five classes of landslides are proposed namely; Type 1, Type 2, Type 3, Type 4 and Type 5 (Fig.31 & 32).

The landslide name is given based on the landslide development process and mechanism. In the type 1 model, the thick sandstone layer loses support on the steep slope after eroding the thin layer of shale. The wide and massive sandstone beds fall or slide due to this mechanism. Type 1 landslides are widespread in the Middle Siwalik and Lower Siwalik. Type 2 landslides are initiated after head erosion with a small and narrow scar. After the continuous erosion process, a large number of debris is transported from the hill slope and covers a large area on the downslope. This type of landslide causes massive fan deposits at the gentle slope. The type 3 model initiates the landslide in the conglomerate bed. The cementing material erodes due to its loose binding mechanism. After eroding the binding materials, the large block of conglomerate bed dissociates into several debris masses and flows down with rainwater. This type of landslide also creates debris flow, resulting in debris fan deposits.

The type 4 model is related to the thrusting and faulting mechanism. The hanging wall of thrusts is found fragile. The rocks are highly jointed and weathered. Due to that, several landslide activities are widespread in the thrust zone. The type 5 model explains the landslide initiation on the slope having old colluviums. Most of the Siwalik Hills have been affected by landslides in the past. The hill slope is covered by colluviums and later covered by thick or partial vegetation. The tall trees are prevalent on colluvium deposits. However, the colluviums consist of steeply dipping bedrock slides due to overload at saturation. Due to that, landslides are common in the forest area in the entire Siwalik hill. The landslide size distribution shows that the landslide size varies from very small to very large. Some landslides are very small, with an area of less than 100 $m^2$, and some are very large, with a

size greater than 1000000 $m^2$. The size-based classification is proposed based on a logarithmic scale to summarize all the landslides on the same scale. It is very easy to classify the landslide, many of which can be included in the same scale. The landslides with areas less than 100 $m^2$ are very small, and greater than 100000 $m^2$ are very large. This classification is accessible for every sized landslide and easier for all the researchers. The state of activity of landslides is divided into five types, namely new, active, inactive, reactivated, and mitigated. WP/WLI (1993) classified the landslide based on the activity state. In that classification, active landslide means the landslide which is currently moving. In many places, a landslide occurs every season, either dry or wet. However, in the case of Nepal, the landslide mainly occurred in the rainy season. The researcher may study the landslide in the winter season (dry season). So, to make the classification clearer and more specific, new definitions are proposed. If the preexisting landslide is moving every year and the movement has occurred in the last 12 months is proposed to say "active" landslide. Similarly, the term "new landslide" is added to the classification. The landslide that occurred last year or this year is called a new landslide. Furthermore, a landslide initiated within 24 months is called a new landslide. If the landslide of last year moves again this year, the landslide is a new one, whereas if the landslide occurred three years ago and moved every year, the landslide is active. The inactive landslide is the landslide that is not been moving for the last 36 months, and there is no particular symbol to activate again. The Siwalik Hills are fragile, so after the landslide, it takes a minimum of two years to regenerate vegetation and seems new and fresh. The vegetation begins to grow from the various parts of the landslide body. Scar seems going to disappear, and tension crack or any rupture do not appear.

The mitigation is either natural or artificial. The reactivated landslide can be easily identified in the field and the image. The temporal series imageries are used for the reactivated landslide in the image. The materials of the new landslide and surface near the recent landslides are the most crucial evidence to recognize reactivated landslides. The old colluvium, rocky slope in the middle of the forest, different vegetation, discontinuous forest, and slope are some evidences of old and stabilized landslides. The stabilized landslide may be covered by forest, settlement, agricultural land, or road and infrastructure.

Sediment analysis, boulder analysis, vegetation differences, and slope discontinuity can be evidence of landslides.

### 4.2.3 Susceptibility analysis

The next objective of the study was to evaluate each causative factor in landslide susceptibility in the Siwalik Hills of Nepal and compare four models of the spatial probability of landslide occurrence using FR, SE, IVM, and WoE models. The four models were based on integrating fourteen weighted causative factors and a landslide spatial inventory.

There are various steps for landslide susceptibility analysis. The susceptibility analysis begins from the landslide inventory map because "the past is key to the future." After the landslide inventory map, the selection of landslide causative factors is the most critical part (Xie et al., 2015). After factor selection, cross tabulation and pixel calculation of sub-factors and landslide pixels in each sub-factor is another step. The appropriate model should be selected for better prediction of the result, so comparing the result of more than two models is essential for better model selection. Finally, the validation of the result should conduct for the model accuracy. A prediction rate of more than 50% can be accepted, and a more than 80% accuracy rate is a more accurate model.

The intense field study showed that the soil thickness factor has no significant effect on the landslide occurrence in the Siwalik. The impacts of colluvium thickness were noted in the case of colluvium deposit; however, the correlation is negligible. Similarly, the relation between elevation and landslide occurrence has no significant correlation. This result may be due to rocky cliffs and bedrock outcrops at the peak or high altitude (Mohammady et al., 2012), so the elevation and soil thickness is excluded from the mapping process. The accumulated effects of various factors may change the level of susceptibility. Generally, the landslide susceptibility increases with increasing slope. In this study, the number of landslides is higher at the slope between $15^{o}$ to $45^{o}$ based on spatial analysis; however, the slope greater than $45^{o}$ is highly susceptible based on susceptibility models. However, models give the result based on the sub-factors and the area of the landslide at the factors.

The shear stress (driving force) rises with increasing hill slope, so the landslide susceptibility increases. In the rainy season, the rock and soil lose the angle of internal friction and material cohesion, which causes to decrease in shear strength. Similarly, the load of material mass increased due to high moisture. Due to this reason, the slope materials slip or slide down. The result shows that the hill slope is crucial in controlling landslides. Previous researchers considered a terrain slope as one of the most effective geo-environmental variables used for susceptibility modeling (Carrara et al., 1991, 1995; Fabbri et al., 2003; Budimir et al., 2015).

In the case of the slope aspect factor, the susceptibility is higher in the SW and SE aspects. The cause may be the flow direction of the river. The river flow direction in the study area is Northeast to Southwest. Due to flow accumulation and direction, the water discharge may cause the toe cut and surface erosion. Due to continuous erosion, the surface becomes concave, and as discussed earlier in the topographical section, the concave slope is more susceptible to landslides. Another cause is rainfall patterns. The rainfall rate is higher in the southern aspect than in the northern aspect of the Nepal Himalayas. The sunlight falls more time on the southern aspect than the northern aspect. The hydraulic action and continuous fall of sunlight may cause environmental alteration of the slope materials and which may ultimately cause soil erosion and landslide. The lateral erosion caused by the river at the meandered area (cut slope) occurred on the side of the SW and SE aspects.

The lithology includes rock composition, texture, or other attributes influencing rocks and soils' physical and chemical behavior. They are essential to determine the shear strength parameters, permeability, and other characteristics of the soil and rock materials. These characters affect the slope stability (Verne's 1984). The Middle Siwalik has the highest susceptible class and more than 25 % land surface with a slope greater than 45$^{o}$. Sparse vegetation covered on the steep slope may be another cause to occur landslides in the Middle Siwalik. For the land use factor, the sparse forest is the most susceptible. It is because the sparse vegetation is found on the steep slope and at the Middle Siwalik. As mentioned above, the steep slope and the Middle Siwalik have higher landslide susceptibility. In the case of rainfall, the classes with high rainfall were more susceptible.

As discussed, water is one of the cru factors to cause a landslide. Water causes some effects on the soil, such as pore water pressure, swelling of clay minerals, and increasing the weight of slope materials which may lead to landslide initiation on the hills. The water plays a lubricating effect on the sliding surface so that a landslide may occur on the slope (Varnes, 1984).

The frequency ratio, Shannon entropy, and information value are higher at the lowest and highest NDVI values. Similarly, we found a higher NDVI value in the landslide-prone area. The NDVI value is noted higher in areas with high precipitation and closer to the river. Mostly, the vegetation can be grown in a suitable environment, and sufficient moisture soil is one of the essential factors for the growth of the plants. So that the NDVI is the higher near distance to drainage, and more importantly, the area near distance to drainage and higher precipitation is highly susceptible, as mentioned previously. In the case of road distance, the near distance to the road has a high FR value, whereas the highest distance from the road has the highest value with the weight of evidence, Shannon entropy, and information value method. The near distance from the road is susceptible due to the natural slope destruction and improper land use management during road construction. The improper deposition of slope cut material during road construction also may cause landslides at the downslope of the road. The road distribution is limited in the study area. The impacts of road construction are seen in less area, so most of the landslides are noted far from the road.

One of the frequent distance variables utilized in susceptibility modeling is the distance to faults (Süzen & Doyuran, 2003). If the region is a tectonically active zone and the fault size is large enough, the result will be more accurate. Furthermore, a fault zone and the area surrounding the fault may respond differently to an earthquake. In the same fault zone also, all faults may not respond equally, and seismic triggers may be different in the different faults (Reichenbach et al., 2018). Due to this reason, including distance to fault in the landslide susceptibility is challenging. There is an unclear relationship between the distance to fault and landslide occurrence. The far distance from the fault is more susceptible than the near distance. It simply means there may be the influence of other

factors on landslide occurrence in this area. In logical thinking, the area nearby the fault may be highly susceptible to landslides; however, some factors may not show a good correlation with landslides due to the greater influence of other factors. During the field visit, the area near the fault plane was noted as a more prone area, so the distance to the fault was not excluded from the mapping. There are various models for landslide susceptibility. Here the four models of bivariate statistics are used. These four models are widespread and broadly discussed susceptibility models, so the accuracy and prediction of these models are compared. The FR model is a widely used landslide susceptibility model, which is easier to use and interpret the result (Lee & Pradhan, 2007).

The literature shows that among the 200 papers related to landslide susceptibility published in the index journal from 2000 to 2021, frequency ratio has been used in 17% of the paper. Similarly, the weight of evidence model has used in 19%, information value has used in 15%, and the entropy model has used in 9%. The rest are machine learning, fuzzy logic, and some multivariate methods. Based on quantitative review and self-analysis, these four models of bivariate methods are selected for the present study.

### 4.2.4 Comparison of model

The success and prediction rates of all four models are obtained (Fig.46). The result shows that the weight of evidence model has higher accuracy and prediction rate. The success rate and prediction rate of the WoE model are 85% and 79.9%, respectively. The accuracy and prediction rate of the rest of the other three models are similar. Comparatively, the prediction rate of the FR model is greater than the IVM and SE models. The hierarchy of success rates from high to low is WoE (79.9%), FR (75.3%), IVM (74.4%), and SE (73.2%).

The accuracy and prediction rate of every model are greater than 70% so that all the models can be applied for landslide susceptibility in the Siwalik Hills of Nepal; however, the weight of evidence model is more reliable and gives more accurate results than others. Similarly, a success rate greater than 75% means the models fit best and can be applied anywhere. Likewise, the success rate of four different models (WoE, FR, IVM, SE) is 85%,

78.75%, 78.57%, and 77.2%, respectively. Ikram et al. (2021) compared the machine learning techniques and three statistical techniques for landslide modeling in the Northwest Himalayas of Pakistan. They compared the frequency ratio, information value method, and weight of evidence model as statistical methods and obtained that the frequency ratio has better prediction than the other two methods.

The medium susceptibility is widely obtained from Information value method whereas low susceptibility is highest in the Shannon Entropy model. High and very high susceptibility were highest weight of evidence and Information value models whereas Shannon Entropy provided very less area of very high susceptibility. There is significant different between four models in case of susceptibility classes.

# CHAPTER 5

## CONCLUSIONS AND RECOMMENDATIONS

### 5.1 Conclusions

The characterization of landslides includes the access of nature, mechanism, classification, and causes of landslides of a particular region as well as identification of potential landslide susceptible zone. In this study, landslide characterization was done using a multidisciplinary approach. Mainly four disciplines, geological, topographical, hydrological, and geotechnical, are chosen for characterization. From the geological point of view, the area is highly susceptible due to its typical geology, stratigraphy, and thrust activity. Among the three geological units, The Middle Siwalik is more potential for landslide due to its characteristic slope and rock formation though the soil is dense and compact. Rockfall is a major landslide type in Middle Siwalik, whereas erosion-induced landslides and soil slides are common in Lower Siwalik. The major problem of Middle Siwalik is rock fall and rock slide, but both of them convert into debris flow where the slope distance is long enough to travel debris material with running water. The soils of the Lower and Upper Siwalik are loose and less compact.

Similarly, the soils of the overall study area are fine; mostly silt/clay ratio is dominant. Due to this reason, long-term rainfall impacts the slope and causes landslides more than short-term rainfall. The total rainfall amount shows a positive correlation with the frequency of landslides. The landslides have direct topographical control. The number of landslides increased with increasing T value. The proposed landslide classification (mechanism, size, and activity state-based) will be helpful to the people as well as stakeholders in understanding landslides. Similarly, this will be the source and reference for future research to discover more mechanism-based landslides in the Siwalik zone. The size-based classification will be easier and more comfortable for researchers to apply in the complex geological terrain in the world as it is common to find landslides of different sizes. Separating the landslide into logarithmic scale gives the proper solution for size-based

landslide classification. The state-based classification will be helpful for any sedimentary terrain of the world, like Siwalik zone of Nepal. Every bivariate technique in this study is applicable and can be accepted for landslide susceptibility in the Siwalik Hills. All models' accuracy and prediction rate is greater than 70%, indicating that these can be applied for susceptibility.

The major conclusions of the study are as follows.

a. The Siwalik of the Babai River watershed has predominantly sand composition, but the silt/clay fraction is higher than sand/clay and sand/silt.
b. The plasticity chart, grainsize analysis, and ternary diagram showed that fine soils are predominant in the study area.
c. Due to the presence of fine soils, long-term rainfall causes several landslides in the monsoon period than short-term rainfall.
d. Mechanism-based classification is suitable and easier for landslide study in the Siwalik Hills.
e. All the applied susceptibility models can be used. However, the weight of evidence model has a better prediction.
f. These findings can be helpful for the concerned departments, policymakers, and researchers.

## 5.2 Recommendations

The following recommendations are suggested based on the result obtained in this research.

a. The investigation revealed that soil composition plays a vital role in the landslide process. On this basis, future research should increase the number of soil sample analyses while investigating the landslide.

b. The soil investigation provided the result based on the dry condition. The future soil investigation should conduct both in the dry and wet seasons to obtain seasonal variation.

c. Landslide classification is essential for landslide investigation. Five types of mechanism-based landslides are identified and proposed in the catchment. Future research covering the wide area of Siwalik may provide an overall landslide mechanism in the Siwalik zone.

d. The result showed that all four bivariate models are useful for landslide susceptibility analysis in the Siwalik. However, the weight of evidence models provided higher prediction and accuracy than the other three models. Further research comparing with multivariate analysis may help to identify the best model for landslide susceptibility in the Siwalik zone.

# CHAPTER 6

## SUMMARY

In this research, the landslide characterization has been conducted based on geological, topographical, hydrological, and geotechnical approaches. Similarly, the landslides were classified based on size, activity state, and mechanism. The characterization includes landslide susceptibility and dynamics. This study is mainly about the spatial and temporal dynamics and the multidisciplinary characterization of landslides in the Sub-Himalaya of Nepal. The Sub-Himalaya of Nepal is composed of fragile sedimentary rock. Landslide activities are a common problem in this region. People of these regions face several problems due to landslides yearly, mainly in the Monsoon season. The mitigation and prevention of landslides in this region are challenging. So, evaluating the landslide mechanism, finding the significant characteristics, giving a new approach for classification, and comparing the accuracy and prediction rate of various bivariate models are the purposes of this study.

The procedure began with a landslide inventory map. Google Earth, Landsat, and Sentinel imageries were used for mapping. The spatial inventory map included all landslides in the research region, whereas the temporal inventory map included new landslides annually from 2010 to 2021. The geological parameters of landslides were assessed in both space and time. The size, length, area, and number of landslides in different geological units were compared. Landslides varied substantially in size, length, and area across the three geological divisions. In addition, the mechanism of landslide beginning in geological units was studied. Based on the literature and a scenario developed from the ground, the slope, aspect, curvature, topographical wetness index, and "T" components were used for topographical characterization. Total yearly rainfall, monsoon rainfall amount, the spatial distribution of rainfall, and distance to the drainage map were used as hydrological characteristics. Data from seven stations from 2010 to 2021 were used to create the rainfall distribution map. The rainfall subclass to landslide pixel frequency ratio was calculated using the GIS spatial analyst tool. Total yearly rainfall, total rainfall during the monsoon

season, is correlated with a total annual landslide. The landslide pixels were correlated with a class pixel of distance to drainage. The shear behavior, phase relation, and index properties of 120 landslide soils were used to calculate geotechnical parameters. The shear behavior and strength parameters were measured using the direct shear test. Grainsize analysis was used to estimate soil composition, and compositional analysis was used to calculate the soil composition ratio. The central log ratios of sand/silt, sand/clay, and silt/clay were obtained to determine the principal constituent responsible for the landslide. The shear stress versus displacement curves of each soil sample from three geological units was obtained to study shear behavior. Shear strength parameters were calculated using the Mohr column failure criterion. Using ASTM guidelines, the laboratory determined the degree of saturation, the void ratio, the moisture content, the specific gravity, the plasticity index, and the dry density. The critical shear strength covariates were determined using multiple regression. The differences in geotechnical parameters between geological units were investigated.

A size-based classification was constructed based on the logarithmic scale of the landslide area. The five sizes proposed for size-based classification are very small, small, medium, large, and very large. Landslides with a surface area of less than 100 $m^2$ are considered very small, while those with a surface area of more than 100,000 $m^2$ are considered very large. Five activity states are recommended for activity-based classification: new, active, inactive, stabilized, and reactivated. The proposed activity state conditions are described. Five types of landslides are postulated based on the landslide mechanism: Type 1, Type 2, Type 3, Type 4, and Type 5. The prerequisites for each class type are proposed. Fourteen landslide-causing elements were chosen for a susceptibility analysis. For factor selection, several literature-based and field-based circumstances are considered. The validation and prediction accuracy of four models were obtained. The prediction rate of models was calculated using the AUC and ROC curves.

The silt/clay proportion present in the Siwalik soil is one of the primary reasons to cause landslides in the saturated condition. The soils of the Middle Siwalik are dense, whereas there are very loose in the Lower and Upper Siwalik. Similarly, the soils of Lower and

Upper Siwalik are well-graded. The average shear strength is also less in the Lower and Upper Siwalik than in the Middle Siwalik. The small and shallow landslides are commonly distributed in the Lower and Upper Siwalik. The "T" factor and landslides are positively correlated with each other. Similarly, the hill slope and landslide events are significantly correlated. Total annual rainfall and total annual landslides have significant positive relation. Likewise, large-size landslides are dominant in the Middle Siwalik. The result shows that the weight of evidence model has higher accuracy and prediction rate. The success rate and prediction rate of the WoE model are 85% and 79.9%, respectively. The accuracy and prediction rate of the rest of the other three models are similar. Comparatively, the prediction rate of the FR model is greater than the IVM and SE models. The hierarchy of prediction rates from high to low is WoE (79.9%), FR(75.3%), IVM(74.4%), and SE(73.2%).

Similarly, the success rate of four different models (WoE, FR, IVM, and SE) is 85%, 78.75%, 78.57%, and 77.2%, respectively. The accuracy and prediction rate of every model are greater than 70% so that all the models can be applied for landslide susceptibility in the Siwalik Hills of Nepal; however, the weight of evidence model is more reliable and gives more accurate results than others. Similarly, a success rate greater than 75% means the models are best fitting and can be applied anywhere.

# REFERENCE


Abella, E. A. C., & Van Westen, C. J. (2008). Qualitative landslide susceptibility assessment by multicriteria analysis: A case study from San Antonio del Sur, Guantánamo, Cuba. *Geomorphology*, *94*(3-4),453-466.https://doi.org/10.1016/j.geomorph.2006.10.038.

Acharya, K. P., Bhandary, N. P., Dahal, R. K., & Yatabe, R. (2015). Numerical analysis on influence of principal parameters of topography on hillslope instability in a small catchment. *Environmental Earth Sciences*, *73*(9), 5643-5656. https://doi.org/10.1007/s12665-014-3819-z.

Achour, Y., Boumezbeur, A., Hadji, R., Chouabbi, A., Cavaleiro, V., & Bendaoud, E. A. (2017). Landslide susceptibility mapping using analytic hierarchy process and information value methods along a highway road section in Constantine, Algeria. *Arabian Journal of Geosciences*, *10*(8), 1-16. https://doi.org/10.1007/s12517-017-2980-6.

Aditian, A., Kubota, T., & Shinohara, Y. (2018). Comparison of GIS-based landslide susceptibility models using frequency ratio, logistic regression, and artificial neural network in a tertiary region of Ambon, Indonesia. *Geomorphology*, *318*, 101-111. https://doi.org/10.1007/s12517-017-2980-6.

Afungang, R. N., de Meneses Bateira, C. V., & Nkwemoh, C. A. (2017). Assessing the spatial probability of landslides using GIS and informative value model in the Bamenda highlands. *Arabian Journal of Geosciences*, *10*(17), 1-15. https://doi.org/10.1007/s12517-017-3155-1

Aghdam, H. H., & Heravi, E. J. (2017). Guide to convolutional neural networks. *New York, NY: Springer*, *10*(978-973), 51.

Agterberg, F. P., Bonham-Carter, G. F., Cheng, Q. M., & Wright, D. F. (1993). Weights of evidence modeling and weighted logistic regression for mineral potential mapping. *Computers in geology*, *25*, 13-32.

Aitchison, C. (2003). From leisure and disability to disability leisure: Developing data, definitions and discourses. *Disability & Society*, *18*(7), 955-969. https://doi.org/10.1080/0968759032000127353.

Aitchison, J. (1982). The statistical analysis of compositional data. *Journal of the Royal Statistical Society: Series B (Methodological)*, *44*(2), 139-160. https://doi.org/10.2307/2345821.

Akgun, A. (2012). A comparison of landslide susceptibility maps produced by logistic regression, multi-criteria decision, and likelihood ratio methods: a case study at İzmir, Turkey. *Landslides*, *9*(1), 93-106. https://doi.org/10.1007/s10346-011-0283-7.

Aleotti, P., & Chowdhury, R. (1999). Landslide hazard assessment: summary review and new perspectives. *Bulletin of Engineering Geology and the environment*, *58*(1), 21-44. https://doi.org/10.1007/s100640050066.

Althuwaynee, O. F., Pradhan, B., & Lee, S. (2012). Application of an evidential belief function model in landslide susceptibility mapping. *Computers & Geosciences*, *44*, 120-135. https://doi.org/10.1016/j.cageo.2012.03.003.

Alvioli, M., & Baum, R. L. (2016). Parallelization of the TRIGRS model for rainfall-induced landslides using the message passing interface. *Environmental Modelling & Software*, *81*, 122-135. https://doi.org/10.1016/j.envsoft.2016.04.002.

Amare, K., Mebrahtu, G., & Gebremiceal, A. (2018). Landslide characterization and distribution in northern Ethiopia: a case study from the Adishu area. *Bulletin of Engineering Geology and the Environment*, *77*(2), 581-593. https://doi.org/10.1007/s10064-017-1064-x.

Anagnostopoulos, G. G., Fatichi, S., & Burlando, P. (2015). An advanced process-based distributed model for the investigation of rainfall-induced landslides: The effect of process representation and boundary conditions. *Water Resources Research*, *51*(9), 7501-7523.http://dx.doi.org/10.1002/2015WR016909.

Arber, M.A. (1941). *The coastal landslips of West Dorset*, Proceedings Geologists' Association, 52, 273-283. https://doi.org/10.1016/S0016-7878(41)80010-8.

Arifianti, Y., Pamela, P., Agustin, F., & Muslim, D. (2020). Comparative Study among Bivariate Statistical Models in Landslide Susceptibility Map. *Indonesian Journal on Geoscience*, *7*(1), 51-63. http://dx.doi.org/10.17014/ijog.7.1.51-63.

ASTM D422-63e2 (2007) *Standard test method for particle size analysis of soils*. ASTM international. West Conshohocken, PA.

Atkinsson, P. M., & Massari, R. (1998). Generalized linear modeling of susceptibility to landsliding in the central appennines, Italy. *Computer & Geoscience*, *24*(4), 373-385. https://doi.org/10.1016/S0098-3004(97)00117-9.

Auden, J. B. (1935). Traverses in the Himalaya. *Records of the Geological Survey of India*, 69(123–167).

Ausilio, E., Zimmaro, P. (2017). Landslide characterization using a multidisciplinary approach. *Measurement* 104, 294-301. https://doi.org/10.1016/j.measurement.2016.01.009

Austin, M. P. (2002). Spatial prediction of species distribution: an interface between ecological theory and statistical modelling. *Ecological modelling*, *157*(2-3), 101-118. https://doi.org/10.1016/S0304-3800(02)00205-3.

Bailey, R. G. (1969). Soil slippage: an indicator of slope instability on chaparral watersheds of southern California. *The Professional Geographer*, *21*(3), 172-177. https://doi.org/10.1111/j.0033-0124.1969.00172.x.

Ballabio, C., & Sterlacchini, S. (2012). Support vector machines for landslide susceptibility mapping: the Staffora River Basin case study, Italy. *Mathematical geosciences*, *44*(1), 47-70. https://doi.org/10.1007/s11004-011-9379-9.

Baltzer, A. (1875). *Über bergstürze in den Alpen*. Verlag der Schabelitz'schen buchhandlung (C. Schmidt).

Banshtu, R. S., Versain, L. D., & Pandey, D. D. (2020). Risk assessment using quantitative approach: central Himalaya, Kullu, Himachal Pradesh, India. *Arabian Journal of Geosciences*, *13*(5), 1-11. https://doi.org/10.1007/s12517-020-5143-0.

Barton, M., & Pearce, R. B. (2015). Landslides and stratigraphy in the coastal outcrop of the Barton clay. *Proceedings of the Geologists' Association*, *126*(6), 731-741. https://doi.org/10.1016/j.pgeola.2015.10.001.

Basharat, M., Shah, H. R., & Hameed, N. (2016). Landslide susceptibility mapping using GIS and weighted overlay method: a case study from NW Himalayas, Pakistan. *Arabian Journal of Geosciences*, *9*(4), 1-19. http://dx.doi.org/10.1007/s12517-016-2308-y.

Bates, R. L., & Jackson, J. A. (1987). Glossary of geology: American geological institute. *Alexandria, Virginia*, *788*.

Baum, R. L., Savage, W. Z., & Godt, J. W. (2008). *TRIGRS: a FORTRAN program for transient rainfall infiltration and grid-based regional slope-stability analysis, version 2.0* (pp. 2008-1159). Reston, VA, USA: US Geological Survey.

Benac, Č., Oštrić, M., & Dugonjić Jovančević, S. (2014). Geotechnical properties in relation to grain-size and mineral composition: case study landslide in the Rječina Valley (Croatia). *Geologia Croatica*, *67*(2), 127-136. https://doi.org/10.4154/GC.2014.11.

Bhandari, B. P., & Dhakal, S. (2018). Lithological control on landslide in the Babai Khola watershed, Siwaliks zone of Nepal. *American Journal of Earth Sciences*, *5*(3), 54-64.

Bhandari, B. P., & Dhakal, S. (2019). Topographical and geological factors on gully-type debris flow in Malai River catchment, Siwaliks, Nepal. *Journal of Nepal Geological Society*, *59*, 89-94. https://doi.org/10.3126/jngs.v59i0.24994.

Bhandari, B. P., & Dhakal, S. (2020). Spatio-temporal dynamics of landslides in the sedimentary terrain: a case of Siwalik zone of Babai watershed, Nepal. *SN Applied Sciences*, *2*(5), 1-17. https://doi.org/10.1007/s42452-020-2628-0.

Bhandari, B. P., & Dhakal, S. (2021). A multidisciplinary approach of landslide characterization: A case of the Siwalik zone of Nepal Himalaya. *Journal of Asian Earth Sciences: X*, *5*, 100061. https://doi.org/10.1016/j.jaesx.2021.100061.

Bicocchi, G., Tofani, V., D'Ambrosio, M., Tacconi-Stefanelli, C., Vannocci, P., Casagli, N., ... & Catani, F. (2019). Geotechnical and hydrological characterization of hillslope deposits for regional landslide prediction modeling. *Bulletin of engineering geology and the environment*, *78*(7), 4875-4891. https://doi.org/10.1007/s10064-018-01449-z.

Blahut, J., Van Westen, C. J., & Sterlacchini, S. (2010). Analysis of landslide inventories for accurate prediction of debris-flow source areas. *Geomorphology*, *119*(1-2), 36-51. http://dx.doi.org/10.1016/j.geomorph.2010.02.017.

Blanford, W. T. (1883). Geological notes on the hills in the neighborhood of the Sind and Punjab Frontier between Quetta and Dera Ghazi Khan. *Memoirs of the geological survey of India*, *20*, 105-240.

Blong, R. J. (1973). A numerical classification of selected landslides of the debris slide-avalanche-flow type. *Engineering Geology*, *7*(2), 99-114. https://doi.org/10.1016/0013-7952%2873%2990040-9.

Bonham-Carter, G. F., & Bonham-Carter, G. (1994). *Geographic information systems for geoscientists: modelling with GIS* (No. 13). Elsevier.

Borga, M., Dalla Fontana, G., & Cazorzi, F. (2002). Analysis of topographic and climatic control on rainfall-triggered shallow land sliding using a quasi-dynamic wetness index. *Journal of Hydrology*, *268*(1-4), 56-71. https://doi.org/10.1016/S0022-1694(02)00118-X.

Bourenane, H., Guettouche, M. S., Bouhadad, Y., & Braham, M. (2016). Landslide hazard mapping in the Constantine city, Northeast Algeria using frequency ratio, weighting factor, logistic regression, weights of evidence, and analytical hierarchy process

methods. *Arabian Journal of Geosciences*, *9*(2), 1-24. https://doi.org/10.1007/s12517-015-2222-8.

Brabb, E.E. (1984). *Innovative approaches to landslide hazard mapping*. In: Proc. 4th Int.

Broothaerts, N., Kissi, E., Poesen, J., Van Rompaey, A., Getahun, K., Van Ranst, E., & Diels, J. (2012). Spatial patterns, causes and consequences of landslides in the Gilgel Gibe catchment, SW Ethiopia. *Catena*, *97*, 127-136. https://doi.org/10.1016/j.catena.2012.05.011.

Brunsden, D., & Jones, D. K. (1972). The morphology of degraded landslide slopes in South West Dorset. *Quarterly Journal of Engineering Geology and Hydrogeology*, *5*(3), 205-222.

Buccianti, A. (2013). Is compositional data analysis a way to see beyond the illusion?. *Computers & geosciences*, *50*, 165-173. https://doi.org/10.1016/j.cageo.2012.06.012.

Budimir, M. E. A., Atkinson, P. M., & Lewis, H. G. (2015). A systematic review of landslide probability mapping using logistic regression. *Landslides*, *12*(3), 419-436. https://doi.org/10.1007/s10346-014-0550-5.

Bui, D. T., Pradhan, B., Lofman, O., Revhaug, I., & Dick, O. B. (2012). Spatial prediction of landslide hazards in Hoa Binh province (Vietnam): a comparative assessment of the efficacy of evidential belief functions and fuzzy logic models. *Catena*, *96*, 28-40. https://doi.org/10.1016/j.catena.2012.04.001.

Burton, A., & Bathurst, J. C. (1998). Physically based modelling of shallow landslide sediment yield at a catchment scale. *Environmental Geology*, *35*(2), 89-99. https://doi.org/10.1007/s002540050296

Carranza, E. J. M., Hale, M., & Faassen, C. (2008). Selection of coherent deposit-type locations and their application in data-driven mineral prospectivity mapping. *Ore geology reviews*, *33*(3-4), 536-558. https://doi.org/10.1016/j.oregeorev.2007.07.001.

Carrara, A. (1983). Multivariate models for landslide hazard evaluation. *Journal of the International Association for Mathematical Geology*, *15*(3), 403-426. https://doi.org/10.1007/BF01031290.

Carrara, A., & Guzzetti, F. (Eds.). (2013). *Geographical information systems in assessing natural hazards* (Vol. 5). Springer Science & Business Media. https://doi.org/10.1007/978-1-4020-4399-4_152.

Carrara, A., Cardinali, M., Detti, R., Guzzetti, F., Pasqui, V., & Reichenbach, P. (1991). GIS techniques and statistical models in evaluating landslide hazard. *Earth surface processes and landforms*, *16*(5), 427-445. https://doi.org/10.1002/esp.3290160505.

Carrara, A., Cardinali, M., Guzzetti, F., & Reichenbach, P. (1995). GIS technology in mapping landslide hazard. In *Geographical information systems in assessing natural hazards* (pp. 135-175). Springer, Dordrecht. https://doi.org/10.1007/978-94-015-8404-3_8.

Carrara, A., Sorriso-Valvo, M., & Reali, C. (1982). Analysis of landslide form and incidence by statistical techniques, Southern Italy. *Catena*, *9*(1-2), 35-62. https://doi.org/10.1016/S0341-8162(82)80004-0

Carrubba, P., & Del Fabbro, M. (2008). Laboratory investigation on reactivated residual strength. *Journal of geotechnical and geoenvironmental engineering*, *134*(3), 302-315. http://dx.doi.org/10.1061/(ASCE)1090-0241(2008)134:3(302).

Casagrande, A. (1932). Research on the Atterberg limits of soils. *Public roads*, *13*(8), 121-136.

Casagrande, A. (1940). Characteristics of cohesionless soils affecting the stability of slopes and earth fills. *Contributions to Soils Mechanics, 1925-1940*.

Cencetti, C., & Conversini, P. (2003). Slope instability in the Bastardo Basin (Umbria, Central Italy)–The landslide of Barattano. *Natural Hazards and Earth System Sciences*, *3*(6), 561-568. https://doi.org/10.5194/nhess-3-561-2003.

Cengiz, L. D., & Ercanoglu, M. (2022). A novel data-driven approach to pairwise comparisons in AHP using fuzzy relations and matrices for landslide susceptibility assessments. *Environmental Earth Sciences*, *81*(7), 1-23. https://doi.org/10.1007/s12665-022-10312-0.

Cernica, J. N. (1995). *Geotechnical engineering: soil mechanics*. University of California, Wiley. ISBN: 0471308846,9780471308843

Cha, K. S., & Kim, T. H. (2011). Evaluation of slope stability with topography and slope stability analysis method. *KSCE Journal of Civil Engineering*, *15*(2), 251-256. https://doi.org/10.1007/s12205-011-0930-5.

Chacón, J., Irigaray, C., Fernandez, T., & El Hamdouni, R. (2006). Engineering geology maps: landslides and geographical information systems. *Bulletin of Engineering Geology and the Environment*, *65*(4), 341-411. http://dx.doi.org/10.1007/s10064-006-0064-z.

Chang, T. C. (2007). Risk degree of debris flow applying neural networks. *Natural hazards*, *42*(1), 209-224. http://dx.doi.org/10.1007/s11069-006-9069-y.

Chaudhary, R. (1982). Petrology of the Siwalik group of Nepal Himalaya. In *Recent researches in geology*.

Chen, T., Niu, R., & Jia, X. (2016). A comparison of information value and logistic regression models in landslide susceptibility mapping by using GIS. *Environmental Earth Sciences*, *75*(10), 1-16. https://doi.org/10.1007/s12665-016-5317-y.

Chen, T., Niu, R., & Jia, X. (2016). A comparison of information value and logistic regression models in landslide susceptibility mapping by using GIS. *Environmental Earth Sciences*, *75*(10), 1-16. https://doi.org/10.1007/s12665-016-5317-y.

Chen, W., Li, W., Hou, E., Bai, H., Chai, H., Wang, D.,& Wang, Q. (2015). Application of frequency ratio, statistical index, and index of entropy models and their comparison in landslide susceptibility mapping for the Baozhong Region of Baoji, China. *Arabian Journal of Geosciences*, *8*(4), 1829-1841. https://doi.org/10.1007/s12517-014-1554-0.

Chen, W., Pourghasemi, H. R., & Naghibi, S. A. (2018). A comparative study of landslide susceptibility maps produced using support vector machine with different kernel functions and entropy data mining models in China. *Bulletin of Engineering Geology and the Environment*, *77*(2), 647-664. https://doi.org/10.1007/s10064-017-1010-y.

Chen, W., Song, B., Wu, W., Sun, Y., & Song, Y. (2021). Direct and reversal shear behaviors of three kinds of slip zone soil in the Northwest of China. *Bulletin of Engineering Geology and the Environment*, *80*(5), 3939-3952. https://doi.org/10.1007/s10064-021-02174-w.

Chen, Y. C., Chang, K. T., Wang, S. F., Huang, J. C., Yu, C. K., Tu, J. Y., ... & Liu, C. C. (2019). Controls of preferential orientation of earthquake-and rainfall-triggered landslides in Taiwan's orogenic mountain belt. *Earth Surface Processes and Landforms*, *44*(9), 1661-1674. https://doi.org/10.1002/esp.4601.

Chigira, M., Mohamad, Z., Sian, L. C., & Komoo, I. (2011). Landslides in weathered granitic rocks in Japan and Malaysia. *Bulletin of the Geological Society of Malaysia*, 57,(1–6). https://10.7186/bgsm2011001.

Chimidi, G., Raghuvanshi, T. K., & Suryabhagavan, K. V. (2017). Landslide hazard evaluation and zonation in and around Gimbi town, western Ethiopia—a GIS-based statistical approach. *Applied Geomatics*, *9*(4), 219-236.https://doi.org/10.1007/s12518-017-0195-x.

Ching, H., Chih-Hsuan, L., Chia-Ming, C. (2018). Numerical investigation of rainfall induced landslide in mudstone using coupled finite and discrete element analysis. *Geofluids,* 1-15. https://doi.org/10.1155/2018/9192019.

Choi, J., Oh, H. J., Won, J. S., & Lee, S. (2010). Validation of an artificial neural network model for landslide susceptibility mapping. *Environmental Earth Sciences*, *60*(3), 473-483. https://doi.org/10.1007/s12665-009-0188-0.

Conway, B. W. (1974). The Black Ven Landslip, Charmouth, Dorset : an Example of the Effect of a Secondary Reservoir of Groundwater in an Unstable Area / B.W. Conway. London: H.M.S.O., 1974. Print.

Craiguie, W.A., Hulbert, J.R., (1942). *Dictionary of American English on Historical Principles*, University of Chicago Press, Chicago.

Crozier, M. J. (1986). Landslides: causes, consequences and environment, Croom Helm. *London. 252pp*.

Cruden, D. M. (1991). A Simple Definition of a Landslide. *Bulletin of the International Association of Engineering Geology*, 43, 27-29. https://doi.org/10.1007/BF02590167.

Cruden, D. M. (2003). The first classification of landslides?. *Environmental & Engineering Geoscience*, *9*(3), 197-200. http://dx.doi.org/10.2113/9.3.197.

Cruden, D.M., & Varnes, D.J. (1996). *Landslide Types and Processes*. Transportation Research Board, U.S. National Academy of Sciences, Special Report, 247: 36-75.

Dahal, R. K. (2012). Rainfall-induced landslides in Nepal. *International Journal of Erosion Control Engineering*, *5*(1), 1-8. http://dx.doi.org/10.13101/ijece.5.1.

Dahal, R. K., & Hasegawa, S. (2008). Representative rainfall thresholds for landslides in the Nepal Himalaya. *Geomorphology*, *100*(3-4),429-443. https://doi.org/10.1016/j.geomorph.2008.01.014.

Dahal, R. K., Hasegawa, S., Bhandary, N. P., Poudel, P. P., Nonomura, A., & Yatabe, R. (2012). A replication of landslide hazard mapping at catchment scale. *Geomatics, Natural Hazards and Risk*, *3*(2), 161-192. https://doi.org/10.1080/19475705.2011.629007.

Dahal, R. K., Hasegawa, S., Nonomura, A., Yamanaka, M., Dhakal, S., & Paudyal, P. (2008). Predictive modelling of rainfall-induced landslide hazard in the Lesser Himalaya of Nepal based on weights-of-evidence. *Geomorphology*, *102*(3-4), 496-510. http://dx.doi.org/10.1016/j.geomorph.2008.05.041.

Dahal, R. K., Hasegawa, S., Nonomura, A., Yamanaka, M., Dhakal, S., & Paudyal, P. (2008). Predictive modelling of rainfall-induced landslide hazard in the Lesser Himalaya of Nepal based on weights-of-evidence. *Geomorphology*, *102*(3-4), 496-510. https://doi.org/10.1016/j.geomorph.2008.05.041.

Dahl, M. P. J., Mortensen, L., Jensen, N. H., & Veihe, A. (2011). Magnitude-frequency characteristics and preparatory factors for debris slide activity in the Northern Faroe Islands. In *Geophysical Research Abstracts* (Vol.13). Copernicus GmbH. https://doi.org/10.1016/j.geomorph.2012.09.015.

Dai, F. C., & Lee, C. F. (2002). Landslide characteristics and slope instability modeling using GIS, Lantau Island, Hong Kong. *Geomorphology*, *42*(3-4), 213-228. https://doi.org/10.1016/S0169-555X(01)00087-3.

Dana, J.D. (1862). *Manual of geology; treating of the principles of the science with special reference to American Geological History for the use of Colleges, Academies, and Schools of Science,*798.

D'appolonia, E., Alperstein, R., & D'Appolonia, D. J. (1967). Behavior of a colluvial slope. *Journal of the Soil Mechanics and Foundations Division*, *93*(4), 447-473. https://doi.org/10.1061/JSFEAQ.0001001.

Das, B. M. (1994). *Principal of geotechnical engineering*. CENGAGE Learning. Eight Edition.

Das, B. M., & Sobhan, K. (2010). *Principles of geotechnical engineering*. CENGAGE Learning. 7th edition, 51-72.

Das, B.M. (2009) Weight- volume relationship. *In Principal of geotechnical engineering*. CENGAGE Learning. Eight Edition.

Davis, R. O. E. (1927). *Grouping of soils on the basis of mechanical analysis* (Vol. 419). US Department of Agriculture.

Demir, G., Aytekin, M., Akgün, A., Ikizler, S. B., & Tatar, O. (2013). A comparison of landslide susceptibility mapping of the eastern part of the North Anatolian Fault Zone (Turkey) by likelihood-frequency ratio and analytic hierarchy process methods. *Natural hazards*, *65*(3), 1481-1506. https://doi.org/10.1007/s11069-012-0418-8.

Denness, B., Conway, B. W., McCann, D. M., & Grainger, P. (1975). Investigation of a coastal landslip at Charmouth, Dorset. *Quarterly Journal of Engineering Geology*, *8*(2), 119-140. https://doi.org/10.1144/GSL.QJEG.1975.008.02.03.

Densmore, A. L., Ellis, M. A., & Anderson, R. S. (1998). Landsliding and the evolution of normal-fault-bounded mountains. *Journal of geophysical research: solid earth*, *103*(B7), 15203-15219. https://doi.org/10.1029/98JB00510.

Derbyshire, E., Dijkstra, T. A., Smalley, I. J., & Li, Y. (1994). Failure mechanisms in loess and the effects of moisture content changes on remoulded strength. *Quaternary international*, *24*, 5-15. https://doi.org/10.1016/1040-6182(94)90032-9.

Devkota, K. C., Regmi, A. D., Pourghasemi, H. R., Yoshida, K., Pradhan, B., Ryu, I. C., ... & Althuwaynee, O. F. (2013). Landslide susceptibility mapping using certainty factor, index of entropy and logistic regression models in GIS and their comparison at Mugling–Narayanghat road section in Nepal Himalaya. *Natural hazards*, *65*(1), 135-165. http://dx.doi.org/10.1007/s11069-012-0347-6.

Dhakal, A. S., & Sidle, R. C. (2003). Long-term modelling of landslides for different forest management practices. *Earth Surface Processes and Landforms: The Journal of the British Geomorphological Research Group*, *28*(8), 853-868. https://doi.org/10.1002/esp.499.

Dhakal, S. (2014). Flood hazard in Nepal and new approach of risk reduction. *International journal of landslide and environment*, *1*(1), 13-14.

Dhakal, S. (2015). Evolution of geomorphologic hazards in Hindu Kush Himalaya. In *Mountain hazards and disaster risk reduction* (pp. 53-72). Springer, Tokyo. http://dx.doi.org/10.1007/978-4-431-55242-0_4.

Dhital, M.R. (2015). *Geology of the Nepal Himalaya*, 1st edn. Springer International Publishing, Switzerland. doi:10.1007/978-3-319-02496-7.

Dietrich, W. E., Reiss, R., Hsu, M. L., & Montgomery, D. R. (1995). A process-based model for colluvial soil depth and shallow landsliding using digital elevation data. *Hydrological processes*, *9*(3-4), 383-400. https://doi.org/10.1002/hyp.3360090311.

Dietrich, W. E., Reneau, S. L., & Wilson, C. J. (1987). Overview: Zero-order basins and problems of drainage density, sediment transport and hillslope morphology. *IAHS-AISH publication*, (165), 27-37.

Dijkstra, T. A., Rogers, C. D. F., Smalley, I. J., Derbyshire, E., Li, Y. J., & Meng, X. M. (1994). The loess of north-central China: geotechnical properties and their relation to slope stability. *Engineering Geology*, *36*(3-4), 153-171. https://doi.org/10.1016/0013-7952(94)90001-9.

Dikau, R. A. (1996). *Landslide recognition: identification, movement and causes* (1) 251. John Wiley & Sons. ISBN: 978-0-471-96477-3.

Dimitrova RS, Yanful EK (2012) Factors affecting the shear strength of mine tailings/clay mixtures with varying clay content and clay mineralogy. Eng Geol 125:11–25. https://doi.org/10.1016/j.enggeo.2011.10.013.

Ding, Q., Chen, W., & Hong, H. (2017). Application of frequency ratio, weights of evidence and evidential belief function models in landslide susceptibility mapping. *Geocarto international*, *32*(6), 619-639. https://doi.org/10.1080/10106049.2016.1165294.

Dou, J., Yamagishi, H., Pourghasemi, H. R., Yunus, A. P., Song, X., Xu, Y., & Zhu, Z. (2015). An integrated artificial neural network model for the landslide susceptibility assessment of Osado Island, Japan. *Natural Hazards*, *78*(3), 1749-1776. https://doi.org/10.1007/s11069-015-1799-2.

Duffera, M., White, J. G., & Weisz, R. (2007). Spatial variability of Southeastern US Coastal Plain soil physical properties: Implications for site-specific management. *Geoderma*, *137*(3-4),327-339. https://doi.org/10.1016/j.geoderma.2006.08.018

Dundulis, K., Gadeikis, S., Gadeikytė, S., Urbaitis, D., & Prunskienė, L. (2010). Problems of usage of soil classification systems for sand soils of Lithuania.*10th Int. Conf, Vilnius Gediminas Technical Univ*., Vilnius, Lithuania.

Egozcue, J. J., & Pawlowsky-Glahn, V. (2005). Groups of parts and their balances in compositional data analysis. *Mathematical Geology*, *37*(7), 795-828. https://doi.org/10.1007/s11004-005-7381-9.

Ercanoglu, M. U. R. A. T., Gokceoglu, C. A. N. D. A. N., & Van Asch, T. W. (2004). Landslide susceptibility zoning north of Yenice (NW Turkey) by multivariate statistical techniques. *NaturalHazards*, *32*(1),1-23. https://doi.org/10.1023/B:NHAZ.0000026786.85589.4a

Eynatten, H. (2004). Statistical modelling of compositional trends in sediments. *SedimentaryGeology*, *171*(1-4),79-89. http://dx.doi.org/10.1016/j.sedgeo.2004.05.011.

Farooq, S., & Akram, M. S. (2021). Landslide susceptibility mapping using information value method in Jhelum Valley of the Himalayas. *Arabian Journal of Geosciences*, *14*(10), 1-16. http://dx.doi.org/10.1007/s12517-021-07147-7.

Fell, R., Corominas, J., Bonnard, C., Cascini, L., Leroi, E., & Savage, W. Z. (2008). Guidelines for landslide susceptibility, hazard and risk zoning for land use planning. *Engineering Geology*, *102*(3-4),85-98. https://doi.org/10.1016/j.enggeo.2008.03.022.

Fernandes, N. F., Guimarães, R. F., Gomes, R. A., Vieira, B. C., Montgomery, D. R., & Greenberg, H. (2004). Topographic controls of landslides in Rio de Janeiro: field evidence and modeling. *Catena*, *55*(2), 163-181. https://doi.org/10.1016/S0341-8162(03)00115-2.

Fleming RW, Johnson AM (1994) Landslides in colluvium. USGS Bulletin 2059-B, Washington, DC. https://doi.org/10.3133/b2059B.

Gabet, E. J., Burbank, D. W., Putkonen, J. K., Pratt-Sitaula, B. A., & Ojha, T. (2004). Rainfall thresholds for landsliding in the Himalayas of Nepal. *Geomorphology*, *63*(3-4), 131-143. https://doi.org/10.1016/j.geomorph.2004.03.011.

Galli, M., Ardizzone, F., Cardinali, M., Guzzetti, F., & Reichenbach, P. (2008). Comparing landslide inventory maps. *Geomorphology*, *94*(3-4), 268-289. http://dx.doi.org/10.1016/j.geomorph.2006.09.023.

Gansser, A. (1964). Geology of the Himalayas. *Interscience*, London, 289.

García-Rodríguez, M. J., Malpica, J. A., Benito, B., & Díaz, M. (2008). Susceptibility assessment of earthquake-triggered landslides in El Salvador using logistic regression. *Geomorphology*, *95*(3-4), 172-191. https://doi.org/10.1016/j.geomorph.2007.06.001

Gerrard, J. (1994). The landslide hazard in the Himalayas: geological control and human action. *Geomorphology and Natural Hazards*, 221-230. https://doi.org/10.1016/B978-0-444-82012-9.50019-0.

Ghimire, M. (2011). Landslide occurrence and its relation with terrain factors in the Siwalik Hills, Nepal: case study of susceptibility assessment in three basins. *Natural hazards*, *56*(1), 299-320.DOI: 10.1007/s11069-010-9569-7.

Gibo, S., Egashira, K., Ohtsubo, M., & Nakamura, S. (2002). Strength recovery from residual state in reactivated landslides. *Geotechnique*, *52*(9), 683-686. http://dx.doi.org/10.1680/geot.2002.52.9.683.

Giuseppe, F., Simoni, S., Godt, J. W., Lu, N., & Rigon, R. (2016). Geomorphological control on variably saturated hillslope hydrology and slope instability. *Water Resources Research*, *52*(6), 4590-4607. https://doi.org/10.1002/2015WR017626.

Goodman, R. E. (1976). Toppling of Rock Slope, ASCE. Speciality Conf. *Rock Engineering for Foundation and Slopes*, *2*, 201-234.

Gorum, T., Fan, X., van Westen, C. J., Huang, R. Q., Xu, Q., Tang, C., & Wang, G. (2011). Distribution pattern of earthquake-induced landslides triggered by the 12 May 2008 Wenchuan earthquake. *Geomorphology*, *133*(3-4), 152-167. https://doi.org/10.1016/j.geomorph.2010.12.030.

Greco, R., Sorriso-Valvo, M., & Catalano, E. (2007). Logistic regression analysis in the evaluation of mass movements susceptibility: the Aspromonte case study, Calabria, Italy. *Engineering geology*, *89*(1-2), 47-66. https://doi.org/10.1016/j.enggeo.2006.09.006.

Griffiths, D. V., Huang, J., & Dewolfe, G. F. (2011). Numerical and analytical observations on long and infinite slopes. *International Journal for Numerical and Analytical Methods in Geomechanics*, *35*(5), 569-585. https://doi.org/10.1002/nag.909.

Griffiths, J. S. (1999). Proving the occurrence and cause of a landslide in a legal context. *Bulletin of Engineering Geology and the Environment*, *58*(1), 75-85. https://doi.org/10.1007/s100640050070.

Guzzetti, F. (2006). *Landslide hazard and risk assessment*. Doctoral dissertation, Universitäts-und Landesbibliothek Bonn, 389 pp.

Guzzetti, F., Cardinali, M., Reichenbach, P., & Carrara, A. (2000). Comparing Landslide Maps: A Case Study in the Upper Tiber River Basin, Central Italy. *Environmental management*, *25*(3). https://doi.org/10.1007/s002679910020.

Guzzetti, F., Carrara, A., Cardinali, M., & Reichenbach, P. (1999). Landslide hazard evaluation: a review of current techniques and their application in a multi-scale study,

Central Italy. *Geomorphology*, *31*(1-4), 181-216. https://doi.org/10.1016/S0169-555X(99)00078-1.

Guzzetti, F., Mondini, A. C., Cardinali, M., Fiorucci, F., Santangelo, M., & Chang, K. T. (2012). Landslide inventory maps: New tools for an old problem. *Earth-Science Reviews*, *112*(1-2), 42-66. https://doi.org/10.1016/j.earscirev.2012.02.001.

Guzzetti, F., Peruccacci, S., Rossi, M., & Stark, C. P. (2008). The rainfall intensity–duration control of shallow landslides and debris flows: an update. *Landslides*, *5*(1), 3-17. https://doi.org/10.1007/s10346-007-0112-1.

Guzzetti, F., Reichenbach, P., Cardinali, M., Galli, M., & Ardizzone, F. (2005). Probabilistic landslide hazard assessment at the basin scale. *Geomorphology*, *72*(1-4), 272-299. https://doi.org/10.1016/j.geomorph.2005.06.002.

Gyawali, P., & Tamrakar, N. K. (2018). Landslide susceptibility assessment of the Chure Khola Catchment area of the Siwalik region, Central Nepal. *Journal of Nepal Geological Society*, *56*(1), 19-30. https://doi.org/10.3126/jngs.v56i1.22696.

Hagen T. (1951). Preliminary note on the geological structure of Central Nepal. Verhandlungen der Schweizerischen Naturforschenden Gesellschaft, Luzern, pp 133–134.

Hagen, T. (1959). Über den Geologischen Bau des Nepal-Himalaya mit besonderer Berücksichtigung der Siwalik-Zone und der Talbildung. *Jahrbuch der St. Gallischen Naturwissenchaftlichen* Gesellschaft, 76(3–48).

Hagen, T. (1969). Report on the Geological survey of Nepal, Vol. 1: preliminary reconnaissance. *Denkschriften der Schweizerischen Naturforschenden Gesellschaft Memoires de la Societe Helvetique des Sciences Naturelles*, *84*(1), 185.

Hamza, T., & Raghuvanshi, T. K. (2017). GIS based landslide hazard evaluation and zonation–A case from Jeldu District, Central Ethiopia. *Journal of King Saud University-Science*, *29*(2), 151-165. https://doi.org/10.1016/j.jksus.2016.05.002.

Hansen, A. (1984). Landslide hazard analysis. In: Brunsen, D. and Prior, D.B., Eds., *Slope Instability*, John Wiley and Sons, New York, 523-602.

Hansen, A., Franks, C. A. M., Kirk, P. A., Brimicombe, A. J., & Tung, F. (1995). Application of GIS to hazard assessment, with particular reference to landslides in Hong Kong. *Geographical information systems in assessing natural hazards*, 273-298. https://doi.org/10.1007/978-94-015-8404-3_14.

Harp, E. L., Reid, M. E., McKenna, J. P., & Michael, J. A. (2009). Mapping of hazard from rainfall-triggered landslides in developing countries: examples from Honduras and Micronesia. *Engineering Geology*, *104*(3-4), 295-311. https://doi.org/10.1016/j.enggeo.2008.11.010.

Hasegawa, S., Dahal, R. K., Yamanaka, M., Bhandary, N. P., Yatabe, R., & Inagaki, H. (2009). Causes of large-scale landslides in the Lesser Himalaya of central Nepal. *Environmental geology*, *57*(6), 1423-1434. https://doi.org/10.1007/s00254-008-1420-z.

Heim, A. (1932). *Bergsturz und Menschenleben*. Fretz und Wasmuth, Zurich, p. 218.

Hennrich, K., Crozier, M.J. (2004). A Hillslope hydrology approach for catchment-scale slope stability analysis. *Earth Surfaces Process Landforms* 29, 599–610. https://doi.org/10.1002/esp.1054.

Hoek, E., & Bray, J. (1981). Rock Slope Engineering, 3rd edn, Inst. *Mining and Metallurgy, London, UK*. https://doi.org/10.1201/9781482267099.

Hong, Y., Adler, R., & Huffman, G. (2007). Use of satellite remote sensing data in the mapping of global landslide susceptibility. *Natural hazards*, *43*(2), 245-256. https://doi.org/10.1007/s11069-006-9104-z.

Howard, A. K. (1984). The revised ASTM standard on the unified classification system. *Geotechnical Testing Journal*, *7*(4), 216-222.

Huabin, W., Gangjun, L., Weiya, X., & Gonghui, W. (2005). GIS-based landslide hazard assessment: an overview. *Progress in Physical geography*, *29*(4), 548-567. https://doi.org/10.1191/0309133305pp462ra.

Huang, F., Yao, C., Liu, W., Li, Y., & Liu, X. (2018). Landslide susceptibility assessment in the Nantian area of China: a comparison of frequency ratio model and support vector machine. *Geomatics, Natural Hazards and Risk*, *9*(1), 919-938. https://doi.org/10.1080/19475705.2018.1482963.

Huang, Y., & Zhao, L. (2018). Review on landslide susceptibility mapping using support vector machines. *Catena*, *165*, 520-529. https://doi.org/10.1016/j.catena.2018.03.003.

Hung, L.Q., Van, N.T.H., Duc, D.M., Ha, L.T.C., Van Son, P., Khanh, N.H., Binh, L.T., (2015). Landslide susceptibility mapping by combining the analytical hierarchy process and weighted linear combination methods: a case study in the upper Lo River catchment (Vietnam). *Landslides,* 1–17. http://dx.doi.org/10.1007/s10346-015-0657-3.

Hungr, O., Evans, S. G., Bovis, M. M., & Hutchinson, J. N. (2002). A review of the classification of landslides of the flow type. *Environmental and Engineering Geosciences. 8*(1), 225. http://dx.doi.org/10.2113/gseegeosci.7.3.221.

Hungr, O., Evans, S.G., Hutchinson, I.N. (2001). A Review of the Classification of Landslides of the Flow Type. *Environment and Engineering Geoscience*.7 (3),221-238.https://doi.org/10.2113/gseegeosci.7.3.221.

Hungr, O., Leroueil, S., & Picarelli, L. (2014). The Varnes classification of landslide types, an update. *Landslides,* 11, 167-194. https://doi.org/10.1007/s10346-013-0436-y.

Hungr, O., Leroueil, S., Picarelli, L. (2013). The Varnes classification of landslide types, an update. *Landslides* **11,** 167–194. https://doi.org/10.1007/s10346-013-0436-y.

Hurst, M. D., Mudd, S. M., Yoo, K., Attal, M., & Walcott, R. (2013). Influence of lithology on hillslope morphology and response to tectonic forcing in the northern Sierra Nevada of California. *Journal of Geophysical Research: Earth Surface*, *118*(2), 832-851.

https://doi.org/10.1002/jgrf.20049.

Hutchinson, J. N. (1968). Mass movement. *Encyclopedia of geomorphology*, Reinhold Publishers, New York, pp 688–695.

Hutchinson, J. N. (1988). General report: morphological and geotechnical parameters of landslides in relation to geology and hydrogeology. In *International symposium on landslides. 5* (pp. 3-35).

Iida, T. (1999). A stochastic hydro-geomorphological model for shallow landsliding due to rainstorm. *Catena, 34*(3-4), 293-313. https://doi.org/10.1016/S0341-8162(98)00093-9.

Ilia, I., & Tsangaratos, P. (2016). Applying weight of evidence method and sensitivity analysis to produce a landslide susceptibility map. *Landslides*, *13*(2), 379-397. https://doi.org/10.1007/s10346-015-0576-3.

Ilia, I., Tsangaratos, P., Koumantakis, I., & Rozos, D. (2010). Application of a Bayesian approach in GIS based model for evaluating landslide susceptibility. Case study KIMI area, Euboea, Greece. *Bulletin of the Geological Society of Greece*, *43*(3), 1590-1600. http://dx.doi.org/10.12681/bgsg.11333

Irwin-Hunt, J. R., (1960). *Some Quantitative Aspects of Mass Movement*. Thesis, Kings College, University of London, London, 76 pp.

Iwashita, F., Friedel, M. J., Ribeiro, G. F., & Fraser, S. J. (2012). Intelligent estimation of spatially distributed soil physical properties. *Geoderma*, *170*, 1-10. https://doi.org/10.1016/j.geoderma.2011.11.002.

Jade, S., & Sarkar, S. (1993). Statistical models for slope instability classification. *Engineering geology*, *36*(1-2), 91-98. https://doi.org/10.1016/0013-7952(93)90021-4.

Kamp, U., Growley, B. J., Khattak, G. A., & Owen, L. A. (2008). GIS-based landslide susceptibility mapping for the 2005 Kashmir earthquake region. *Geomorphology*, *101*(4), 631-642. https://doi.org/10.1016/j.geomorph.2008.03.003.

Kannaujiya, S., Chattoraj, S. L., Jayalath, D., Bajaj, K., Podali, S., & Bisht, M. P. S. (2019). Integration of satellite remote sensing and geophysical techniques (electrical resistivity tomography and ground penetrating radar) for landslide characterization at Kunjethi (Kalimath), Garhwal Himalaya, India. *Natural Hazards*, *97*(3), 1191-1208. https://doi.org/10.1007/s11069-019-03695-0.

Kanungo, D. P., Arora, M. K., Sarkar, S., & Gupta, R. P. (2012). Landslide Susceptibility Zonation (LSZ) Mapping–A Review. *Journal of South Asia Disaster Study*, 2 (1), 81–105.

Kayastha, P., Dhital, M. R., & De Smedt, F. (2012). Landslide susceptibility mapping using the weight of evidence method in the Tinau watershed, Nepal. *Natural hazards*, *63*(2), 479-498. https://doi.org/10.1007/s11069-012-0163-z.

Kayastha, P., Dhital, M.R., De Smedt, F., (2013). Application of the analytical hierarchy process (AHP) for landslide susceptibility mapping: a case study from the Tinau watershed, west Nepal. *Computer and Geosciences* 52, 398–408. https://doi.org/10.1016/j.cageo.2012.11.003.

Kim, K. D., Lee, S., Oh, H. J., Choi, J. K., & Won, J. S. (2006). Assessment of ground subsidence hazard near an abandoned underground coal mine using GIS. *Environmental Geology*, *50*(8), 1183-1191. https://doi.org/10.1007/s00254-006-0290-5.

Kitutu, M. G., Muwanga, A., Poesen, J., & Deckers, J. A. (2009). Influence of soil properties on landslide occurrences in Bududa district, Eastern Uganda. *African journal of agricultural research*, *4*(7), 611-620.

Knapen, A., Kitutu, M. G., Poesen, J., Breugelmans, W., Deckers, J., & Muwanga, A. (2006). Landslides in a densely populated county at the footslopes of Mount Elgon (Uganda): characteristics and causal factors. *Geomorphology*, *73*(1-2), 149-165.

https://doi.org/10.1016/j.geomorph.2005.07.004.

Korup, O., & Stolle, A. (2014). Landslide prediction from machine learning. *Geology today*, *30*(1), 26-33. https://doi.org/10.1111/gto.12034.

Kumar, R., & Anbalagan, R. (2019). Landslide susceptibility mapping of the Tehri reservoir rim area using the weights of evidence method. *Journal of Earth System Science*, *128*(6), 1-18. https://doi.org/10.1007/s12040-019-1159-9.

Ladd, G. E. (1935). Landslides, subsidence and rock-falls. *American Railway Engineering Association.*

Larsen, I. J., Montgomery, D. R., & Korup, O. (2010). Landslide erosion controlled by hillslope material. *Nature Geoscience*, *3*(4), 247-251.
https://doi.org/10.1038/ngeo776.

Lee, I. K., White, W., & Ingles, O. G. (1983). Soil formation, classification and exploration. *Principal of Geotechnical engineering*, 1(1-56).

Lee, S. (2007). Landslide susceptibility mapping using an artificial neural network in the Gangneung area, Korea. *International Journal of Remote Sensing*, *28*(21), 4763-4783. https://doi.org/10.1080/01431160701264227.

Lee, S., & Choi, J. (2004). Landslide susceptibility mapping using GIS and the weight-of-evidence model. *International Journal of Geographical Information Science*, *18*(8), 789-814. https://doi.org/10.1080/13658810410001702003.

Lee, S., & Pradhan, B. (2006). Probabilistic landslide hazards and risk mapping on Penang Island, Malaysia. *Journal of Earth System Science*, *115*(6), 661-672. https://doi.org/10.1007/s12040-006-0004-0.

Lee, S., & Pradhan, B. (2007). Landslide hazard mapping at Selangor, Malaysia using frequency ratio and logistic regression models. *Landslides*, *4*(1), 33-41. https://doi.org/10.1007/s10346-006-0047-y.

Lee, S., & Sambath, T. (2006). Landslide susceptibility mapping in the Damrei Romel area, Cambodia using frequency ratio and logistic regression models. *Environmental Geology*, *50*(6), 847-855. https://doi.org/10.1007/s00254-006-0256-7.

Lee, S., & Talib, J. A. (2005). Probabilistic landslide susceptibility and factor effect analysis. *Environmental Geology*, *47*(7), 982-990. https://doi.org/10.1007/s00254-005-1228-z.

Lee, S., Hwang, J., & Park, I. (2013). Application of data-driven evidential belief functions to landslide susceptibility mapping in Jinbu, Korea. *Catena*, *100*, 15-30. https://doi.org/10.1016/j.catena.2012.07.014.

Lee, S., Ryu, J. H., Won, J. S., & Park, H. J. (2004). Determination and application of the weights for landslide susceptibility mapping using an artificial neural network. *Engineering Geology*, *71*(3-4), 289-302. https://doi.org/10.1016/S0013-7952(03)00142-X.

Lepore, C., Kamal, S. A., Shanahan, P., & Bras, R. L. (2012). Rainfall-induced landslide susceptibility zonation of Puerto Rico. *Environmental Earth Sciences*, *66*(6), 1667-1681. https://doi.org/10.1007/s12665-011-0976-1.

Leroueil, S., Locat, A., Eberhardt, E., & Kovacevic, N. (2012). Progressive failure in natural and engineered slopes. *Landslides and Engineered Slope, Taylor & Francis Group, London*, *3146*.

Li, D., Yin, K., Glade, T., & Leo, C. (2017). Effect of over-consolidation and shear rate on the residual strength of soils of silty sand in the Three Gorges Reservoir. *Scientific Reports*, *7*(1), 1-11. https://doi.org/10.1038/s41598-017-05749-4.

Li, L., Yu, B., Zhu, Y., Chu, S., & Wu, Y. (2015). Topographical factors in the formation of gully-type debris flows in Longxi River catchment, Sichuan, China. *Environmental Earth Sciences*, *73*(8), 4385-4398. https://doi.org/10.1007/s12665-014-3722-7.

Londe, P. (1965). Une méthode d'analyse à trois dimensions de la stabilité d'une rive rocheuse. *Ann Ponts Chaussees*, *135*(1), 37-60.

Lyell, C. (1833). *Principles of geology, being an attempts to explain the former changes of the Earth's surface.* London: John Murray, 3.

Maheshwari, B. K. (2019). Earthquake-induced landslide hazard assessment of chamoli district, uttarakhand using relative frequency ratio method. *Indian Geotechnical Journal*, *49*(1), 108-123. http://dx.doi.org/10.1007/s40098-018-0334-2.

Mandal, S., & Mondal, S. (2019). Probabilistic approaches and landslide susceptibility. In *Geoinformatics and Modelling of Landslide Susceptibility and Risk*, 145-163. http://dx.doi.org/10.1007/978-3-030-10495-5_6.

Mansouri, D., Reza, M., (2014). Landslide susceptibility zonation using analytical hierarchy process and GIS for the Bojnurd region, northeast of Iran. *Landslides* 11 (6), 1079–1091. https://doi.org/10.1007/s10346-013-0458-5.

Marr, J.E. (1916). The geology of the Lake District and the scenario as influenced by geological structure, University Press. Cambridge.

Martha, T. R., van Westen, C. J., Kerle, N., Jetten, V., & Kumar, K. V. (2013). Landslide hazard and risk assessment using semi-automatically created landslide inventories. *Geomorphology*, *184*,139-150.
https://doi.org/10.1016/j.geomorph.2012.12.001.

Mathew, J., Jha, V. K., & Rawat, G. S. (2007). Weights of evidence modelling for landslide hazard zonation mapping in part of Bhagirathi valley, Uttarakhand. *Current science*, 628-638.

Medlicott, H. B. (1875). Note on the geology of Nepal. *Record of the Geological Survey of India*, 8, (93–101).

Medlicott, H.B. (1879). Sub-Himalayas, a manual of the geology of India. *Government of India,* 517–571.

Meyerhof, G. G. (1957). The mechanism of flow slides in cohesive soils. *Geotechnique*, *7*(1), 41-49.

Mezughi, T. H., Akhir, J. M., Rafek, A. G., & Abdullah, I. (2011). Landslide susceptibility assessment using frequency ratio model applied to an area along the EW highway (Gerik-Jeli). *American Journal of Environmental Sciences*, *7*(1), 43. http://dx.doi.org/10.3844/ajessp.2011.43.50.

Middlemiss, C. S. (1890). Physical geology of the Sub-Himalaya of Garhwal and Kumaun. *Memoirs of the geological survey of India*, 24, (2) 59–200.

Ministry of Home Affairs (2020). *Nepal Disaster Report 2019*. Flood Resilience Portal (MoHA)

Mohammady, M., Pourghasemi, H. R., & Pradhan, B. (2012). Landslide susceptibility mapping at Golestan Province, Iran: a comparison between frequency ratio, Dempster–Shafer, and weights-of-evidence models. *Journal of Asian Earth Sciences*, *61*, 221-236. https://doi.org/10.1016/j.jseaes.2012.10.005.

Mondal, S., & Maiti, R. (2013). Integrating the analytical hierarchy process (AHP) and the frequency ratio (FR) model in landslide susceptibility mapping of Shiv-khola watershed, Darjeeling Himalaya. *International Journal of Disaster Risk Science*, *4*(4), 200-212. https://doi.org/10.1007/s13753-013-0021-y.

Mondini, A. C., Guzzetti, F., Reichenbach, P., Rossi, M., Cardinali, M., & Ardizzone, F. (2011). Semi-automatic recognition and mapping of rainfall induced shallow landslides using optical satellite images. *Remote sensing of environment*, *115*(7), 1743-1757. https://doi.org/10.1016/j.rse.2011.03.006.

Montgomery, D. R., & Dietrich, W. E. (1994). A physically based model for the topographic control on shallow landsliding. *Water resources research*, *30*(4), 1153-1171. https://doi.org/10.1029/93WR02979.

Morgenstern, N. R. (1993). The evaluation of slope stability—A 25 year perspective. In *Stability and performance of slopes and embankments II* (pp. 1-26). ASCE. https://doi.org/10.1016/0148-9062%2893%2993166-u.

Morrow, C. A., Shi, L. Q., & Byerlee, J. D. (1982). Strain hardening and strength of clay-rich fault gouges. *Journal of Geophysical Research: Solid Earth*, *87*(B8), 6771-6780. https://doi.org/10.1029/JB087iB08p06771.

Mugagga, F., Kakembo, V., & Buyinza, M. (2012). A characterisation of the physical properties of soil and the implications for landslide occurrence on the slopes of Mount Elgon, Eastern Uganda. *Natural hazards*, *60*(3), 1113-1131. https://doi.org/10.1007/s11069-011-9896-3.

Nemčok, A., Pašek, J., & Rybář, J. (1972). Classification of landslides and other mass movements. *Rock mechanics*, *4*(2), 71-78.

Neuhäuser, B., Damm, B., & Terhorst, B. (2012). GIS-based assessment of landslide susceptibility on the base of the weights-of-evidence model. *Landslides*, *9*(4), 511-528. https://doi.org/10.1007/s10346-011-0305-5.

Neuland, H. (1976). A prediction model of landslips. *Catena*, *3*(2), 215-230. https://doi.org/10.1016/0341-8162(76)90011-4.

Nilsen, T. H., & Brabb, E. E. (1977). Slope stability studies in the San Francisco Bay region, California. *Reviews in Engineering Geology-GSA*, *3*, 235-243. https://doi.org/10.1130/REG3-p233.

Nugraha, H., Wacano, D., Dipayana, G. A., Cahyadi, A., Mutaqin, B. W., & Larasati, A. (2015). Geomorphometric characteristics of landslides in the Tinalah watershed, Menoreh

Mountains, Yogyakarta, Indonesia. *Procedia Environmental Sciences*, *28*, 578-586. https://doi.org/10.1016/j.proenv.2015.07.068.

Oh, H. J., Lee, S., Chotikasathien, W., Kim, C. H., & Kwon, J. H. (2009). Predictive landslide susceptibility mapping using spatial information in the Pechabun area of Thailand. *Environmental Geology*, *57*(3), 641-651. https://doi.org/10.1016/j.proenv.2015.07.068.

Onions, C.T. (1933). *The Oxford English Dictionary*. Oxford University Press, Oxford.

Ozdemir, A. (2020). A comparative study of the frequency ratio, analytical hierarchy process, artificial neural networks and fuzzy logic methods for landslide susceptibility mapping: Taşkent (Konya), Turkey. *Geotechnical and Geological Engineering*, *38*(4), 4129-4157. https://doi.org/10.1007/s10706-020-01284-8.

Ozdemir, A., & Altural, T. (2013). A comparative study of frequency ratio, weights of evidence and logistic regression methods for landslide susceptibility mapping: Sultan Mountains, SW Turkey. *Journal of Asian Earth Sciences*, *64*, 180-197. https://doi.org/10.1016/j.jseaes.2012.12.014.

Pack, R. T., Tarboton, D. G., & Goodwin, C. N. (1999). SINMAP 2.0-A stability index approach to terrain stability hazard mapping, user's manual.

Pal, S. C., & Chowdhuri, I. (2019). GIS-based spatial prediction of landslide susceptibility using frequency ratio model of Lachung River basin, North Sikkim, India. *SN Applied Sciences*, *1*(5), 1-25. https://doi.org/10.1007/s42452-019-0422-7.

Panchal, S., & Shrivastava, A. K. (2021). A comparative study of frequency ratio, Shannon’s entropy and analytic hierarchy process (AHP) models for landslide susceptibility assessment. *ISPRS International Journal of Geo-Information*, *10*(9), 603. https://doi.org/10.3390/ijgi10090603.

Pardeshi, S. D., Autade, S. E., & Pardeshi, S. S. (2013). Landslide hazard assessment: recent trends and techniques. *SpringerPlus*, *2*(1), 1-11. https://doi.org/10.1186/2193-1801-2-523.

Park, H. J., Jang, J. Y., & Lee, J. H. (2017). Physically based susceptibility assessment of rainfall-induced shallow landslides using a fuzzy point estimate method. *Remote Sensing*, *9*(5), 487. https://doi.org/10.3390/rs9050487.

Park, N. W. (2011). Application of Dempster-Shafer theory of evidence to GIS-based landslide susceptibility analysis. *Environmental Earth Sciences*, *62*(2), 367-376. https://doi.org/10.1007/s12665-010-0531-5.

Park, S., Choi, C., Kim, B., & Kim, J. (2013). Landslide susceptibility mapping using frequency ratio, analytic hierarchy process, logistic regression, and artificial neural network methods at the Inje area, Korea. *Environmental earth sciences*, *68*(5), 1443-1464. https://doi.org/10.1007/s12665-012-1842-5.

Pearson, K. (1895). Correlation coefficient. *Proceedings of the royal society of London*, *58*, (347-352).

Piacentini, D., Troiani, F., Soldati, M., Notarnicola, C., Savelli, D., Schneiderbauer, S., & Strada, C. (2012). Statistical analysis for assessing shallow-landslide susceptibility in South Tyrol (south-eastern Alps, Italy). *Geomorphology*, *151*, 196-206. http://dx.doi.org/10.1016/j.geomorph.2012.02.003.

Pilgrim, G.E. (1910) Preliminary note on a revised classification of the tertiary freshwater deposits of India. *Records of the geological survey of India*, 11(3), 185–205.

Pirasteh, S., & Li, J. (2017). Landslides investigations from geoinformatics perspective: quality, challenges, and recommendations. *Geomatics, natural hazards and risk*, *8*(2), 448-465. https://doi.org/10.1080/19475705.2016.1238850.

Pokhrel, K., & Bhandari, B. P. (2019). Identification of potential landslide susceptible area in the lesser Himalayan Terrain of Nepal. *Journal of Geoscience and Environment Protection*, *7*(11), 24-38. https://doi.org/10.4236/gep.2019.711003.

Porwal, A., Carranza, E. J. M., & Hale, M. (2004). A hybrid neuro-fuzzy model for mineral potential mapping. *Mathematical geology*, *36*(7), 803-826. https://doi.org/10.1023/B:MATG.0000041180.34176.65.

Pourghasemi, H. R., Mohammady, M., & Pradhan, B. (2012). Landslide susceptibility mapping using index of entropy and conditional probability models in GIS: Safarood Basin, Iran. *Catena*, *97*, 71-84. https://doi.org/10.1016/j.catena.2012.05.005.

Pradhan, B. (2010). Landslide susceptibility mapping of a catchment area using frequency ratio, fuzzy logic and multivariate logistic regression approaches. *Journal of the Indian Society of Remote Sensing*, *38*(2), 301-320. https://doi.org/10.1007/s12524-010-0020-z.

Pradhan, B., & Lee, S. (2010). Landslide susceptibility assessment and factor effect analysis: backpropagation artificial neural networks and their comparison with frequency ratio and bivariate logistic regression modelling. *Environmental Modelling & Software*, *25*(6),747-759. https://doi.org/10.1016/j.envsoft.2009.10.016.

Pradhan, B., & Youssef, A. M. (2010). Manifestation of remote sensing data and GIS on landslide hazard analysis using spatial-based statistical models. *Arabian Journal of Geosciences*, *3*(3), 319-326. http://dx.doi.org/10.1007/s12517-009-0089-2.

Rahardjo, H., Nio, A. S., Leong, E. C., & Song, N. Y. (2010). Effects of groundwater table position and soil properties on stability of slope during rainfall. *Journal of geotechnical and geoenvironmental engineering*, *136*(11), 1555-1564. http://dx.doi.org/10.1061/(ASCE)GT.1943-5606.0000385.

Ramesh, V., & Anbazhagan, S. (2015). Landslide susceptibility mapping along Kolli hills Ghat road section (India) using frequency ratio, relative effect and fuzzy logic models. *Environmental Earth Sciences*, *73*(12), 8009-8021.

http://dx.doi.org/10.1007/s12665-014-3954-6.

Ramiah, B. K., Purushothamaraj, P., & Tavane, N. G. (1973). Thixotropic effects on residual strength of remoulded clays. *Indian Geotech. J, 3*(3), 189-197.

Razavizadeh, S., Solaimani, K., Massironi, M., & Kavian, A. (2017). Mapping landslide susceptibility with frequency ratio, statistical index, and weights of evidence models: a case study in northern Iran. *Environmental Earth Sciences*, *76*(14), 1-16. https://doi.org/10.1007/s12665-017-6839-7.

Regmi, A. D., Devkota, K. C., Yoshida, K., Pradhan, B., Pourghasemi, H. R., Kumamoto, T., & Akgun, A. (2014). Application of frequency ratio, statistical index, and weights-of-evidence models and their comparison in landslide susceptibility mapping in Central Nepal Himalaya. *Arabian Journal of Geosciences*, *7*(2), 725-742. https://doi.org/10.1007/s12517-012-0807-z.

Regmi, A. D., Yoshida, K., Pourghasemi, H. R., DhitaL, M. R., & Pradhan, B. (2014). Landslide susceptibility mapping along Bhalubang—Shiwapur area of mid-Western Nepal using frequency ratio and conditional probability models. *Journal of Mountain Science*, *11*(5), 1266-1285. https://doi.org/10.1007/s11629-013-2847-6.

Reichenbach, P., Mondini, A. C., & Rossi, M. (2014). The influence of land use change on landslide susceptibility zonation: the Briga catchment test site (Messina, Italy). *Environmental management*, *54*(6), 1372-1384. https://doi.org/10.1007/s00267-014-0357-0.

Reichenbach, P., Rossi, M., Malamud, B. D., Mihir, M., & Guzzetti, F. (2018). A review of statistically-based landslide susceptibility models. *Earth-science reviews*, *180*, 60-91. https://doi.org/10.1016/j.earscirev.2018.03.001.

Reis, S., Yalcin, A., Atasoy, M., Nisanci, R. E. C. E. P., Bayrak, T., Erduran, M. U. R. A. T., ... & Ekercin, S. (2012). Remote sensing and GIS-based landslide susceptibility

mapping using frequency ratio and analytical hierarchy methods in Rize province (NE Turkey). *Environmental Earth Sciences*, *66*(7), 2063-2073. https://doi.org/10.1007/s12665-011-1432-y.

Remondo, J., Yu, L., Cao, Y., Zhou, C., Wang, Y., & Huo, Z. (2019). Landslide susceptibility mapping combining information gain ratio and support vector machines: a case study from Wushan segment in the Three Gorges Reservoir area, China. *Applied Sciences*, *9*(22), 4756. https://doi.org/10.3390/app9224756.

Rib, H. T., & Liang, T. (1978). Recognition and identification. *Transportation Research Board Special Report*, (176).

Rice, R. M., Crobett, E. S., & Bailey, R. G. (1969). Soil slips related to vegetation, topography, and soil in southern California. *Water Resources Research*, *5*(3), 647-659.

Riemer, M. F., Collins, B. D., Badger, T. C., Toth, C., & Yu, Y. C. (2015). *Geotechnical soil characterization of intact Quaternary deposits forming the March 22, 2014 SR-530 (Oso) landslide, Snohomish County, Washington*. US Department of the Interior, US Geological Survey. https://doi.org/10.3133/ofr20151089.

Roback, K., Clark, M. K., West, A. J., Zekkos, D., Li, G., Gallen, S. F., ... & Godt, J. W. (2018). The size, distribution, and mobility of landslides caused by the 2015 Mw7. 8 Gorkha earthquake, Nepal. *Geomorphology*, *301*, 121-138. https://doi.org/10.1016/j.geomorph.2017.01.030

Rossi, M., & Reichenbach, P. (2016). LAND-SE: a software for statistically based landslide susceptibility zonation, version 1.0. *Geoscientific Model Development*, *9*(10), 3533-3543. https://doi.org/10.5194/gmd-9-3533-2016.

Ruff, M., & Czurda, K. (2008). Landslide susceptibility analysis with a heuristic approach in the Eastern Alps (Vorarlberg, Austria). *Geomorphology*, *94*(3-4), 314-324. https://doi.org/10.1016/j.geomorph.2006.10.032,

Rundsen, D., Jones, D.K.C.(1976). *The evolution of landslide slopes in South-West Dorset, Philosophical Transactions of the Royal Society of London*. Series A, 283, 605-631.

Sabokbar, H. F., Roodposhti, M. S., & Tazik, E. (2014). Landslide susceptibility mapping using geographically-weighted principal component analysis. *Geomorphology*, *226*, 15-24. https://doi.org/10.1016/j.geomorph.2014.07.026.

Saha, A. K., Gupta, R. P., Sarkar, I., Arora, M. K., & Csaplovics, E. (2005). An approach for GIS-based statistical landslide susceptibility zonation—with a case study in the Himalayas. *Landslides*, *2*(1), 61-69. https://doi.org/10.1007/s10346-004-0039-8.

Salvatici, T., Tofani, V., Rossi, G., D'Ambrosio, M., Tacconi Stefanelli, C., Masi, E. B., ... & Casagli, N. (2018). Application of a physically based model to forecast shallow landslides at a regional scale. *Natural Hazards and Earth System Sciences*, *18*(7), 1919-1935. https://doi.org/10.5194/nhess-18-1919-2018.

Sarda, V. K., & Pandey, D. D. (2019). Landslide susceptibility mapping using information value method. *Jordan Journal of Civil Engineering*, *13*(2).

Sarkar, S., Kanungo, D.P., Patra, A.K., Kumar, P. (2012). GIS Based Landslide Susceptibility Mapping–A Case Study in Indian Himalaya. In: *Disaster Mitigation of Debris Flows, Slope Failures and Landslides.* Universal Academy Press, Inc. Tokyo, Japan, p 838.

Sarkar, S., Roy, A. K., & Martha, T. R. (2013). Landslide susceptibility assessment using information value method in parts of the Darjeeling Himalayas. *Journal of the Geological Society of India*, *82*(4), 351-362. https://doi.org/10.1007/s12594-013-0162-z.

Selby, M. J. (1993). Hillslope Materials and Processes Oxford Univ. *Press, New York*.

Shadman Roodposhti, M., Aryal, J., Shahabi, H., & Safarrad, T. (2016). Fuzzy shannon entropy: A hybrid gis-based landslide susceptibility mapping method. *Entropy*, *18*(10), 343. https://doi.org/10.3390/e18100343.

Shafique, M., van der Meijde, M., & Khan, M. A. (2016). A review of the 2005 Kashmir earthquake-induced landslides; from a remote sensing prospective. *Journal of Asian Earth Sciences*, *118*,68-80. https://doi.org/10.1016/j.jseaes.2016.01.002.

Shannon, C. E. (1948). A mathematical theory of communication. *The Bell system technical journal*, *27*(3), 379-423. https://doi.org/10.1002/j.1538-7305.1948.tb01338.x.

Sharma, L. P., Patel, N., Ghose, M. K., & Debnath, P. (2015). Development and application of Shannon's entropy integrated information value model for landslide susceptibility assessment and zonation in Sikkim Himalayas in India. *Natural hazards*, *75*(2), 1555-1576. http://dx.doi.org/10.1007/s11069-014-1378-y.

Sharma, M., & Kumar, R. (2008). GIS-based landslide hazard zonation: a case study from the Parwanoo area, Lesser and Outer Himalaya, HP, India. *Bulletin of Engineering Geology and the Environment*, *67*(1), 129-137. https://doi.org/10.1007/s10064-007-0113-2.

Sharma, R. K., & Mehta, B. S. (2012). Macro-zonation of landslide susceptibility in Garamaura-Swarghat-Gambhar section of national highway 21, Bilaspur District, Himachal Pradesh (India). *Natural Hazards*, *60*(2), 671-688. https://doi.org/10.1007/s11069-011-0041-0.

Sharma, S., & Mahajan, A. K. (2019). A comparative assessment of information value, frequency ratio and analytical hierarchy process models for landslide susceptibility mapping of a Himalayan watershed, India. *Bulletin of Engineering Geology and the Environment*, *78*(4), 2431-2448. https://doi.org/10.1007/s10064-018-1259-9.

Sharpe, C. F. S.(1938). Landslides and Related Phenomena: A Study of Mass-Movements of Soil and Rock: *Columbia University Press, New York*, 137 p.

Shoaei, G., & Sidle, R. C. (2009). Variation in soil characteristics and hydrologic properties associated with historic land use near a recent landslide, Nagano Prefecture, Japan. *Geoderma*, *153*(1-2), 37-51. https://doi.org/10.1016/j.geoderma.2009.07.012.

Sidle, R., & Ochiai, H. (2006). Processes, prediction, and land use. *Water resources monograph. American Geophysical Union, Washington, 525*.

Silalahi, F. E. S., Arifianti, Y., & Hidayat, F. (2019). Landslide susceptibility assessment using frequency ratio model in Bogor, West Java, Indonesia. *Geoscience Letters*, *6*(1), 1-17. https://doi.org/10.1186/s40562-019-0140-4.

Singh, K., & Kumar, V. (2018). Hazard assessment of landslide disaster using information value method and analytical hierarchy process in highly tectonic Chamba region in bosom of Himalaya. *Journal of Mountain science*, *15*(4), 808-824. https://doi.org/10.1007/s11629-017-4634-2.

Sivakugan, N., & Das, B. M. (2009). *Geotechnical engineering: a practical problem solving approach*. J. Ross Publishing.

Skempton, A. W. (1953). Soil mechanics in relation to geology. *Proceedings of the Yorkshire Geological Society*, *29*(1), 33-62.

Skempton, A. W. (1985). Residual strength of clays in landslides, folded strata and the laboratory. *Geotechnique*, *35*(1), 3-18.

Skempton, A. W., & Hutchinson, J. (1969). Stability of natural slopes and embankment foundations. *International conference of soil mechanics and foundation engineering*, Mexico, State of the Art volume, 291–340.

Sterlacchini, S., Ballabio, C., Blahut, J., Masetti, M., & Sorichetta, A. (2011). Spatial agreement of predicted patterns in landslide susceptibility maps. *Geomorphology*, *125*(1), 51-61. https://doi.org/10.1016/j.geomorph.2010.09.004.

Stiny, J. (1910). *Die Muren: Versuch einer Monographie mit besonderer berücksichtigung der verhältnisse in Den Tiroler Alpen*. Wagner.

Süzen, M. L., & Doyuran, V. (2004). A comparison of the GIS based landslide susceptibility assessment methods: multivariate versus bivariate. *Environmental geology*, *45*(5), 665-679. https://doi.org/10.1007/s00254-003-0917-8.

Süzen, M. L., & Doyuran, V. (2004). Data driven bivariate landslide susceptibility assessment using geographical information systems: a method and application to Asarsuyu catchment, Turkey. *Engineering geology*, *71*(3-4), 303-321. https://doi.org/10.1016/S0013-7952(03)00143-1.

Talebi, A., Uijlenhoet, R., & Troch, P. A. (2008). A low-dimensional physically based model of hydrologic control of shallow landsliding on complex hillslopes. *Earth Surface Processes and Landforms: The Journal of the British Geomorphological Research Group*, *33*(13), 1964-1976. http://dx.doi.org/10.1002/esp.1648.

Talebi, A., Uijlenhoet, R., & Troch, P. A. (2008). A low-dimensional physically based model of hydrologic control of shallow landsliding on complex hillslopes. *Earth Surface Processes and Landforms: The Journal of the British Geomorphological Research Group*, *33*(13), 1964-1976. http://dx.doi.org/10.1002/esp.1648.

Talebi, A., Uijlenhoet, R., Troch, P. A. (2008). A low-dimensional physically based model of hydrologic control of shallow landsliding on complex hillslopes. *Earth Surf. Process Landforms* 33, 1964–1976. http://dx.doi.org/10.1002/esp.1648.

Tehrany, M. S., Jones, S., & Shabani, F. (2019). Identifying the essential flood conditioning factors for flood prone area mapping using machine learning techniques. *Catena*, *175*, 174-192. https://doi.org/10.1016/j.catena.2018.12.011.

Terzaghi, K. (1950). Mechanism of landslides. Application of geology to engineering practice (Berkey volume). *Paige, Chairman, Geological Society of America Bulletin*, *83*. https://doi.org/10.1130/Berkey.1950.83.

Terzaghi, K. (1957). Varieties of submarine slope failures, NGI Publication No. 25. *Norwegian Geotechnical Institute, Oslo*.

Thapa, D., & Bhandari, B. P. (2019). GIS-Based frequency ratio method for identification of potential landslide susceptible area in the Siwalik zone of Chatara-Barahakshetra section, Nepal. *Open Journal of Geology*, *9*(12), 873. https://doi.org/10.4236/ojg.2019.912096.

Thiery, Y., Malet, J. P., Sterlacchini, S., Puissant, A., & Maquaire, O. (2007). Landslide susceptibility assessment by bivariate methods at large scales: application to a complex mountainous environment. *Geomorphology*, *92*(1-2), 38-59. https://doi.org/10.1016/j.geomorph.2007.02.020.

Thomas, C. W., & Aitchison, J. (2005). Compositional data analysis of geological variability and process: a case study. *Mathematical Geology*, *37*(7), 753-772. https://doi.org/10.1007/s11004-005-7378-4.

Tian, Y., Owen, L. A., Xu, C., Ma, S., Li, K., Xu, X., ... & Maharjan, S. B. (2020). Landslide development within 3 years after the 2015 Mw 7.8 Gorkha earthquake, Nepal. *Landslides*, *17*(5), 1251-1267. https://doi.org/10.1007/s10346-020-01366-x.

Tika-Vasilikou, T., Vaughan, P. R., & Lemos, L. J. (1996). *Fast shearing of pre-existing shear zones in soil* (No. RefW-25-38095). Aristotle University of Thessaloniki. https://doi.org/10.1680/geot.1996.46.2.197.

Tiwari, B., Brandon, T. L., Marui, H., & Tuladhar, G. R. (2005). Comparison of residual shear strengths from back analysis and ring shear tests on undisturbed and remolded specimens. *Journal of Geotechnical and Geoenvironmental Engineering*, *131*(9), 1071-1079. http://dx.doi.org/10.1061/(ASCE)1090-0241(2005)131:9(1071).

Tofani, V., Bicocchi, G., Rossi, G., Segoni, S., D'Ambrosio, M., Casagli, N., & Catani, F. (2017). Soil characterization for shallow landslides modeling: a case study in the Northern Apennines (Central Italy). *Landslides*, *14*(2), 755-770. https://doi.org/10.1007/s10346-017-0809-8.

Tomita, H., Nakata, A. M., Konagai, K., Matsushima, T., Shiga, M., Ikeda, T., & Pokhrel, R. M. (2018). Landslides triggered by the 2015 Gorkha Earthquake and analysis of their long-lasting impact. *Journal of Nepal Geological Society*, *55*(1), 77-84. https://doi.org/10.3126/jngs.v55i1.22793.

Troch, P., Van Loon, E., & Hilberts, A. (2002). Analytical solutions to a hillslope-storage kinematic wave equation for subsurface flow. *Advances in Water Resources*, *25*(6), 637-649. https://doi.org/10.1016/S0309-1708(02)00017-9.

Tsou, C. Y., Higaki, D., Chigira, M., Yagi, H., Dangol, V., Amatya, S., ... & Kato, H. (2018). Topographic characteristics of landslides induced by the 2015 Gorkha earthquake, Nepal. *Journal of Nepal Geological Society*, *55*(1), 69-75.

Umar, Z., Pradhan, B., Ahmad, A., Jebur, M. N., & Tehrany, M. S. (2014). Earthquake induced landslide susceptibility mapping using an integrated ensemble frequency ratio and logistic regression models in West Sumatera Province, Indonesia. *Catena*, *118*, 124-135. https://doi.org/10.1016/j.catena.2014.02.005.

Vakhshoori, V., & Zare, M. (2016). Landslide susceptibility mapping by comparing weight of evidence, fuzzy logic, and frequency ratio methods. *Geomatics, Natural Hazards and Risk*, *7*(5), 1731-1752. https://doi.org/10.1080/19475705.2016.1144655.

Van Westen, C. J., Castellanos, E., & Kuriakose, S. L. (2008). Spatial data for landslide susceptibility, hazard, and vulnerability assessment: An overview. *Engineering geology*, *102*(3-4), 112-131. https://doi.org/10.1016/j.enggeo.2008.03.010.

Van Westen, C. J., Rengers, N., & Soeters, R. (2003). Use of geomorphological information in indirect landslide susceptibility assessment. *Natural hazards*, *30*(3), 399-419. https://doi.org/10.1023/B:NHAZ.0000007097.42735.9e.

Van Westen, C. J., Rengers, N., Terlien, M. T. J., & Soeters, R. (1997). Prediction of the occurrence of slope instability phenomenal through GIS-based hazard zonation. *Geologische Rundschau*, *86*(2), 404-414.

https://doi.org/10.1007/s005310050149.

Varnes, D. J. (1954). Landslide types and processes. *Landslides and engineering practice-special report*, 24, 20–47. Highway research board, National Academy of Sciences, Washington, DC.

Varnes, D. J. (1978). *Slope movement types and processes*. *Special report*, *176*, 11-33. Transportation research board, National Academy of Sciences, Washington, DC.

Varnes, D.J. (1984). *Landslide hazard zonation: A review of principles and practice*. UNESCO Press, Paris.

Vijith, H., & Madhu, G. (2008). Estimating potential landslide sites of an upland sub-watershed in Western Ghat's of Kerala (India) through frequency ratio and GIS. *Environmental Geology*, *55*(7), 1397-1405. http://dx.doi.org/10.1007/s00254-007-1090-2.

Wang, H. B., & Sassa, K. (2005). Comparative evaluation of landslide susceptibility in Minamata area, Japan. *Environmental Geology*, *47*(7), 956-966. http://dx.doi.org/10.1007/s00254-005-1225-2.

Wang, Q., & Li, W. (2017). A GIS-based comparative evaluation of analytical hierarchy process and frequency ratio models for landslide susceptibility mapping. *Physical Geography*, *38*(4), 318-337. https://doi.org/10.1080/02723646.2017.1294522.

Ward, W.H. (1948). A Coastal Landslip. *Second International Conference on Soil Mechanics and Foundation Engineering.* Rotterdam, Vol. 2, pp. 33-38.

Wati, S. E., Hastuti, T., Widjojo, S., & Pinem, F. (2010). Landslide susceptibility mapping with heuristic approach in mountainous area: A case study in Tawangmangu sub district Central Java, Indonesia. *International archives of the photogrammetry, remote sensing and spatial information science*, *38*(Part 8).

Wen, B. P., & Aydin, A. (2004). Deformation history of a landslide slip zone in light of soil microstructure. *Environmental & Engineering Geoscience*, *10*(2), 123-149. https://doi.org/10.2113/10.2.123.

Wen, B., & Ji, B. (2019). Variation in residual strength of the large-scale landslides' slip zones in the Three Gorges Reservoir of China. In *IAEG/AEG Annual Meeting Proceedings, San Francisco, California, 2018-Volume 1* (pp. 11-18). Springer, Cham. https://doi.org/10.1007/978-3-319-93124-1_2.

Working Party on World Landslide Inventory, (1990). A suggested method for reporting a landslide. *Bulletin International Association for Engineering Geology*, *41*, 5-12. https://doi.org/10.1007/BF02590201.

Wu, W., & Sidle, R. C. (1995). A distributed slope stability model for steep forested basins. *Water resources research*, *31*(8), 2097-2110. https://doi.org/10.1029/95WR01136.

Wu, Y., Li, W., Wang, Q., Liu, Q., Yang, D., Xing, M., ... & Yan, S. (2016). Landslide susceptibility assessment using frequency ratio, statistical index and certainty factor models for the Gangu County, China. *Arabian Journal of Geosciences*, *9*(2), 1-16. https://doi.org/10.1007/s12517-015-2112-0.

Wubalem, A., & Meten, M. (2020). Landslide susceptibility mapping using information value and logistic regression models in Goncha Siso Eneses area, northwestern Ethiopia. *SN Applied Sciences*, *2*(5), 1-19. https://doi.org/10.1007/s42452-020-2563-0.

Xu, C., Dai, F., Xu, X., & Lee, Y. H. (2012). GIS-based support vector machine modeling of earthquake-triggered landslide susceptibility in the Jianjiang River watershed, China. *Geomorphology*, *145*, 70-80. https://doi.org/10.1016/j.geomorph.2011.12.040.

Yalcin, A. (2007). The effects of clay on landslides: A case study. *Applied Clay Science*, *38*(1-2), 77-85. https://doi.org/10.1016/j.clay.2007.01.007.

Yalcin, A. (2011). A geotechnical study on the landslides in the Trabzon Province, NE, Turkey. *Applied Clay Science*, *52*(1-2), 11-19. https://doi.org/10.1016/j.clay.2011.01.015.

Yao, X., Tham, L. G., & Dai, F. C. (2008). Landslide susceptibility mapping based on support vector machine: a case study on natural slopes of Hong Kong, China. *Geomorphology*, *101*(4), 572-582. https://doi.org/10.1016/j.geomorph.2008.02.011.

Yatsu, E. (1967). Some problems on mass movements. *Geografiska Annaler: Series A, Physical Geography*, *49*(2-4), 396-401. https://doi.org/10.1080/04353676.1967.11879767

Yilmaz, I. (2009). Landslide susceptibility mapping using frequency ratio, logistic regression, artificial neural networks and their comparison: a case study from Kat landslides (Tokat—Turkey). *Computers & Geosciences*, *35*(6), 1125-1138. https://doi.org/10.1016/j.cageo.2008.08.007.

Yin, K. L., & Yan, T. Z. (1988). Statistical prediction models for instability of metamorphosed rocks. In *International symposium on landslides. 5* (pp. 1269-1272). https://doi.org/10.1016/0148-9062%2890%2990358-9.

Youssef, A. M. (2015). Landslide susceptibility delineation in the Ar-Rayth area, Jizan, Kingdom of Saudi Arabia, using analytical hierarchy process, frequency ratio, and logistic regression models. *Environmental earth sciences*, *73*(12), 8499-8518. https://doi.org/10.1007/s12665-014-4008-9.

Youssef, A. M., Al-Kathery, M., & Pradhan, B. (2015). Landslide susceptibility mapping at Al-Hasher area, Jizan (Saudi Arabia) using GIS-based frequency ratio and index of entropy models. *Geosciences Journal*, *19*(1), 113-134. https://doi.org/10.1007/s12303-014-0032-8.

Yufeng, S., & Fengxiang, J. (2009). Landslide stability analysis based on generalized information entropy. In *2009 international conference on environmental science and information application technology* (Vol. 2, pp. 83-85). IEEE. https://doi.org/10.1109/ESIAT.2009.258.

Zaruba, Q. and Mencl, V. (1969). *Landslides and their Control*. Elsevier, Amsterdam, 205 pp.

Zêzere, J. L. (2002). Landslide susceptibility assessment considering landslide typology. A case study in the area north of Lisbon (Portugal). *Natural Hazards and Earth System Sciences*, *2*(1/2), 73-82. https://doi.org/10.5194/nhess-2-73-2002.

Zhang, F., Chen, W., Liu, G. et al. (2012). Relationship between landslide types and topographic attributes in a loess catchment, China. *Journal of Mountain Science,* 9(742-751). https://doi.org/10.1007/s11629-012-2377-7.

Zhang, J. Q., Liu, R. K., Deng, W., Khanal, N. R., Gurung, D. R., Murthy, M. S. R., & Wahid, S. (2016). Characteristics of landslide in Koshi River basin, central Himalaya. *Journal of Mountain Science*, *13*(10), 1711-1722. https://doi.org/10.1007/s11629-016-4017-0.

Zhao, H. F., Zhang, L. M., Xu, Y., & Chang, D. S. (2013). Variability of geotechnical properties of a fresh landslide soil deposit. *Engineering Geology*, *166*, 1-10. https://doi.org/10.1016/j.enggeo.2013.08.006.

Zhou, J.W., Cui, P.,Yang, X.G. (2016). Effects of material composition and moisture content on the mechanical properties of landslide deposits triggered by the Wenchuan earthquake. *Acta Geologica Sinica-English Edition* 90(1), 242–257. https://doi.org/10.1111/1755-6724.12655.

Zydroń, T., & Zawisza, E. (2011). Shear strength investigation of soils in landslide areas. *Geologija*, *53*(3).

## ANNEX 1

Calculation of frequency ratio value of subclasses of 14 factors. Where, A is the number of pixel of sub classes of each factor, B is the landslide pixel present in the sub classes, FR is general frequency ratio, RF is percent of frequency ratio of each sub classes.

| SN | Rainfall (mm) | A | B | A% | B% | FR | RF | RF% | RF (INT) |
|---|---|---|---|---|---|---|---|---|---|
| 1 | 2148-2182 | 109128 | 85 | 9.827447 | 2.856183 | 0.290633 | 0.018697 | 1.869672 | 1 |
| | 2183-2218 | 380072 | 651 | 34.22712 | 21.875 | 0.639113 | 0.041115 | 4.111477 | 4 |
| | 2218-2253 | 346537 | 859 | 31.20715 | 28.86425 | 0.924924 | 0.059501 | 5.950128 | 5 |
| | 2253-2288 | 155242 | 290 | 13.98021 | 9.744624 | 0.69703 | 0.044841 | 4.484061 | 4 |
| | 2288-2323 | 61297 | 337 | 5.520059 | 11.32392 | 2.051414 | 0.131969 | 13.19695 | 13 |
| | 2323-2357 | 40284 | 348 | 3.627748 | 11.69355 | 3.223363 | 0.207362 | 20.73621 | 20 |
| | 2357-2392 | 17881 | 406 | 1.610261 | 13.64247 | 8.472212 | 0.545026 | 54.50257 | 54 |
| 2 | Land use | | | | | | | | |
| | Water body | 30586 | 196 | 2.597074 | 6.581598 | 2.534236 | 0.343018 | 34.30179 | 34 |
| | Dense forest | 213574 | 77 | 18.13469 | 2.585628 | 0.142579 | 0.019299 | 1.92986 | 1 |
| | Sparse forest | 850664 | 1903 | 72.23035 | 63.90195 | 0.884697 | 0.119747 | 11.97469 | 11 |
| | Sediment deposit | 82886 | 802 | 7.037896 | 26.93083 | 3.826545 | 0.517937 | 51.79366 | 51 |
| 3 | Aspect | | | | | | | | |
| | N | 67962 | 66 | 6.241476 | 2.214022 | 0.354727 | 0.047514 | 4.751372 | 4 |
| | NE | 190818 | 160 | 17.52429 | 5.367326 | 0.306279 | 0.041024 | 4.102437 | 4 |
| | E | 53363 | 63 | 4.900737 | 2.113385 | 0.431238 | 0.057762 | 5.776191 | 5 |
| | SE | 189176 | 740 | 17.3735 | 24.82388 | 1.428836 | 0.191385 | 19.13846 | 19 |
| | S | 107356 | 571 | 9.859332 | 19.15465 | 1.942793 | 0.260226 | 26.02262 | 26 |
| | SW | 217182 | 844 | 19.9455 | 28.31265 | 1.4195 | 0.190134 | 19.0134 | 19 |
| | W | 110010 | 322 | 10.10307 | 10.80174 | 1.069155 | 0.143207 | 14.32072 | 14 |
| | NW | 153010 | 215 | 14.05209 | 7.212345 | 0.513258 | 0.068748 | 6.874797 | 6 |
| 4 | NDVI | | | | | | | | |
| | 0.086-0.016 | 3365 | 254 | 0.285892 | 8.520631 | 0.033553 | 0.005649 | 0.564865 | 0 |
| | 0.016-0.119 | 144108 | 850 | 12.2435 | 28.54478 | 0.428923 | 0.072209 | 7.22092 | 7 |
| | 0.119-0.222 | 706062 | 1564 | 59.98746 | 52.49111 | 1.142812 | 0.192393 | 19.23926 | 19 |
| | 0.222-0.326 | 307724 | 195 | 26.14442 | 6.550822 | 3.991014 | 0.671888 | 67.18878 | 67 |
| | 0.326-0.429 | 15757 | 116 | 1.338724 | 3.892653 | 0.34391 | 0.057897 | 5.789739 | 5 |
| 5 | Profile curvature | | | | | | | | |
| | Convex | 78052 | 401 | 7.168119 | 13.45186 | 1.876624 | 0.477684 | 47.76839 | 47 |
| | Planar | 477124 | 987 | 43.81799 | 33.10969 | 0.755619 | 0.192338 | 19.23385 | 19 |
| SN | | A | B | A% | B% | FR | RF | RF% | RF (INT) |
| | Concave | 533701 | 1593 | 49.01389 | 53.43844 | 1.090271 | 0.277522 | 27.75224 | 27 |
| 6 | Plan curvature | | | | | | | | |
| | Convergent | 81615 | 500 | 7.495337 | 16.7729 | 2.237777 | 0.569613 | 56.96135 | 56 |
| | Planar | 655747 | 1512 | 60.22232 | 50.72123 | 0.842233 | 0.214386 | 21.43857 | 21 |

| | | | | | | | | | |
|---|---|---|---|---|---|---|---|---|---|
| | Divergent | 351515 | 969 | 32.28234 | 32.50587 | 1.006924 | 0.256307 | 25.63068 | 25 |
| 7 | Geology | | | | | | | | |
| | Lower Siwalik | 338784 | 740 | 28.78078 | 24.96626 | 0.867463 | 0.308275 | 30.82748 | 30 |
| | Middle Siwalik | 537627 | 1906 | 45.67312 | 64.30499 | 1.40794 | 0.500347 | 50.03467 | 50 |
| | Upper Siwalik | 234511 | 318 | 19.92245 | 10.72874 | 0.538525 | 0.191378 | 19.13785 | 19 |
| | Quaternary deposit | 66197 | 0 | 5.623646 | 0 | 0 | 0 | 0 | 0 |
| 8 | Slope | | | | | | | | |
| | <15 | 599731 | 439 | 50.95213 | 14.7266 | 0.289028 | 0.00087 | 0.087021 | 0 |
| | 15-30 | 483542 | 1266 | 41.08091 | 42.46897 | 1.033789 | 0.003113 | 0.311256 | 0 |
| | 30-45 | 91411 | 1094 | 7.766123 | 36.69909 | 4.725536 | 0.014228 | 1.422779 | 1 |
| | 45-60 | 2360 | 179 | 0.200502 | 6.004696 | 29.94837 | 0.090169 | 9.016947 | 9 |
| | >60 | 4 | 3 | 0.00034 | 0.100637 | 296.1375 | 0.89162 | 89.16199 | 89 |
| 9 | TWI | | | | | | | | |
| | 2.79-6.79 | 772012 | 2421 | 65.97344 | 84.65035 | 1.283097 | 0.488197 | 48.81968 | 48 |
| | 6.79-10.79 | 362424 | 395 | 30.97149 | 13.81119 | 0.445932 | 0.16967 | 16.96697 | 16 |
| | 10.79-14.79 | 34707 | 43 | 2.965939 | 1.503497 | 0.506921 | 0.192875 | 19.28748 | 19 |
| | 14.79-19.07 | 1043 | 1 | 0.089131 | 0.034965 | 0.392288 | 0.149259 | 14.92588 | 14 |
| 10 | Distance to road (m) | | | | | | | | |
| | <100 | 19645 | 69 | 9.76547 | 2.31466 | 0.237025 | 0.099599 | 9.959871 | 9 |
| | 100-200 | 19061 | 39 | 9.475165 | 1.308286 | 0.138075 | 0.05802 | 5.801971 | 5 |
| | 200-300 | 18589 | 21 | 9.240535 | 0.704462 | 0.076236 | 0.032035 | 3.203464 | 3 |
| | 300-400 | 17989 | 19 | 8.942277 | 0.63737 | 0.071276 | 0.02995 | 2.995044 | 2 |
| | 400-500 | 17448 | 29 | 8.673348 | 0.972828 | 0.112163 | 0.047131 | 4.713125 | 4 |
| | >500 | 108436 | 2804 | 53.90321 | 94.0624 | 1.745024 | 0.733265 | 73.32654 | 73 |
| 11 | Distance to river (m) | | | | | | | | |
| | <100 | 19645 | 688 | 9.76547 | 23.0795 | 2.363379 | 0.253983 | 25.39832 | 25 |
| | 100-200 | 19061 | 619 | 9.475165 | 20.76484 | 2.191502 | 0.235512 | 23.55123 | 23 |
| | 200-300 | 18589 | 497 | 9.240535 | 16.67226 | 1.804252 | 0.193896 | 19.38961 | 19 |
| SN | Distance to River (m) | A | B | A% | B% | FR | RF | RF% | RF (INT) |
| | 300-400 | 17989 | 388 | 8.942277 | 13.01577 | 1.455532 | 0.15642 | 15.64204 | 15 |
| | 400-500 | 17448 | 308 | 8.673348 | 10.3321 | 1.191247 | 0.128019 | 12.80188 | 12 |
| | >500 | 108436 | 481 | 53.90321 | 16.13552 | 0.299343 | 0.032169 | 3.21692 | 3 |
| 12 | Distance to fault (m) | | | | | | | | |
| | <500 | 196961 | 253 | 16.73273 | 8.487085 | 0.507215 | 0.092206 | 9.220581 | 9 |
| | 500-1000 | 188220 | 237 | 15.99015 | 7.950352 | 0.497203 | 0.090386 | 9.038588 | 9 |
| | 1000-1500 | 173870 | 327 | 14.77105 | 10.96947 | 0.742633 | 0.135002 | 13.50023 | 13 |
| | 1500-2000 | 157578 | 304 | 13.38697 | 10.19792 | 0.76178 | 0.138483 | 13.84829 | 13 |
| | 2000-2500 | 117856 | 386 | 10.0124 | 12.94867 | 1.293263 | 0.235101 | 23.51005 | 23 |
| | >2500 | 342615 | 1474 | 29.1067 | 49.44649 | 1.698801 | 0.308823 | 30.88226 | 30 |
| 13 | Stream power index | | | | | | | | |

| | | | | | | | | | |
|---|---|---|---|---|---|---|---|---|---|
| | -11.57 | 59 | 100 | 0.005426 | 3.354571 | 618.2907 | 0.969562 | 96.95624 | 96 |
| | -5.57 | 7207 | 247.0067 | 0.662746 | 8.286015 | 12.50256 | 0.019606 | 1.960568 | 1 |
| | -0.73 | 136846 | 2584 | 12.58417 | 86.68213 | 6.888191 | 0.010802 | 1.08016 | 1 |
| | 3.33 | 943334 | 50 | 86.74766 | 1.677286 | 0.019335 | 3.03E-05 | 0.003032 | 0 |
| 14 | Relief | | | | | | | | |
| | 0-71.19 | 216735 | 285 | 19.2022 | 9.403754 | 0.489723 | 0.076771 | 7.67711 | 7 |
| | 71.19-142.38 | 368190 | 936 | 32.62074 | 30.88391 | 0.946757 | 0.148418 | 14.84177 | 14 |
| | 142.38-213.58 | 345975 | 1015 | 30.65255 | 33.49056 | 1.092587 | 0.171279 | 17.12787 | 17 |
| | 213.58-284.77 | 150061 | 648 | 13.29504 | 21.38117 | 1.608206 | 0.252109 | 25.21094 | 25 |
| | 284.77-355.97 | 29126 | 96 | 2.580493 | 3.16758 | 1.22751 | 0.19243 | 19.24298 | 19 |
| | 355.97-427.16 | 18612 | 50.70444 | 1.648978 | 1.673025 | 1.014583 | 0.15905 | 15.90505 | 15 |

# ANNEX 2

Calculation of weighted value by using weight of evidence model of subclasses of 14 factors. Where, A is the number of pixels of sub classes of each factor, Np1 is the landslide pixel present in the sub classes, Np2 is landslide pixel not present in the sub class, Np3 is sub classes not present in thus class and Np4 is neither sub classes nor landslides of other classes present in this class. FR is general frequency ratio, and RF is percent of frequency ratio of each sub classes.

| **Rainfall (mm)** | A | Np1 | Np2 | Np3 | Np4 | a/b | W+ | c/d | W- | C=W+ - W- |
|---|---|---|---|---|---|---|---|---|---|---|
| 2148-2182 | 109128 | 85 | 2891 | 1001313 | 998422 | 0.0570412 | -1.2438114 | 1.9456892 | 0.289 | -1.5328849 |
| 2183-2218 | 380072 | 651 | 2325 | 730369 | 728044 | 0.4368036 | -0.3597137 | 1.5649949 | 0.194 | -0.5542267 |
| 2218-2253 | 346537 | 859 | 2117 | 763904 | 761787 | 0.576485 | -0.239212 | 1.4246919 | 0.153 | -0.3929329 |
| 2253-2288 | 155242 | 290 | 2686 | 955199 | 952513 | 0.1946185 | -0.710816 | 1.8076526 | 0.257 | -0.967931 |
| 2288-2323 | 61297 | 337 | 2639 | 1049144 | 1046505 | 0.2261937 | -0.6455196 | 1.7757577 | 0.2493 | -0.8949033 |
| 2323-2357 | 40284 | 348 | 2628 | 1070157 | 1067529 | 0.2335838 | -0.6315573 | 1.7683029 | 0.2475 | -0.8791139 |
| 2357-2392 | 17881 | 406 | 2570 | 1092560 | 1089990 | 0.2725286 | -0.564588 | 1.7291867 | 0.237 | -0.8024299 |
| **Land use** | | | | | | | | | | |
| Water body | 30586 | 196 | 2780 | 1147124 | 1077075 | 0.1276987 | -0.8938136 | 1.9290326 | 0.285 | -1.1791531 |
| Dense forest | 213574 | 77 | 2899 | 964136 | 893968 | 0.0498643 | -1.3022105 | 2.0247124 | 0.306 | -1.6085738 |
| Sparse forest | 850664 | 1903 | 1073 | 327046 | 258704 | 1.1452738 | 0.0589093 | 0.8163492 | 0.088 | 0.1470334 |
| Sediment deposit | 82886 | 802 | 2174 | 1094824 | 1025381 | 0.5218852 | -0.282425 | 1.5104947 | 0.17 | -0.4615442 |
| **Aspect** | | | | | | | | | | |
| N | 67962 | 66 | 2910 | 1020915 | 1039569 | 0.0447601 | -1.3491093 | 1.9380991 | 0.287 | -1.6364853 |
| NE | 190818 | 160 | 2816 | 898059 | 916807 | 0.1086493 | -0.9639732 | 1.8731233 | 0.272 | -1.2365396 |
| E | 53363 | 63 | 2913 | 1035514 | 1054165 | 0.04272 | -1.3693688 | 1.9403432 | 0.287 | -1.6572473 |
| SE | 189176 | 740 | 2236 | 899701 | 919029 | 0.5026536 | -0.2987312 | 1.4868867 | 0.172 | -0.4710091 |
| S | 107356 | 571 | 2405 | 981521 | 1000680 | 0.3874818 | -0.4117487 | 1.600791 | 0.204 | -0.6160833 |
| SW | 217182 | 844 | 2132 | 871695 | 891127 | 0.5735264 | -0.2414466 | 1.4171739 | 0.151 | -0.3928697 |
| W | 110010 | 322 | 2654 | 978867 | 997777 | 0.2184881 | -0.6605723 | 1.7667006 | 0.247 | -0.9077352 |
| NW | 153010 | 215 | 2761 | 935867 | 954670 | 0.1459408 | -0.8358234 | 1.8372379 | 0.264 | -1.0999888 |
| **NDVI** | | | | | | | | | | |
| 0.086-0.016 | 3365 | 254 | 2722 | 1173651 | 1104354 | 0.1656596 | -0.7807835 | 1.8866944 | 0.275 | -1.0564851 |
| 0.016-0.119 | 144108 | 850 | 2126 | 1032908 | 964207 | 0.5522395 | -0.2578726 | 1.4796641 | 0.170 | -0.4280357 |
| 0.119-0.222 | 706062 | 1564 | 1412 | 470954 | 402967 | 0.9752086 | -0.0109025 | 1.0289741 | 0.012 | -0.023307 |
| 0.222-0.326 | 307724 | 195 | 2781 | 869292 | 799936 | 0.1258206 | -0.9002483 | 1.9499725 | 0.290 | -1.1902768 |
| 0.326-0.429 | 15757 | 116 | 2860 | 1161259 | 1091824 | 0.0756264 | -1.1213268 | 1.9831596 | 0.297 | -1.4186845 |
| **Profile curvature** | | | | | | | | | | |
| Convex | 78052 | 401 | 2575 | 1010825 | 1029814 | 0.2720205 | -0.5653983 | 1.7145561 | 0.234 | -0.79955 |
| Planar | 477124 | 987 | 1989 | 611753 | 631328 | 0.6739188 | -0.1713925 | 1.3159707 | 0.119 | -0.2906387 |
| Concave | 533701 | 1593 | 1383 | 555176 | 575357 | 1.0900224 | 0.0374354 | 0.9131352 | 0.03 | 0.0769003 |
| **Plan curvature** | | | | | | | | | | |
| Convergent | 81615 | 500 | 2476 | 1007262 | 1026350 | 0.3392054 | -0.4695373 | 1.6485052 | 0.217 | -0.6866276 |
| Planar | 655747 | 1512 | 1464 | 433130 | 453230 | 1.0397065 | 0.0169107 | 0.9620544 | -0.0168 | 0.0337111 |

| | | | | | | | | | | |
|---|---|---|---|---|---|---|---|---|---|---|
| Divergent | 351515 | 969 | 2007 | 737362 | 756919 | 0.6598457 | -0.1805576 | 1.3313655 | 0.124 | -0.3048549 |
| **Geology** | | | | | | | | | | |
| Lwer Siwalik | 338784 | 740 | 2236 | 838335 | 769421 | 0.4768715 | -0.3215987 | 1.5699831 | 0.195 | -0.5174936 |
| Middle Siwalik | 537627 | 1906 | 1070 | 639492 | 571744 | 1.2130637 | 0.0838836 | 0.7616896 | -0.118 | 0.2021056 |
| Upper Siwalik | 234511 | 318 | 2658 | 942608 | 873272 | 0.2058497 | -0.6864498 | 1.8572042 | 0.268 | -0.9553094 |
| Quaternary deposit | 66197 | 0 | 2976 | 1110922 | 1041268 | 0 | 0 | 2.0668934 | 0.315 | -0.3153181 |
| **Slope** | | | | | | | | | | |
| <15 | 599731 | 439 | 2537 | 577317 | 508173 | 0.2773595 | -0.5569569 | 1.8209658 | 0.260 | -0.8172587 |
| 15-30 | 483542 | 1266 | 1710 | 693506 | 625189 | 0.8089001 | -0.0921051 | 1.2119821 | 0.083 | -0.1756013 |
| 30-45 | 91411 | 1094 | 1882 | 1085637 | 1017148 | 0.712024 | -0.1475054 | 1.3073667 | 0.116 | -0.2639028 |
| 45-60 | 2360 | 179 | 2797 | 1174688 | 1105284 | 0.116742 | -0.9327729 | 1.9387204 | 0.287 | -1.2202881 |
| >60 | 4 | 3 | 2973 | 1177044 | 1107464 | 0.0019565 | -2.7085117 | 2.0607488 | 0.31 | -3.0225367 |
| **TWI** | | | | | | | | | | |
| 2.79-6.79 | 772012 | 2421 | 555 | 398174 | 337874 | 1.5038174 | 0.1771951 | 0.4062669 | -0.39 | 0.5683837 |
| 6.79-10.79 | 362424 | 395 | 2581 | 807762 | 745436 | 0.2552158 | -0.5930924 | 1.8070557 | 0.256 | -0.850064 |
| 10.79-14.79 | 34707 | 43 | 2933 | 1135479 | 1072801 | 0.0281003 | -1.5512894 | 2.0286826 | 0.307 | -1.8585035 |
| 14.79-19.07 | 1043 | 1 | 2975 | 1169143 | 1106423 | 0.000654 | -3.1844111 | 2.0559961 | 0.31 | -3.4974334 |
| **Distance to road (m)** | | | | | | | | | | |
| <100 | 19645 | 69 | 2907 | 181523 | 1087889 | 0.1621389 | -0.7901129 | 1.1398038 | 0.056 | -0.846943 |
| 100-200 | 19061 | 39 | 2937 | 182107 | 1088443 | 0.0914317 | -1.0389032 | 1.1520122 | 0.061 | -1.1003603 |
| 200-300 | 18589 | 21 | 2955 | 182579 | 1088897 | 0.049141 | -1.3085563 | 1.1594337 | 0.064 | -1.3728022 |
| 300-400 | 17989 | 19 | 2957 | 183179 | 1089495 | 0.044357 | -1.3530378 | 1.1606742 | 0.064 | -1.4177482 |
| 400-500 | 17448 | 29 | 2947 | 183720 | 1090046 | 0.0675613 | -1.1703017 | 1.1571563 | 0.06 | -1.2336937 |
| >500 | 108436 | 2804 | 172 | 92732 | 1001833 | 0 | 0 | 0.0631454 | -1.19 | 1.1996583 |
| **Distance to river (m)** | 201168 | | | | | | | | | |
| <100 | 19645 | 688 | 2288 | 181523 | 1088508 | 1.6174772 | 0.2088382 | 0.8970276 | -0.04 | 0.2560324 |
| 100-200 | 19061 | 619 | 2357 | 182107 | 1089023 | 1.4518477 | 0.1619211 | 0.9244418 | -0.034 | 0.1960415 |
| 200-300 | 18589 | 497 | 2479 | 182579 | 1089373 | 1.1634383 | 0.0657434 | 0.9726077 | -0.012 | 0.0778056 |
| 300-400 | 17989 | 388 | 2588 | 183179 | 1089864 | 0.9060793 | -0.0428338 | 1.0157857 | 0.006 | -0.0496359 |
| 400-500 | 17448 | 308 | 2668 | 183720 | 1090325 | 0.7177052 | -0.1440539 | 1.0475667 | 0.0201 | -0.1642356 |
| >500 | 108436 | 481 | 2495 | 92732 | 999510 | 1.9037126 | 0.2796014 | 0.9161558 | -0.038 | 0.317632 |
| **Distance to fault (m)** | 201168 | | | | | | | | | |
| <500 | 196961 | 253 | 2723 | 980139 | 910757 | 0.164009 | -0.7851324 | 1.8996773 | 0.278 | -1.0638123 |
| 500-1000 | 188220 | 237 | 2739 | 988880 | 919482 | 0.1536854 | -0.8133674 | 1.9101903 | 0.281 | -1.094444 |
| 1000-1500 | 173870 | 327 | 2649 | 1003230 | 933922 | 0.2121671 | -0.673322 | 1.8462994 | 0.266 | -0.9396241 |
| 1500-2000 | 157578 | 304 | 2672 | 1019522 | 950191 | 0.1973545 | -0.704753 | 1.8612108 | 0.269 | -0.9745486 |
| 2000-2500 | 117856 | 386 | 2590 | 1059244 | 989995 | 0.2509291 | -0.600449 | 1.8014676 | 0.255 | -0.8560755 |
| >2500 | 342615 | 1474 | 1502 | 834485 | 766324 | 0.9501355 | -0.0222145 | 1.0542997 | 0.022 | -0.0451786 |
| **SPI** | 1177100 | | | | | | | | | |
| -11.57 | 59 | 100 | 2876 | 1087387 | 1107506 | 0.067826 | 0 | 1.9152401 | 0.282 | -0.2822232 |
| -5.57 | 7207 | 247.0067 | 2728 | 1080239 | 1100505 | 0.1675563 | -0.7758394 | 1.8171141 | 0.259 | -1.0352216 |

| | | | | | | | | | | |
|---|---|---|---|---|---|---|---|---|---|---|
| -0.73 | 136846 | 2584 | 392 | 950600 | 973203 | 1.7572048 | 0.2448224 | 0.2603816 | -0.584 | 0.8292121 |
| 3.33 | 943334 | 50 | 2926 | 144112 | 164181 | 0.0359419 | -1.4443994 | 1.8462145 | 0.266 | -1.7106816 |
| **Relief** | | | | | | | | | | |
| 0-71.19 | 216735 | 285 | 2691 | 911964 | 891015 | 0.1893324 | -0.7227751 | 1.8297275 | 0.26 | -0.9851615 |
| 71.19-142.38 | 368190 | 936 | 2040 | 760509 | 740211 | 0.6206378 | -0.2071618 | 1.389765 | 0.142 | -0.3501031 |
| 142.38-213.58 | 345975 | 1015 | 1961 | 782724 | 762505 | 0.6733135 | -0.1717827 | 1.3353491 | 0.125 | -0.2973775 |
| 213.58-284.77 | 150061 | 648 | 2328 | 978638 | 958052 | 0.4309036 | -0.3656199 | 1.5813248 | 0.199 | -0.564641 |
| 284.77-355.97 | 29126 | 96 | 2880 | 1099573 | 1078435 | 0.063896 | -1.1945263 | 1.9544522 | 0.291 | -1.4855513 |
| 355.97-427.16 | 18612 | 50.70444 | 2925. | 1110087 | 1088903.7 | 0.0337504 | -1.4717206 | 1.9850468 | 0.297 | -1.7694913 |

# ANNEX 3

Calculation of weighted value by using Shannon entropy model of subclasses of 14 factors. Where, A is the number of pixel of sub classes of each factor, B is the landslide pixel present in the sub classes, FR is general frequency ratio, Wj is the Shannon entropy index.

| **Rainfall (mm)** | A | B | A% | B% | FR | Pij | Ej | 1-Ej | Wj |
|---|---|---|---|---|---|---|---|---|---|
| 2148-2182 | 109128 | 85 | 9.8274469 | 2.8561828 | 0.2906332 | 0.0178324 | -0.0311852 | 1.0311852 | 0.0669 |
| 2183-2218 | 380072 | 651 | 34.227122 | 21.875 | 0.639113 | 0.0392142 | -0.055157 | 1.055157 | |
| 2218-2253 | 346537 | 859 | 31.207151 | 28.864247 | 0.9249241 | 0.0567508 | -0.0707131 | 1.0707131 | |
| 2253-2288 | 155242 | 290 | 13.980211 | 9.7446237 | 0.6970298 | 0.0427678 | -0.0585441 | 1.0585441 | |
| 2288-2323 | 61297 | 337 | 5.5200591 | 11.323925 | 2.0514137 | 0.125869 | -0.1132923 | 1.1132923 | |
| 2323-2357 | 40284 | 348 | 3.6277479 | 11.693548 | 3.223363 | 0.1977766 | -0.1392001 | 1.1392001 | |
| 2357-2392 | 17881 | 406 | 1.6102611 | 13.642473 | 8.4722116 | 0.5198314 | -0.1477036 | 1.1477036 | |
| **Land use** | | | | | | | | | |
| Water body | 30586 | 196 | 2.597074 | 6.5815984 | 2.534236 | 0.3430206 | -0.1593947 | 1.1593947 | 0.2604 |
| Dense forest | 213574 | 77 | 18.134685 | 2.5856279 | 0.1425791 | 0.0192987 | -0.0330871 | 1.0330871 | |
| Sparse forest | 850664 | 1903 | 72.230345 | 63.901948 | 0.8846967 | 0.1197478 | -0.1103754 | 1.1103754 | |
| Sediment deposit | 82886 | 802 | 7.0378956 | 26.930826 | 3.8265453 | 0.5179406 | -0.147986 | 1.147986 | |
| **Aspect** | | | | | 7.3880571 | | | | |
| N | 67962 | 66 | 6.2414763 | 2.2140221 | 0.3547273 | 0.0475187 | -0.0628737 | 1.0628737 | 0.051 |
| NE | 190818 | 160 | 17.524293 | 5.3673264 | 0.3062792 | 0.0410287 | -0.0569032 | 1.0569032 | |
| E | 53363 | 63 | 4.9007372 | 2.1133848 | 0.4312381 | 0.057768 | -0.0715348 | 1.0715348 | |
| SE | 189176 | 740 | 17.373496 | 24.823885 | 1.4288365 | 0.1914048 | -0.1374377 | 1.1374377 | |
| S | 107356 | 571 | 9.8593321 | 19.154646 | 1.9427935 | 0.2602536 | -0.1521451 | 1.1521451 | |
| SW | 217182 | 844 | 19.945503 | 28.312647 | 1.4195002 | 0.1901541 | -0.137081 | 1.137081 | |
| W | 110010 | 322 | 10.103069 | 10.801744 | 1.0691547 | 0.1432223 | -0.1208781 | 1.1208781 | |
| NW | 153010 | 215 | 14.052092 | 7.2123449 | 0.5132577 | 0.0687552 | -0.0799413 | 1.0799413 | |
| **NDVI** | | | | | 7.4657873 | | | | |
| 0.086-0.016 | 3365 | 254 | 0.2858925 | 8.5206307 | 0.033553 | 0.0056486 | -0.0126985 | 1.0126985 | 0.053 |
| 0.016-0.119 | 144108 | 850 | 12.243504 | 28.544784 | 0.4289226 | 0.0722092 | -0.0824201 | 1.0824201 | |
| 0.119-0.222 | 706062 | 1564 | 59.98746 | 52.49111 | 1.1428118 | 0.1923926 | -0.1377168 | 1.1377168 | |
| 0.222-0.326 | 307724 | 195 | 26.144419 | 6.5508219 | 3.9910136 | 0.6718878 | -0.1160372 | 1.1160372 | |
| 0.326-0.429 | 15757 | 116 | 1.3387244 | 3.8926535 | 0.3439105 | 0.0578974 | -0.0716388 | 1.0716388 | |
| **Profile curvature** | | | | | 5.9402115 | | | | |
| Convex | 78052 | 401 | 7.1681191 | 13.451862 | 1.8766236 | 0.5041976 | -0.149948 | 1.149948 | 0.0557 |
| Planar | 477124 | 987 | 43.817989 | 33.109695 | 0.7556188 | 0.2030142 | -0.140582 | 1.140582 | |
| Concave | 533701 | 1593 | 49.013892 | 53.438443 | 1.0902714 | 0.2929262 | -0.1562005 | 1.1562005 | |
| **Plan curvature** | | | | | | | | | |
| Convergent | 81615 | 500 | 7.4953369 | 16.772895 | 2.2377773 | 0.5476694 | -0.1432054 | 1.1432054 | 0.0552 |
| Planar | 655747 | 1512 | 60.222321 | 50.721234 | 0.8422331 | 0.2061266 | -0.1413752 | 1.1413752 | |
| Divergent | 351515 | 969 | 32.282342 | 32.505871 | 1.0069242 | 0.2464327 | -0.1499054 | 1.1499054 | |
| **Geology** | | | | | | | | | |
| Lower Siwalik | 338784 | 740 | 28.780777 | 24.966262 | 0.8674631 | 0.3087057 | -0.1575805 | 1.1575805 | 0.0559 |

| | | | | | | | | | |
|---|---|---|---|---|---|---|---|---|---|
| Middle Siwalik | 537627 | 1906 | 45.673122 | 64.304993 | 1.4079395 | 0.5010461 | -0.1503751 | 1.1503751 | |
| Upper Siwalik | 234511 | 318 | 19.922455 | 10.728745 | 0.5385253 | 0.191646 | -0.1375061 | 1.1375061 | |
| Quaternary deposit | 66197 | 0 | 5.6236455 | 0 | 0 | 0 | 0 | 1 | |
| **Slope** | | | | | | | | | |
| <15 | 599731 | 439 | 50.952128 | 14.726602 | 0.2890282 | 0.0008702 | -0.0026632 | 1.0026632 | 0.0484 |
| 15-30 | 483542 | 1266 | 41.080907 | 42.46897 | 1.0337885 | 0.0031126 | -0.0078029 | 1.0078029 | |
| 30-45 | 91411 | 1094 | 7.7661234 | 36.699094 | 4.7255358 | 0.014228 | -0.026277 | 1.026277 | |
| 45-60 | 2360 | 179 | 0.2005016 | 6.0046964 | 29.948372 | 0.0901706 | -0.0942224 | 1.0942224 | |
| >60 | 4 | 3 | 0.0003398 | 0.1006374 | 296.13754 | 0.8916314 | -0.0444163 | 1.0444163 | |
| **Topographical wetness index** | | | | | | | | | |
| 2.79-6.79 | 772012 | 2421 | 65.973444 | 84.65035 | 1.2830973 | 0.488241 | -0.1520215 | 1.1520215 | 0.0556 |
| 6.79-10.79 | 362424 | 395 | 30.971487 | 13.811189 | 0.4459324 | 0.1696851 | -0.130718 | 1.130718 | |
| 10.79-14.79 | 34707 | 43 | 2.9659387 | 1.5034965 | 0.506921 | 0.1928923 | -0.1378573 | 1.1378573 | |
| 14.79-19.07 | 1043 | 1 | 0.0891311 | 0.034965 | 0.3922876 | 0.1492723 | -0.123302 | 1.123302 | |
| **Distance from Road (m)** | | | | | | | | | |
| <100 | 19645 | 69 | 9.7654697 | 2.3146595 | 0.2370249 | 0.0996322 | -0.0997916 | 1.0997916 | 0.0531 |
| 100-200 | 19061 | 39 | 9.475165 | 1.3082858 | 0.1380753 | 0.0580392 | -0.0717526 | 1.0717526 | |
| 200-300 | 18589 | 21 | 9.2405353 | 0.7044616 | 0.076236 | 0.0320454 | -0.0478833 | 1.0478833 | |
| 300-400 | 17989 | 19 | 8.9422771 | 0.63737 | 0.071276 | 0.0299605 | -0.0456434 | 1.0456434 | |
| 400-500 | 17448 | 29 | 8.6733476 | 0.9728279 | 0.1121629 | 0.0471471 | -0.0625427 | 1.0625427 | |
| >500 | 108436 | 2804 | 53.903205 | 94.062395 | 1.7450242 | 0.7335116 | -0.0987255 | 1.0987255 | |
| **Distance from River (m)** | | | | | | | | | |
| <100 | 19645 | 688 | 9.7654697 | 23.079504 | 2.3633788 | 0.2541267 | -0.1511926 | 1.1511926 | 0.0556 |
| 100-200 | 19061 | 619 | 9.475165 | 20.764844 | 2.1915021 | 0.2356454 | -0.1479243 | 1.1479243 | |
| 200-300 | 18589 | 497 | 9.2405353 | 16.672258 | 1.8042524 | 0.1940056 | -0.138168 | 1.138168 | |
| 300-400 | 17989 | 388 | 8.9422771 | 13.015767 | 1.4555316 | 0.1565088 | -0.1260618 | 1.1260618 | |
| 400-500 | 17448 | 308 | 8.6733476 | 10.332103 | 1.1912475 | 0.1280911 | -0.1143189 | 1.1143189 | |
| >500 | 108436 | 481 | 53.903205 | 16.135525 | 0.2993426 | 0.0321874 | -0.0480337 | 1.0480337 | |
| **Distance from fault (m)** | | | | | | | | | |
| <500 | 196961 | 253 | 16.732733 | 8.4870849 | 0.5072145 | 0.0922208 | -0.0954643 | 1.0954643 | 0.0529 |
| 500-1000 | 188220 | 237 | 15.990145 | 7.9503522 | 0.4972033 | 0.0904006 | -0.0943627 | 1.0943627 | |
| 1000-1500 | 173870 | 327 | 14.771047 | 10.969473 | 0.7426334 | 0.1350243 | -0.1174155 | 1.1174155 | |
| 1500-2000 | 157578 | 304 | 13.386968 | 10.19792 | 0.7617797 | 0.1385054 | -0.1189115 | 1.1189115 | |
| 2000-2500 | 117856 | 386 | 10.012403 | 12.948675 | 1.2932634 | 0.2351388 | -0.1478261 | 1.1478261 | |
| >2500 | 342615 | 1474 | 29.106703 | 49.446494 | 1.6988009 | 0.3088729 | -0.1575932 | 1.1575932 | |
| **Stream power index** | | | | | | | | | |
| -11.57 | 59 | 100 | 0.0054256 | 3.3545715 | 618.29074 | 0.9695636 | -0.0130151 | 1.0130151 | 0.0489 |
| -5.57 | 7207 | 247.0067 | 0.6627456 | 8.2860152 | 12.502559 | 0.0196057 | -0.033479 | 1.033479 | |
| -0.73 | 136846 | 2584 | 12.584165 | 86.682128 | 6.8881906 | 0.0108016 | -0.0212415 | 1.0212415 | |
| 3.33 | 943334 | 50 | 86.747664 | 1.6772857 | 0.0193352 | 3.032E-05 | -0.000137 | 1.000137 | |
| **Relief** | | | | | | | | | |
| 0-71.19 | 216735 | 285 | 19.202197 | 9.4037543 | 0.4897228 | 0.0767711 | -0.0855846 | 1.0855846 | 0.0529 |

| | | | | | | | | |
|---|---|---|---|---|---|---|---|---|
| 71.19-142.38 | 368190 | 936 | 32.620743 | 30.883909 | 0.9467568 | 0.1484177 | -0.1229662 | 1.1229662 |
| 142.38-213.58 | 345975 | 1015 | 30.652548 | 33.490564 | 1.0925866 | 0.1712787 | -0.1312503 | 1.1312503 |
| 213.58-284.77 | 150061 | 648 | 13.295041 | 21.381168 | 1.6082062 | 0.2521094 | -0.150865 | 1.150865 |
| 284.77-355.97 | 29126 | 96 | 2.5804931 | 3.1675804 | 1.2275097 | 0.1924298 | -0.1377273 | 1.1377273 |
| 355.97-427.16 | 18612 | 50.70444 | 1.6489782 | 1.673025 | 1.0145829 | 0.1590505 | -0.1269962 | 1.1269962 |

# ANNEX 4

Calculation of weighted value by using information value model of subclasses of 14 factors. Where, A is the number of pixel of sub classes of each factor, B is the landslide pixel present in the sub classes, cPr is conditional probability and pPr is prior probability, infv is information value.

| **Rainfall (mm)** | A | B | cPr | pPr | cPr/pPr | InfV |
|---|---|---|---|---|---|---|
| 2148-2182 | 109128 | 85 | 0.0007789 | 0.00268 | 0.290635 | -0.5366521 |
| 2183-2218 | 380072 | 651 | 0.0017128 | 0.00268 | 0.6391169 | -0.1944197 |
| 2218-2253 | 346537 | 859 | 0.0024788 | 0.00268 | 0.9249298 | -0.0338912 |
| 2253-2288 | 155242 | 290 | 0.0018681 | 0.00268 | 0.697034 | -0.156746 |
| 2288-2323 | 61297 | 337 | 0.0054978 | 0.00268 | 2.0514261 | 0.3120559 |
| 2323-2357 | 40284 | 348 | 0.0086387 | 0.00268 | 3.2233826 | 0.5083119 |
| 2357-2392 | 17881 | 406 | 0.0227057 | 0.00268 | 8.4722631 | 0.9279994 |
| **Land use** | | | | | | |
| Water body | 30586 | 196 | 0.0064082 | 0.002529 | 2.5338713 | 0.4037846 |
| Dense forest | 213574 | 77 | 0.0003605 | 0.002529 | 0.1425586 | -0.8460065 |
| Sparse forest | 850664 | 1903 | 0.0022371 | 0.002529 | 0.8845694 | -0.0532681 |
| Sediment deposit | 82886 | 802 | 0.0096759 | 0.002529 | 3.8259946 | 0.5827444 |
| **Aspect** | | | | | | |
| N | 67962 | 66 | 0.0009711 | 0.0027377 | 0.3547273 | -0.4501054 |
| NE | 190818 | 160 | 0.0008385 | 0.0027377 | 0.3062792 | -0.5138825 |
| E | 53363 | 63 | 0.0011806 | 0.0027377 | 0.4312381 | -0.3652828 |
| SE | 189176 | 740 | 0.0039117 | 0.0027377 | 1.4288365 | 0.1549825 |
| S | 107356 | 571 | 0.0053188 | 0.0027377 | 1.9427935 | 0.2884266 |
| SW | 217182 | 844 | 0.0038861 | 0.0027377 | 1.4195002 | 0.1521355 |
| W | 110010 | 322 | 0.002927 | 0.0027377 | 1.0691547 | 0.0290406 |
| NW | 153010 | 215 | 0.0014051 | 0.0027377 | 0.5132577 | -0.2896645 |
| **NDVI** | | | | | | |
| 0.086-0.016 | 3365 | 254 | 0.0754829 | 0.0025327 | 29.803621 | 1.474269 |
| 0.016-0.119 | 144108 | 850 | 0.0058984 | 0.0025327 | 2.3289021 | 0.3671512 |
| 0.119-0.222 | 706062 | 1564 | 0.0022151 | 0.0025327 | 0.8746097 | -0.0581857 |
| 0.222-0.326 | 307724 | 195 | 0.0006337 | 0.0025327 | 0.2502036 | -0.6017064 |
| 0.326-0.429 | 15757 | 116 | 0.0073618 | 0.0025327 | 2.906731 | 0.4634048 |
| **Profile curvature** | | | | | | |
| Convex | 78052 | 401 | 0.0051376 | 0.0027377 | 1.8766236 | 0.2733772 |
| Planar | 477124 | 987 | 0.0020686 | 0.0027377 | 0.7556188 | -0.1216973 |
| Concave | 533701 | 1593 | 0.0029848 | 0.0027377 | 1.0902714 | 0.0375346 |
| **Plan curvature** | | | | | | |
| Convergent | 81615 | 500 | 0.0061263 | 0.0027377 | 2.2377773 | 0.3498169 |
| Planar | 655747 | 1512 | 0.0023058 | 0.0027377 | 0.8422331 | -0.0745677 |

| **Rainfall (mm)** | A | B | cPr | pPr | cPr/pPr | InfV |
|---|---|---|---|---|---|---|
| Divergent | 351515 | 969 | 0.0027566 | 0.0027377 | 1.0069242 | 0.0029968 |
| **Geology** | | | | | | |
| Lwer Siwalik | 338784 | 740 | 0.0021843 | 0.002518 | 0.8674631 | -0.061749 |
| Middle Siwalik | 537627 | 1906 | 0.0035452 | 0.002518 | 1.4079395 | 0.148584 |
| Upper Siwalik | 234511 | 318 | 0.001356 | 0.002518 | 0.5385253 | -0.2687939 |
| Quaternary deposit | 66197 | 0 | 0 | 0.002518 | 0 | |
| **Slope** | | | | | | |
| <15 | 599731 | 439 | 0.000732 | 0.0025326 | 0.2890282 | -0.5390598 |
| 15-30 | 483542 | 1266 | 0.0026182 | 0.0025326 | 1.0337885 | 0.0144317 |
| 30-45 | 91411 | 1094 | 0.0119679 | 0.0025326 | 4.7255358 | 0.6744511 |
| 45-60 | 2360 | 179 | 0.0758475 | 0.0025326 | 29.948372 | 1.4763732 |
| >60 | 4 | 3 | 0.75 | 0.0025326 | 296.13754 | 2.4714935 |
| **Topographical wetness index** | | | | | | |
| 2.79-6.79 | 772012 | 2421 | 0.003136 | 0.0024441 | 1.2830973 | 0.1082596 |
| 6.79-10.79 | 362424 | 395 | 0.0010899 | 0.0024441 | 0.4459324 | -0.350731 |
| 10.79-14.79 | 34707 | 43 | 0.0012389 | 0.0024441 | 0.506921 | -0.2950598 |
| 14.79-19.07 | 1043 | 1 | 0.0009588 | 0.0024441 | 0.3922876 | -0.4063954 |
| **Distance from Road (m)** | | | | | | |
| <100 | 19645 | 688 | 0.0350216 | 0.0148185 | 2.3633788 | 0.3735333 |
| 100-200 | 19061 | 619 | 0.0324747 | 0.0148185 | 2.1915021 | 0.3407419 |
| 200-300 | 18589 | 497 | 0.0267362 | 0.0148185 | 1.8042524 | 0.2562973 |
| 300-400 | 17989 | 388 | 0.0215687 | 0.0148185 | 1.4555316 | 0.1630216 |
| 400-500 | 17448 | 308 | 0.0176525 | 0.0148185 | 1.1912475 | 0.076002 |
| >500 | 108436 | 481 | 0.0044358 | 0.0148185 | 0.2993426 | -0.5238315 |
| **Distance from River (m)** | | | | | | |
| <100 | 19645 | 253 | 0.0128786 | 0.0148185 | 0.8690913 | -0.0609346 |
| 100-200 | 19061 | 237 | 0.0124338 | 0.0148185 | 0.8390727 | -0.0762004 |
| 200-300 | 18589 | 327 | 0.017591 | 0.0148185 | 1.1871037 | 0.0744886 |
| 300-400 | 17989 | 304 | 0.0168992 | 0.0148185 | 1.1404165 | 0.0570635 |
| 400-500 | 17448 | 386 | 0.0221229 | 0.0148185 | 1.492927 | 0.1740386 |
| >500 | 108436 | 1474 | 0.0135933 | 0.0148185 | 0.9173201 | -0.0374791 |
| **Distance from fault (m)** | | | | | | |
| <500 | 196961 | 285 | 0.001447 | 0.0025325 | 0.5713681 | -0.243084 |
| 500-1000 | 188220 | 936 | 0.0049729 | 0.0025325 | 1.9636382 | 0.2930615 |
| 1000-1500 | 173870 | 1015 | 0.0058377 | 0.0025325 | 2.3051159 | 0.3626928 |
| 1500-2000 | 157578 | 648 | 0.0041122 | 0.0025325 | 1.6237935 | 0.2105308 |
| 2000-2500 | 117856 | 96 | 0.0008146 | 0.0025325 | 0.3216406 | -0.4926291 |
| >2500 | 342615 | 50 | 0.0001459 | 0.0025325 | 0.0576255 | -1.239385 |

| **Rainfall (mm)** | A | B | cPr | pPr | cPr/pPr | InfV |
|---|---|---|---|---|---|---|
| **Stream power index** | | | | | | |
| -11.57 | 59 | 100 | 1.6949153 | 0.0027413 | 618.29212 | 2.7911937 |
| -5.57 | 7207 | 247 | 0.0342722 | 0.0027413 | 12.502249 | 1.0969882 |
| -0.73 | 136846 | 2584 | 0.0188825 | 0.0027413 | 6.888206 | 0.8381061 |
| 3.33 | 943334 | 50 | 5.3E-05 | 0.0027413 | 0.0193353 | -1.7136498 |
| **Relief** | | | | | | |
| 0-71.19 | 216735 | 285 | 0.001315 | 0.0026845 | 0.4898426 | -0.3099434 |
| 71.19-142.38 | 368190 | 936 | 0.0025422 | 0.0026845 | 0.9469883 | -0.0236554 |
| 142.38-213.58 | 345975 | 1015 | 0.0029337 | 0.0026845 | 1.0928538 | 0.0385621 |
| 213.58-284.77 | 150061 | 648 | 0.0043182 | 0.0026845 | 1.6085995 | 0.2064479 |
| 284.77-355.97 | 29126 | 96 | 0.003296 | 0.0026845 | 1.2278099 | 0.0891311 |
| 355.97-427.16 | 18612 | 50 | 0.0026864 | 0.0026845 | 1.0007318 | 0.0003177 |

# ANNEX 5

**Factor maps for landslide susceptibility analysis**

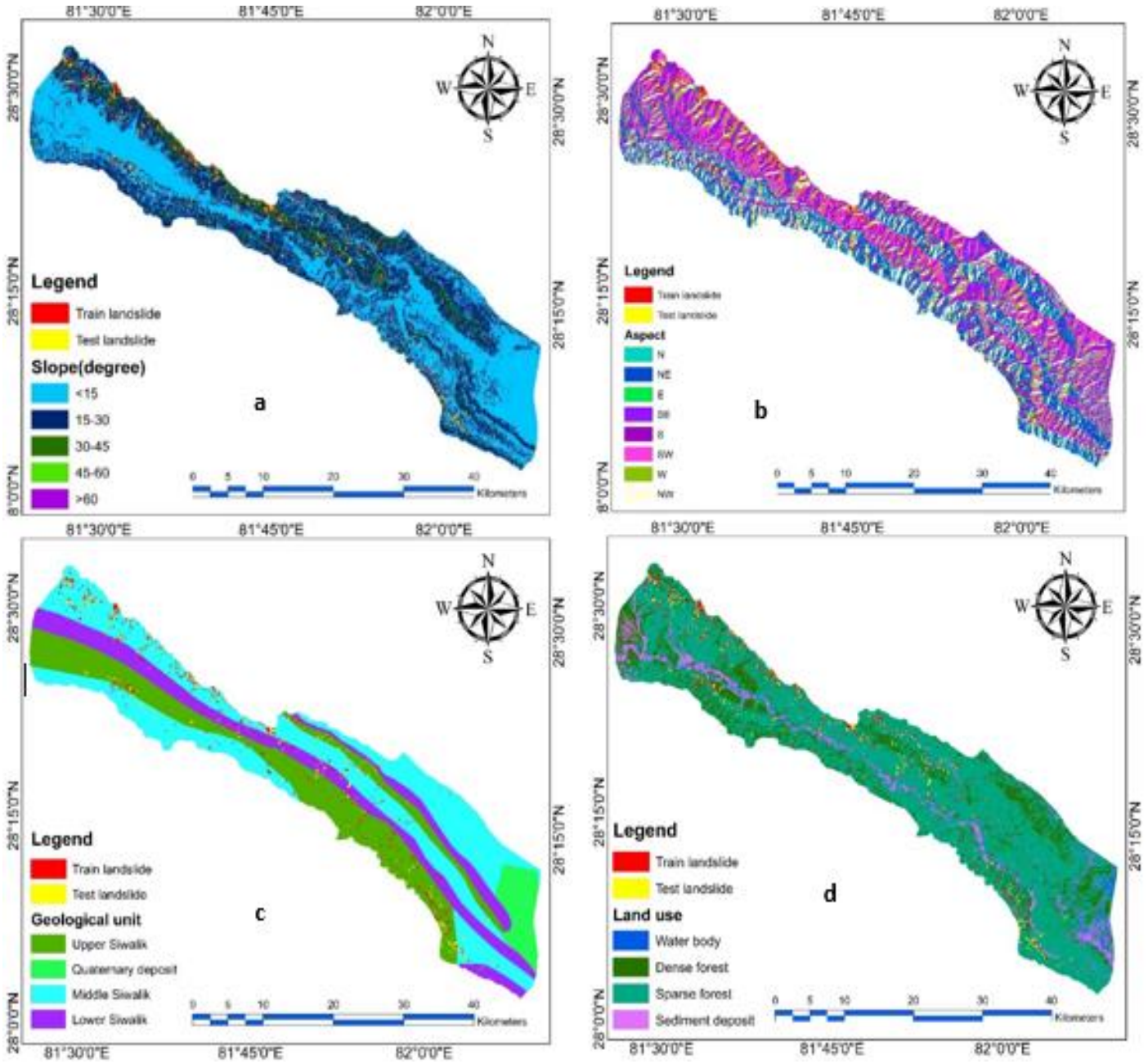


**Figure**:Landslide causative factor maps a) Slope b) Aspect c) Geology d) Landuse

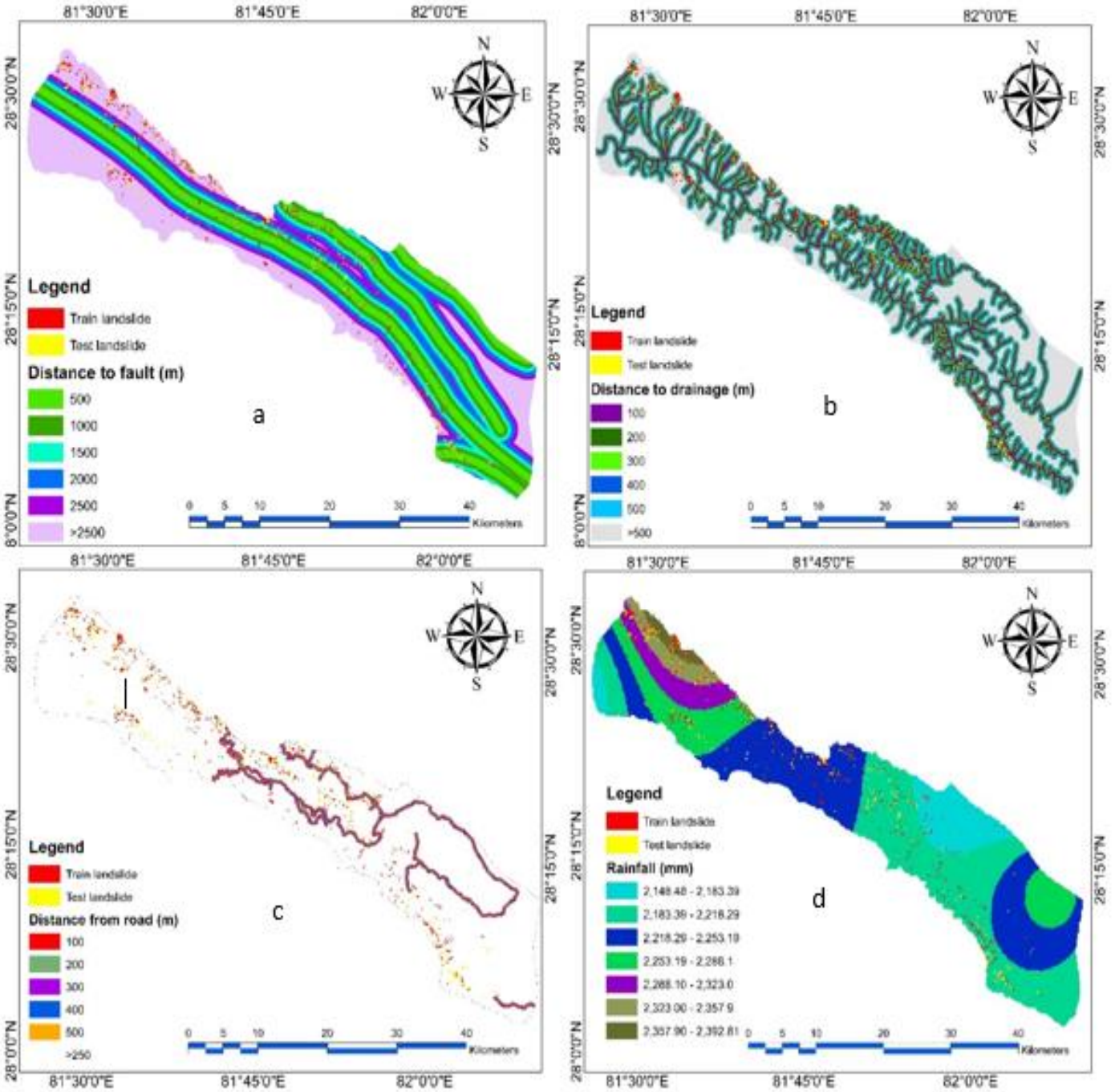


**Figure:** Landslide causative factors map a) Distance to fault b) Distance to drainage c)Distance to road d) Rainfall

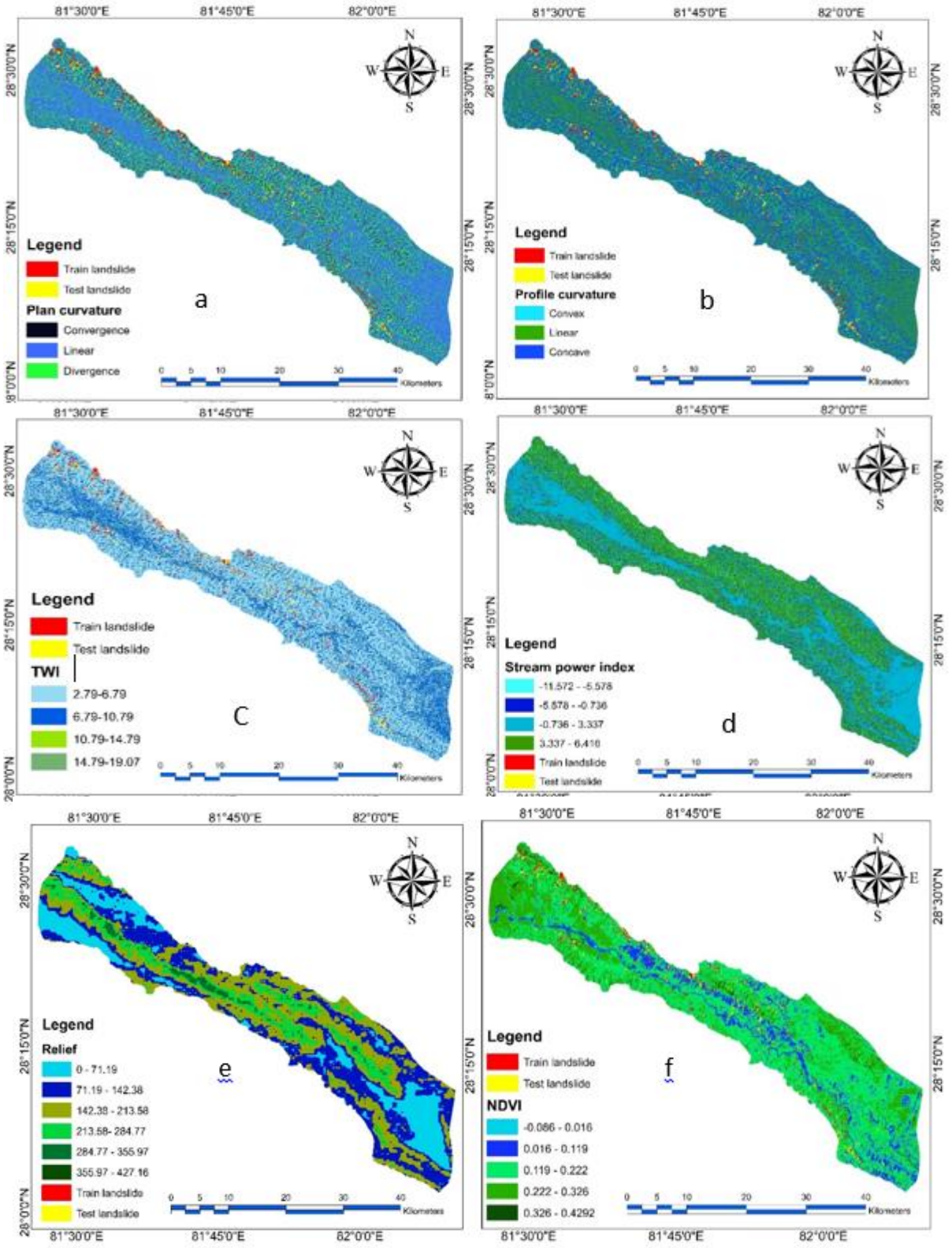


**Figure:** landslide causative factors map: a) Plan curvature b) Profile curvature c) Topographical wetness index d) Stream power index e) Relative relief f) NDVI

# ANNEX 6

## Photographs

**Figure**: Soil sample collection from the landslide of Babai valley –Harre road section.

**Figure**: Preparing sample for soil gradation analysis.

**Figure**: Preparing sample for Atturburg limit test.

**Figure**: Conducting Pycnometer test for specific gravity determination.

Photographs

**Figure**: Participant and presenter of "World Geological Congress" in London, UK, 2019.


**Figure**: Presenting paper in IAEG Arc 11 in Kathmandu in 2018.

**Figure**: Received certificate from Prof. JJ Dong at National Central University, Taiwan in 2018.

## Field Photographs

**Figure**: New landslides occurred at the ommunity forest of Ranagaun, Dang.

**Figure**: Reactivated landslide at the road section near Babai valley.

**Figure**: Active landslide observed at the Bhirkhet of Babai valley.

**Figure**: Soria Rubusta seccession in the mitigated landslide at the Fulbari of Dang District.

Engineering Geology 278 (2020) 105851

Contents lists available at ScienceDirect

Engineering Geology

journal homepage: www.elsevier.com/locate/enggeo

# Compositional analysis and phase relations of soil mass from the active landslides of Babai River watershed, Siwalik zone of Nepal

Bharat Prasad Bhandari[a], Subodh Dhakal[b,*]

[a] Central Department of Environment Science, Tribhuvan University, Kirtipur, Nepal
[b] Department of Geology, Tri-Chandra Campus, Tribhuvan University, Kathmandu, Nepal

ARTICLE INFO

*Keywords:*
Landslides
Siwalik
Compositional analysis
Phase relation

ABSTRACT

The present study focuses on the compositional analysis and phase relationship of soil mass and their role to trigger landslides in the Babai River watershed, Siwalik zone of Nepal. A total of 76 landslides are selected for sampling and further analysis among 769 active landslides from the total study area. For the classification of soil, the Unified Soil Classification System (USCS) is adopted by using both the sieve and hydrometer analysis. The centered log-ratio (clr) and mean component fraction of sand, silt, and clay are obtained from the compositional analysis by using R and CoDapac v.2.02.21 software. Correlation of phase relationships like moisture content, unit weight, specific gravity, void ratio, porosity, and degree of saturation of each soil samples are obtained. The results indicate that the degree of saturation is highly correlated with moisture content and void ratio but less correlated with the specific gravity and dry density. Furthermore, the highly correlated variables are checked by multiple regression analysis and the best-fitted regression equation was obtained from the phase relation. The centered log-ratio and mean log of silt/clay fraction indicate that silt and clay constituents in the soil are responsible for the landslide initiation in the study area.

## 1. Introduction

Grain size distribution analysis and classification is a very important task in the engineering and geotechnical field to depict the properties and behaviors of soil (Casagrande, 1948; Howard, 1984; Das, 2009; Dundulis et al., 2010; Das and Sobhan, 2013; Kovačevi'c and Juri'c-Ka'cuni'c, 2014). The engineering properties of the soil are influenced by their shape, size, and arrangement. Phase relationship is the interrelationship between mass volume and weight of different phases of the soil. It defines the condition or the physical make-up of the soil. The phase relationship of the soil includes dry unit weight, bulk unit weight, porosity, void ratio, specific gravity, moisture content, and degree of saturation (Bicochhi et al., 2019). So that, to identify the interrelationship among the different phases of soil is very important to understand the soil behaviors.

In the recent year, many researchers studied the classification and phase relationship of soil for the geotechnical study of landslides (Cencetti and Conversini, 2003; Meisina, 2006; Mugagga et al., 2011; Yalcin, 2011; Zhao et al., 2013; Riemer et al., 2015; Tofani et al., 2017; Bicocchi et al., 2019). The soil classification provides the compositional structure of soil which is useful to relate its composition with other geotechnical properties. The soil components (gravel, sand, silt, and clay) and their proportion significantly impact for landslide initiation. The high water content of the clay is the main cause of shallow landslide (Yalcin, 2007; Yalcin, 2011). The classification of the landslide based on grain size distribution provides a better understanding of the soil nature in various aspects. The soil classification can be linked with the nature of the soil in the presence of moisture and shear stress. Generally, soils are classified based on particle size distribution from fine-grained to coarse-grained according to the Unified Soil Classification System (USCS). Fine soils either silt or clay are determined by the soil mass passing through the 0.075 mm sieve, whereas coarse soils are considered as the soil mass that retain in the 0.075 mm sieve. Moreover, the fine-grained soils are further classified into clay or silt using the hydrometer test (ASTM D422-63, 2007). The study of soil component identification and soil classification alone is not sufficient to understand the soil behavior. The component analysis of soil provides the role of each components for landslide initiation and it will be easy to evaluate the sources of particles present in the soil (Bicocchi et al., 2019).

Generally, the soil is composed of solid, liquid, and gas components. The ratio of these components mainly determines the behavior of soil. The relationship between each ratio is referred to the phase relationship. Commonly, the value of moisture content, void ratio, porosity, dry unit weight, degree of saturation, and specific gravity are determined

* Corresponding author.
*E-mail address:* subodhdhakal@geology.edu.np (S. Dhakal).

https://doi.org/10.1016/j.enggeo.2020.105851
Received 4 May 2020; Received in revised form 20 September 2020; Accepted 29 September 2020
Available online 02 October 2020

based on the phase relation. The phase relation consists of the weight volume relationship of soil in the various states which provides the proportion of weight and volume of solid, water, and air presence in the soil. Relating the phase relationship with the particle size of soil will provide better information about landslide initiation in the slope soil (Yalcin, 2007; Yalcin, 2011).

The Siwalik hill is considered one of the most fragile and vulnerable regions in the Himalaya where soil erosion and landslides processes are very common. It is due to its location within the zone of active crustal movement (Hurtrez and Lucazeau, 1999; Dhakal, 2014; Dhakal, 2015; Bhandari and Dhakal, 2019a). The Siwalik hill is the youngest Mountain of the world characterized by steep and highly dissected terrains. The region is located between the Terai plain and the Lesser Himalayan zone. Intense monsoon, higher relief, steep slope, and weak geological units have led to the formation of landforms such as rills, gullies, and shallow landslides (Higaki, 2003). Landslides of the Siwalik zone have been studied by many researchers in the past (Ghimire, 2011: Dahal et al., 2012; Devkota et al., 2013; Regmi et al., 2014a, 2014b; TU-CDES, 2017; Bhandari and Dhakal, 2018; Bhandari and Dhakal, 2019a; Bhandari and Dhakal, 2019b; Thapa and Bhandari, 2019; Bhandari and Dhakal, 2020). There is a lack of studies about the geotechnical properties (phase relationship and soil compositional analysis) of landslides in the Siwalik zone of Nepal though there occur severe landslides and slope stability problems.

This study aims to analyze the soil composition based on the particle size from the active landslides emphasizing the phase relationship and other geotechnical properties of soil. Furthermore, the study focuses to identify the role of soil compositions (clay, silt and sand) for triggering landslides. The site-specific geotechnical data obtained from the laboratory analysis in this study will be useful for landslide susceptibility analysis, landslide mitigation, and further detailed analysis of landslides with numerical modeling.

## 2. Materials and methods

### 2.1. Study area

The present study covered the Siwalik zone of Babai River watershed (Fig. 1) which is located in Dang and Bardia districts of province no. 5 and Salyan district of Karnali province. The Babai River is the east-west trending river and located between 27°57′59.03”N, 82°33′42.80″ E in the east, 28°28′30.14” N, 81°28′30.14″E in the west, 28°12′47.90”N, 82°15′46.08″ in the north and 28°01′03.89”N, 82°12′39.61″E in the south (Fig. 1). The total area covered by the whole watershed of the Babai River is 1952 km$^2$ but the study area covered only 1157 km$^2$ after avoiding the plain area and river terraces. After originating from the Siwalik, the Babai River flows through the widely distributed flat Dang valley where there is no sloppy area for the possibilities of landslide occurrences. Due to that the flat wide valley has been excluded from this study.

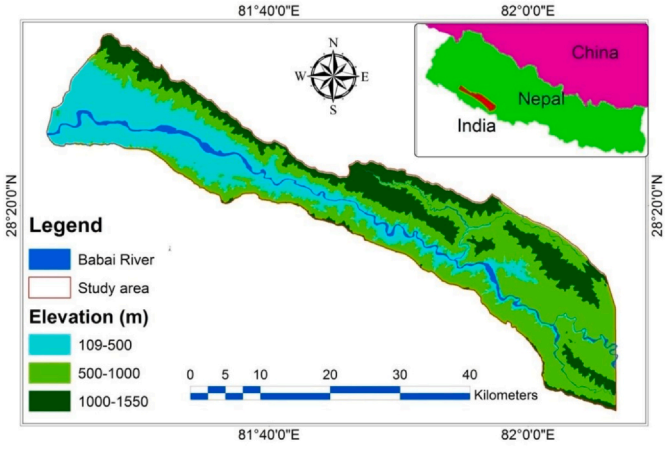


**Fig. 1.** Map shows the location of the study area in the Babai River catchment, Siwalik zone of Nepal.

### 2.2. Geology of study area

The bedrock geology of the study area is dominated by younger (Neogene) sedimentary rocks (Dhital, 2015) like sandstone, mudstone, and conglomerate. Based on lithostratigraphy, the rocks of the study area are divided into three geological formations. From bottom to top they are Lower Siwaliks, Middle Siwaliks, and Upper Siwaliks, respectively (Auden, 1935; Hagen, 1969; Chaudhari, 1982; Bhandari and Dhakal, 2018; Bhandari and Dhakal, 2019b; Bhandari and Dhakal, 2020). Interbedding of fine to very fine-grained grey-green, thinly bedded sandstone and red-purple, brown, thickly bedded mudstone is the major composition of the Lower Siwalik. The characteristics feature of the Middle Siwaliks is of medium to coarse-grained thickly bedded salt and pepper as well as pebbly sandstone and thinly bedded variegated mudstone. Sandstone beds are massive, less compact, and weathered due to poor intergranular bonding (Bhandari and Dhakal, 2018; Bhandari and Dhakal, 2019b). The Upper Siwalik consists of cobble and pebble bearing conglomerate interbedding with yellow to brown mudstone. The area consists of three major *E*-W trending and North dipping thrusts namely MBT (Main Boundary Thrust), BT (Babai Thrust), and BHT (Bheri Thrust) including one minor thrust namely Malai Thrust (Fig. 2).

The Babai catchment is characterized by various landscapes, from the upper Dang valley to the lower Babai valley with several ridges extended up to 1500 m from mean sea level. There are several gullies and steep slopes on peak elevation of the range. The topography of the study area is characterized by several erosional landforms likes rugged hills, numerous deep gorges, steep slopes, cliffs, and active gullies, as well as depositional landform, likes river terraces, alluvial fans, and talus cones. The area falls on a sub-tropical climate as a whole, where the winter temperature falls below 0$^0$ and varies between 0 to −3$^0$C and summer temperature reaches up to 40$^0$ to 45$^0$ (Bhandari and Dhakal, 2020). The average annual rainfall over the period 1990–2019 is in the range of 1800–3300 mm. Some representative landslides of the study area are shown in Fig. 3(a-d).

### 2.3. Methods

#### 2.3.1. Landslide inventory mapping

The landslide inventory is widely used for different aspects of landslide management. Mainly, the landslide inventory map is prepared for landslide susceptibility analysis (Guzzetti et al., 2005; Cardinali

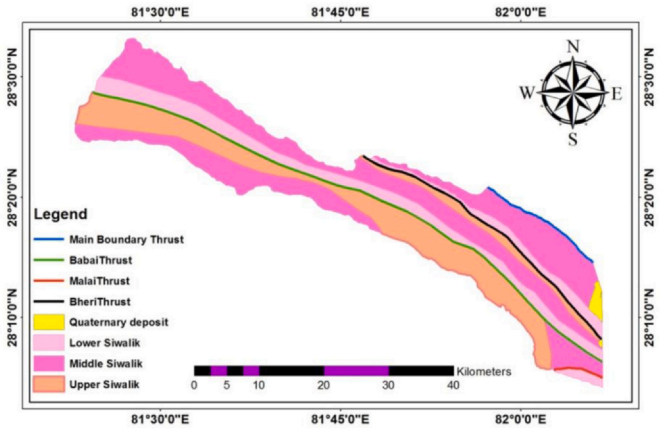


**Fig. 2.** Stratigraphical map of the study area.


**Fig. 3.** (a) Landslide on the thick soil surface in Babai Valley (b) Landslide on the saturated soil at Bankhet village of Bardia (c) A typical soil slide in the thick forest region of Gothi area (Source: Google earth) (d) A deep landslide in Bangaun of Bardia district.

et al., 2006; Van Westen et al., 2006; Devkota et al., 2013; Regmi et al., 2014a; Regmi et al., 2014b; Rosi et al., 2018; Thapa and Bhandari, 2019) and to study the evolution and dynamics of landslides (Hovius et al., 1997; Malamud et al., 2004; Parker et al., 2011; Bhandari and Dhakal, 2020). Similarly, some of the past researchers have prepared landslide inventory maps for the landslide distribution, classification, and characterization (Guzzetti et al., 1996; Dai et al., 2010; Ausilio and Zimmaro, 2017; Bhandari and Dhakal, 2018). In this study, the landslide inventory map has been prepared for tracing out the distribution of landslides in the entire study area and selecting the proper landslides site for soil sampling.

First of all, the landslide inventory map was generated with 769 landslide polygons. According to Guzzetti et al. (2012), remote sensing techniques and aerial photographs are mainly used for landslide inventories. The data used in this work were taken by Landsat-8, sentinel-2, and Google Earth imagery of 30 m resolution from the date 2017 to 2019. We only mapped new and active landslide for soil sampling and the term new and active landslide was adopted from Bhandari and Dhakal (2020). After the field observation and verification, the prepared map is finally determined. We verified all the new and active landslides in the field by direct observation. The final inventory map was prepared after obtaining the KML file of inventory into the GIS layer (Fig. 4).

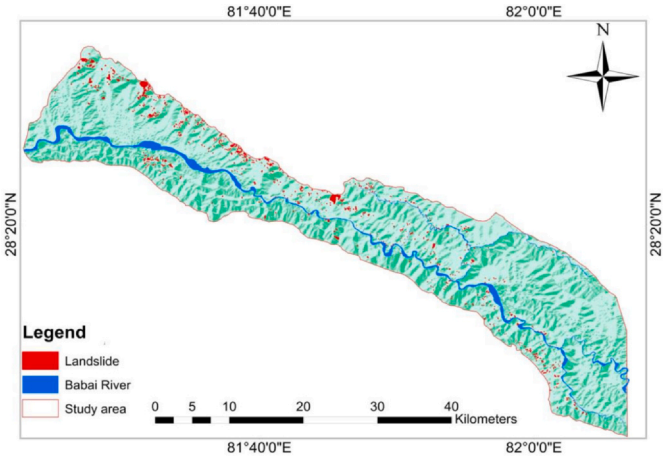


**Fig. 4.** Landslide inventory map of new and active landslides of the study area.

### 2.3.2. Sampling area selection

For the geotechnical study of landslide slope soil, a total of 76 samples were collected from 76 different landslides where a sampled landslide having an area greater than 10,000 $m^2$. Only one representative sample from each landslides was collected. The sample sites have been selected so that the spatial distribution of a representative sample of landslides caused by soil characters is obtained. Among the 769 landslides, 76 landslides were chosen based on the size, geological heterogeneity, and spatial distribution (Fig. 5) from the east to the west of the study area based on the stratigraphical map and the landslide inventory map. The samples were collected from the new and active landslides. Old and inactive landslides were excluded for sampling and further analysis.

### 2.3.3. Sampling techniques

All the samples were collected in the dry season from September 2017 to December 2019. The temporal data analysis and seasonal variation of soil are beyond the scope of this study. The soil samples were obtained from scar or slip surface area at the depth ranging from 80 to 100 cm below the ground surface by using a hand auger and soil driller after removing disturbed soil surface (Fig. 6). The depth of soil samples can be considered significant to characterize soil materials involved in the landslide (Tofani et al., 2017). We have tested the depth of disturbed soil in 20 landslides. As our observation, the depth of disturbed soil on the slip surface and scar of the landslide in the study area mostly varied between 40 and 80 cm. So, we have collected soil samples from either scar area or slip surface area because the deposited materials consist of disturbed soil. The collected samples were kept in a sealed protected plastic bag and wrapped in the paper to protect

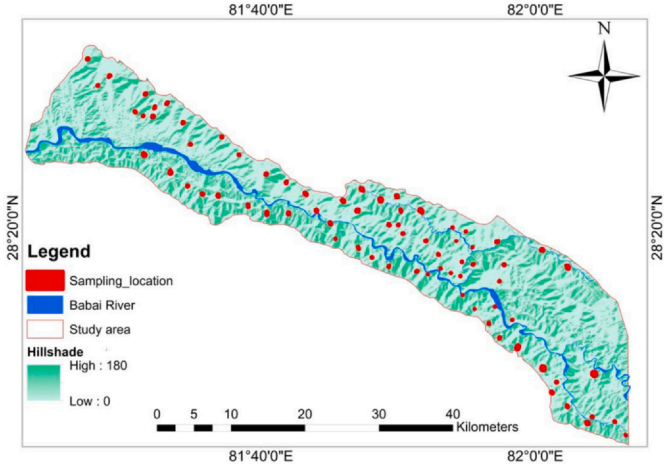


**Fig. 5.** Sampling locations of the study area.

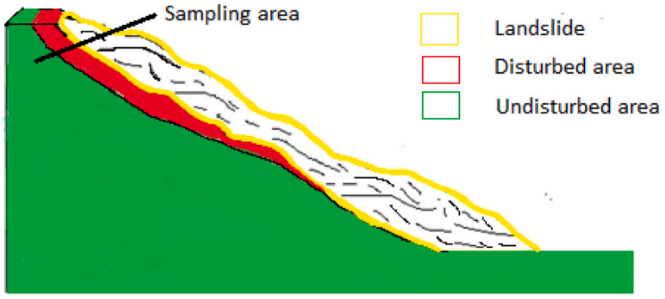


**Fig. 6.** Schematic diagram to show the soil sampling locations in the studied landslides

moisture content.

### 2.3.4. Laboratory analysis

To identify the soil phase relationship and particle size distribution, the samples collected from 76 landslides were analyzed at the Central Material Testing Laboratory, Pulchwok Engineering College, Tribhuvan University. The analysis was focused on the particle size distribution, Atterberg limit, wet density, dry density, moisture content, and specific gravity.

*2.3.4.1. Moisture content test.* The moisture content is one of the most significant properties used in establishing a correlation between soil behavior and its index properties as well as expressing the phase relationships of air, water, and solids in a given volume of material. The moisture content of each soil sample was calculated by the ASTM D4643-17 by microwave oven heating. The mass of water was obtained by subtracting dry mass from the bulk mass of soil. The final value of moisture content was obtained by the ratio of the weight of water to the weight of solids in a given volume (Eq. (1)) (Lee et al., 1983).

$$\text{Moisture content (w)} = \frac{\boldsymbol{Ww}}{\boldsymbol{Ws}} \text{ x } 100\% \quad (1)$$

Ww = Weight of moist soil–weight of dry soil

Where Ww is the weight of water and Ws is the weight of solid.

*2.3.4.2. Soil density test.* Dry density and bulk density of soil were determined by the ASTM D7263–09 standards. Dry density was obtained after taking the mass of the oven-dried soil sample. The ratio of dry soil mass with its total volume is dry density whereas the ratio of the bulk mass of wet samples with total volume is bulk density. Both bulk and dry densities are used to convert the water fraction of soil from the mass basis to the volume basis and vice-versa. Dry density can be used to calculate porosity and void ratio as well as for determining the degree of soil compaction. The dry unit weight ($\gamma_d$) was obtained from dry density (Eq. (2)) (Lee et al., 1983; Das, 2009).

$$\text{Dry unit weight } (\gamma d) = \frac{\boldsymbol{Wd}}{\boldsymbol{V}} \quad (2)$$

Where V is volume and Wd is the weight of soil.

*2.3.4.3. Atterberg limit test.* Atterberg limit is another important component for soil analysis. Atterberg limit gives the expansion potential of soil at different moisture content and clay content (Selby, 1993; Mugagga et al., 2011). The Plastic Limit (PL) and liquid limit (LL) were determined by using ASTM D4318 standard. The plasticity index (PI) was calculated by subtracting the plastic limit (PL) by liquid limit (LL). The plasticity index and liquid limit of the soil were plotted on the Casagrande plasticity chart (Casagrande, 1932) for further USCS classification of fine soil.

*2.3.4.4. Specific gravity test.* The specific gravity was determined by the ASTM D 854–00 – Standard test of Soil solids by the phase relationship of air, water, and solids in a given volume of the soil. The specific gravity of soil is defined as the unit weight of the soil mass divided by the unit weight of distilled water at 4 °C (Eq. (3)). The specific gravity of soil is mainly used to find the various phase relationships such as void ratio, porosity, and degree of saturation.

$$\text{Gs} = \frac{\gamma s}{\gamma w} \quad (3)$$

Where Gs is specific gravity, $\gamma s$ is the unit weight of soil, $\gamma_w$ is the unit weight of water (Lee et al., 1983; Das, 2009).

*2.3.4.5. Phase relationship.* The void ratio, porosity, and degree of saturation were obtained by numerical relation. The void ratio was obtained by using specific gravity, dry unit weight, and dry density of soil (Das, 2009) (Eq. (4)).

$$\text{Void ratio (e)} = \frac{\text{Gs } \gamma w}{\gamma d} - 1 \quad (4)$$

Where Ws is the specific gravity of the soil sample, $\gamma_w$ is the unit weight of water and $\gamma_d$ is the dry unit weight of soil.

Similarly, porosity was determined by using the special relation of the void ratio (Lee et al., 1983; Das, 2009) (Eq. (5)).

$$\text{Porosity (n)} = \frac{\text{e}}{1 + \text{e}} \quad (5)$$

Where n is porosity and e is the void ratio.

The degree of saturation is the volume of water content in the total pore volume of soil. The degree of saturation was calculated by the special relation of water content, specific gravity, and void ratio (Lee et al., 1983; Das, 2009).

$$\text{Degree of saturation (Sr)} = \frac{\text{wGs}}{\text{e}} \quad (6)$$

Where w is moisture content, Gs is specific gravity and e is the void ratio.

*2.3.4.6. Particle size distribution.* The particle size distribution of soil was conducted according to ASTM (American Society for Testing and Materials) standard (ASTM D422). For grain size distribution, both sieve analysis and hydrometer analysis were conducted. Sieve analysis was conducted for the soil having grain size greater than 75 μ and hydrometer analysis was done for the fine soil having a grain size less than 75 μ. For hydrometer analysis, the sample was prepared by passing the soil from U.S. No. 200 sieve (ASTM D422-632007).

*2.3.4.7. Soil classification.* The soil was classified based on results

obtained from both analyses. The particle distribution curve and ternary diagram of clay silt and sand (Davis and Bennet, 1927), as well as liquid limit value, was used to classify the soil. The obtained information was compared with the Unified Soil Classification table for soil classification. Furthermore, the plasticity index and liquid limit of the soil were plotted on the Casagrande plasticity chart (Casagrande, 1932) for further USCS classification of fine soil.

#### 2.3.5. Data analysis

For a detailed analysis of grain size distribution, the compositional statistics (Aitchison, 1982) have been carried out. Previously, some researchers have used compositional statistics for data analysis in the geosciences researches (Eynatten, 2004; Thomas and Aitchison, 2005; Buccianti, 2013; Bicocchi et al., 2019).

For quantitative assessment of compositional data, an appropriate measure of central tendency may be represented by geometric mean "$g_c$" (Bicocchi et al., 2019). The parts of the compositional dataset (sand, silt, clay) is represented by "D" variable. A compositional data point can be represented by a real vector "x" with positive components (x1, x2 …..xD). The sample space for compositional data is called composed data (Simplex). The abundance of part of composition (% by weight) is called the "center" of compositional data and is represented by a closed geometric mean $g_c$ (Aitchison, 1982; Bicocchi et al., 2019), where, the "center" $g_c$ is defined as,

$$g_c = C(g_1, g_2, \ldots g_D) \tag{7}$$

Where "C" stands for closer operation for any vector of real positive component (Aitchison, 1982).

Where C with the positive vector component(x) is defined as,

$$C(x) = \left[ \frac{x1}{\sum_{i=1}^{D} zi}, \frac{x2}{\sum_{i=1}^{D} zi} \ldots \frac{xD}{\sum_{i=1}^{D} zi} \right] \tag{8}$$

And the geometrical mean $g_i$ is calculated by.

$$g_i = \sqrt{\prod_{j=1}^{n} xij} \quad i = 1, 2, 3 \ldots D \tag{9}$$

Furthermore, we have analyzed the relationship between parts of composition because the only center value cannot provide information about the variability of the analyzed dataset (Bicocchi et al., 2019). For further information, the variation array of the mean value of log-ratio between the centroid of the data and the variance of the same log-ratio was prepared. The variance of the same log-ratio gives a measure of the dispersion of the values around the centroid. Finally, the centered log-ratio (clr) transformation was obtained. Similarly, the clr (centered log-ratio) variance for each part was also obtained to evaluate for each grain size fraction after center log-ratio transformation (Aitchison, 2003; Egozcue and Pawlowsky-Glahn, 2005; Bicocchi et al., 2019).

$$\mathrm{clr}(x) = y = [y_1, y_2, y_3 \ldots\ldots y_D] \tag{10}$$

$$\text{Where } y_i = \left[ \ln \frac{x1}{g(x)}, \ln \frac{x2}{g(x)} \ldots \ln \frac{xD}{g(x)} \right] \tag{11}$$

and g(x) is the geometric mean of the components of the compositional vector x.

Similarly, descriptive statistics were used to analyze the obtained data by using MS excel, R software (Van den Boogaart et al., 2014), and CoDapack v.2.02.21. The distribution of each parameters was plotted on the histogram and the maximum frequency class was noted. The minimum, maximum, arithmetic means, standard deviation, and coefficient of variation of each data were obtained for identification of landslide initiation range and data variation. The maximum count of value was considered as the cause for landslide initiation. Karl Pearson Correlation among five variables (moisture content, dry unit weight, specific gravity, void ratio, and degree of saturation) was obtained and plotted in the correlation matrix.

To check the validity and significance of phase relation, we obtained the regression equation between the degree of saturation, void ratio, moisture content, and specific gravity. For that, multiple regression models were used. The data were checked for normality of the response variable to run multiple regression models using qq-plot and Shapiro-test (Shapiro and Wilk, 1965). The degree of saturation was taken as the response variable and other variables (moisture content, dry unit weight, specific gravity, and void ratio) were taken as predictor variables. The predictor variables were fit in the model starting with the most complex model, that included all the variables and subsequently simplifying the model with manual updates until the minimum adequate model was obtained. The model checking was carried out with visual model diagnostics. Finally, the regression equation of best-fitted variables was obtained.

## 3. Results

### 3.1. Soil classification and compositional statistics

The major soil types according to the USCS classification are CL, ML, CL-ML, and SC. The particle size distribution curve and hydrometer analysis showed that 52 samples have more than 15% clay composition. The ternary diagram of sand, silt, and clay indicates that CL type soils dominantly present in the landslides of the study area (Fig. 7). The liquid limit values were obtained in the range of 16.4% and 38.67% with mean values of 25.49%. The samples were collected in the dry season but also the ranges values are considered as higher values. Similarly, the plastic limit varies between 6.37% and 29.52% with a mean value of 14.78%. The plasticity index values range between 7.56 and 16.21 with a mean value of 10.706 which indicates that the soil types are medium plastic but according to the plotted data on the plasticity chart the soil is defined as clay-rich having low plastic behavior (Fig. 8). Altogether 33 samples are found CL type (Fig. 9) out of 76.

### 3.2. Compositional statistics

A quantitative assessment through compositional statistics of soil has been carried out to obtain detailed information into the grain size distribution. The 3D scattered plot of the component of soil was plotted to predict the center value (Fig. 10). The center of the 3 parts composition has been obtained (Sand = 40.9%, Silt = 36.67% and Clay = 22.36%). The obtained values are consistent with the USCS classification. The predictive region of the center (Fig. 11) was obtained first

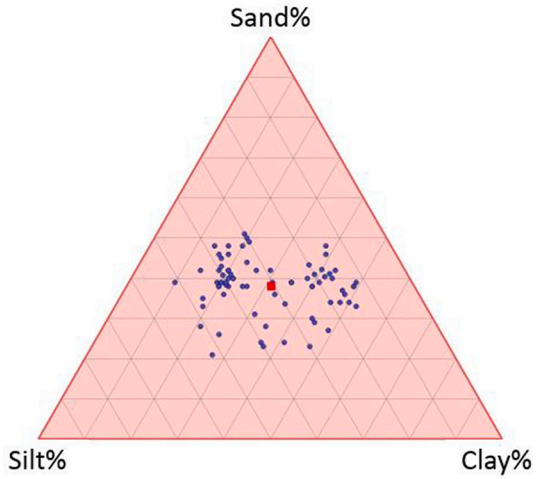


**Fig. 7.** Ternary diagram shows the soil type based on the particle size distribution.

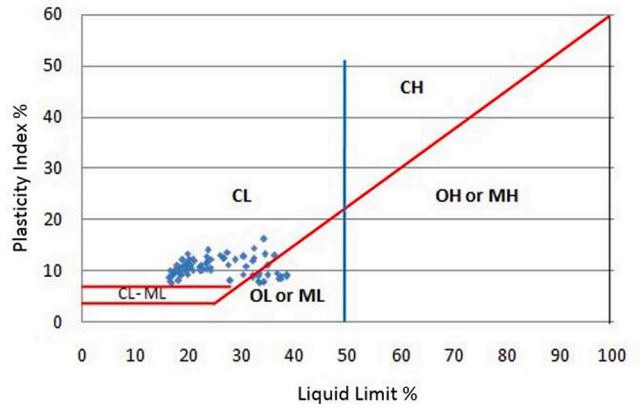


**Fig. 8.** Casagrande plasticity chart shows the liquid limit/ plasticity index and soil classification.

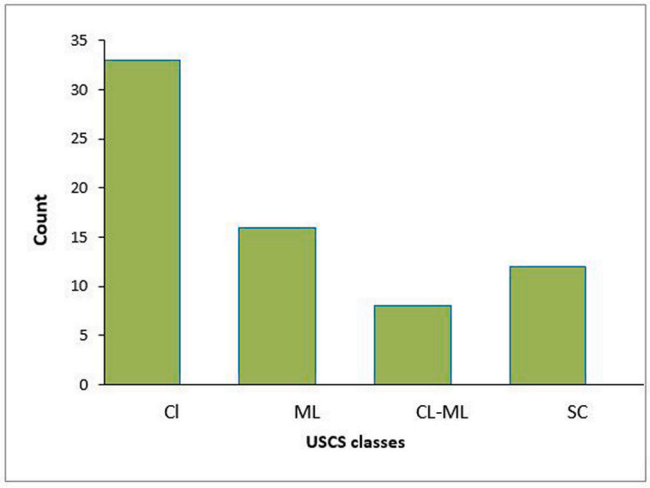


**Fig. 9.** The distribution of the soil type according to Unified Unified Soil Classification System (USCS)

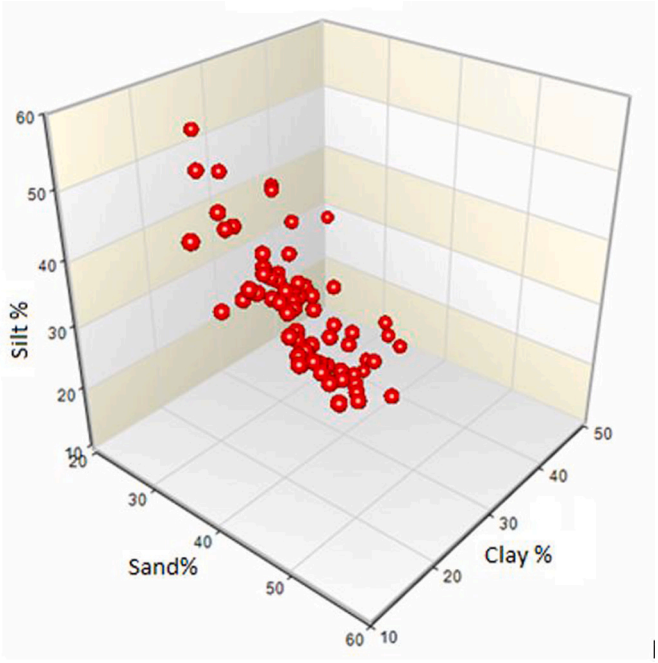


**Fig. 10.** The 3D scattered plot of three components of soil.

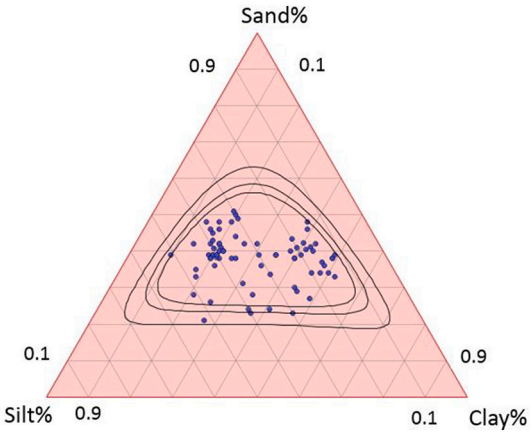


**Fig. 11.** Figure shows the predictive region of center (gi)

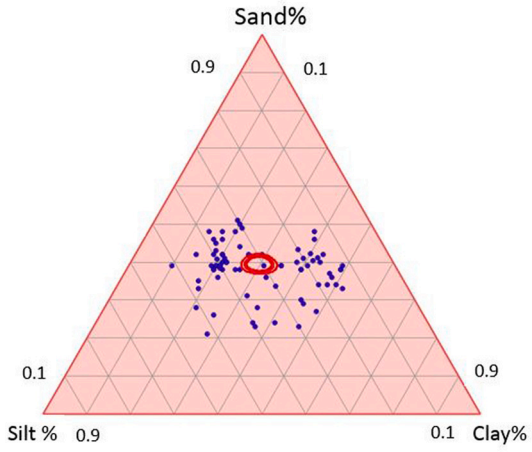


**Fig. 12.** The figure shows the consistency of a centered confidence region of center (gi) with the maximum concentration zone of sand, silt, and clay

and further process provided the center plot. The center value lies in the maximum point concentrated location in the ternary diagram (Fig. 12).

In the next step, the relationship between parts of the composition have been analyzed. The variation array is used to get the relation between the mean value of log-ratio and variance of the same log-ratio (Table 1). The variation array is computed by using CoDapack v.2.02.21 developed by the research group in statistics and compositional data analysis at the University of Girona which is freely available. CoDapack v.2.01.15 has been used by other researchers in the past for a similar purpose (Bicocchi et al., 2019). Finally, the centered log-ratio (clr) variance was obtained (Table 1).

The result shows that, the silt-clay log-ratio has a high variance (0.2296) whereas sand-clay and sand-silt log-ratio have low variance. The sand-clay log-ratio has a lower variance than the silt-clay log-ratio but has higher variance than sand–silt log ratio. The centered log-ratio value of a single component indicates that the silt and clay fraction has

**Table 1**
Variation array of the soil grain size distribution.

| | Variance ln(Xi/Xj) | | | |
|---|---|---|---|---|
| Xi/Xj | Sand | Silt | Clay | clr variance |
| Sand | – | 0.1152 | 0.1867 | 0.0416 |
| Silt | −0.1108 | – | 0.2296 | 0.0559 |
| Clay | −0.6058 | −0.4950 | – | 0.0797 |
| | Mean ln(Xi/Xj) | | | 0.1772 |

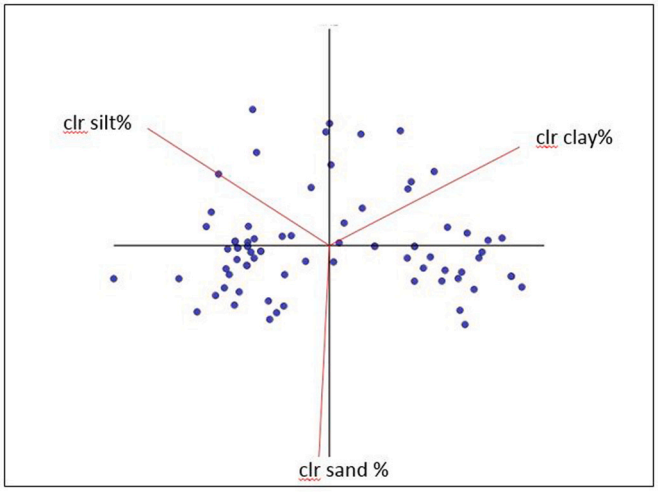


**Fig. 13.** The plot of centered log ratio (clr) of sand, silt, and clay fraction

a variance greater than 76% which is the highest fraction. Sand-silt and sand-clay fraction have 54% and 68% respectively. The clr plots of silt, sand, and clay fraction are shown in Fig. 13.

### 3.3. Phase relationship analysis

The obtained phase relationship of soils is shown in Table 2**.** The value of dry unit weight is ranged between 13.134 and 17.464 kN/m$^3$ with the coefficient of variance 5.89. The values are highly concentrated around the mean value. The majority of values (37 counts) lie in the interval of 16–17. The maximum count of void ratio value is at the interval of 40–45. The mean value of the void ratio is 47.22 and the coefficient of variance is 10.86. The values are nearly concentrated around the mean value. The value of specific gravity ranges between 2.03 and 2.62 with a standard deviation of 0.139. That means there is less variation in data.

The value distributions of different phase relationships are shown in Fig. 14(a-f) respectively.

### 3.4. Correlation analysis

Correlation is a very useful statistical tool to identify the potential associates between different variables. Karl Pearson correlation coefficient was obtained to find out the interrelationship between each variable (Table 3**).** The correlation matrix and heat map of the correlation matrix were obtained to find the strength of the correlation between the variables. According to the result, the degree of saturation and moisture contents are highly correlated positively to each other (correlation coefficient 0.88). Similarly, specific gravity and dry unit weight have a higher positive correlation between each other. But the degree of saturation and dry unit weight have a less positive correlation to each other. To obtain the exact relationship between the variables, the linear regression between variables was tested.

**Table 2**
Descriptive statistics of seven variables.

| Phase relationship | Min. value | Max. value | Am | Sd | CV % |
|---|---|---|---|---|---|
| Sp. Gravity Gs (kN/m3) | 2.03 | 2.62 | 2.4 | 0.139 | 5.79 |
| Moisture content ω (%) | 6.38 | 12.38 | 9.375 | 1.461 | 15.58 |
| Dry unit weight γd (kN/m3) | 13.134 | 17.462 | 16 | 0.943 | 5.89 |
| Wet unit weight γω (kN/m3) | 14.224 | 18.83 | 17.156 | 0.994 | 5.79 |
| Void ratio e (%) | 35.63 | 56.79 | 47.22 | 5.13 | 10.86 |
| Porosity n (%) | 25.2 | 36.2 | 31.84 | 2.54 | 7.97 |
| Degree of saturation Sr (%) | 0.285 | 0.752 | 0.48 | 0.118 | 24.58 |

Where Am is an arithmetic mean, Sd is a standard deviation, CV is the coefficient of variance.

#### 3.4.1. Multiple regressions

We checked the linear relationship between some variables. The data were checked for normality of the response variable to run multiple regression models using qq-plot and Shapiro-test. For that, we selected one response variable and other predictor variables to run multiple regression models. Degree of saturation (Sr) was taken as the response variable whereas dry unit weight, void ratio, moisture content, and specific gravity were taken as the predictor variables. In the model, only two variables are statistically significant (Table 4). The moisture content and void ratio are statistically significant (*p*-value less than 0.05) but other variables are not statistically significant (*p*-value greater than 0.05). So, we again run the model by using two statistically significant variables (moisture content and void ratio) and another less significant variable (Specific gravity).

Again, the multiple regressions were run by taking only three predictor variables (moisture content, void ratio, and specific gravity) and the response variable (degree of saturation). The summary of significant covariates is shown in Table 5. In the new model, the variables are highly significant to each other.

The linear relation of the degree of saturation with void ratio, moisture content, and specific gravity was obtained on the scatter plot. The degree of saturation has an inverse relation with the void ratio (Fig. 15a) in a linear fashion but positive relation with moisture content (Fig. 15b) and specific gravity. Among the two positive variables, moisture content has strong regression with the degree of saturation.

## 4. Discussions

The nature and types of soil play a significant role to control mass movements and landslides. Various geotechnical properties, as well as grain size composition of the soil, play a direct role for landslide occurrence in the saturated or dry condition. The clay, sand, and silt have different nature in case of cohesion and water infiltration. Sand is non-cohesive and can infiltrate water easily through it but clay is cohesive, retains the water on it, and does not allow it to infiltrate. Therefore particle size and compositional analysis of soil are necessary.

This study depicts that most of the soil samples have more than 15% clay in them. Only four USCS classes of soils are obtained namely CL, ML, CL-ML, and SC. All three classes except SC are clay-rich but the compositional percentage of SC is less in number. Despite collecting samples in the dry season, the highest and mean value of liquid limit was 38.67% and 25.49% respectively, which also indicate that the soil has high clay content. The result obtained from the plasticity chart is similar to the result obtained from grain size analysis. But grain size distribution and classification merely are not sufficient to analyze the soil in the landslide area.

As shown in the variation array (Table 1), the compositional analysis of grain size distribution highlighted that the silt-clay and sand-silt log-ratio are characterized by higher variance whereas sand-silt log-ratio has the lowest variance. Low variance in the ratio indicates that the proportion between sand-silt grain size fractions is preserved independently in the soil. The transformation of components (sand-silt, silt-clay, and sand-clay) was carried out for confining the components to compare the source. The value of log-ratio provided the inter-particle transformation. The mean value of the silt-clay log ratio and variance of log-ratio indicate the physical mechanism of the formation of the soil component. The high variance in the silt-clay log-ratio indicates the transformation of mudstone or shale into the soil. Indeed, silt-clay abundance in the soil of hill slope depends on the weathering of shale or mudstone.

Furthermore, to identify the major role for landslide initiation among three components, Principal Component Analysis was conducted by using CoDapack software (Bhandari and Dhakal, 2019a, 2019b). The result of Principal Component Analysis (PCA) of 76

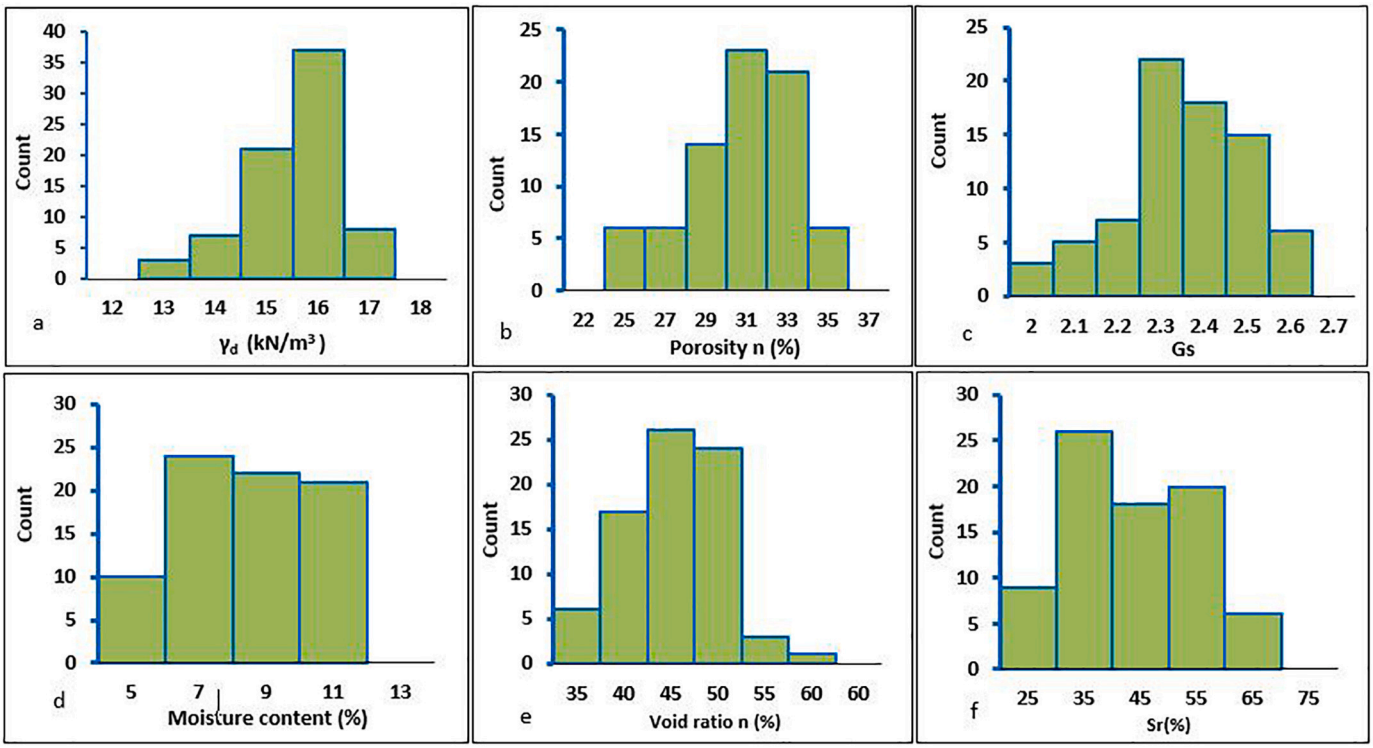


**Fig. 14.** The frequency distribution of a) dry unit weight b) porosity c) specific gravity d) moisture content e) void ratio f) degree of saturation.

**Table 3**
Correlation matrix of variables obtained from Karl Pearson correlation test.

| Variables | Sr | γd | e | w | Gs |
|---|---|---|---|---|---|
| Sr | 1.0000 | 0.2159 | −0.4027 | 0.8820 | −0.0172 |
| γd | 0.2159 | 1.0000 | −0.3116 | −0.1325 | 0.8190 |
| e | −0.4027 | −0.3116 | 1.0000 | 0.0024 | 0.2864 |
| w | 0.8820 | −0.1325 | 0.0024 | 1.0000 | −0.1237 |
| Gs | −0.0172 | 0.8190 | 0.2864 | −0.1237 | 1.0000 |

**Table 4**
Summary table showing covariates of degree of saturation for model selection.

| Variables | Estimate | Std.Error | t-value | p-value |
|---|---|---|---|---|
| Intercept | −16.8649 | 11.9919 | −1.408 | 0.1640 |
| γd | 3.9600 | 2.2484 | 1.781 | 0.0825 |
| e | −0.6532 | 0.2472 | −2.642 | 0.0101 |
| w | 5.2152 | 0.0685 | 76.087 | 0.0000 |
| Gs | −6.8888 | 15.0249 | −0.458 | 0.6480 |

**Table 5**
Summary table showing significant covariates of degree of saturation.

| Variables | Estimate | Std. Error | t-value | p-value |
|---|---|---|---|---|
| Intercept | 3.7338 | 2.668 | 1.389 | 0.000 |
| e | −1.0858 | 0.0288 | −37.622 | 0.000 |
| w | 5.1981 | 0.0689 | 75.440 | 0.000 |

Gs 19.508 1.0678 18.289 0.000.

samples for three variables is shown in Table 6. Bartles's test was performed to find the validity of PCA before conducting the analysis. Only two principal components having Eigen-value greater than 1 were selected which explained about 96.49% of the total variance.

The PCs features were classified based on their loading value. The PCs with a loading value greater than 0.75 are considered as strong and PCs value between 0.5 and 0.75 is considered as moderate. This standard was adopted by previous researchers (Li and Zhang, 2010; Pant et al., 2020) for the identification of major factors influencing water quality. The $PC_1$ has 61.05% of the total variance. It has a strong positive loading on clay (0.99). $PC_2$ has 35.44% of the total variance and has moderate positive loading on silt (0.484). The result showed that the two major components namely silt and clay are highly responsible for landslide initiation in the study area. The result is consistent with the compositional analysis. The results of clr and CA are similar and highly consistent. This result indicates that landslide mostly occurs in clayey soil. It has been established from the previous studies that higher clay fraction is more susceptible for landslide due to its extreme expansion potential (Mugagga et al., 2011; Knapen et al., 2006; Yang et al., 2007; Kitutu et al., 2009; Wati et al., 2010; Ohlmacher, 2000; Yalcin, 2007; Yalcin, 2011).

The dry unit weight varied from 13.134 to 17.462 whereas the void ratio varied from 35.63% to 56.79%. The dry unit weight has a negative correlation with the void ratio. It means the dry unit weight decreases with increasing void ratio. The voids allow passing water slowly in the clayey soil but clay holds and stores the water for longer. The fine clay stops the drain at the basal part on the bedrock, due to that, the clay retains and stores water on it. The mechanism caused high pore pressure and the landslides are triggered. Similar results were obtained by previous researchers in the different areas (Yang et al., 2007; Jadda et al., 2009; Wati et al., 2010; Yalcin, 2011; Mugagga et al., 2011). Their results show that clayey soils with fine texture have numerous small pores and liberate water gradually, which causes susceptible to landslides on the soil slope. In our result, the plasticity chart revealed that the soils are inorganic clays and silts having medium plasticity. But some of the previous researchers obtained high plasticity of fine-grained inorganic clay and silts (Orazulike, 1988; Chartwin et al., 1994; Isik and Keskin, 2008). From our result, it can be concluded that the medium to the low plastic (Burmister, 1949; Casagrande, 1932) inorganic soils are prone to initiate landslide in the study area because it is a part of the Siwalik zone consisting of sedimentary rocks. Dai et al. (2002) also have reported that highly plastic inorganic soils are prone to sliding during rainfall events; due to the reduction of shear resistance

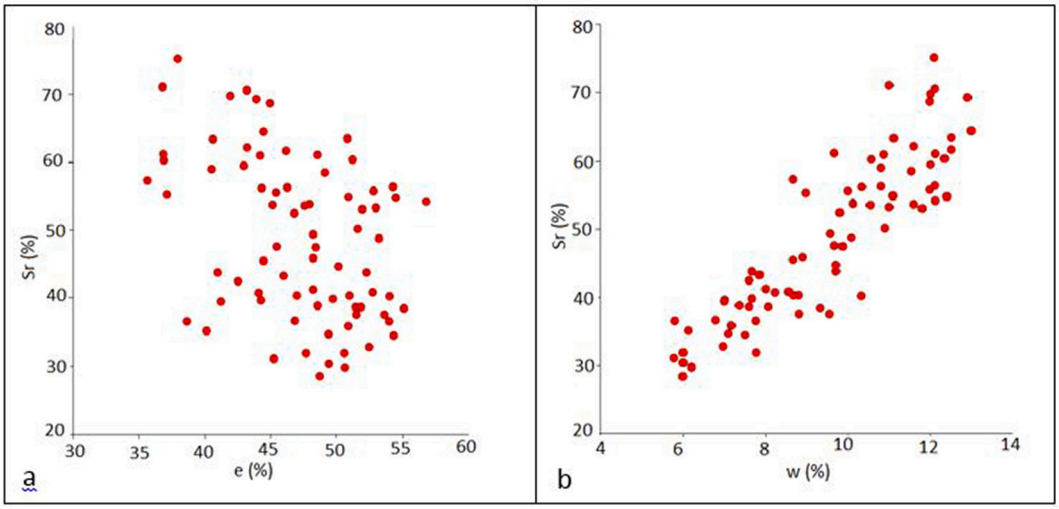


**Fig. 15.** a) Linear scatter plot of the degree of saturation and void ratio b) Linear scatter plot of the degree of saturation and moisture content.

**Table 6**
Loading of the component on the Principal Component is shown in the table below.

| Particles | PC1 | PC2 |
|---|---|---|
| Sand | −0.36 | −0.93 |
| Silt | −0.869 | 0.484 |
| Clay | 0.99 | 0.086 |
| Eigenvalue | 1.86 | 1.108 |
| Variance | 61.05 | 35.44 |

occurs.

The correlation matrix (Table. 3) showed that the degree of saturation (Sr) is highly correlated positively with moisture content but negatively correlated with void ratio and specific gravity. The numerical relation of the degree of saturation (Sr) to the moisture content (w) and void ratio (e) shows that there should be a positive relationship between the degree of saturation (Sr) and specific gravity (Gs). To signify the numerical relation of the degree of saturation, we used multiple regressions of five variables. We used the degree of saturation as a response variable and the other four variables (void ratio, specific gravity, moisture content, and dry unit weight) are taken as a predictor variable. After running the model, the best-selected model provided the regression equation (Eq. (12)). We checked the model with a visual model diagnostic and obtained the residual plot with a significant variable (Fig. 16a,b) and the normal probability plot of residual (Fig. 17a,b). The plot showed that the model is statistically significant.

$$Sr = 3.7338 - 1.0858 * e + 5.1991 * w + 19.5086 * Gs \quad (12)$$

If we compare this equation with Eq. (6) (relation of the degree of saturation to void ratio, specific gravity, and moisture content), the relation is true. The compositional analysis and phase relationship provided better results to understand soil from the landslide area. The soil is clay-rich so that the degree of saturation and moisture content is comparatively higher though the samples were collected in the dry season.

In the study area, all the geological units are extended from the east

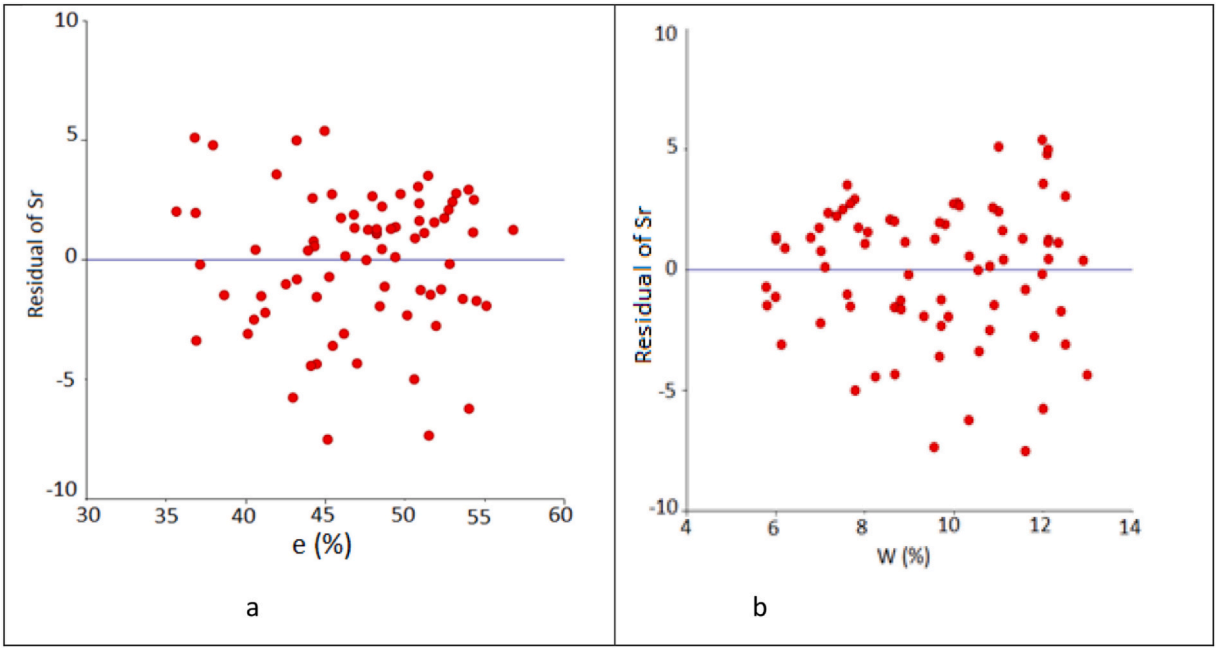


**Fig. 16.** Residual plot of the response variable with a) void ratio b) moisture content.

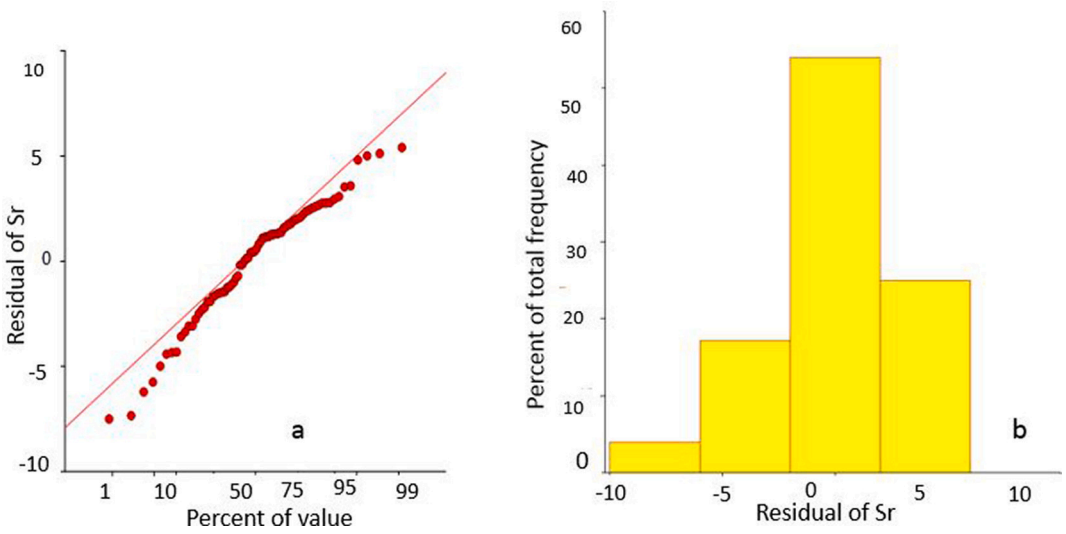


**Fig. 17.** a) Normal Probability plot of residual b) histogram of the residual plot shows normal behavior.

to the west as shown in Fig. 2. The inventory mapping and field mapping revealed that the landslide types and mechanisms in a particular geological unit are similar throughout the study area. For example, the rock falls and rockslides are very common in the Middle Siwalik whereas debris slides are common in the Lower Siwalik (Bhandari and Dhakal, 2020). About 10% of soil samples were studied in the laboratory out of 769 landslide sites but the spatial coverage of sampled landslide locations is such that all the geological units are represented (Fig. 5). The laboratory analysis result has provided the distribution of a principal component of soil in different geological units with precise soil classification. The results revealed that the clay/silt fraction is mainly responsible for landslide in the study area. As the shear strength parameters are directly related to the moisture content, Atterberg limits, and particle size distribution (Ael et al., 2020), the laboratory geotechnical data obtained from this study will be useful for landslide prediction modeling (Carrière et al., 2018), landslide susceptibility analysis (Ael et al., 2020), slope stability analysis (Tofani et al., 2017) and landslide mitigation purposes (Uyeturk et al., 2020).

## 5. Conclusions

The major objective of this study was to evaluate the soil component and the phase relation of soil for landslide initiation in the Siwalik zone of the Babai River watershed. In this study, the compositional analysis and phase relationship of 76 soil samples from 76 active landslides were conducted. The laboratory analysis results provided the distribution of the principal component of soil in different geological units with precise soil classification. This laboratory study followed by statistical analysis of the result depicted that three USCS classes of soils are dominantly present in the landslides of the study area namely CL, ML, and CL-ML. Similarly, the principal component has higher loading on clay and silt. The centered log-ratio indicates that the main source of clay in the landslide of the Siwalik zone may be either shale or weak mudstone. This study concluded that the silt-clay fraction having less void ratio is mainly responsible to trigger landslides in the study area as it retains the water in it for a long time. The results of laboratory analysis conducted in the present study can be useful for the landslide prediction modeling, landslide susceptibility analysis, and also for site-specific landslide mitigation purposes in the study area.

## Author statement

The authors declare that the work described in this paper has not been published previously, that it is not under consideration for publication elsewhere, that its publication is approved by both the authors, and that, if accepted, it will not be published elsewhere in the same form, in English or in any other language, including electronically without the written consent of the copyright-holder.

## Declaration of Competing Interest

The authors declare that they have no known competing financial interests or personal relationships that could have appeared to influence the work reported in this paper.

## Acknowledgments

The authors want to acknowledge the support of the Central Material Testing Laboratory, Pulchwok Engineering Campus, Tribhuvan University for the arrangement of laboratory work. Our sincere thanks go to the local people of Babai valley for their continuous support during field study and soil sampling.

## References

Ael, Jazouli, Barakat, A., Khellouk, R., 2020. Geotechnical studies for Landslide susceptibility in the high basin of the Oum Er Rbia river (Morocco). Geol. Ecol. Landscapes. https://doi.org/10.1080/24749508.2020.1743527.

Aitchison, J., 1982. The statistical analysis of compositional data. J. R. Stat. Soc. Ser. B Methodol. 44 (2), 139–177. https://doi.org/10.1111/j.2517-6161.1982.tb01195.x.

Aitchison, J., 2003. The Statistical Analysis of Compositional Data. Blackbum, Caldwell, NJ. USA ISBN 978193066578.

ASTM D422-63e2, 2007. Standard Test Method for Particle Size Analysis of Soils. ASTM international, West Conshohocken, PA.

Auden, J.B., 1935. Traverses in the Himalaya. Geol. Survey India 69, 123–167.

Ausilio, E., Zimmaro, P., 2017. Landslide characterization using a multidisciplinary approach. Measurement 104, 294–301.

Bhandari, B.P., Dhakal, S., 2018. Lithological Control on Landslide in the Babai Khola Watershed, Siwaliks Zone of Nepal. Am. J. Earth Sci. 5, 54–64.

Bhandari, B.P., Dhakal, S., 2019a. Topographical and geological factors on gully-type debris flow in Malai River catchment, Siwaliks, Nepal. J. Nepal Geol. Soc. 59, 89–94 DOI: doi.103126/jngs.v59i0.24994.

Bhandari, B.P., Dhakal, S., 2019b. Evolutional Characteristics of Debris Flow in the Siwalik Hills of Nepal. Int. J. Geosci. 10, 1049–1067. https://doi.org/10.4236/ijg.2019.101206.

Bhandari, B.P., Dhakal, S., 2020. Spatio temporal dynamics of landslide in the sedimentary terrain: a case of Siwalik zone of Babai watershed, Nepal. SN Appl. Sci. 2, 854. https://doi.org/10.1007/s42452-020-2628-0.

Bicocchi, G., Tofani, V., D'Ambrosio, M., et al., 2019. Geotechnical and Hydrological characterization of hillslope deposits for regional landslide prediction modeling. Bull. Eng. Geol. Environ. 78, 4875–4891.

Buccianti, A., 2013. Is compositional data analysis a way to see beyond the illusion? Comput. Geosci. 50, 165–173.

Burmister, D.M., 1949. Principal and techniques of soil identification. In: Proceeding Annual Highway Research Board Meeting. 29. National Research Council,

Washington D.C, pp. 402–434.
Cardinali, M., Galli, M., Guzzetti, F., Ardizzone, F., Reichenbach, P., Bartoccini, P., 2006. Rainfall induced landslide in December 2004 in South- western Umbria, Central Italy: types, extent, damage and risk assessment. Nat. Hazards Earth Syst. Sci. 6, 237–260.
Carrière, S.R., Jongmans, D., Chambon, G., Bièvre, et al., 2018. Rheological properties of clayey soils originating from flow-like landslides. Landslides 15 (8), 1615–1630. https://doi.org/10.1007/s10346-018-0972-6.
Casagrande, A., 1932. Research of Atterberg limit of soils. Public Roads 13 (8), 121–136.
Casagrande, A., 1948. Classification and identification of soil transaction. ASCE 113, 901–930.
Cencetti, C., Conversini, P., 2003. Slope instability in the Bastardo Basin (Umbria, Central Italy) – the landslide of Barattano. Nat. Hazards Earth Syst. Sci. 3, 561–568.
Chartwin, S.C., Howes, D.E., Schwab, J.W., Swanston, D.N., 1994. A Guide for Management of Landslide-Prone Terrain in the Pacific Northwest. Ministry of Forests, Victoria.
Chaudhari, R.S., 1982. Petrology of the Siwalik Group of Nepal Himalaya. Recent Res. Himalaya 8, 424–466.
Dahal, R.K., Hasegawa, S., Bhandary, N.P., Poudel, P.P., Nonomura, A., Yatabe, R., 2012. A replication of landslide hazard mapping at catchment scale. Geomat. Nat. Hazards Risk 3 (2). https://doi.org/10.1080/19475705.2011.629007. 161 192.
Dai, F.C., Lee, C.F., Ngai, Y.Y., 2002. Landslide risk assessment and management: An overview. Eng. Geol. 64 (1), 65–87.
Dai, F.C., Xua, C., Yaob, X., Xua, L., Tua, X.B., Gongc, Q.M., 2010. Spatial distribution of landslides triggered by the 2008 Ms 8.0 Wenchuan earthquake. J. Asian Earth Sci. 40, 383–895.
Das, B.M., 2009. Weight- volume relationship. In: Principal of Geotechnical Engineering.
Das, B.M., Sobhan, K., 2013. Principles of geotechnical engineering. In: Cengage Learning Cengage learning, 7th edition. pp. 51–72.
Davis, R.O.E., Bennet, H.H., 1927. Grouping of soils on the basis of mechanical analysis. In: Dep. Circ. 419 US Department of Agriculture, Washington DC.
Devkota, K.C., Regmi, A.D., Pourghasemi, H.R., et al., 2013. Landslide susceptibility mapping using certainty factor, index of entropy and logistic regression models in GIS and their comparison at Mugling–Narayanghat road section in Nepal Himalaya. Nat. Hazards 65, 135–165. https://doi.org/10.1007/s11069-012-0347-6.
Dhakal, S., 2014. Disaster in Nepal. In: In: Disaster Risk Management: Concept, Policy and Practices in Nepal, Central Department of Environmental Science (CDES), Tribhuvan University Kirtipur.
Dhakal, S., 2015. Evolution of geomorphologic hazards in Hindu Kush Himalaya. In: Shaw, R., Nibanupudi, H.K. (Eds.), Mountain Hazards and Disaster Risk Reduction. Springer, Japan, pp. 53–72. https://doi.org/10.1007/978-4-431-55242-0_4.
Dhital, M.R., 2015. Geology of the Nepal Himalaya, 1st edn. Springer International Publishing, Switzerland. https://doi.org/10.1007/978-3-319-02496-7.
Dundulis, K., Gadeikis, S., Gadeikytė, S., Urbaitis, D., Prunskienė, L., 2010. Problems of usage of soil classification systems for sand soils of Lithuania. In: 10th Int. Conf, Vilnius Gediminas Technical Univ., Vilnius, Lithuania.
Egozcue, J.J., Pawlowsky-Glahn, V., 2005. Groups of parts and their balances in compositional data analysis. Math. Geol. 37 (7), 795–828. https://doi.org/10.1007/s11004-005-7381-9.
Eynatten, V.H., 2004. Statistical modeling of compositional trends in sediments. Sediment. Geol. 171, 79–89.
Ghimire, M., 2011. Landslide occurrence and its relation with terrain factors in the Siwalik Hills, Nepal:Case study of susceptibility assessment in three basins. Nat. Hazards 56 (1), 299–320. https://doi.org/10.1007/s11069-010-9569-7.
Guzzetti, F., Cardinali, M., Reichenbach, P., 1996. The influence of structural setting lithology on landslide type and pattern. Environ. Eng. Geosci. 2 (4), 531–555.
Guzzetti, F., Reichenbach, P., Cardinali, M., Galli, M., Ardizzone, F., 2005. Probabilistic landslide hazard assessment at the basin scale. Geomorphology 72, 272–299.
Guzzetti, F., Mondini, A.C., Cardinali, M., Fiorucci, F., Santangelo, M., Chang, K.T., 2012. Landslide inventory maps: New tools for an old problem. Earth Sci. Rev. 112, 42–66. https://doi.org/10.1016/j.earscirev.2012.02.001.
Hagen, T., 1969. Report on the geological survey on Nepal. Denschr. Schweiz. Naturf. Gesell 86, 1–185.
Higaki, D., 2003. Landslides and Erosion Study in Siwalik Region Using Geomorphological Approach, 1st ed. Kathmandu, Nepal, Seminar of Nepal Landslide Society (NLS).
Hovius, N., Stark, C.P., Allen, P.A., 1997. Sediment flux from a mountain belt derived by landslide mapping. Geology 25, 231–234.
Howard, A.K., 1984. The revised ASTM standard on the unified classification system. Geotech. Test. J. 7 (4), 216–222.
Hurtrez, J.E., Lucazeau, F., 1999. Investigation of the relationships between basin morphology, tectonic uplift, and denudation from the study of an active fold belt in the Siwalik Hills, Central Nepal. J. Geophys. Res. 104, 12779–12796. https://doi.org/10.1029/1998JB900098.
Isik, Y., Keskin, Y., 2008. GIS based statistical and physical approaches to landslide susceptibility mapping (Sebinkarahisar, Turkey). Bull. Eng. Geol. Environ. 68, 459–471.
Jadda, M., Shafri, H.Z., Mansor, S., Sharifikia, M., 2009. Landslide susceptibility evaluation and factor effect analysis using probabilistic–frequency ratio model. Eur. J. Sci. Res. 33, 654–668.
Kitutu, M.G., Muwanga, A., Poesen, J., Deckers, J.A., 2009. Influence of soil properties on landslide occurrence in Bududa district, Eastern Uganda. Afr. J. Agric. Res. 4 (7), 611–620.
Knapen, A., Kitutu, M.G., Poesen, J., Breugelmans, W., Deckers, J., Muwanga, A., 2006. Landslides in a densely populated county at the footsteps of Mount Elgon (Uganda): characteristics and causal factors. Geomorphology 73, 149–165.
Kovačevi'c, M.S., Juri'c-Ka'cuni'c, D., 2014. European soil classification system for engineering purposes. Grad-evinar 66 (9), 801–810.
Lee, I.K., White, W., Ingles, O.G., 1983. Soil formation, classification and exploration. In: Principal of Geotechnical Engineering. Pitman Publishing Inc., pp. 1–56.
Li, S., Zhang, Q., 2010. Spatial characterization of dissolved trace elements and heavy metals in the upper Han River (China) using multivariate statistical techniques. J. Hazard. Mater. 176, 579–588. https://doi.org/10.1016/j.jhazmat.2009.11.069.
Malamud, B.D., Turcotte, D.L., Guzzetti, F., Reichenbach, P., 2004. Landslide inventories and their statistical properties. Earth Surf. Process. Landf. 29 (6), 687–711.
Meisina, C., 2006. Characterization of weathered clayey soils responsible for shallow landslides. In: Natural Hazards and Earth System Science. Copernicus Publications on behalf of the European Geosciences Union 6 (5):825–838. Hal-00299368.
Mugagga, F., Kakembo, V., Buyinza, M., 2011. A characterization of the physical properties of soil and the implications for landslide occurrence on the slopes of Mount Elgon, Eastern Uganda. Nat. Hazard 52.
Ohlmacher, G.C., 2000. The relationship between geology and landslide hazards at Atchison, Kansas and vicinity. Curr. Res. Earth Sci. 244 (3), 1–16.
Orazulike, D.M., 1988. Hazardous earth processes in parts of Bauchi state, Nigeria. Their causes and environmental implications. Nat. Hazards 1 (2), 155–160. https://doi.org/10.1007/bf00126612.
Pant, R.R., Zhang, F., Ur, Faizan Rehman, et al., 2020. Spatiotemporal characterization of dissolved trace elements in the Gandaki River, Central Himalaya Nepal. J. Hazard. Mater. 389, 121913.
Parker, R.N., Densmore, A.L., Rosser, N.J., et al., 2011. Mass wasting triggered by the 2008 Wenchuan earthquake is greater than orogenic growth. Nat. Geosci. 4 (7), 449–452.
Regmi, A.D., Yoshida, K., Pourghasemi, H.R., et al., 2014a. Landslide susceptibility mapping along Bhalubang–Shiwapur area of mid-western Nepal using frequency ratio and conditional probability models. J. Mt. Sci. 11 (5). https://doi.org/10.1007/s11629-013-2847-6.
Regmi, A.D., Devkota, K.C., Yoshida, K., et al., 2014b. Application of frequency ratio, statistical index, and weights-of-evidence models and their comparison in landslide susceptibility mapping in Central Nepal Himalaya. Arab. J. Geosci. 7, 725–742. https://doi.org/10.1007/s12517-012-0807-z.
Riemer, M.F., Collins, B.D., Badger, T.C., Toth, C., Yat, C.Y., 2015. Geotechnical Soil Characterization of Intact Quaternary Deposits Forming the March 22, 2014 SR-530 (Oso) Landslide. U.S. Geological Survey Open-File Report 2015–1089, Snohomish County, Washington, pp. 17. https://doi.org/10.3133/ofr20151089.
Rosi, A., Tofani, V., Tanteri, L., et al., 2018. The new landslide inventory of Tuscany(Italy) updated with PS-InSAR: Geomorphological features and landslide distribution. Landslides 15, 5–19.
Selby, M.G., 1993. Hillslope Materials and Processes. Oxford University Press, New York.
Shapiro, S.M., Wilk, M.B., 1965. An analysis of variance test for normality (complete samples). Biometrika 52, 591–611.
Thapa, D., Bhandari, B., 2019. GIS-based frequency ratio method for identification of potential landslide susceptible area in the Siwalik Zone of Chatara-Barahakshetra Section, Nepal. Open J. Geol. 9, 873–896. https://doi.org/10.4236/ojg.2019.912096.
Thomas, C.W., Aitchison, J., 2005. Compositional data analysis of geological variability and process: a case study. Math. Geol. 37, 753–772.
Tofani, V., Bicocchi, G., et al., 2017. Soil characterization for shallow landslides modeling: a case study in the Northern Appennines (Central Italy). Landslides 14, 755–770. https://doi.org/10.1007/s10346-017-0809-8.
TU-CDES, 2017. Landslide Inventory Characterization and Engineering Design for Mitigation Works of Chure Area in Ten Districts. Central Department of Environmental Science, Tribhuvan University and Government of Nepal, President. Chure-Tarai Madhesh Conservation Development Board, Kathmandu.
Uyeturk, C.E., Huvaj, N., Bayraktaroglu, H., Huseyinpasaoglu, M., 2020. Geotechnical characteristics of residual soils in rainfall-triggered landslides in Rize, Turkey. Eng. Geol. 264, 105318. https://doi.org/10.1016/j.enggeo.2019.105318.
Van den Boogaart, K.G., Tolosana-Delgado, R., Bren, M., 2014. Compositional Data Analysis. R package version. 1. pp. 40–41. https://CRAN.R-project.org/package=compositions.
Van Westen, C.J., Van Asch, T.W.J., Soeters, R., 2006. Landslide hazard and risk zonation why is it still so difficult? Bull. Eng. Geol. Environ. 65, 167–184.
Wati, S.E., Hastuti, T., Wijojo, S., Pinem, F., 2010. Landslide susceptibility mapping with heuristic approach in mountainous area. A case study in Tawangmangu sub District, Central Java, Indonesia. Int Arch Photo RS Spat. Inf. Sci. 38 (8), 248–253.
Yalcin, A., 2007. The effects of clay on landslides: a case study. Appl. Clay Sci. 38, 78–85.
Yalcin, A., 2011. A geotechnical study on landslides in the Trabon Province, NE Turkey. Appl. Clay Sci. 52, 11–19.
Yang, H., Adler, R., Huffman, G., 2007. Use of satellite remote sensing in the mapping of global landslide susceptibility. Nat. Hazards 43 (2), 245–256. https://doi.org/10.1007/s11069-006-9104-z.
Zhao, H.F., Zhang, L.M., Xu, Y., Chang, D.S., 2013. Variability of geotechnical properties of a fresh landslide soil deposit. Eng. Geol. 166, 1–10. https://doi.org/10.1016/j.enggeo.2013.08.006.

Journal of Asian Earth Sciences: X 5 (2021) 100061

Contents lists available at ScienceDirect

Journal of Asian Earth Sciences: X

journal homepage: www.sciencedirect.com/journal/journal-of-asian-earth-sciences-x

# A multidisciplinary approach of landslide characterization: A case of the Siwalik zone of Nepal Himalaya

Bharat Prasad Bhandari [a], Subodh Dhakal [b,*]

[a] Central Department of Environmental Science, Tribhuvan University, Kirtipur, Nepal
[b] Department of Geology, Tri-Chandra Campus, Tribhuvan University, Kathmandu, Nepal

ARTICLE INFO

*Keywords:*
Siwalik
Landslide characterization
Multidisciplinary approach
GIS

ABSTRACT

The landslide is a common problem in the Siwalik zone of Nepal Himalaya during the monsoon period. The heterogeneity of lithology comprising of thickly bedded sandstone and mudstone, weakly cemented conglomerate beds, and permeable quaternary deposits on moderate to steep slopes are primarily responsible for the landslide in this zone. In this study, a multidisciplinary approach is used for the landslide characterization. The polygon-based landslide inventory map was prepared by using Sentinel-2, Landsat-8, and Google Earth imageries. The draft inventory map was verified and updated by several field visits. The final inventory map was overlaid with topographical, geological, and hydrological maps in Q-GIS and explored the landslide characteristics. Landslide distribution to geological units, thrust zone, slope, aspect, and rainfall amount along with the geotechnical properties are manifested and the relation between each selected factor is discussed. The study shows that a multidisciplinary technique provides the better option for landslide characterization.

## 1. Introduction

Landslides are complex natural phenomena that occur due to the impact of a large number of factors. The geological (Bhandari & Dhakal, 2018; Tsou et al., 2018; Gerrard 1994; Hasegawa et al., 2009), geotechnical (Yalcin, 2011; Yalcin 2011; Tofani et al., 2017), topographical (Tsou et al., 2018; Zhang et al., 2016) and hydrological (Dahal et al.,2008a; Dahal et al.,2008b) conditions are crucial factors that need to be studied for a better understanding of the landslide process. Weak and fragile geology is one of the major reasons for landslide initiation (Devkota et al., 2013; Regmi et al., 2014; Regmi et al., 2012a,b; Dahal et al., 2008; Bhandari & Dhakal, 2018; Gadtaula & Dhakal, 2019; Bhandari & Dhakal, 2020a). Similarly, the soil in the slopes has typical geotechnical properties that play a vital role in landslide initiation (Bhandari & Dhakal, 2020b; Yalcin, 2011; Yalcin, 2011; Tofani et al., 2017; Bicocchi et al., 2019). Continuous rainfall on adverse topography and geology leads to the landslide process in the mountainous areas of the Himalayan region (Weidinger, 1998; Borga et al., 2002; Fernandes et al., 2004; Zhang et al., 2012; Ching et al., 2018; Hennrich and Crozier, 2004; Talebi et al., 2008; Kayastha et al., 2013).

When we talk about the Nepal Himalaya, it is diversified into different geographical regions, namely mountainous regions, hilly regions, and the Terai region, based on geography. Every year, many people become homeless and property less due to landslides in Nepal (MoHA, 2019).

Generally, landslides are caused by intense rainfall adverse topography, deep and continuous erosion, and geometry modification. However, the soil properties also play a significant role in triggering landslides on the hill slope. The pore water pressure is generated in the unsaturated zone after heavy and continuous rainfall causing landslides (Yalcin, 2011; Hakro and Harahap, 2015, Bhandari & Dhakal, 2020b). Tohari et al. (2007) concluded that the continuous rainfall for a long time develops the hydrologic condition in the less permeable soil slopes which leads to failure initiation. The continuous rainfall increases the volumetric moisture content. If the moisture content of dry soil is excessively increased, the soil saturation increases rapidly and leads to failure initiation. Hence, landslide characterization incorporating the triggering factors like rainfall is necessary to understand the process, manage them properly and reduce the disaster risk associated with them.

Characterization of landslides broadly means understanding or unraveling the mechanisms or interplay of all the determining factors that lead to any slope failure (Varnes, 1978). A single factor cannot provide effective landslide characterization in complex geological and

* Corresponding author.
*E-mail address:* dhakalsubodh@gmail.com (S. Dhakal).

https://doi.org/10.1016/j.jaesx.2021.100061
Received 7 February 2021; Received in revised form 7 April 2021; Accepted 10 April 2021
Available online 16 April 2021

topographical conditions. A multidisciplinary approach is taken as a powerful tool for landslide characterization (Ausilio and Zimmaro, 2017) which involves the combination of different techniques that provides an adequate characterization of the landslide. Therefore, it is imperative to characterize the landslides from different important aspects including the geotechnical and hydrological properties, in addition to the geology and the topography, so that the process can be better understood, and the landslides can be better managed. This study aims to identify the landslide process by evaluating the characteristics of the landslides in the Siwalik zone of Nepal Himalaya using multidisciplinary approach including geological, hydrological, topographical, and geotechnical properties. This study will be useful for a better understanding of the landslide initiation mechanism in the Siwalik zone of Nepal Himalaya.

## 2. Materials and methods

### 2.1. Study area

The present study area lies in the Babai River catchment of Western Nepal (Fig. 1). The Babai River is initiated from the Siwalik hill and extends through the Dun Valley, reinter into Siwalik and finally run through the Terai plain of Nepal. The River extends over the eastern hill of the Dang Valley to the southeastern Indian border and enters the Indian Territory. The study area is highly sensitive to gully erosions, landslides, and many other mass movements (Bhandari & Dhakal 2019; Bhandari & Dhakal 2020a).

The study area is characterized by a sub-tropical climate moderated by hilly topography varying between 109 m and 1550 m above the mean sea level. The area has mainly two seasons in terms of precipitation: a long dry season and a long rainy season. The long rainy season can be divided into three parts: pre-monsoon, monsoon, and post-monsoon periods. March, April, and May are considered as the pre-monsoon period. Similarly June, July, August and September are the monsoon periods whereas October and November are considered as the post-monsoon periods. Generally speaking, June to September is considered as a long-term rainy season in Nepal. The long-term dry season is completely dry. However, moderate to low-intensity rainfall occurs in the dry season which is very low in comparison to the rainy season. The winter temperature falls below 0 °C and the summer temperature rises above 40 °C. The range of total yearly rainfall from 1990 to 2019 is 1800–3300 mm as obtained from the analysis of data of Department of Hydrology and Meteorology, government of Nepal. The amount of rainfall only in the monsoon period is 1500 – 2400 mm and the overall climate is sub-tropical. The area consists of a large number of erosional landforms and the downstream consists of a huge amount of valley fill due to sediments deposited by landslides and soil erosion. The rocks are highly jointed and fractured. The topography is characterized by a gentle to steep slope along with the high cliff and continuously extended ridges. Stratigraphically, the area is divided into three geological units in terms of bedrock lithology (Fig. 2).

The bedrock lithology consists of sandstone, mudstone, shale, and conglomerate beds with minute limestone beds. Previous researchers have divided the Siwalik group into three geological units namely; Lower Siwalik, Middle Siwalik, and Upper Siwalik (Auden, 1935; Hagen, 1969; Dhakal, 2015; Chaudari, 1982; Thapa & Bhandari, 2019). Similarly, the study area is also divided into three geological units by Bhandari & Dhakal, 2018; Bhandari & Dhakal, 2020a. Lower Siwalik is reach in mudstone and shale with the alternate bed of sandstone whereas, Middle Siwalik is rich in sandstone with the alternate bed of medium to thinly layered mudstone (Bhandari & Dhakal, 2019). Similarly, the Upper Siwalik is composed of calcite and clay bonded pebbly conglomerate with a thin layer of shale. The Northern boundary of the study area is separated by Main Boundary Thrust (MBT) with Lesser Himalaya but bounded by the Siwalik hills in the all directions. Babai Thrust, Bheri Thrust, and Malai Thrust are other thrusts extending to the East-West and dipping towards North. Due to its topographical and geological nature, the Babai watershed is prone to various mass movements and landslides (Bhandari & Dhakal, 2020a).

### 2.2. Landslide inventory mapping

Mostly, the landslide inventory map was prepared by using satellite images or aerial photographs (Guzzetti et al., 2012; Bhandari & Dhakal, 2020b). However, there are difficulties to obtain clear imagery of either technique in the hilly region of Nepal because of vegetation cover and frequent cloud cover. Even then, the remote sensing technique is considered as the best tool for the preliminary landslide inventory mapping. In this study, the process of landslide inventory mapping involves the following steps; (a) landslides were recognized from the images of Google Earth imagery (Fig. 3a), infrared imagery of Landsat 8 (Fig. 3b) and Sentinel-2. The white color band from the infrared imagery was followed for landslide mapping. The detected landslides in the infrared imagery were re-identified in the Sentinel and Google Earth imagery. The Landsat images were used by previous researchers for landslide inventory (Yu & Chen, 2017; Yu et al., 2020; Bhandari &

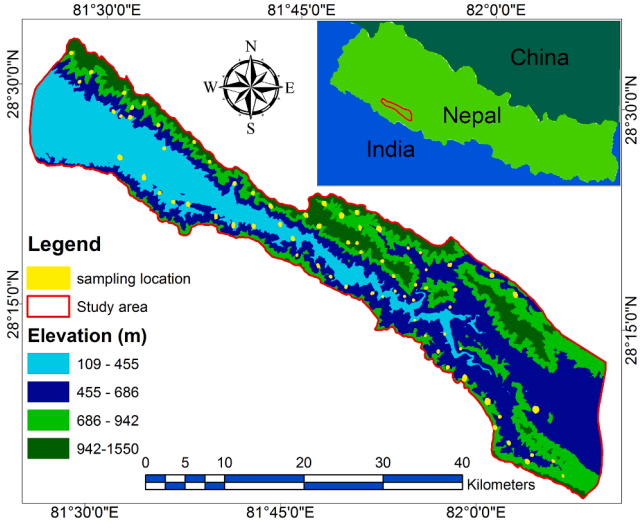


**Fig. 1.** Location map of the study area. The yellow dots show the soil sampling locations. (For interpretation of the references to color in this figure legend, the reader is referred to the web version of this article.)

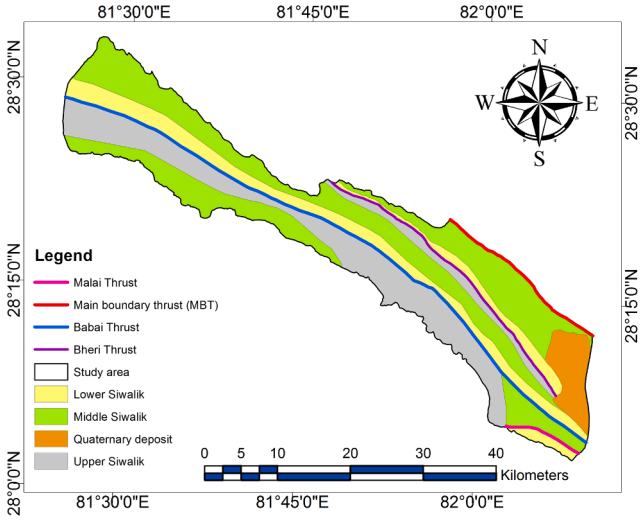


**Fig. 2.** Stratigraphical map of the study area.

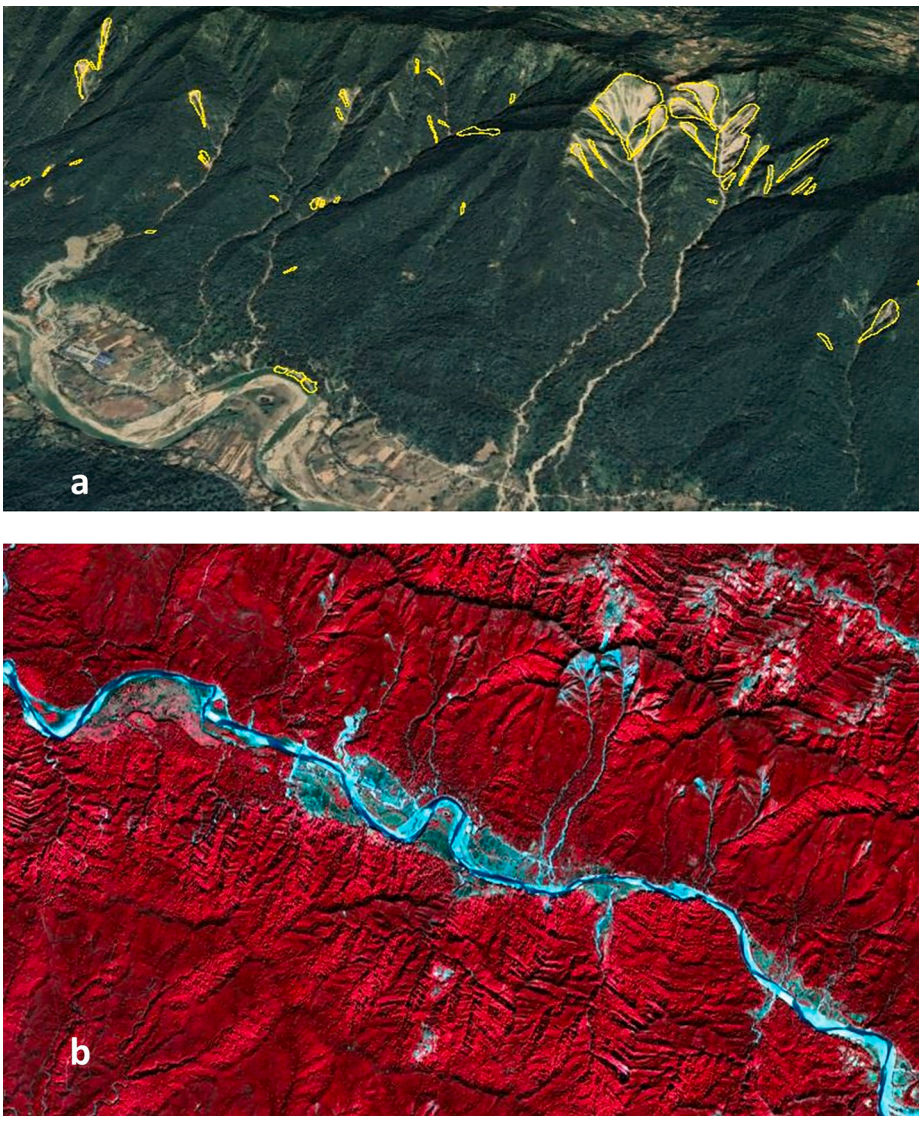


**Fig. 3.** a) Google earth imagery (yellow polygons show the landslide b) Landsat infrared imagery of Babai valley area (white color with scar shows the landslide. (For interpretation of the references to color in this figure legend, the reader is referred to the web version of this article.)

Dhakal, 2020a; Devkota et al., 2013). The recognized landslides were recorded in the imageries (b) The polygons were drawn from scar to toe of each landslide recorded on Google Earth imagery (c) The landslides were observed and verified in the field (d) The missing landslides in the image were traced out in the topographical map during the field visit and digitized in the layer. The final landslide inventory map was obtained on Q-GIS in the computer application system (Fig. 4). The time series imageries from 2010 to 2019 of Google earth were used for temporal landslide inventories (Fig. 5) and verified by past data obtained from the local government, Nepal police along with the local people in the field. The old scars, deposited sediments, vegetation status, heterogeneous surface curvature were observed and studied to identify the old landslides.

### 2.3. Topographical analysis of landslides

The area and length of landslides were obtained from Q GIS. The topographical factor maps (slope, aspect, curvature, and topographical wetness index) were prepared by using the Digital Elevation Model (DEM). The DEM of 30/30 m resolution was obtained from Alaska Satellite Facility. The topographical factors, their classes, and pixel numbers were obtained from the 3D analyst process of Q-GIS. The slope

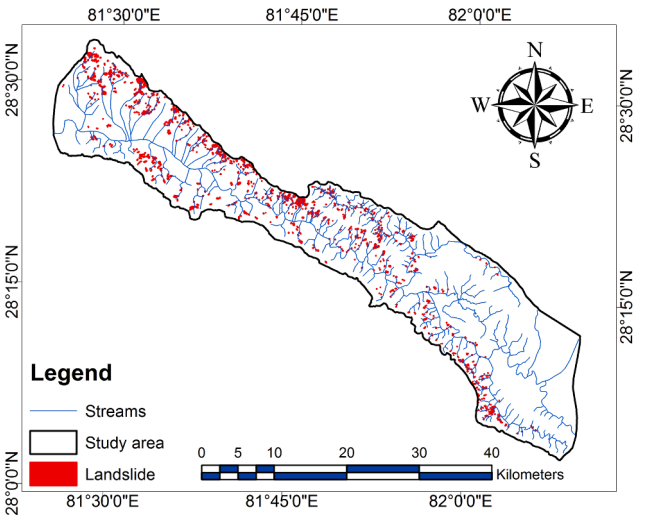


**Fig. 4.** Updated landslide inventory map of the study area.

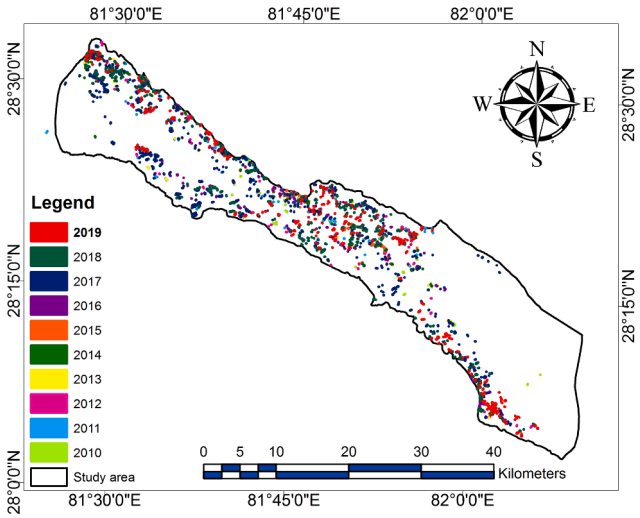


**Fig. 5.** Updated temporal landslide inventory map of the study area.

angle is classified into four classes based on landslide potential (Bhandari & Dhakal, 2020a) : (a) $< 15^0$ (b) $15^0$-$30^0$ (c) $30^0$-–$45^0$ (d) $> 45^0$ (Fig. 6a). The aspect class is divided into four classes (a) NE (b) SE (c) SW (d) NW (Fig. 6b). The curvature is classified into three classes based on low to high value: (a) convex (b) planar (c) concave (Fig. 6c). The topographical wetness index is classified into four classes based on equal interval division from low to high pixel numbers (Fig. 6d). The vector polygon-based inventory was obtained on the raster map and the pixel-based area of the raster was calculated by using cell size (29.138) and pixel number. The size and number of landslides in each parameter of raster maps were obtained.

### 2.4. Hydrological study

The rainfall data from seven different stations of ten years (2010 to 2019) were obtained and the average rainfall was calculated from the total station. The maximum 24 h rainfall, total annual rainfall, and total rainfall in the monsoon period (June-September) were calculated from raw data obtained from DHM, Nepal. Similarly, the drainage map of the study area was obtained from DEM and buffered into 5 classes. The landslide pixels of each buffered unit were measured. The distance to the drainage map was used to identify the significant role of water flow in triggering landslides during the rainy period.

### 2.5. Field study

The landslide inventory map was verified in the field by several routes walk. All the mapped landslides were visually observed in the field. The landslides missed in the image were traced out in the topo map of 1:25,000 scales, prepared by the department of the survey, Government of Nepal. Among the 1198 landslides, the length of the landslide, width of the toe and scar of 120 landslides were measured manually to

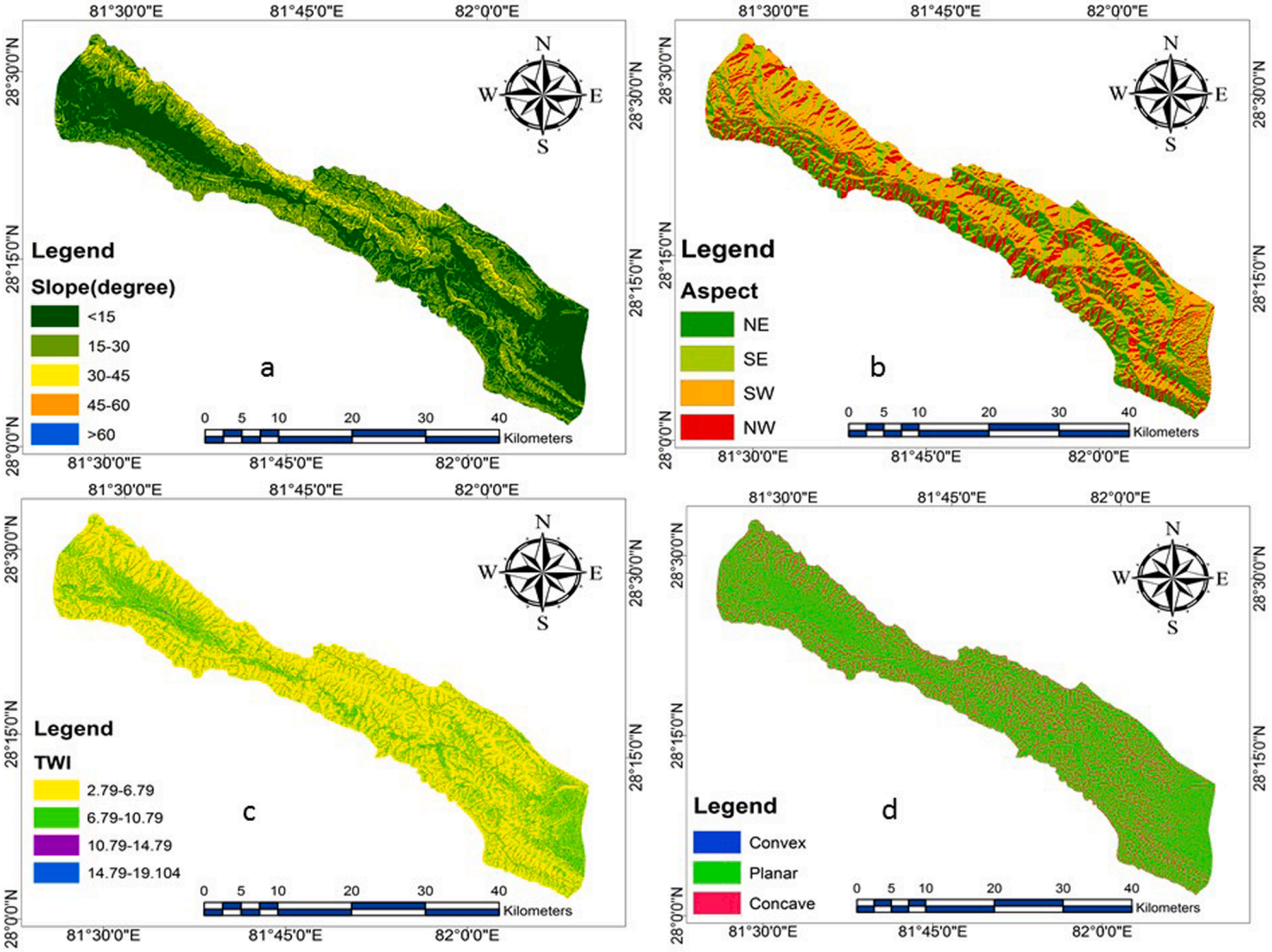


**Fig. 6.** The figure shows a) slope map b) Aspect map c) Topographical wetness index map d) Curvature map of the study area.

verify the inventory map. The focus group discussion was conducted with the Salghari women group and Gidde Khola conservation group. The members of both groups were called for discussion. The questions were asked and discussed between the members about the past and present situation of landslides in the study area. The historical landslides and their dynamism were discussed with the community people.

### 2.6. Geotechnical data

The selected geotechnical properties (specific gravity, moisture content, and soil composition and plasticity index) of 70 landslides were obtained from the laboratory analysis. The samples sites were selected based on spatial distribution and geological heterogeneity. The geological units are extended from east to west and the lithology of particular unit is same in the whole areas (Bhandari & Dhakal, 2020b). The average distance between each sampling locations is 2–3 km. These samples have represented all the geological units and topographical factors more or less equally. The sampling points were selected in such a way that the spatial distribution as well as geological and topographical heterogeneity could be proportionately covered. The ASTM D 854–00 – Standard test was performed to identify the specific gravity of each soil sample. The mathematical relationship of specific gravity is given in equation (1) (Lee et al., 1983; Das and Sobhan, 2013).

$$Gs = \frac{\gamma s}{\gamma w} \quad (1)$$

Where Gs is specific gravity, γs is the unit weight of soil, $\gamma_w$ is the unit weight of water.

The ASTM D4643-17 by microwave oven heating method was used to determine the moisture content of the soil samples. The Plastic Limit (PL) and liquid limit (LL) were determined by using The ASTM D4318 standard was adopted for the identification of the Plasticity index (PI). The percentage of sand, silt, and clay presence in the geological units were obtained. The composition and classification of soil were conducted based on the unified soil classification system (USCS) and ASTM-D2487 standard. The obtained percentage of sand, silt and clay was plotted in the ternary diagram for the soil classification (Fig. 7).

Soil composition, specific gravity, moisture content, and plasticity index data were published previously for compositional analysis and phase relationship of soils (Bhandari & Dhakal, 2020b). But these data are used here for further analysis with topography and geology. The previously published data are compared with different geological units and topographical units in this study.

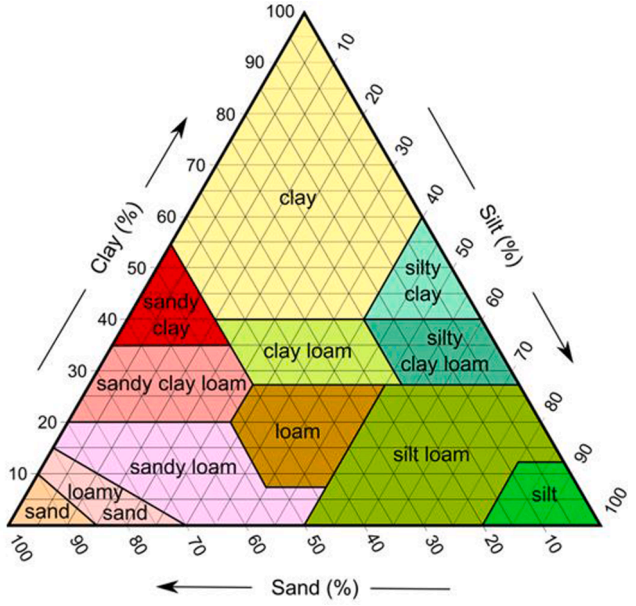


**Fig. 7.** Ternary diagram of silt, sand, and clay with soil types.

### 2.7. Data availability

Rainfall data from seven stations of the year 2010 to 2019 were obtained from the Department of Hydrology and Meteorology (DHM), Government of Nepal. The mean annual rainfall, maximum of 24 h rainfall, and total rainfall only in the Monsoon period were evaluated. The topographical factor maps considered for this study (slope, aspect, curvature, and topographical wetness index) were extracted from the Digital Elevation Model (DEM) obtained from the Alaska Satellite Facility of USGS.

### 2.8. Data analysis

Based on the field study and the past studies of landslides in different parts of Nepal Himalaya, mainly four landslide probable factors namely: geology (Bhandari & Dhakal, 2018; Tsou et al., 2018; Gerrard 1994; Hasegawa et al., 2009, Dahal et al 2008; Dhakal 2015) topography (Tsou et al., 2018; Zhang et al., 2016; Bhandari & Dhakal, 2019a), geotechnical (Yalcin, 2011; Yalcin 2011;Tofani et al., 2017; Bhandari & Dhakal, 2020b; Bicocchi et al., 2019), and hydrology (Dahal et al 2008a; Dahal et al 2008b; Zhang et al., 2016) were selected for the characterization of the landslides in this study. The lithological units and thrusts were taken for the geological attributes; slope, aspect, curvature, and topographical wetness index were taken for topographical attributes whereas rainfall data and drainage to distance is taken as the hydrological attributes. The specific gravity, dry density, wet density, plasticity index, and particle size analysis were taken as geotechnical attributes. The data obtained from the Q-GIS were analyzed statistically by using MS Excel and R (4.0.3) computing system. The $R^2$ value in 5% significance was obtained to identify the correlation between the two variables. The landslide distribution into the different geological units, slope classes, curvature, and aspects was analyzed. Similarly, geotechnical properties of soil of landslides were compared with geological factors. The relation between landslide numbers with geology, slope, aspect, curvature, and rainfall was analyzed.

## 3. Results

### 3.1. Geological characteristics

The geological distribution of landslides was obtained based on the stratigraphic unit. Landslide distribution in the geological units and

**Table 1**
Landslide distribution in different geological units and the thrust structures.

| Size of landslide | Number of landslides in different geological units | | |
|---|---|---|---|
| | Lower Siwalik | Middle Siwalik | Upper Siwalik |
| Very Small | 4 | 0 | 3 |
| Small | 116 | 118 | 67 |
| Medium | 201 | 398 | 121 |
| Large | 49 | 69 | 19 |
| very large | 0 | 4 | 0 |
| **Length (m)** Lower Siwalik | | Middle Siwalik | Upper Siwalik |
| <100 | 75 | 98 | 122 |
| 100–200 | 202 | 148 | 84 |
| 200–300 | 102 | 63 | 9 |
| 300–400 | 24 | 6 | 2 |
| 400–500 | 8 | 3 | 0 |
| >500 | 4 | 2 | 0 |
| **Thrust** | **Number of landslide in the Fault structure** | | |
| | Hanging wall | Foot wall | Fault plain |
| Babai Thrust | 272 | 77 | 96 |
| Bheri Thrust | 122 | 53 | 26 |
| Malai Thrust | 72 | 42 | 21 |

thrust structures is given in Table 1. The total area of landslides present in the Middle Siwalik is 4.67 km$^2$ whereas the area of the landslide in the Lower Siwalik is 0.88 km$^2$ (Fig. 8a).

The number of medium-sized (1000–10000 m$^2$) landslide is greater in every geological units. The total length of the landslides varied significantly in each stratigraphic units (Fig. 8b). Upper Siwalik consists of significantly large number of landslides with a length <100 m (Fig. 8c). The study area consists of four geological thrusts namely Babai thrust, Bheri thrust, Malai thrust, and Main boundary thrust. The number of landslides is significantly higher in the Babai thrust zone. The average area of landslide is also greater in the Babai thrust zone. The hanging wall has large number of landslide than foot wall (Fig. 8d). The maximum number of landslides is present within 1 km from the fault. The number of the landslides is higher around the fault zone in this area.

### 3.2. Topographical characteristics

The result shows that most of the landslides are distributed on the moderate to steep slope (15$^0$–45$^0$). The distribution of landslides is higher in the SW aspect and then in the SE aspect. Similarly, the landslides are significantly higher on the planar surface. The topographical wetness index (TWI) gives topographic control on hydrological processes. The index is a function of the slope and the upstream contributing area per unit width perpendicular to the flow direction. The landslides are significantly higher in the low topographical wetness index. The topographical distribution of landslides is shown in Table 2.

### 3.3. Hydrological characteristics

Rainfall is considered one of the major causes of the landslide in the Himalaya region. The maximum 24 h rainfall, rainfall in the monsoon period, total annual rainfall and total annual new landslides are shown in Table 3.The rainfall pattern in the monsoon period is shown in Fig. 9a. The maximum 24 h rainfall and total annual rainfall were compared with a total number of annual landslide during the period 2010–1019. There is less correlation ($R^2 = 0.52$) between a maximum 24 h rainfall and landslide occurrence (Fig. 9b). The total annual rainfall and number of landslides are highly correlated with adjusted $R^2 = 0.964$. In Fig. 9c, the total landslide and total annual rainfall have the same trend of distribution. Similarly, the rainfall that occurred only during the monsoon period (June-September) was calculated. The total landslides and rainfalls in the monsoon period are shown in Fig. 9d. The $R^2$ and adjusted $R^2$ value between the landslides and rainfall of only the monsoon period is 0.678 and 0.668 respectively.

The drainage to distance analysis was carried out by calculating the landslide pixel of drainage to distance from < 100 m to > 500 m. The landslides that occurred nearby the drainage signifies the effect of runoff for landslide initiation. The area of landslide and distance from drainage is shown in the Table 4. The drainage to distance map and landslides area distribution is shown in Fig. 10a & b. The landslides and distance to drainage showed significant relation. The distribution of landslides is greater at the near distance from drainage. The $R^2$ value is 0.68 at 1 degree of freedom and 4.1% significant level. The result showed that the number of landslides increases with decreasing distance from drainage.

### 3.4. Geotechnical characteristics

Geotechnical properties of 70 samples were obtained from Bhandari & Dhakal, (2020b) and analyzed here. The obtained values were compared with geological units, slope and aspect. The plasticity index was selected to compare the results with parameters of slope, geology and aspect. The plasticity index showed positive correlation with moisture content. Similarly, the plasticity index showed significant relation with other geotechnical properties of soil. So the plasticity index was selected to compare the result with selected factors. There is significant difference in mean of plasticity index in three geological units

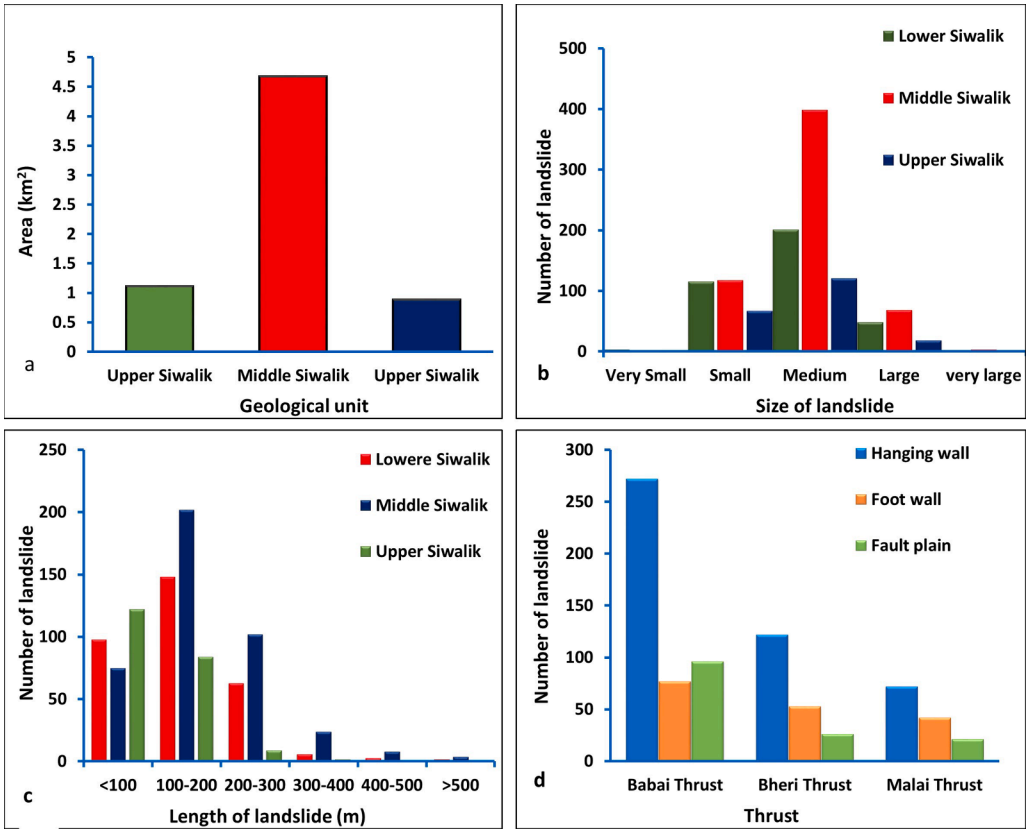


**Fig. 8.** Distribution of landslides in different geological formations a) Area distribution b) Size distribution c) Length distribution d) Thrust distribution.

**Table 2**
Landslide area distribution in various topographic factors.

| Slope angle ($^0$) | Area ($km^2$) | Aspect | Area ($km^2$) | Curvature | Area ($km^2$) | TWI | Area ($km^2$) |
|---|---|---|---|---|---|---|---|
| <15 | 0.8 | NE | 0.66 | Convex | 0 | 2.79–6.79 | 5.42 |
| 15–30 | 3.01 | SE | 2.23 | Planar | 4.32 | 6.70–10.79 | 1.15 |
| 30–45 | 2.41 | SW | 2.93 | Concave | 2.35 | 10.79–14.79 | 0.09 |
| >45 | 0.66 | NW | 0.84 | | | 14.79–19.10 | 0.0008 |

**Table 3**
The year-wise landslide distribution and rainfall pattern.

| Year | Maximum 24 h rainfall (mm) | Rainfall in monsoon Period (mm) | Total annual Rainfall (mm) | Total yearly Landslides (number) |
|---|---|---|---|---|
| 2010 | 112.5 | 892.4 | 1666 | 398 |
| 2011 | 124.4 | 1424.1 | 2089 | 556 |
| 2012 | 138.2 | 985 | 1700 | 422 |
| 2013 | 187.5 | 1957.7 | 2151 | 575 |
| 2014 | 215.6 | 1609.5 | 1978 | 464 |
| 2015 | 198.4 | 1481 | 1750 | 428 |
| 2016 | 212.3 | 1633.8 | 2270 | 600 |
| 2017 | 215.1 | 1841.41 | 2380 | 622 |
| 2018 | 220.7 | 1887.76 | 2416 | 698 |
| 2019 | 186.4 | 1914.8 | 2584 | 726 |

but the mean value is significantly greater in the Lower Siwalik than other geological units. Similarly, the average value of plasticity index is significantly greater in the steep slope (slope angle $30^0$-$45^0$). The soil type in the different landslide of different geological units according to gradation is shown in Table 5.

The loam soil is dominant in the Middle Siwalik whereas clay soil and clay loam is dominant in the Lower Siwalik and Upper Siwalik respectively. After gradation analysis, the amount of individual components was obtained. Typically, the soils of the Lower Siwalik and Upper Siwalik are clay rich whereas the soils of the Middle Siwalik are sand rich. But the proportion of clay/silt/sand in the Lower Siwalik is similar to the proportion of sand/silt/clay in the Middle Siwalik. In case of slope angle, the loam soil is dominant in the steep slope. The characteristics of soils in the slope are given in Table 6 and Table 7. The result shows that the loam, clay, and clay loam are common soil types in the study area. Similarly, the value of dry unit weight is significantly greater in Middle Siwalik and very steep slope ($>45^0$).

**Table 4**
Area distribution of landslides with respect to distance from drainage.

| Distance from drainage (m) | Area of landslide ($km^2$) |
|---|---|
| <100 | 2.15 |
| 100–200 | 1.76 |
| 200–300 | 1.1 |
| 300–400 | 0.96 |
| 400–500 | 0.42 |
| >500 | 0.37 |

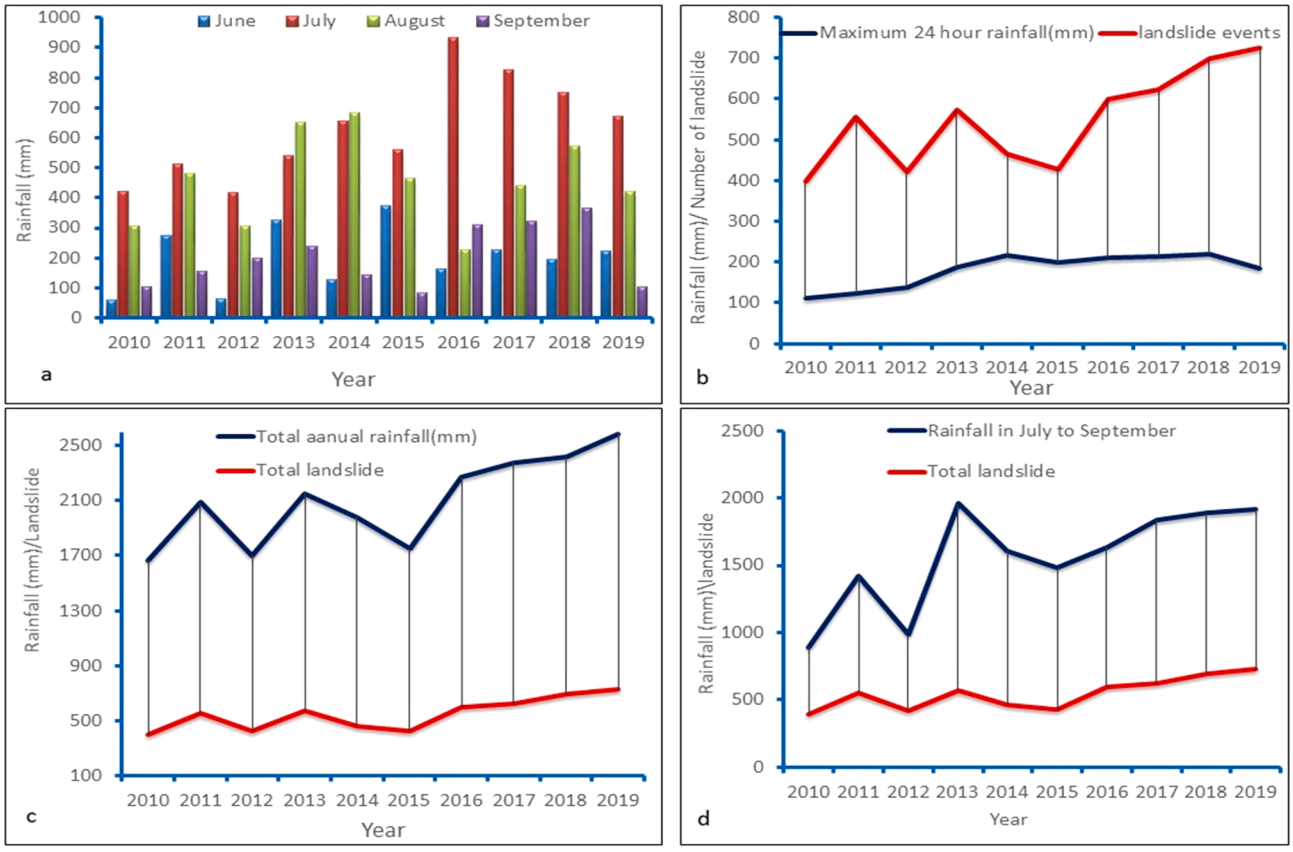


**Fig. 9.** a) Year wise rainfall distribution in the Monsoon period b) Maximum 24 h rainfall and landslide events c) Total annual rainfall and total new landslide d) Rainfall in the monsoon period and total new landslide events.

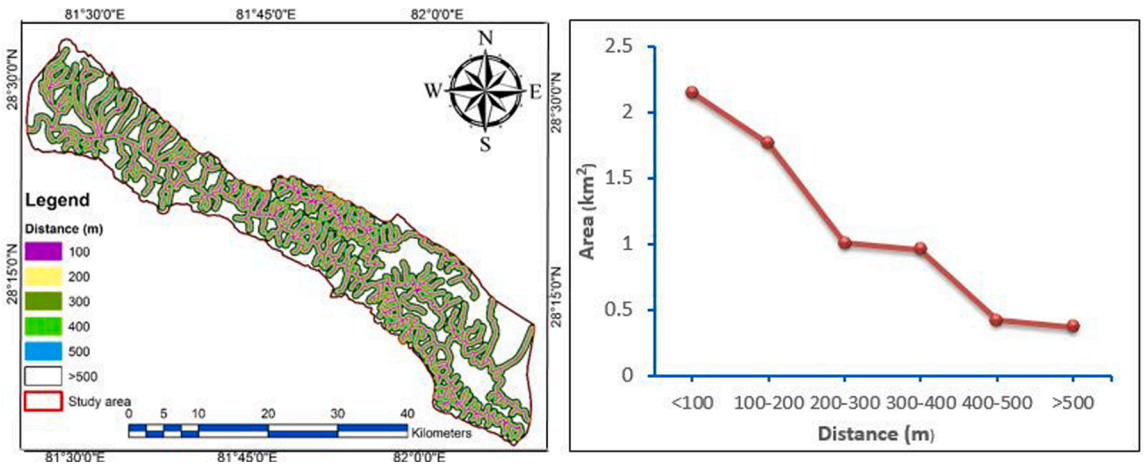


**Fig. 10.** a) Distance to drainage map b) Area of landslides with respect to distance to drainage.

**Table 5**
Distribution of geotechnical properties of soil with respect to different geological units.

| Properties | Geological units | | |
|---|---|---|---|
| | Lower Siwalik | Middle Siwalik | Upper Siwalik |
| **Geotechnical properties** | **Average value** | | |
| Plasticity index | 13.39 | 10.26 | 9.56 |
| Moisture content (%) | 1.56 | 1.47 | 1.52 |
| Specific gravity | 1.73 | 1.67 | 1.68 |
| Dry unit weight (kN/m$^3$) | 2.24 | 2.68 | 2.66 |
| **Composition** | **Average Percentage** | | |
| Sand % | 29.24 | 39.28 | 31.48 |
| Silt % | 35.25 | 33.19 | 31.56 |
| Clay % | 37.67 | 30.87 | 31.46 |
| **Soil types** | **Number of landslides** | | |
| Loam | 4 | 7 | 5 |
| Clay loam | 11 | 5 | 6 |
| Sandy clay | 5 | 8 | 4 |
| Silt loam | 6 | 4 | 5 |

**Table 6**
Average values and percentages of geotechnical properties of soils in the slopes.

| Properties | Slope Angle (degree) | | |
|---|---|---|---|
| | 15–30 | 30–45 | >45 |
| **Geotechnical properties** | **Average value** | | |
| Plasticity index | 13.36 | 12.16 | 8.56 |
| Moisture content (%) | 14.34 | 13.44 | 9.84 |
| Specific gravity | 1.67 | 1.64 | 1.62 |
| Dry unit weight (kN/m$^3$) | 2.46 | 2.63 | 2.65 |
| **Composition** | **Average percentage** | | |
| Sand % | 33.68 | 37.07 | 29.25 |
| Silt % | 36.32 | 31.52 | 32.16 |
| Clay % | 39.97 | 32.58 | 27.45 |
| **Soil types** | **Number of landslides** | | |
| Loam | 5 | 9 | 4 |
| Clay loam | 10 | 6 | 4 |
| Sandy clay | 6 | 5 | 4 |
| Silt loam | 6 | 5 | 7 |

The average value of moisture content is greater in the Lower Siwalik and the moderate slope. The average value of specific gravity of soils is significantly greater in the Lower Siwalik. The average moisture content of soils is slightly greater in the Lower Siwalik and on the moderate slope $(15^0 - 30)^0$. The moisture content of soil is significantly higher in the NW slope. But the plasticity index of soil is significantly greater in SE aspect. Similarly, the loam soil is common in SE aspect whereas clay loam is common in NW aspect.

**Table 7**
Average values and percentages of different geotechnical properties of soils with respect to slope aspect.

| Properties | Slope Aspect | | | |
|---|---|---|---|---|
| | NE | NW | SE | SW |
| **Geotechnical properties** | **Average value** | | | |
| Plasticity index | 10.36 | 9.16 | 14.56 | 11.1 |
| Moisture content (%) | 9.34 | 14.44 | 9.84 | 8.8 |
| Specific gravity | 1.67 | 1.64 | 1.62 | 1.58 |
| Dry unit weight (kN/m$^3$) | 2.48 | 2.64 | 2.62 | 2.42 |
| **Composition** | **Average percentage** | | | |
| Sand % | 32.18 | 34.21 | 27.2 | 29.55 |
| Silt % | 34.11 | 30.12 | 33.16 | 32.11 |
| Clay % | 23.13 | 27.18 | 25.25 | 28.68 |
| **Soil types** | **Number of landslides** | | | |
| Loam | 4 | 4 | 7 | 2 |
| Clay loam | 5 | 8 | 4 | 3 |
| Sandy clay | 4 | 5 | 4 | 2 |
| Silt loam | 4 | 5 | 6 | 3 |

## 4. Discussions

Various factors contribute to trigger the landslide. The major contributing factors to trigger landslides are geology, slope, aspect, structures, elevation, drainage, surface curvature but all the factors may not have an equal role in every region. The lithological study is very important for the study of the landslide (Bhandari & Dhakal, 2018; Yalcin, 2011). The mineralogical composition is considered as one of the major causes to make the slope unstable. The clay minerals formed by the rock weathering reduce the shear strength of rocks and causes landslide (Regmi et al., 2012b). Some mineral loses cohesion and friction after increasing moisture content. Weathering of rock of one layer from an alternate layer causes to disintegrate the remaining rock which causes rock slope failure (Bhandari & Dhakal, 2018). Regmi et al., 2012a studied the relationship between geology and rock weathering with slope instability of Muglin-Narayangad road section of Nepal and concluded that rock weathering is crucial factor for rock slope instability.

The area is a part of Siwalik as well as Lesser Himalayan zone. The rock weathering has various stages and each stages of rock weathering is susceptible for slope failure (Durgin, 1977). The weathering process of rock leads to reduce shear strength and ultimately causes surface slide (Miscevic & Vlastelica, 2014). In this study, landslide behaviors compiled with geological units. Among the three geological units, Middle Siwalik covers a large number and area of the landslide (Bhandari & Dhakal, 2018; Bhandari & Dhakal, 2020a,b). The data from 2010 to 2019 shows that both area and number of the landslide is greater in

Middle Siwalik however, the medium to large size landslides are dominant in all the formations (Bhandari & Dhakal, 2020a). The size distribution of landslide is similar in every formation. In general, the landslide occurrence trend is similar in all rock types as well as all geological units. Similarly, landslide having length 100 m to 200 m is dominant in Middle Siwalik. The landslides occurred in Middle Siwalik can travel in longer distances because the elevation of Middle Siwalik ranges between 800 m and 1300 m. The elevation difference of Middle Siwalik is ranges between 300 m and 500 m however the slope length varies from 432 m to 1400 m. Another important factor to trigger landslide in the study area is the presence of thrust. Due to active thrust, the rocks of the hanging wall are crumbled and fragile (Fig. 11a). The rocks are highly jointed (Fig. 11b) and tending to slide or fall. Most of the landslides are in the thrust zone mostly on the hanging wall (Bhandari & Dhakal, 2020a). Several new landslides occurred in the area in a decade indicate that the thrusts are active and the movement of thrusts is mainly responsible to trigger landslide. The uprooted trees are found on the landslide of Babai thrust and mostly the landslides are very common at the alternate bed of sandstone and mudstone on the thrust zone (Fig. 11c & 11d).

The flexural toppling and wedge failure is very common on the hanging wall of the Babai thrust. The rocks are highly jointed and highly fractured. The pole concentration of joints is plotted using freely available Dips8 software designed by Rockscience for the analysis of features related to the engineering analysis of rock structures. It is shown in Fig. 12, and it reveals that the joints are highly intersected and concentrated in the critical zone. The main cause of large size landslide in Middle Siwalik is found as the effects of active Babai thrust (Bhandari & Dhakal, 2020a). The slope is another major factor for landslide occurrence in this area. The maximum numbers of landslides are found in the moderate slope. The stratigraphy of the Siwalik zone is not homogeneous. The alternate beds of thickly bedded sandstone and thinly bedded weak mudstone are dominant in the Middle Siwalik. The weathering and erosion of mudstone causes the sandstone weak and fragile; and sandstone beds loose support of thin mudstone layers causing landslides (Bhandaari & Dhakal, 2018). Similarly, the weak and concretion structured mudstone of Lower Siwalik is crumble and easily erodible due to which small and shallow landslides are very common in the Lower Siwalik even in the moderate slope. Moreover, the surface of moderate slope is dominant in the Lower Siwalik and Upper Siwalik (Table 8). When landslides and curvature are taken into consideration, it is found that the area of landslides is higher on the planar slopes. The landslides of Middle Siwaliks were noticed on the planar slope and higher numbers of landslides were noticed in Middle Siwalik. Mostly, the Landslides in Lower and Upper Siwaliks are significantly high on the concave slope. The runoff activity increases on the concave slope during rainy season, due to that the erosive and sliding mechanism increases in the concave slope. The low value of the topographical wetness index (TWI) is correlated with the number of landslides. The landslides area decreased with increasing TWI. It indicated that, initiating the drainage or stream in the upslope causes the landslide on the slope.

The landslides are rich in the southern aspect. Most of the articles related to landslides show that the southern aspect has a good correlation with landslide occurrence. >60% area of Middle Siwalik, 54% area of Lower Siwalik and 37% of Upper Siwalik lies in the southern aspect. 68% of landslides are encountered in the southern aspect. The rainfall data revealed that rainfall frequency and magnitude is higher in the Southern aspect. The rainfall amount cannot separate formation wise because the formations are distributed parallels and rainfall pattern is the same in every formation. The result shows that there is no good correlation between maximum 24 h of rainfall and landslide occurrence but total annual rainfall has a good correlation with landslide occurrence. The result shows that the long term and continuous rainfall is required for landslide initiation in the study area. Most of the landslides are initiated in the August and September. After consulting with the local people, it is found that August and September have a typical


**Fig. 11.** a) Fragile and broken rocks of Middle Siwalik (hanging wall of Babai thrust) b) Plain failure on the highly jointed rocks of thrust zone c) Uprooted tree on the landslide of hanging wall d) Landslide occurred on the alternate bed of sandstone and mudstone.

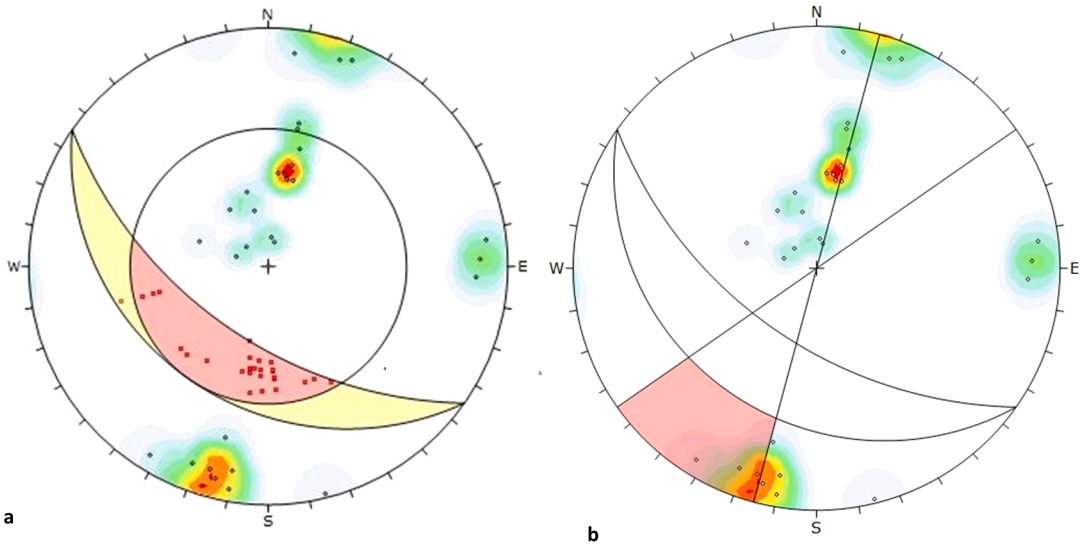


**Fig. 12.** Lower hemispheric plot of the poles of the discontinuity planes.

**Table 8**
Relation of slope angle and landslide area in different geological formations.

| Slope angle (degree) | Total area of landslide ($km^2$) | | |
|---|---|---|---|
| | Lower Siwalik | Middle Siwalik | Upper Siwalik |
| <15 | 0.38 | 0.13 | 0.29 |
| 15–30 | 1.89 | 0.28 | 0.84 |
| 30–45 | 0.14 | 1.96 | 0.31 |
| >45 | 0.09 | 0.21 | 0.06 |

weather period with very sunny in the day and heavy rainfall in the night. Due to the continuous variation of changing temperature, the large scale landslide might have occurred in the area. The area of the planar slope is dominant in every geological unit. The area of both planar and concave slope is dominant in the Middle Siwalik.

The soil of landslides in the Middle Siwalik is sand rich whereas the soil of the Lower and Upper Siwalik is clay-rich. The average clay amount is higher in the soil of the Lower Siwalik than in the Upper and Middle Siwalik. The amount of clay is less but the amount of silt and sand is greater in the Middle Siwalik. The value of wet density of the soil of the Lower Siwalik is comparatively greater than that of the Middle and Upper Siwalik. It is due to the presence of a higher amount of clay and silt. The mechanism caused high pore pressure and the landslides are triggered (Yang et al. 2007; Jadda et al. 2009; Wati et al. 2010; Yalcin 2011; Mugagga et al.2011). In the wet state, the clay loses cohesion and internal friction that causes erosion and landslide. The average value of plasticity index and moisture content is comparatively greater in the Lower Siwalik. The result shows that plasticity index is greater than moisture content in the soil. The main cause of having high plasticity index in the soil is the presence of higher amount of clay and silt fraction. Bhandari and Dhakal (2020b) investigated the higher silt/clay fraction in the soil of study area. The average value of plasticity index is greater in the moderate slope. In the Middle Siwalik, the steep slope, SE aspect, clay/silt rich soil with average plasticity index are the critical factors for landslide.

## 5. Conclusions

The multidisciplinary technique was carried out for landslide characterization in the Siwalik of the Babai River catchment. The topographical, hydrological, geological, and geotechnical information were adopted in the multidisciplinary approach. The landslide size distribution in each geological unit is similar. The slope angle, aspect and the topographical wetness index were taken as topographical factors whereas lithological unit (geological formation) and fault area were taken as geological factors. The geotechnical properties including specific gravity, moisture content, and soil composition and plasticity index of soil from different lithological units were determined and analyzed. The hydrological factors comprising of maximum 24 h rainfall, rainfall in the monsoon period and total annual rainfall in the study area were analyzed with the landslide process.

The result indicates that the moderate to steep slope, alternate beds of sandstone and mudstone along with the southern aspect, characterized by loamy soil consists of a higher number of landslides. The total annual new landslides are highly significant with the total rainfall in the monsoon period and the total annual rainfall. The maximum 24 hours rainfall shows less significance with the landslide. Near distance from drainage is highly sensitive for landslide. It is found that the Lower Siwalik is clay rich and clay loom soil is dominant due to which landslide initiation rate is higher during monsoon period. Generally, the combination of the conditioning factors comprising of Lower Siwalik zone, higher plasticity index, higher moisture content, moderate slope, long term rainfall and clay loom soil are highly significant with the landslide process. The overall result shows that a multidisciplinary approach provides better option for landslide characterization providing detailed information that are necessary to understand the landslide process and manage them properly.

## CRediT authorship contribution statement

**Bharat Prasad Bhandari:** Investigation, Writing - original draft. **Subodh Dhakal:** Conceptualization, Methodology, Supervision.

## Declaration of Competing Interest

The authors declare that they have no known competing financial interests or personal relationships that could have appeared to influence the work reported in this paper.

## Acknowledgments

Our sincere thanks go to the Nepal Army of Bardia National Park as well as local people of Babai valley for their support during field study.

## References


Auden, J.B., 1935. Traverses in the Himalaya. Geological Survey of India 69, 123–167.

Ausilio, E., Zimmaro, P., 2017. Landslide characterization using a multidisciplinary approach. Measurement 104, 294–301.

Bhandari, B.P., Dhakal, S., 2020a. Spatio temporal dynamics of landslide in the sedimentary terrain: A case of Siwalik zone of Babai watershed. Nepal. SN Applied Sciences 2, 854. https://doi.org/10.1007/s42452-020-2628-0.

Bhandari, B.P., Dhakal, S., 2020b. Compositional analysis and phase relationship of soil mass from the active landslides of Babai River watershed, Siwalik zone of Nepal. Eng. Geol. 278, 105851 https://doi.org/10.1016/j.enggeo.2020.105851.

Bhandari, B.P., Dhakal, S., 2019a. Topographical and geological factors on gully-type debris flow in Malai River catchment, Siwaliks, Nepal, Journal of Nepal Geological Society, 2019, vol. 59, pp. 89–94.

Bhandari, B.P., Dhakal, S., 2019. Evolutional Characteristics of Debris Flow in the Siwalik Hills of Nepal. International Journal of Geosciences 10 (1049), 1067. https://doi.org/10.4236/ijg.2019.101206.

Bhandari, B.P., Dhakal, S., 2018. Lithological Control on Landslide in the Babai Khola Watershed, Siwaliks Zone of Nepal. American Journal of Earth Sciences. 5 (3), 54–64.

Bicocchi, G., Tofani, V., D'Ambrosio, M., et al., 2019. Geotechnical and Hydrological characterization of hillslope deposits for regional landslide prediction modeling. Bulletin of Engineering Geology and Environment 78, 4875–4891.

Borga, M., Fontana, D.G., Cazorzi, F., 2002. Analysis of topographic and climatic control on rainfall triggered shallow landslide using a quassi-dynamics wetness index. J. Hydrol. 268, 56–71.

Chaudhari, R.S., 1982. Petrology of the Siwalik Group of Nepal Himalaya. Recent Researches in Himalaya 8, 424–466.

Ching, H., Chih-Hsuan, L., Chia-Ming, C., 2018. Numerical investigation of rainfall induced landslide in mudstone using coupled finite and discrete element analysis. Geofluids 2018, 1–15. https://doi.org/10.1155/2018/9192019.

Dahal, R.K., Hasegawa, S., Nonomura, A., Yamanaka, M., Dhakal, S., Paudyal, P., 2008. Predictive modeling of rainfall-induced landslide hazard in the Lesser Himalaya of Nepal based on weights-of evidence. Geomorphology 102, 496–510.

Dahal, R.K., Hasegawa, S., 2008. Representative rainfall thresholds for landslides in the Nepal Himalaya. Geomorphology 100 (3–4), 429–443. https://doi.org/10.1016/j.geomorph.2008.01.014.

Devkota, K.C., Regmi, A.D., Pourghasemi, H.R., et al., 2013. Landslide susceptibility mapping using certainty factor, index of entropy and logistic regression models in GIS and their comparison at Mugling–Narayanghat road section in Nepal Himalaya. Nat Hazards 65, 135–165 (2013). https://doi.org/10.1007/s11069-012-0347-6.

Das, B.M., Sobhan, K., 2013. Principles of geotechnical engineering. Cengage learning, 7th edition:51–72.

Dhakal, S., 2015. Evolution of Geomorphologic Hazards in Hindu Kush Himalaya, In: Shaw, R. & Nibanupudi, H.K (Eds.), Mountain Hazards and Disaster Risk Reduction (pp. 53-72), Springer Japan, DOI: 10.1007/978-4-431-55242-0_4.

Durgin, P.B., 1977. Landslides and the weathering of granitic rocks, Landslides, Geological Society of America. Reviews in Engineering Geology 3, 127–131.

Fernandes, N.F., Guimaraes, R.F., Gomes, R.A.T., et al., 2004. Topographical controls of landslides in Reo de Janeiro: field evidence and modeling. CATENA 55, 163–181.

Gadtaula, A., Dhakal, S., 2019. Landslide susceptibility mapping using Weight of Evidence Method in Haku. Rasuwa District, Nepal, Journal of Nepal Geological Society 58, 163–172. https://doi.org/10.3126/jngs.v58i0.24601.

Gerrard, J., 1994. The landslide hazard in the Himalayas: geological control and human action. Geomorphology and Natural Hazards 221–230. https://doi.org/10.1016/B978-0-444-82012-9.50019-0.

Guzzetti, F., Mondini, A.C., Cardinali, M., Fiorucci, F., Santangelo, M., Chang, K.T., 2012. Landslide inventory maps: New tools for an old problem. Earth Sci. Rev. 112, 42–66. https://doi.org/10.1016/j.earscirev.2012.02.001.

Hagen, T., 1969. Report on the geological survey on Nepal. Denschr. Schweiz. Naturf. Gesell 86, 1–185.

Hasegawa, S., Dahal, R.K., Yamanaka, M. et al., 2009. Causes of large-scale landslides in the Lesser Himalaya of central Nepal. Environmental Geology 57, 1423–1434 (2009). https://doi.org/10.1007/s00254-008-1420-z.

Hennrich, K., Crozier, M.J., 2004. A hillslope hydrology approach for catchment-scale slope stability analysis. Earth Surfaces Process Landforms 29, 599–610.

Hakro, M.R., Harahap, I.S.H., 2015. Laboratory experiments on rainfall-induced flowslide from pore pressure and moisture content measurements. Nat. Hazards Earth Syst. Sci. Discuss. 3, 1575–1613. https://doi.org/10.5194/nhessd-3-1575-2015.

Jadda, M., Shafri, H.Z., Mansor, S., Sharifikia, M., 2009. Landslide susceptibility evaluation and factor effect analysis using probabilistic–frequency ratio model. Eur J Sci Res 33, 654–668.

Kayastha, P., Dhital, M.R., Smedt, F. De., 2013. Application of the Analytical hierarchy process (AHP) for landslide susceptibility mapping: A case study from the Tinau watershed, west Nepal. Computer and Geosciences 52, 398–408. https://doi.org/10.1016/j.cageo.2012.11.003.

Lee, I.K., White, W., Ingles, O.G., 1983. Soil formation, Classification and Exploration. In: In. Principal of Geotechnical engineering. Pitman Publishing Inc., pp. 1–56

Mišćević, P., Vlastelica, G., 2014. Impact of weathering on slope stability in soft rock mass. J. Rock Mech. Geotech. Eng. 6, 240–250. https://doi.org/10.1016/j.jrmge.2014.03.006.

Mugagga, F., Kakembo, V., Buyinza, M., 2011. A characterization of the physical properties of soil and the implications for landslide occurrence on the slopes of Mount Elgon. Eastern Uganda, Natural hazard, p. 52.

Nepal Disaster Report 2019. Ministry of Home Affairs, Government of Nepal.

Regmi, A.D., Devkota, K.C., Yoshida, K., et al., 2014. Application of frequency ratio, statistical index, and weights-of-evidence models and their comparison in landslide susceptibility mapping in Central Nepal Himalaya. Arab J Geosci 7, 725–742. https://doi.org/10.1007/s12517-012-0807-z.

Regmi, A.D., Yoshida, K., Dhital, M.R., Devkota, K., 2012a. Effect of rock weathering, clay mineralogy and geological structures in the formation of large landslide, a case study from Dumre Besei landslide, Lesser Himalaya Nepal. Landslides 10, 1–13. https://doi.org/10.1007/s10346-011-0311-7.

Regmi, A.D., Yoshida, K., Nagata, H., Pradhan, A.M.S., Pradhan, B., Pourghasemi, H.R., 2012b. The relationship between geology and rock weathering on the rock instability along Mugling-Narayanghat road corridor, Central Nepal Himalaya. Nat. Hazards 66, 501–532. https://doi.org/10.1007/s11069-012-0497-6.

Thapa, D., Bhandari, B., 2019. GIS-Based Frequency Ratio Method for Identification of Potential Landslide Susceptible Area in the Siwalik Zone of Chatara-Barahakshetra Section. Nepal. Open Journal of Geology 9, 873–896. https://doi.org/10.4236/ojg.2019.912096.

Talebi, A., Uijlenhoet, R., Troch, P.A., 2008. A low-dimensional physically based model of hydrologic control of shallow landsliding on complex hillslopes. Earth Surf. Process Landforms 33, 1964–1976.

Tofani, V., Bicocchi, G., et al., 2017. Soil characterization for shallow landslides modeling: a case study in the Northern Appennines (Central Italy). Landslides 14, 755–770. https://doi.org/10.1007/s10346-017-0809-8.

Tohari, A., Nishigaki, M., Komatsu, M., 2007. Laboratory Rainfall-Induced Slope Failure with Moisture Content Measurement. J. Geotech. Geoenviron. Engineering 133 (5), 575.

Tsou, C.Y., Chigira, M., Higaki, D., et al., 2018. Topographic and geologic controls on landslides induced by the 2015 Gorkha earthquake and its aftershocks: an example from the Trishuli Valley, central Nepal. Landslides 15, 953–965. https://doi.org/10.1007/s10346-017-0913-9.

Varnes, D.J., 1978. Slope movement types and processes. In: Schuster, R.L., Krizek, R.J. (Eds.), Landslides, analysis and control, special report 176: Transportation research board. National Academy of Sciences, Washington, DC, pp. 11–33.

Wati, S.E., Hastuti, T., Wijojo, S., Pinem, F., 2010. Landslide susceptibility mapping with heuristic approach in mountainous area. A case study in Tawangmangu sub District, Central Java, Indonesia. Int Arch Photo RS Spat. Inf Sci 38 (8), 248–253.

Weidinger, J.T., 1998. Case history and hazard analysis of two lake-damming landslides in the Himalayas. J. Asian Earth Sci. 16, 323–331.

Yalcin, A., 2011. A geotechnical study on landslides in the Trabon Province, NE Turkey. Appl. Clay Sci. 52, 11–19.

Yang, H., Adler, R., Huffman, G., 2007. Use of satellite remote sensing in the mapping of global landslide susceptibility. Nat Hazards. 43 (2), 245–256. https://doi.org/10.1007/s11069-006-9104-z.

Yu, B., Chen, F., 2017. A new technique for landslide mapping from a large-scale remote sensed image: A case study of Central Nepal. Comput. Geosci. 100, 115–124. https://doi.org/10.1016/j.cageo.2016.12.007.

Yu, B., Chen, F., Xu, C., 2020. Landslide detection based on contour-based deep learning framework in case of national scale of Nepal in 2015. Comput. Geosci. 135, 104388.

Zhang, F., Chen, W., Liu, G., et al., 2012. Relationship between landslide types and topographic attributes in a loess catchment. China. Journal of Mountain Science. 9, 742–751. https://doi.org/10.1007/s11629-012-2377-7.

Zhang, Jq, Liu, Rk, Deng, W., et al., 2016. Characteristics of landslide in Koshi River Basin. Central Himalaya. Journal of Mountain science. 13, 1711–1722. https://doi.org/10.1007/s11629-016-4017-0.

Research Article

# Spatio-temporal dynamics of landslides in the sedimentary terrain: a case of Siwalik zone of Babai watershed, Nepal

**Bharat Prasad Bhandari**[1] · **Subodh Dhakal**[2]

Received: 21 January 2020 / Accepted: 30 March 2020 / Published online: 8 April 2020


**Abstract**
Topographical, geological and hydrological attributes of mountainous region play significant role for landslide occurrence. In this study, the spatial and temporal behaviors of landslides in the Siwalik zone of Babai watershed are evaluated on the basis of topographical, geological and hydrological attributes. For this work, polygon based landslide spatial inventory and spatio-temporal inventory from the years 2010 to 2019 were prepared by using Santeniel-2, USGS and temporal series of Google earth images. Further analysis of landslides including the numbers, area and other geometrical parameters were carried out using Q-GIS. The geological map prepared by the Department of Mines and Geology of Nepal government was referred and validated from the field. The precipitation data was obtained from department of hydrology and meteorology, Government of Nepal. The state of activity of landslides was evaluated in different geological formations in temporal basis. The result shows that the landslides in study area are highly dynamic in nature showing reactivation, expansion and even self stabilization in some parts. The new and active landslides are identified every year in every geological formation since a decade. It is also found that the hanging wall of the thrust zone is more sensitive for the distribution of medium to large scale landslides. The total annual rainfall shows positive correlation with the landslide frequency. The study will be useful for the researchers and policy makers to understand landslide mechanics and to manage the safe settlements in the area.

**Keywords** Landslides · Spatio-temporal dynamics · Siwalik · State of activity

## 1 Introduction

Landslide is common geological hazard in the mountainous terrain like Nepal that causes long term threat to the people and properties. Lying on the convergent plate boundary between Tibetan plate and Indian plate, the Nepalese Mountain is considered as an active Mountain of the world and the geological structures are very common in the Nepalese hills. Topographical and hydrological attributes of mountainous region play significant role for landslide occurrence in the hills of Nepal [2]. Many people loose their life and property every year due to landslide mostly in the monsoon period which is the great challenges in the entire Nepalese Himalaya.

Spatial and temporal dynamics of landslide give causes and evolution mechanism of landslide. The temporal study helps to understand the series of landslide initiation and development. For the spatial and temporal study, landslide inventory is essential. The number and area of landslide can be obtained from systematic and accurate landslide inventory map [18, 30].

The adverse topography, dynamic geomorphology, weak geology and presence of geological structures are the contributing factors for landslide occurrence in the Nepal Himalaya [16, 17]. TU-CDES [38] studied about the

✉ Subodh Dhakal, subodhdhakal@geology.edu.np | [1]Central Department of Environmental Science, Tribhuvan University, Kirtipur, Nepal. [2]Department of Geology, Tri-Chandra Multiple Campus, Kathmandu, Nepal.

characterization of landslide of Siwaliks zone and prepared landslide susceptibility map. The research concluded that the major causes of landslide in Siwaliks zone is toe cutting of hillslopes, heavy soil erosion and geological composition. Bhandari and Dhakal [4] studied the landside of Babai River catchment of Siwaliks and reported that lithostratigraphy is the main cause for landslide occurrence in Siwaliks region of Nepal. Lithologically, the rocks may be strong but stratigraphy may adverse and cause the landslide. Most of the landslides of Siwalik zone are originated on the steep slope convert in to the debris flow and deposit huge amount of sediment in to the river channel [3]. Dahal et al. [13] studied the landslides of Eastern Siwaliks region and prepared the landslide hazard map in catchment scale. They concluded that the slopes of Siwaliks zone are prone to landslide during intense rainfall due to rugged and fragile topography. To reduce the future risk and to cope with them, the evolution mechanism of landslide should be identified. The landslide characters should be identified on spatial and temporal basis to judge the landslide dynamics.

The landslide evolution and dynamic has been studied by several researchers in the past globally. Carrara et al. [6], Crozier [11], Guzzetti et al. [21] discussed about the role of intrinsic (lithology, elevation and soil thickness) and extrinsic factors (extreme rainfall, earthquake and human interference) for landslide occurrence. Iverson [25], Msilimba and Holmes [28], Wang et al. [40], Sassa et al. [35], Guzzetti et al. [21] studied about the role of discontinuity, slope materials, rock weathering, nature of soil for landslide occurrence. Geomorphological characterization of landslide is important task for the study of landslide evolution.

The characteristics of rainfall induced landslide are controlled by rainfall pattern as well as geological and geomorphological conditions. According to Chen et al. [8], the rainfall induced landslide tended to occur on dip slope rather than windward slope and concluded that geological settings were a more effective control of the mass wasting processes on hill slope scale than the rainfall condition. Chigira et al. [9] studied the geological and geomorphological characters of rain and earthquake induced landslide of Japan. According to Chigira et al. [9], the response shown by different geological materials are different with rain and ground shaking. Triggering of landslide is majorly controlled by a stability or safety criterion, which depends on material strength loss [26], precipitation [13, 21, 25] through pore pressure and water table height. According to Densmore et al. [14], the landslides are supposed to occur along the steep slope. The threshold slope angle for sliding may be dependent on climate or on lithology [19, 24].

Despite so many studies globally, landslide dynamics and evolution process are still lacking in the important geological zone of Nepal Himalaya. In this context, the main objective of this study is to identify the decadal evolution process and dynamic behaviors of landslide in catchment scale at the Siwaliks zone of Nepal. The study will be useful for the policy makers and different stake holders of Siwalik region to understand landslide and to manage the safe settlement in the days to come.

## 2 Materials and methods

### 2.1 Study area

The study area lies in the Babai River catchment, Mid-western Nepal which is extended into the three districts of Mid-Western Development region namely Dang, Salyan and Bardiya. The Babai River is east–west trending river originated from Siwalik hill and located between 27°57′59.03″ N, 82°33′42.80″ E at east, 28°28′30.14″ N, 81°28′30.14″ E at west, 28°12′47.90″N, 82°15′46.08″ at north and 28°01′03.89″ N, 82°12′39.61″ E at south. Total area covered by whole watershed of Babai River is 1952 km$^2$ and perimeter is 316.640 km but the study area covered only 1157 km$^2$ (Fig. 1). The Babai catchment is characterized by various landscapes, from upper Dang valley to lower Babai valley with several ridges extended up to 1500 m from mean sea level. The large flat Dang valley is extruded for the study because the flat land is considered as landslide free area. The Siwaliks in the study area have altitudes ranging from 109 to 1500 m and exhibits a very rugged topography with highly dissected gullies and steep slopes.

Most of the hill ridges in the study area extend in the east–west direction, parallel to the main geological structures. The landforms of the study area are mainly controlled by the tectonic processes and subordinately by mass wasting and weathering. The erosional landforms predominate over the depositional ones. There are rugged hills, numerous deep gorges, steep slopes, cliffs, and active gullies representing the erosional landforms, whereas river terraces, alluvial fans, and talus cones are the examples of depositional landforms. Drainage density is higher toward North-East and lower towards South-West. As a whole, the climate of study area is sub tropical. The winter is very cold (0° to – 3 °C) and summer is very hot (40° to 45°). The rainfall is heavy and occasionally intense during rainy season. The average annual rainfall over the period 1990–2017 AD is in the range of 1800–3300 mm. More than 80% of rainfall occurs in rainy season.

### 2.2 Geological setting

The geological setting of the area is similar to the overall Siwalik region. The area lies between two major thrusts

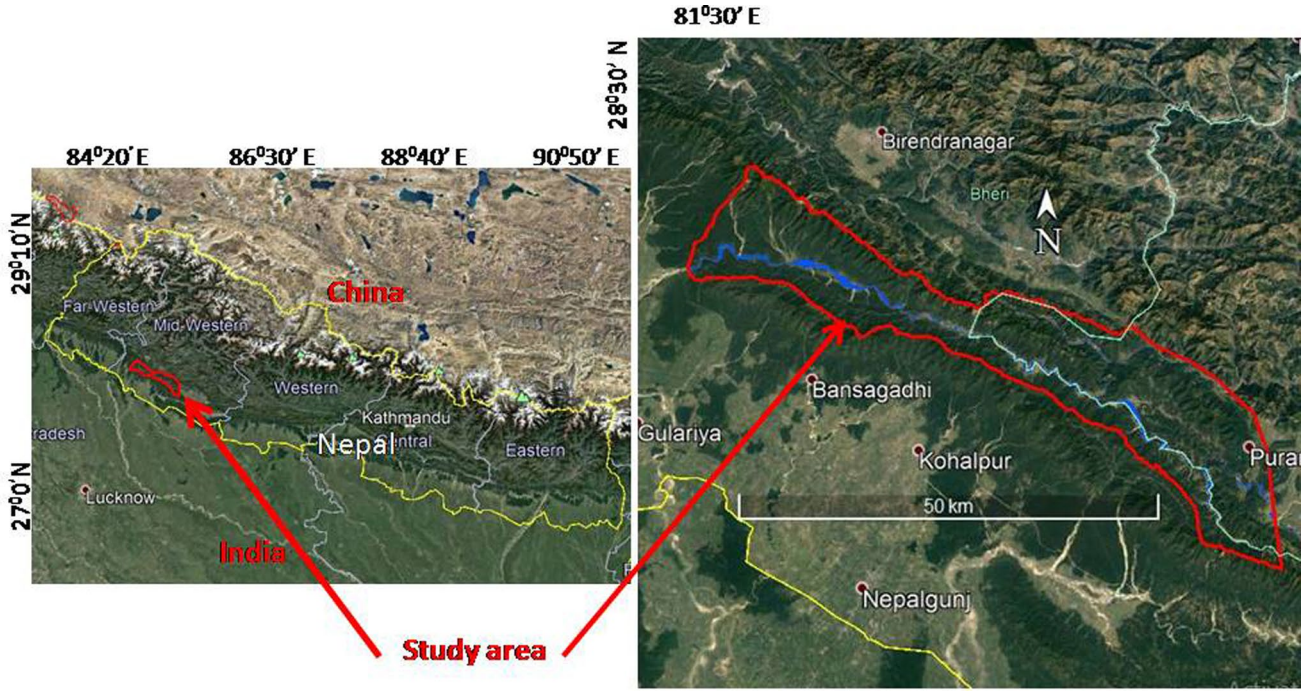


**Fig. 1** Location map of study area. *Source* Google Earth

namely Himalayan Frontal Thrust (MFT) and Main Boundary Thrust (MBT) that is bounded by Indogangetic plain in the south and the Lesser Himalayan rocks in the north. The bed rock geology of study area is dominated by younger (Neogene) sedimentary rocks. The study area has three major thrust and one minor thrust [3, 4]. Main Boundary Thrust, Babai Back Thrust and Bheri Thrust are major thrust where as Malai Thrust is one minor thrust. All the Thrust are E-W trending and north dipping (Fig. 2).

The sedimentary rocks of the study area divided in three geological formations [1, 3, 4, 7, 23]. From bottom to top they are Lower Siwaliks, Middle Siwaliks and Upper Siwaliks, respectively. The Lower Siwalik consists of interbedding of fine to very fine grained grey-green sandstone and red–purple, brown mudstone. Mudstone bed is medium to thick, highly fractured and highly weathered. Sandstone bed is of thinly bedded and spheroidically weathered [4]. Thin layer of sandstone lies between thick layers of mudstone in the overall Lower Siwalik zone. The characteristics feature of Middle Siwaliks is of medium to coarse grained thickly bedded salt and pepper as well as pebbly sandstone and variegated mudstone. Sandstone beds are massive, less compact and weathered due to poor intergranular bonding [3, 4]. The sandstone of Middle Siwaliks consists of minerals like quartz, feldspar, muscovite and biotite. The bed of sandstone is thicker than mudstone. The thickness of sandstone bed varies from 0.3 to 3.4 m whereas thickness of mudstone bed varies from 7 to 92 cm [3, 4].

Upper Siwaliks consists of cobble and pebble bearing conglomerate interbedding with yellow to brown mudstone. The cementing material of conglomerate is calcite and mostly clay. The size of clast in conglomerate varies from 5 to 100 mm. Most of the flat lying area is covered by superficial quaternary deposits.

The colluviums of hilly terrain include debris-flow and other slope debris deposits and landslide deposit mostly of late-quaternary period [3]. Colluviums occur as relatively thick deposits filling drainage courses. However, there are deposits which are considerably thinner and of greater areal extent on some hill slopes in the study area. The colluviums derived from erosion and landslide typically consists of sub angular cobbles and boulders of sandstone and mudstone with some conglomeratic fragments. Huge amount of alluvial deposits occur in river terrace and valley fill.

## 2.3 Methods

The remote sensing data and satellite images are essential to identify the landslide evolution process but field investigation is very important to understand the mechanism of land sliding. Morphological analysis is another important factor for the landslide study. Varnes [39], Guzzetti et al.

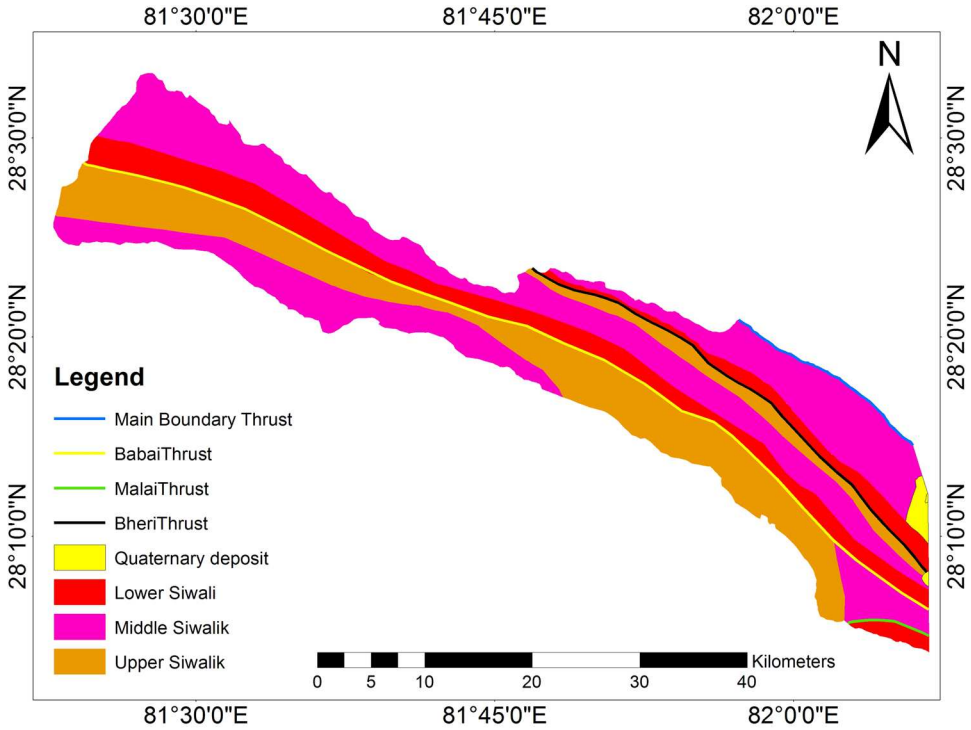


**Fig. 2** Stratigraphical map of study area. *Source* Bhandari and Dhakal [3]

[22], Bucci et al. [5] proposed several geomorphological characters to identify landslide probable area. By the study of surficial process such as rock weathering, soil erosion, deposition and status of vegetation, the morphological features of old landslide can be identified. For the early stage of landslide investigation, various factors such as aerial photography, remote sensing images and mostly field observation are considered the necessary task [33, 34]. For the study of landslide mechanism, the land surface condition before and after the land sliding are identified. Detail methodology is described in the following section.

## 2.4 Landslide inventory

The polygon based landslide inventory of study area was prepared on spatial and temporal basis by using 12.5 m resolution satellite images and 952 landslides were identified in images (Fig. 3). The temporal inventory of landslide from 2010 to 2019 AD (Fig. 4) was prepared on the basis of state of activity (Fig. 5), slope (Fig. 6) and size by using USGS images, Santeniel-2 and time series data of Google earth of resolution 12.5 m. The acquisition dates of imagery used to map landslides ranged from August to December and April to Jun of each year from 2010 to 2019 AD. Some imagery as badly affected by cloud but the multiple set of imagery from different dates helped to avoid the problems. Some area badly disturbed due to cloud and steep terrain has been excluded for analysis but has been included in map after field verification. The scar to toe area of each landslide was identified in the image. The landslides were recognized by the color variation and topographical differences. We were able to identify the scar area and deposit area of landslide due to that the polygon based landslide inventory was possible. The landslide boundaries in the satellite images were identified based on attributes such as headwall scarps, chutes representing material movement pathways, and lobes of transferred materials [20]. The prepared inventory map was updated by using topographical map of 1:25,000, geological map [3] and Digital Elevation Model (DEM) of 12.5 m resolution. The slope and elevation maps were obtained from DEM. The perimeter, length and area of landslides were obtained on temporal basis by using polygon in images. The polygons were obtained in a GIS framework to analyzed topographical, hydrological and geological factors.

## 2.5 Field study

All the mapped landslides using remote sensing techniques were verified in the field by visual observation in the landslide site. Among 952 landslides, 100 landslides were selected randomly for field study. The landslide having area greater than 100 $m^2$ were taken for detailed field study. The length of landslide, slip surfaces, tow length, distance travelled by slide materials, slope, aspect and elevation of 100 landslides were measured manually. The area and length of landslide measured in the polygon were compared to each other.

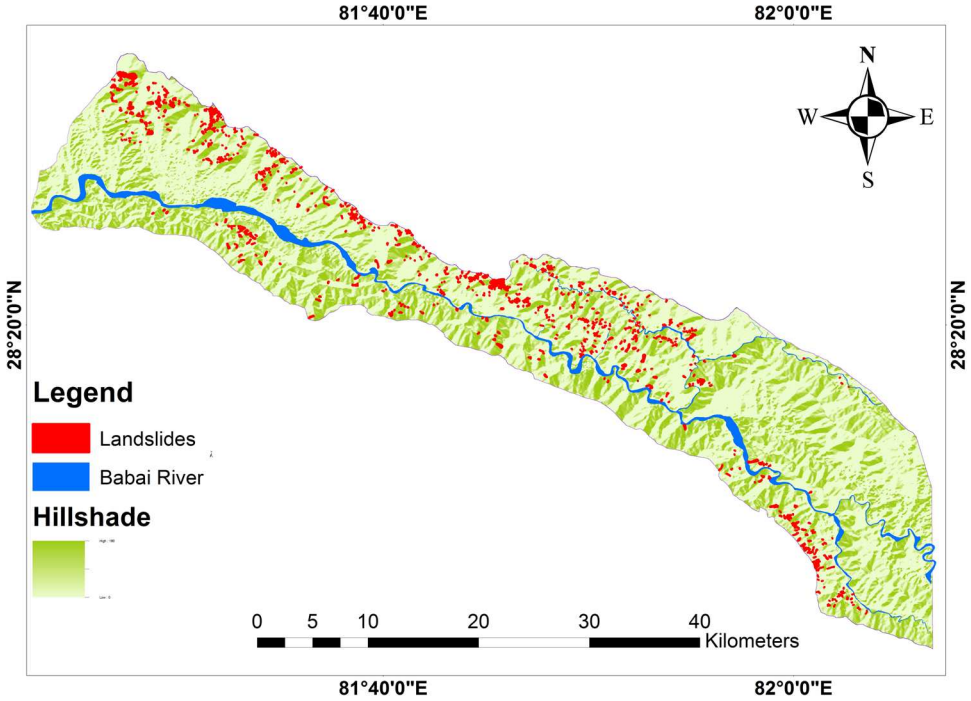


**Fig. 3** Landslide inventory map of Siwalik hill of Babai catchment

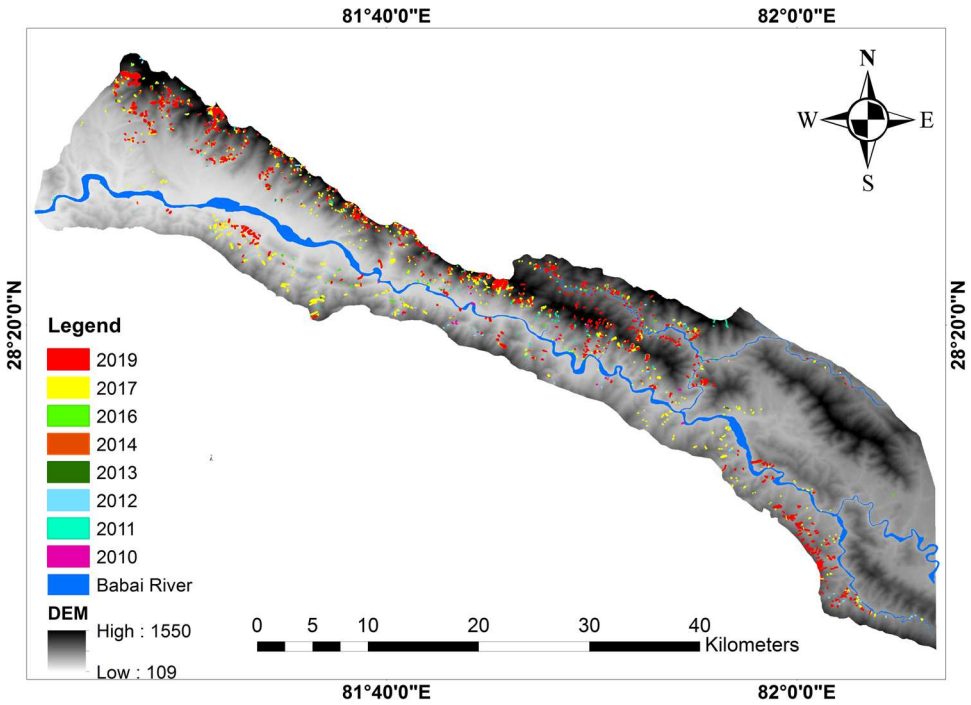


**Fig. 4** Multi temporal inventory map of Siwalik zone of Babai watershed

The geological structures, formations and their impacts on landslide occurrence were also studied in the field. Physical characteristics of landslides, including landslide description, the physical parameters contributing to the initiation of landslides were analyzed. The landslide initiation mechanisms were studied and analyzed based on the field observation.

## 2.6 Data analysis

The landslides in the inventory map were compared with the field data for the validation of landslide distribution in the study area. This is followed by the characterization and analysis of landslides. Major four landslide probable factors: geology, slope, fault and rainfall were selected

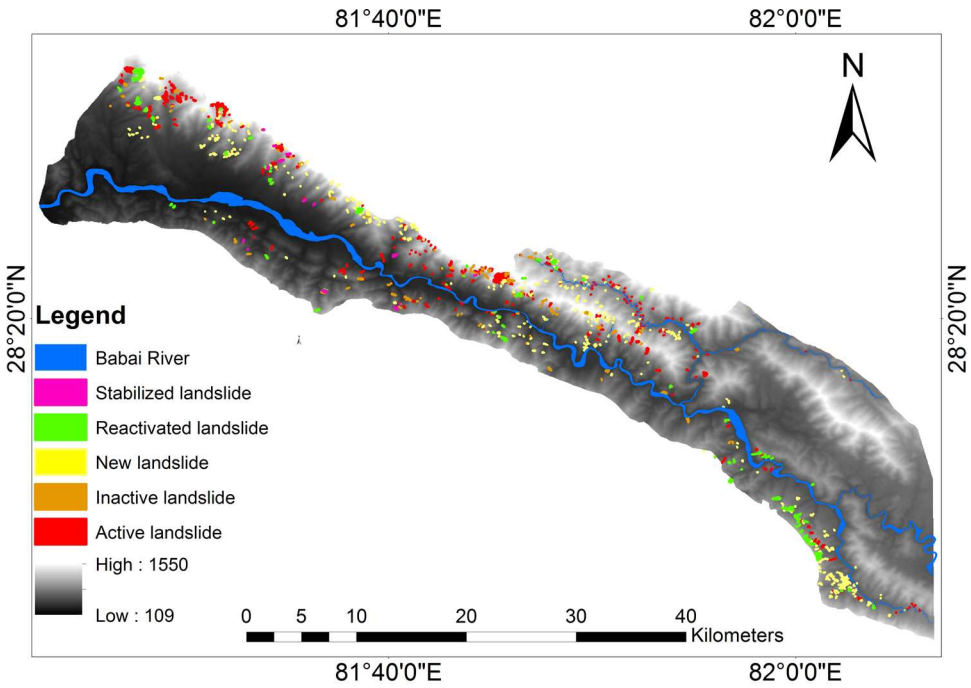


**Fig. 5** Inventory of state of activity of landslides

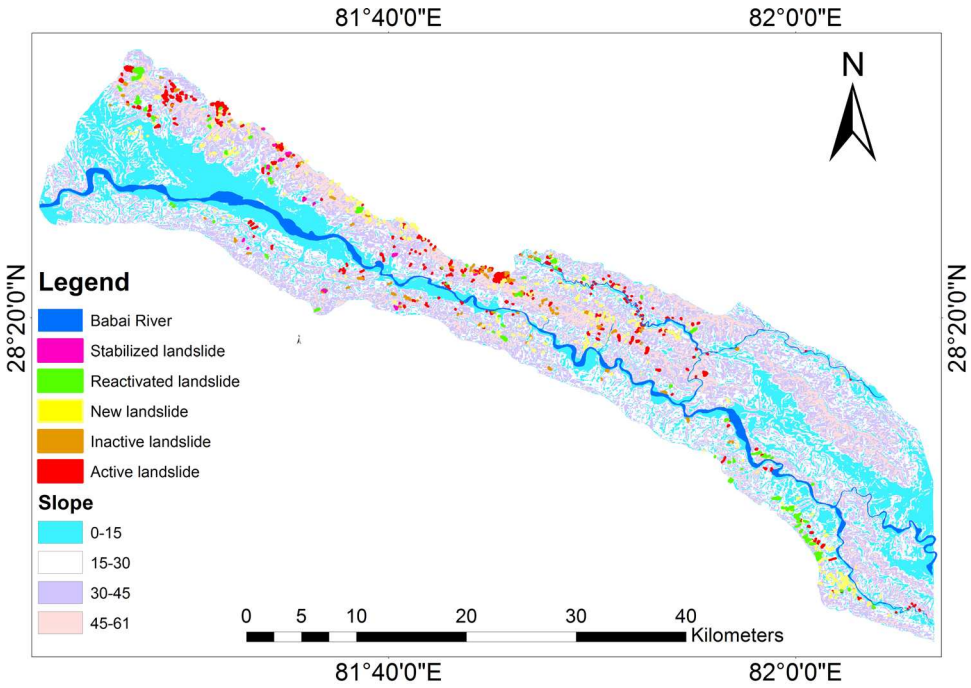


**Fig. 6** State of activity of landslides in different slopes

for the evaluation of landslide dynamics. The geological formation and thrusts were taken for geological attribute, slope was taken for topographical attribute and rainfall data was taken for hydrological attribute. The pre existing landslides were used to analyze the different attributes. MS excel and R-software was used for data analysis. More than thousand landslides were encountered but only 952 are of size having area greater than 100 $m^2$.

## 2.7 Activity classes

Most of the landslides that were unclear in the images were confirmed in the field by visual observations and different social survey. The term to define activity classes were adopted from some of the past researches. The multilingual landslide glossary [41], distinguishing the following four classes of sates of activity:

**Table 1** Landslide classification based on its activities

| Name | Characters |
|---|---|
| New (N) | Landslides that has occurred in last 36 months |
| Active (A) | Landslides that has been moving every year/ Movement has occurred in last 12 months |
| Inactive (I) | No movement has occurred since three years and having no prior probability to reactivate in near future |
| Reactivated (R) | Landslide reoccurred in the inactive or stabilized landslide |
| Stabilized (S) | The landslide mitigated naturally or structurally and seems stable at present |

**Table 2** Landslide size on the basis of area

| SN | Area ($m^2$) | Size class |
|---|---|---|
| 1 | < 100 | Very small |
| 2 | 100–1000 | Small |
| 3 | 1000–10,000 | Medium |
| 4 | 10,000–100,000 | Large |
| 5 | 100,000–1,000,000 | Very large |

**Stabilized (S):** not affected by their original causes anymore.

**Dormant (D):** potentially being reactivated.

**Active (A):** currently moving.

**Reactivated (R):** moving after being inactive.

Cigna et al. (2013) proposed three classes of activity of landslide on the basis of VACT (Distinguishing moving from non moving area) and Vp (Present velocity) namely; stabilized, Dormant and Active. We proposed five activity classes and established for this study namely: new, active, inactive, reactivated and stabilized. The basis of classification of landslides based on activities is as given in Table 1.

### 2.8 Size of landslide

Five landslide size classes are proposed on the basis of logarithmic scale. The proposed landslide size classes are adopted on the basis of area for the size based classification (Table 2).

## 3 Results

### 3.1 Landslide inventory

Altogether 952 landslides (old and new) were identified in the image and from the field verification. The landslide area and frequency has been investigated and the result showed that the area of landslides are log-normally distributed (Fig. 7). The five different sizes of landslide were adopted for size based classification namely very small, small, medium, large and very large on the basis of area. The medium sized landslide covered 67.7% whereas the large and small sized landslide covered only 16.5% and 14.7% respectively. The result indicates that the landslides

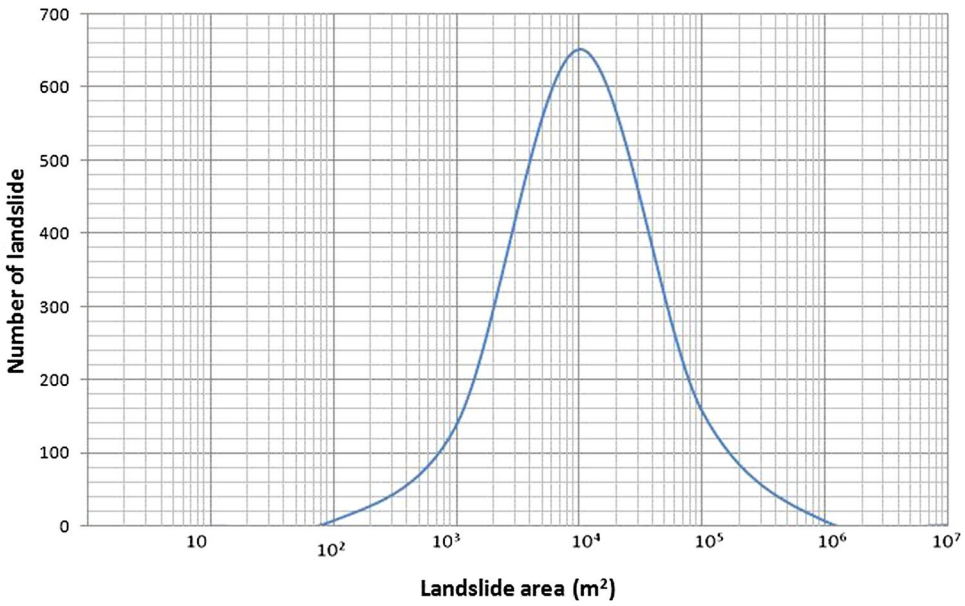


**Fig. 7** Figure showing the landslide size and number relationship

having area between 1000 $m^2$ to 10,000 $m^2$ (medium sized) are dominant in the study area.

### 3.2 State of activity

After the study of state of activity of landslides, five major states of activities are taken namely new, active, inactive, reactivated and stabilized. The maximum, minimum and total area of different states is given in Fig. 8. In the study area, 40% of area is covered by active landslide whereas 26% area is covered by reactivated landslide. Area covered by new landslide is 18.45%. The stabilized landslide is only 3.3% and inactive landslide is 11.63% (Fig. 8), thus the result snowed that the most of the landslides are being active every year since a decade. The occurrence of new landslides is less than active landslide. Similarly, the rate of reactivation of landslide is 26% which is second highest rate of landslide occurrence. Most of the past landslide deposits are reactivated.

### 3.3 Geological distribution

The geological distribution of landslide was found on the basis of geological formation. The area is divided in to three formations namely Lower Siwalik, Middle Siwalik and Upper Siwalik [3, 4]. Figure 9a shows that every state of landslides is dominant in Middle Siwalik whereas the active and new landslides are majorly found in Middle Siwalik but new landslides are major in Lower Siwalik. The landslides having area 1000–100,000 $m^2$ is dominant in all the geological formations (Fig. 9b). There is no significant difference in the size-frequency of landslide in all the geological formation. Less number of very large sized landslides was encountered in the decade from 2010 to 2019 AD. The size distribution of landslide in every geological formations of study area is normal distribution. The result shows that the landslide size distribution in all the geological formations is same. The total length of landslide is significantly different in all geological formations. The landslides having total length < 200 m is dominant in every formation (Fig. 9c). The landslides distributions in the structure of different thrust zone are given in Fig. 9d. Among the three major thrusts of the study area, Babai thrust is more potential for landslide. Hanging wall of thrust zone has higher number of landslides. Most of the landslides lie on the fault zone either in hanging wall or on foot wall. The rock of hanging wall are crumbling, highly jointed and crushed and due to that hanging wall consists of large number of landslides in comparison with foot wall.

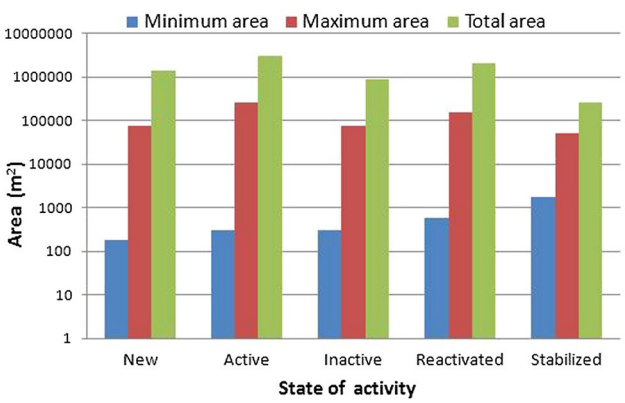


**Fig. 8** The area of different state of activity of landslides

### 3.4 Temporal dynamics of landslide

The landslide distribution from 2010 to 2019 AD was performed (Fig. 10a). During the period of 2010 to 2019 AD, the annual landslide frequency varies significantly. In 2010 AD, there were only 198 landslide events but in 2011 AD, the landslide number increased significantly and reached 398. But in 2012, again the landslide number decreased. The landslide events increased significantly from 2013 to 2019 AD. In case of geological formation, the landslide trend can be described in three patterns. Firstly, the landslides number increased significantly from 2010 to 2011 AD. Secondly, the landslide number decreased in 2012 AD and again increased from 2013 to 2019 AD. These trends are similar for every geological formation. The annual change in area of landslide in geological formations is not in positive trend. The area has fluctuated annually. In case of Lower Siwalik, area increased from 2010 to 2011 AD but decreased in 2012 AD. Again the area increased from 2013 to 2017 AD. The area decreased in 2018 AD and again increased in 2019 AD. Similar result is found in Middle Siwalik but the result is slightly different in Upper Siwalik. The area decreased from 2011 to 2013 AD and increased up to 2017 AD. The result shows that the number of landslide event decreased significantly in 2018 AD and increased in 2019 AD. The number of landslide is found highest in 2019 AD in all the geological formations since 2010 AD. It is also found that the area and number of landslide is higher in Middle Siwalik every year (Fig. 10b). The result concluded that the Middle Siwalik is potential for landslide occurrence.

Discussing the state of activity of landslide, the area of new landslide decreased in 2011, increased in 2012 and 2013 and again decreased in the year 2014 but increased from the year 2016 to 2019 (Fig. 11). The active landslide rate is increasing trend from 2010 to 2016 but slightly decreased in 2017 and increased in 2018 and 2019. The reactivation rate decreased in 2011 and 2012 but increased from the year 2013 to 2019. The result shows that the number and area of landslides decreased mostly

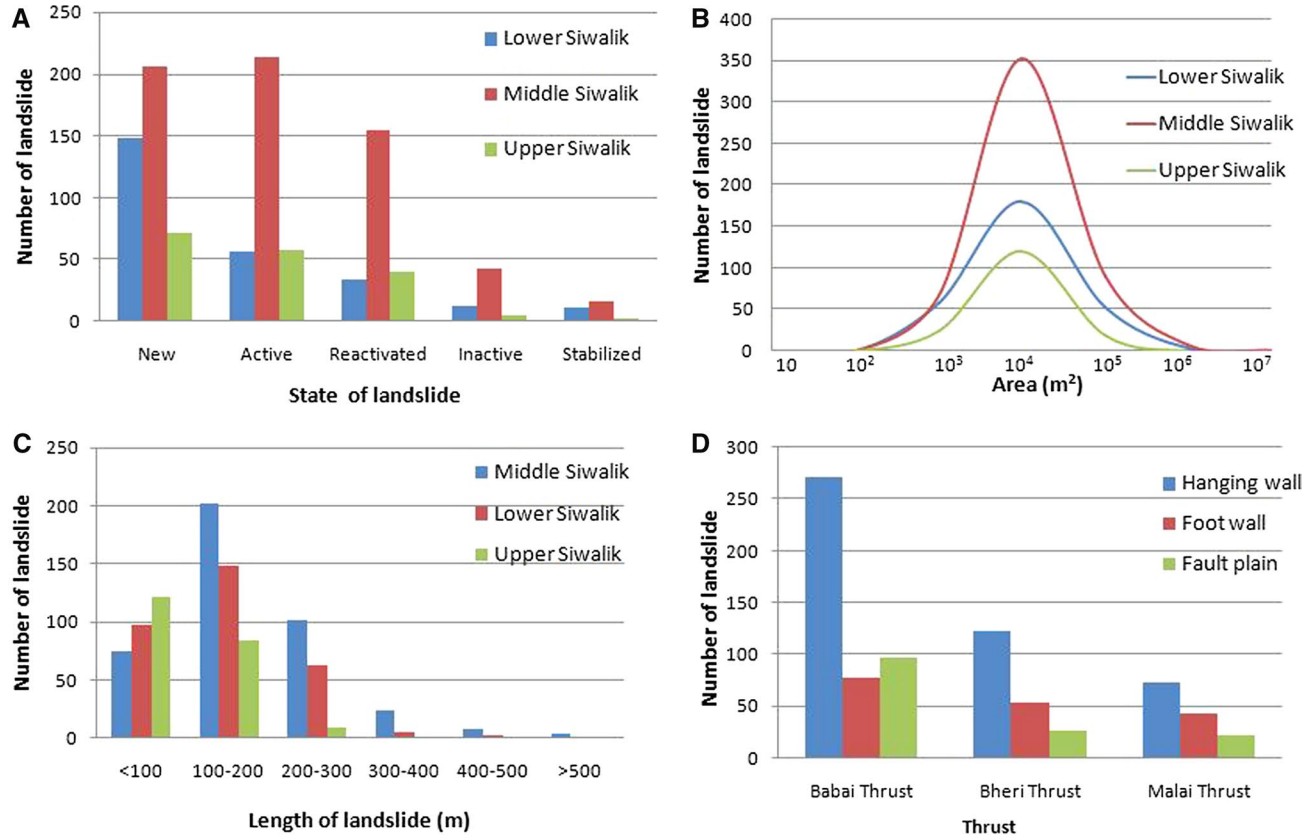


**Fig. 9** **a** Figure shows the number of state of landslide activity in different geological formations, **b** area and number relation of landslides in the geological formations, **c** length and number distribution of landslide in different geological formations, **d** landslide distribution into different thrust zone

in two years; that is 2012 and 2018. In other years, the landslides area and frequency has increased. Since the decade, the area and number relation is in normal distribution. The medium sized landslide (having area 10,000 $m^2$–100,000 $m^2$) is dominant every year. The trend of landslide area and number curve is same in every year since the years 2010–2019 (Fig. 12). It indicates that the landslide size is not significantly difference in every year. The landslide number has been increasing every year since 2010.

### 3.5 Slope angle

The landslide number distribution in different slope angles with geological formation is given in the Fig. 13a. In every geological formations, the landslide number is higher above the slope angle > 45°. Middle Siwalik has higher number of landslide in every slope greater than 15°. New and active landslides are predominant at the slope > 30° (Fig. 13b).

### 3.6 Rainfall and landslide

Rainfall is considered as one of the major cause of landslide. We compared the maximum 24 h rainfall and total number of landslide, total annual rainfall with total annual landslide from 2010 to1019 AD. There is no exact correlation between maximum 24 h rainfall and landslide (Fig. 14a, b). But the total annual rainfall and number of landslides are relatively correlated. Comparatively, the maximum 24 h rainfall amount is less in 2016, 2017 and 2019 AD but the landslide events are higher in these years. Figure 14a and b shows that maximum 24 h rainfall is not major cause of landslide. In Fig. 14c and d, the total landslide and total annual rainfall give the more a less same trend line. It can be said that landslide occurrence depends upon the total annual rainfall. The magnitude of rainfall, events of landslide and landslide intensity are summarized in Table 3.

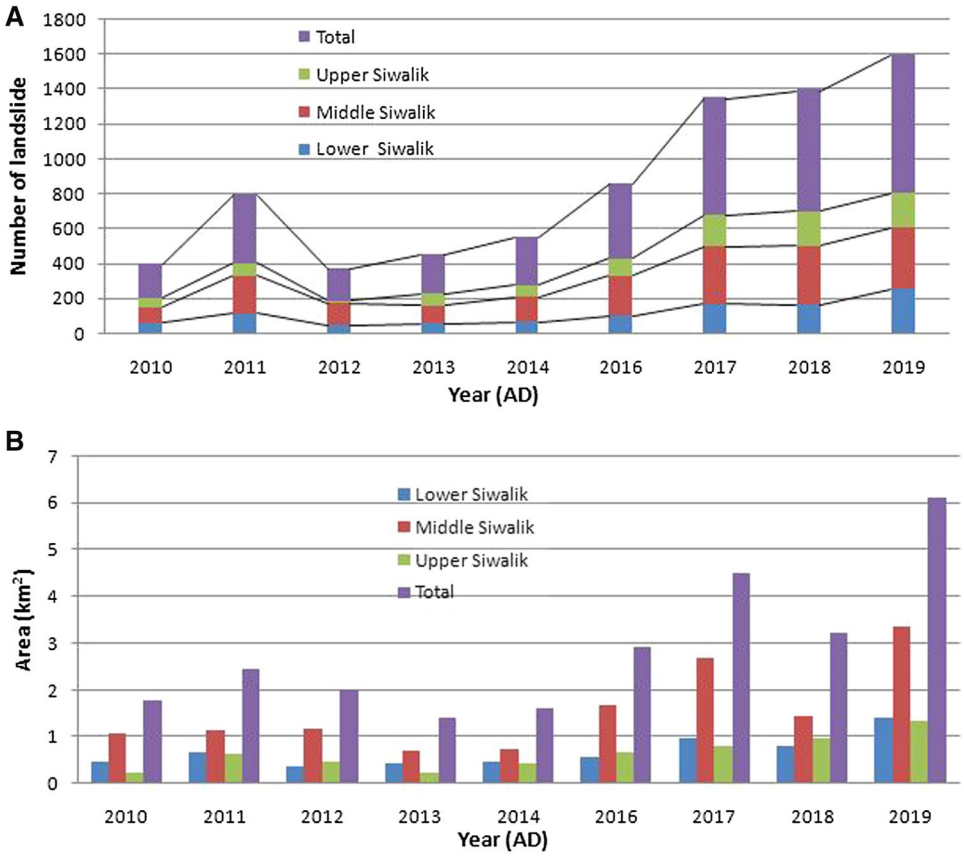


**Fig. 10** **a** Temporal landslide and number in different geological formations, **b** temporal distribution of area of landslides in geological formations

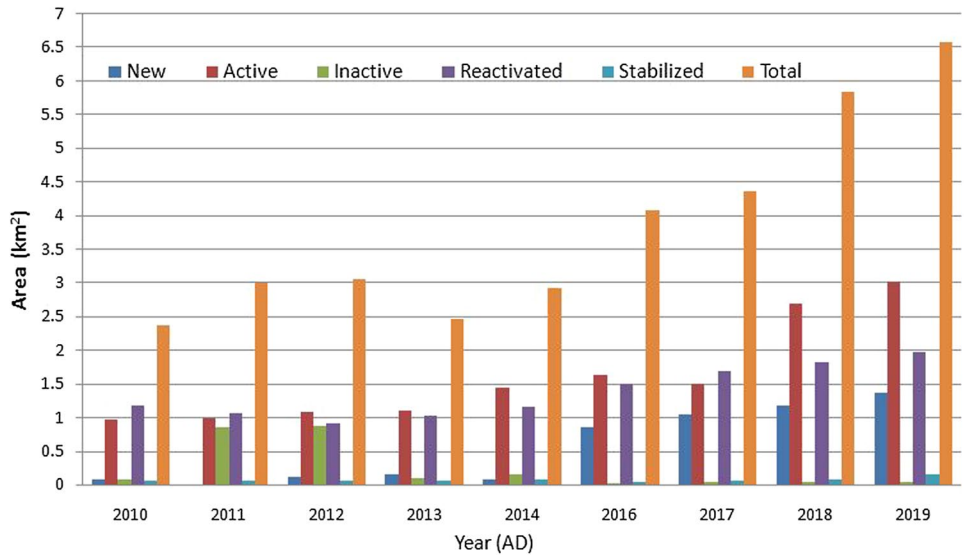


**Fig. 11** The temporal distribution of landslide area with state of activity

### 3.7 Initiation of landslide

Field study indicates that the failures generally occurred along the colluviums, bedrock contact, colluviums-bedrock contact, geological contact, and the fault zone. Landslides of sandstones start from slides or fall and quickly convert to flows (debris flow) because of the water involved and the steep terrain below the landslide sources. From our analysis, the landslide distribution can be summarized in the five types based on their initiation as discussed in the following section.

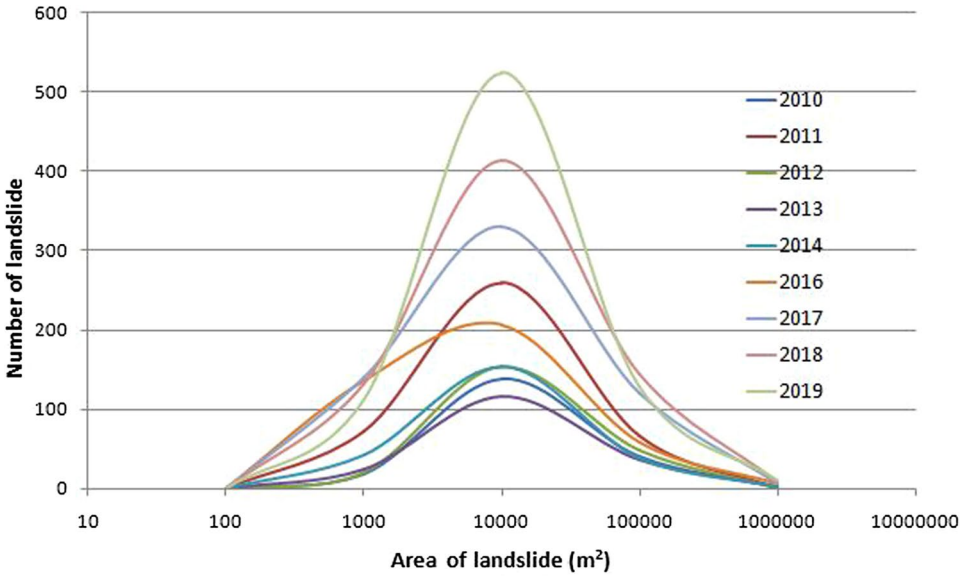


**Fig. 12** The area and number relationship of landslides since 2010 to 2019

*Type 1* Thin layer of shale is present between the massive sandstone beds of Middle Siwalik (Fig. 15). The shale is permeable in nature. In the saturation state, the shale weathers and erodes out. It reduces the friction angle and weakens the support of sandstone beds, causing massive sandstone beds slide or fall from the steep slope.

*Type 2* Landslides in mudstone begin from erosion with small channel and rill. The thick layers of mudstones are highly jointed, highly weathered and concreational in nature. The landslide with short scar begins from slope erosion. Landslides of mudstone have short scar and longer toe (Fig. 16). Landslides of mudstone resulted alluvial fan at bottom after transporting huge amount of landslide mass (debris) during heavy rain. Slope has played vital role to transport such huge landslide debris towards bottom of hill through the channel.

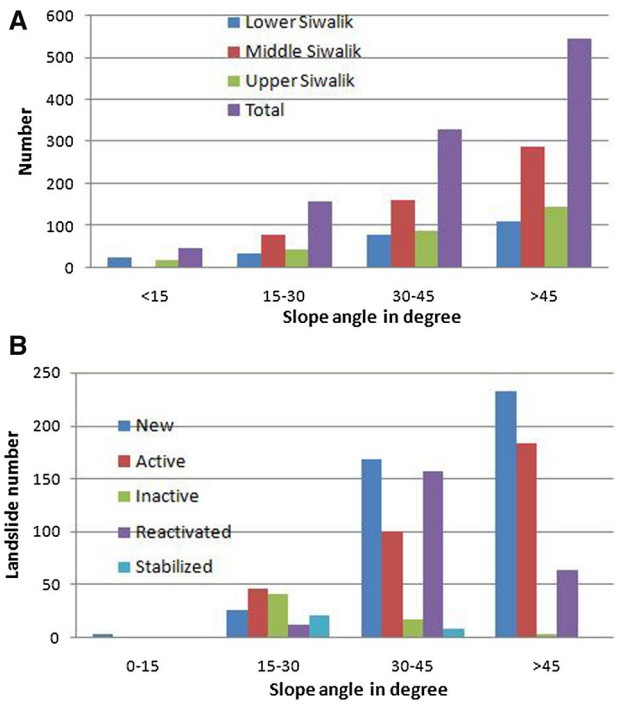


**Fig. 13** **a** Slope and landslide number relation in different geological formations, **b** slope and landslide number relationship with state of activity

*Type 3* Conglomerate beds of study area are basically two types. One is calcite binding and another is clay binding [4]. Due to environmental alteration, the loose binding of cementing material gets weak. The detached rock fragments and clay rich soil layer flow with water during heavy rain fall. Similarly, the mud/clay vein present on conglomerate beds weathers and jointed to the rock bed. The large block separated from intact rock.

*Type 4* The rocks and soils of the fault zone are crumble and fragile. The tension cracks and joints are common in fault zone. Seismic wave or any active stress applying on the area causes the rock/soil to slide or fall. When the water inters from the cracks and joints, there exist pore water presser and also reduces the friction and ultimately caused landslide.

*Type 5* The colluviums deposit of old landslide has been covered by thin layer of soil causing devolvement of forest. The density of soil increased in saturated state in rainy season. The colluviums loose the bedrock- colluviums contact. The trees and forest increased the soil density and causing landslide.

The major initiation models of type 1 to type 5 are shown in Fig. 17. In Fig. 17a, the type 1 model is shown. After eroding the thin layer of shale, the thick layer of sandstone looses the support on the steep slope. The thick and massive sandstone beds fall or slide due to this

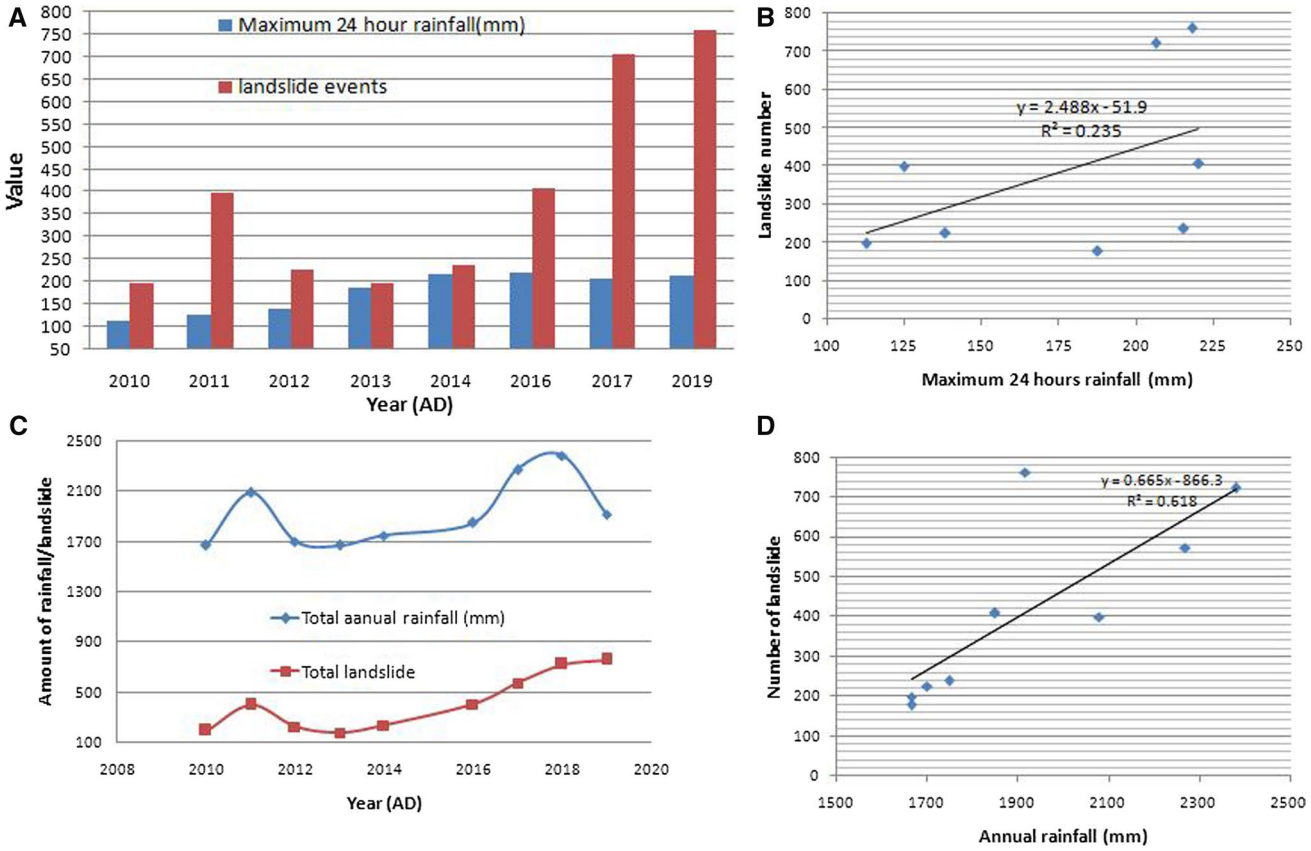


**Fig. 14** **a** Landslide and rainfall events of Babai River catchment from 2010 to 2019. **b** Regression of maximum 24 h rainfall and landslide frequency. **c** Trend analysis of landslide and total annual rainfall. **d** Regression of total annual rainfall and landslide frequency

mechanism. The type 2 model is shown in Fig. 17b. The gulley erosion is the initiation in this type model. The landslide begins from erosion with small and narrow scar. After continuous erosion process, huge amount of debris transported from hill slope and covers large area on the down slope. This type of landslide causes huge fan deposit at the gentle slope. The type 3 model is shown in Fig. 17c. In this model, the landslide initiation in conglomerate bed is shown. The cementing material erodes out due to its loose binding mechanism. After eroding the binding materials, the large block of conglomerate bed dissociate into granular debris masses and flows down like granular flow [15] with or without rain water. This type of landslide also creates debris flow and results debris fan deposits. The type 4 model is related to thrusting and faulting mechanism. The hanging wall of thrusts is found fragile and weak. The rocks are highly jointed and weathered. Due to this process, landslide activities are very common on thrust zone (Fig. 17d). The type 5 model is shown in Fig. 17e. This model explains about the landslide initiation on the slope comprising of old colluvium. Most of the Siwalik hills are affected by landslides in the past. Later on, the hill slopes made this way and comprised of colluvium are covered by vegetation. The tall trees are very common on these colluvium deposits. At many places, these colluvium become unstable due to the overload at saturation state. As a result, landslides are very common even in the forest area of the entire study area.

## 4 Discussions

Geologically, the Siwalik zone of study area has been divided into three formations on the basis of lithology and stratigraphy by various researchers [2, 3, 4, 16, 38]. This threefold classification is the most followed classification system dividing the Siwalik zone into three formations namely: Lower Siwalik, Middle Siwalik and Upper Siwalik. The Siwalik zone consists of Quaternary fluvial sedimentary succession. There is typical lithology and stratigraphy in the sedimentary sequence. The rocks are north dipping sequence in general trend except some folding and faulting cases. Both Middle and Lower Siwalik consists of sandstone and mudstone bed but the proportion of rocks are different. Lower Siwalik consists of thick layer of mudstone alternated by thin layer of

**Table 3** Rainfall amount, landslide events and intensity in temporal series of representative landslides

| SN | Rainfall date | Rainfall amount (mm) | Rainfall duration (h) | Landslide date | Size ($m^2$) | Location |
|---|---|---|---|---|---|---|
| 1 | 7-2-2010 | 100.6 | 3.0 | 7-6-2010 | 14,678 | Babai village |
| 2 | 8-30-2010 | 39.4 | 1.5 | 9-06-2010 | 1,34,342 | Ban gaun |
| 3 | 7-23-2011 | 96.6 | 6.0 | 7-26-2011 | 45,231 | Mulkharka |
| 4 | 8-23-2011 | 120.2 | 4.3 | 8-23-2011 | 53,125 | Khahare |
| 5 | 7-02-2012 | 77.5 | 3.2 | 7-04-2012 | 45,567 | Purandanda |
| 6 | 9-04-2012 | 40.6 | 1.2 | 9-04-2012 | 1,23,187 | Guhiyachaur |
| 7 | 7-02-1013 | 56.78 | 1.2 | 7-05-2013 | 24,156 | Sarada Khola |
| 8 | 8-09-2013 | 86.21 | 1.6 | 8-09-2013 | 9,786 | Damdawali |
| 9 | 6-28-2014 | 116.5 | 1.4 | 7-04-2014 | 96,176 | Gidde Khola |
| 10 | 7-16-2014 | 154.0 | 6.0 | 7-17-2014 | 1,56,342 | Gidde Khola |
| 11 | 7-17-2014 | 215.0 | 8.0 | 7-17-2014 | 2,77,879 | Gidde Khola |
| 12 | 6-02-2015 | 175.2 | 2.5 | 6-04-2015 | 1,34,456 | Harre |
| 13 | 6-21-2015 | 263.3 | 5.0 | 6-26-2015 | 39,213 | Lekhparajul |
| 15 | 7-06-2016 | 95.6 | 1.5 | 7-11-2016 | 6,22,362 | Lekhparajul |
| 16 | 7-28-2016 | 120.5 | 2.5 | 8-06-2016 | 9,62,409 | Babai Village |
| 17 | 8-09-2017 | 157.5 | 4.3 | 8-09-2017 | 4,34,980 | Bardia National park |
| 18 | 8-18-2017 | 125.0 | 3.2 | 8-19-2017 | 2,13,435 | Bardia |
| 19 | 7-22-2018 | 122.5 | 1.2 | 7-22-2018 | 99,876 | Salyantari |
| 20 | 8-17-2019 | 178.5 | 3.5 | 8-22-2019 | 3,66,178 | Bardia |

Data from Department of Meteorology, Nepal government and field study

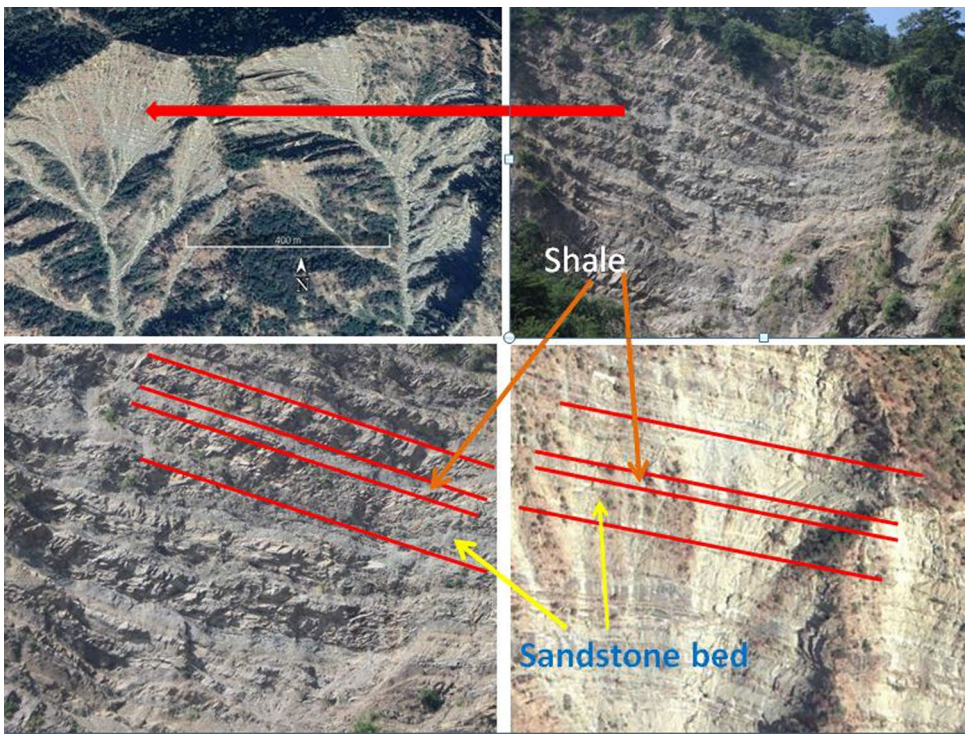


**Fig. 15** Landslide (rock slide) in sandstone bed of Middle Siwaliks. Landslide occurred in the alternate layer of sandstone and shale of Middle Siwaliks due to erosion of shale. Photo taken at Gidde Khola landslide of Bardiya district

sandstone. The mudstone of lower Siwalik consist clay rick mud that is soft and easily breakable. The mudstone gets weathered after continuous interface with water. The concretions are developed in the mudstone in dry condition. Both dry and wet conditions make the mudstone bed easy to slide, erode or fall. The Lower Siwalik

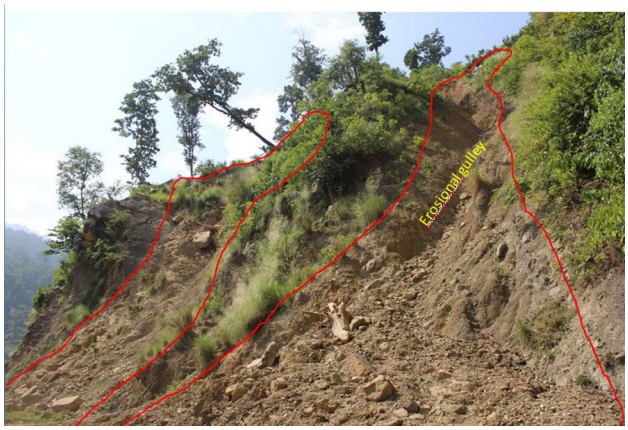


**Fig. 16** Landslide caused by weathered mudstone in between the alternate layer of Mudstone and Sandstone of Lower Siwaliks (Photo taken at Upper Damdawali of Salyan district)

is in the range of 900 m elevation in the study area. Only 8% area of Lower Siwalik consists of slope greater than 45°. The distance to travel by landslide mass is less and slopes to increase flow velocity also less in Lower Siwalik. So that, the area and length of landslides in Lower Siwalik is significantly less than Middle Siwalik. New and active but small landslides are most common every year but possibility to stabilize is seem less in Lower Siwalik because the scar erosion and lateral movement occurs in every monsoon period. In the Middle Siwalik, there consist alternate layer of thickly bedded sandstone and thinly bedded mudstone or shale. The sandstone consists of Feldspar and Mica (Muscovite and Biotite) with little Quartz [32]. The sandstone beds are loosely bonded and less compacted [4].

The Babai thrust, Tui Khola thrust, Bheri thrust caused the sandstone beds crumble and highly jointed. The feldspar has higher weathering rate causing the sandstone weathered both physically and chemically. The thin layered, weak and fragile mudstone/shale when get weathered, it erodes out time by time. 39% area of Middle Siwalik consists of slope greater than 30° and this slope class is potential for landslide occurrence in this area. The Middle Siwalik lies in the range of elevation 1100 m to 1500 m in the study area. When thickly bedded sandstone bed slide or fall, the block crumbled and crushed resulting fragments into cobble, pebble and boulder size. The fragmented rocks flow down with flowing water during or after rainfall through the gulley or valley and reaches to the longer distance as debris flow. The landslide mass of Middle Siwalik travels longer because there exists steep slope on higher elevation to increase flow velocity and to travel longer distance. Both new and active landslide having medium to large size is very common in this formation.

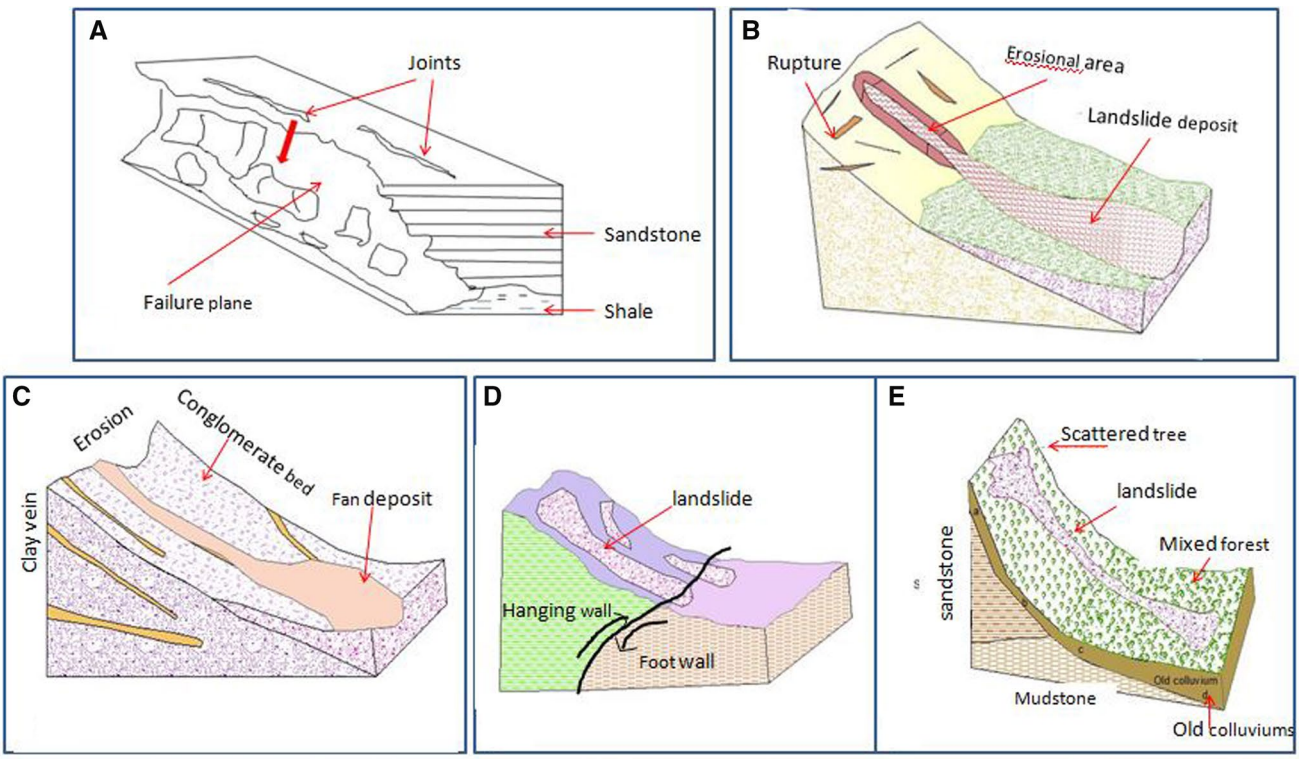


**Fig. 17** Landslide models at different geological conditions, **a** alteration of sandstone and shale followed by weathering of shale, **b** lower Siwalik having alternate layer of sandstone and mudstone, **c** conglomerate bed, **d** in the thrust zone, **e** in the colluvium deposit

In the Upper Siwalik, clay bonded conglomerate alternately found with thin layer of shale. The quaternary fluvial conglomerate belts are weakly bonded and loose in nature. At the saturation condition, the beds weather and erode out after losing inter particular bonding. The eroded rock fragments and materials flow with running water resulting debris flow and gravel flow. If the conglomerate is in steep slope, the large blocks separate and slide/fall down and remain as the boulder conglomerate. The Upper Siwalik rocks are found in the elevation of 400 m to 700 m. Only 7% area of Upper Siwalik lies in the slope > 40°.

The landslide size shows log-normal distribution in the study area. Medium to large scale landslides are commonly found. The result is similar in every year since 2010. The area distribution in all three formations is in the similar trend. The area and frequency of medium to large sized landslides are higher in every formation. The Middle Siwalik consists of larger area as well as number of landslide than Lower and Upper Siwalik since 2010. The decadal data shows that Middle Siwalik is landslide prone area in the Siwalik zone. Bhandari and Dhakal [4] and TU-CDES [38] reported the similar result of this area.

The activity classes proposed by previous researchers are not sufficient to classify the state of activity in Siwalik zone. So, we proposed the states of activity into five classes on the basis of activity time and processes. The active and landslides are very common in the study area. Most of the landslides move every year. The landslides nearby thrust zone and the landslides of the colluviums bedrock contact are active landslide. The new landslides are found in the contact between two formations, colluvium deposit as well as hanging wall area of thrust zone. The hanging wall of thrusts is more sensitive for landslide and debris flow than the foot wall. The active landslides are dominant in the Middle Siwalik. Both in spatial and temporal cases, number of landslides are higher in Middle Siwalik.

Thrust zones are found highly susceptible for landslide occurrence. Most of the large sized landslides are found concentrated on the hanging wall of the thrust. Bucci et al. [5] tested the landscape evolution model in the Peloritani range of Italy and concluded that large landslides and their cumulated volume are sensitive to local rates of tectonic deformation, and the large sized landslides are controlled by the active faults.

Among the 9 rainfall stations, the average rainfall for 24 h and total average annual rainfall was calculated. There is very weak correlation between 24 h rainfall and landslide occurrence but total annual rainfall and landslide frequency has positive correlation. Dahal and Hasewaga [12] found that 140 mm maximum 24 h rainfall is the threshold for landslide in Nepalese hill. However, our result shows that only 24 h rainfall cannot cause the landslide in every formations but average rainfall in rainy season may cause medium to large scale landslides.

Regarding the seismic activities, catastrophic Gorkha Earthquake of 7.8 MW was occurred in Nepal on 25th of April 2015. Several aftershocks were occurred after the major earthquake. The major earthquakes and several aftershocks caused the surface potential for landslide occurrence. Continuing rainfall after earthquakes and strong aftershock shaking are key factors affecting continued landslides in the earthquake-affected areas [27, 29, 31, 36]. Our result shows that the landslide number has increased in 2016 and 2017 after 7.8 MW Gorkha Earthquake. Several aftershocks were occurred within a year. Tsou et al. [37] mapped 13,847 earthquake induced landslides in most affected parts of Central Nepal due to 7.8 MW Gorka Earthquake. Among them 750 were enlarged preexisting landslide and 13,097 landslides were new. Although, the data on the landslides triggered by Gorkha Earthquake 2015 in our study area was not found and the precise differentiation of earthquake induced landslides was beyond the scope of this study, this earthquake and its major aftershocks may have triggered landslides as indicated by the increased numbers of landslides in 2016 and 2017 in this study area.

## 5 Conclusions

The study concludes that landslides of Siwalik region are highly dynamic in nature. There are spatial differences of landslide on the basis of geology and structures. The Middle Siwalik is the major geological Formation which is comprised of large number of landslides. The hanging wall of thrust zone is more sensitive for landslide. The result shows that total annual rainfall has positive role for landslide occurrence rather than maximum 24 h rainfall. The typical sizes of the landslides in the area are between 10,000 $m^2$ and 100,000 $m^2$. The landslides are potentially found larger in number at the hanging wall of thrust. In terms of landslide activity, 40% of area is covered by the active landslides. The rapid increment of landslides is found after 2015, which can be due to the effect of Mw 7.8 Gorkha earthquake in Nepal.

### Compliance with ethical standards

**Conflict of interest** The authors declare that there are no conflicts of interest regarding the publication of this manuscript.

## References


1. Auden JB (1935) Traverses in the Himalaya. Geol Surv India 69:123–167
2. Bhandari BP, Dhakal S (2019) Topographical and geological factors on gully-type debris flow in Malai River catchment, Siwaliks. Nepal J Nepal Geol Soc 59:89–94
3. Bhandari BP, Dhakal S (2019) Evolutional characteristics of debris flow in the Siwalik Hills of Nepal. Int J Geosci 10:1049–1067. https://doi.org/10.4236/ijg.2019.101206
4. Bhandari BP, Dhakal S (2018) Lithological control on landslide in the Babai Khola Watershed, Siwaliks Zone of Nepal. Am J Earth Sci 5:54–64
5. Bucci F, Santangelo M, Cardinali M, Fiorucci F, Guzzetti F (2016) Landslide distribution and size in response to Quaternary fault activity: the Peloritani Range, NE Sicily, Italy. Earth Surf Process Land 41:711–720
6. Carrara A, Guzzetti F, Cardinali M, Reichenbach P (1999) Use of GIS technology in the prediction and monitoring of landslide hazard. Nat Hazards 20:117–135. https://doi.org/10.1023/A:1008097111310
7. Chaudhari RS (1982) Petrology of the Siwalik group of Nepal Himalaya. Rec Res Himalaya 8:424–466
8. Chen YC, Chang KT, Wang F et al (2019) Controls of preferential orientation of earthquake-and rainfall-triggered landslides in Taiwan's orogenic mountain belt. Earth Surf Proc Land 44(9):1661–1674
9. Chigira M, MohaMad Z, Sian LC, KoMoo I (2011) Landslides in weathered granitic rocks in Japan and Malaysia. Bull Geol Soc Malays 57:1–6. https://doi.org/10.7186/bgsm2011001
10. Cigna F, Bianchini S, Casagli N (2013) How to assess landslide activity and intensity with persistent scatterer interferometry (PSI): the PSI-based matrix approach. Landslides 10:267–283. https://doi.org/10.1007/s10346-012-0335-7
11. Crozier MJ (1986) Landslides: causes, consequences and environment. Croom Helm Australia Pty. Ltd., London, p 252
12. Dahal RK, Hasewaga S (2008) Representative rainfall thresholds for landslides in the Nepal Himalaya. Geomorphology 105:429–443
13. Dahal RK, Hasegawa S, Bhandary NP, Poudel PP, Nonomura A, Yatabe R (2012) A replication of landslide hazard mapping at catchment scale. Geomat Nat Hazards Risk 3(2):161. https://doi.org/10.1080/19475705.2011.629007
14. Densmore AL, Ellis MA, Anderson RS (1998) Landsliding and the evolution of normal fault-bounded mountains. J Geophys Res 103(B7):15203–15219. https://doi.org/10.1029/98JB00510
15. Dhakal S (2017) Experimental study of particle interactions in moderate to dense granular shear flows of disks. Condens Matter 2017(2):2
16. Dhakal S (2015) Evolution of geomorphologic hazards in Hindu Kush Himalaya. Mountain hazards and disaster risk reduction. Springer, Japan. https://doi.org/10.1007/978-4-431-55242-0_4
17. Dhakal S (2014) Disaster in Nepal, In: Disaster risk management: concept, policy and practices in Nepal, Central Department of Environmental Science (CDES), Tribhuvan University Kirtipur
18. Galli M, Ardizzone F, Cardinali M, Guzzetti F, Reichenbach P (2008) Comparison of landslide inventory maps. Geomorphology 94:268–289
19. Gabet EJ, Burbank DW, Putkonen JK, Pratt-Sitaula BA, Ojha T (2004) Rainfall thresholds for landsliding in the Himalayas of Nepal. Geomorphology 63(3–4):131–143
20. Goswami R, Mitchell NC, Brocklehurst SH (2011) Distribution and causes of landslides in the eastern Peloritani of NE Sicily and western Aspromonte of SW Calabria, Italy. Geomorphology 132:111–122
21. Guzzetti F, Peruccacci S, Rossi M, Stark CP (2008) The rainfall intensity-duration control of shallow landslides and debris flows: an update. Landslides 5(1):3–17
22. Guzzetti F, Mondini AC, Cardinali M, Fiorucci F, Santangelo M, Chang KT (2012) Landslide inventory maps: new tools for an old problem. Earth Sci Rev 112:42–66. https://doi.org/10.1016/j.earscirev.2012.02.001
23. Hagen T (1969) Report on the geological survey on Nepal. Denschr Schweiz Naturf Gesell 86:1–185
24. Hurst MD, Mudd SM, Yoo K, Attal M, Walcott R (2013) Influence of lithology on hillslope morphology and response to tectonic forcing in the northern Sierra Nevada of California. J Geophys Res Earth Surf 118:832–851
25. Iverson RM (2000) Landslide triggering by rain infiltration. Water Resour 36(7):1897–1910
26. Larsen IJ, Montgomery DR, Korup O (2010) Landslide erosion controlled by hill slope material. Nat Geosci 3:247–251. https://doi.org/10.1038/ngeo776
27. Lin CW, Liu SH, Chang WS, Chen MM (2009) The impact of the Chi-Chi earthquake on the subsequent rainfall induced landslides in the epicentral area of central Taiwan. In: Proceeding of international conference in commemoration of 10th anniversary of the Chi-Chi Earthquake, pp. 336–338
28. Msilimba G, Holmes P (2010) Landslides in the Rumphi district of northern Malawi: characteristics and mechanisms of generation. Nat Hazards 54(3):657–677
29. Owen LA, Kamp U, Khattak GA, Harp EL, Keefer DK, Bauer MA (2008) Landslides triggered by the 8 October 2005 Kashmir earthquake. Geomorphology 94:1–9
30. Park JW, Choi BK, Cha DS (2017) spatial distribution and casual causes of shallow landslides in Jinbu area of Korea. J Environ Sci 32(2):130–135
31. Parker RN, Densmore AL, Rosser NJ, de Michele M, Li Y, Huang R, Whadcoat S, Petley DN (2011) Mass wasting triggered by the 2008 Wenchuan earthquake is greater than orogenic growth. Nat Geosci 4:449–452. https://doi.org/10.1038/ngeo1154
32. Regmi AD, Dhital MR, Gadtaula R, Tamrakar NK, Yoshida K (2011) Lithostratigraphy and structure of the Siwaliks rocks in the southern parts of dang and its surrounding area, South eastern Nepal. J FAC Sci Shishnu Univ 43:1–41
33. Santangelo M, Gioiac D, Cardinalia M, Guzzettia F, Schiattarella M (2015) Landslide inventory map of the upper Sinni River valley. South Italy J Maps 11:444–453
34. Santangelo M, Marchesini I, Bucci F, Cardinali M, Fiorucci F, Guzzetti F (2015) An approach to reduce mapping errors in the production of landslide inventory maps. Nat Hazards Earth Syst Sci 15:2111–2126. https://doi.org/10.5194/nhess15-2111-2015
35. Sassa K, Wang G, Fukuoka H, Wang FW, Ochiai T, Sugiyama ST (2004) Landslide risk evaluation and hazard mapping for rapid and long-travel landslides in urban development areas. Landslides 1(3):221–235
36. Tian Y, Owen LA, Xu C et al (2020) Landslide development within 3 years after the 2015 $M_w$ 7.8 Gorkha earthquake, Nepal. Landslides. https://doi.org/10.1007/s10346-020-01366-x
37. Tsou CY, Higaki D, Chigira M, Yagi H, Dangol V, Amatya S, Hayashi K, Kato H (2018) Topographic characteristics of landslides induced by the 2015 Gorkha earthquake. Nepal J Nepal Geol Soc 55:69–75. https://doi.org/10.3126/jngs.v55i1.22792
38. TU-CDES (2016) Landslide Inventory Characterization and Engineering Design for Mitigation Works of Chure Area in Ten Districts. Central Department of Environmental Science, Tribhuvan University and Government of Nepal, President. Chure-Tarai Madhesh Conservation Development Board, Kathmandu
39. Varnes DJ (1978) Slope movement types and processes. In: Schuster RL, Krizek RJ (eds) Landslides, analysis and control,

special report 176: Transportation research board. National Academy of Sciences, Washington, DC, pp 11–33
40. Wang FW, Sassa K, Wang G (2002) Mechanism of a long run out landslide triggered by the August 1998 heavy rainfall in Fukushima prefecture. Japan Eng Geol 63(1–2):169–185
41. WP/WLI (1993) Working Party on World Landslide Inventory (1993) Multilingual glossary for landslides. The Canadian Geotechnical Society, BiTech, Richmond BC

*Journal of Nepal Geological Society, 2019, vol. 59, pp. 89–94*
DOI: https://doi.org/103126/jngs.v59i0.24994

# Topographical and geological factors on gully-type debris flow in Malai River catchment, Siwaliks, Nepal

***Bharat Prasad Bhandari[1] and Subodh Dhakal[2]**
[1]*Central Department of Environment Science, Tribhuvan University, Kirtipur*
[2]*Department of Geology, Trichandra Multiple Campus, Tribhuvan University,*

**Corresponding author: bbhandari@cdes.edu.np*

## ABSTRACT

The Siwalik hill of Nepal lies in between the two major thrusts; Main boundary Thrust and Main Frontal Thrust. Thrusting and continuous erosion of material from surface causes several landslides and debris flow problem in the Siwalik region. Debris flow commonly occurs after landslide during heavy rainfall in the steep slope. This paper described about the topographical and geological controls on debris flow occurring in gullies in the Siwaliks of the Malai River catchment of mid-Western Nepal. The length of gully, length of debris channel, area of debris channel, area of catchment of debris flow, area of gully without debris flow were found using Google earth pro, a free version online database. Similarly, a form factor (F), average gradient of stream, slope area ratio and a topographical factor (T) were calculated. Lithology and geological structure were studied in the field. The relation between each factor was identified.

Gully having larger debris flow event had T value greater than 0.01 and that having small debris flow event had T value less than 0.01. Gully without debris flow had T value less than 0.001. Gully having debris flow had F more than 0.1 and that free from debris flow had F less than 0.1. Both topograohic and form factors were found greater than 0.1 at the hanging wall of the Malai Thrust, where large size debris flows were encountered. The T and F values obtained from the Middle and Upper Siwaliks were greater than 0.1. The number of debris flow events and large debris flows were found high the in the Middle and the Upper Siwaliks, and hanging wall of the Malai Thrust.

**Keywords:** Debris flow, Topographical factors, Gully-type debris flow, Malai Thrust, Siwaliks

**Paper Received:** 5 Apr 2019 **Paper Accepted:** 6th Jun 2019

## INTRODUCTION

Debris flow is defined as a flow of mixture of sediment and water in a way such that it acts as a flow of continuous fluid driven by gravity. It achieves large movement from the enlarged void space saturated with water or slurry (Takahashi, 2007). Debris flow is a flood in mountain region that carries a bulk load with increased amount of sediment that leads it to change into viscous mass comprising of water, soil, sand, gravel, rock block and wood mixture flowing like lava into a valley (Stiny 1910). Gully-type debris flow is very common in the Siwalik Hills of Nepal. The Siwalik hills of Nepal lie in between the Terai and the Lesser Himalaya. Due to an active thrust and continuous erosion of material from the surface in rainy season, several landslide and debris flow in the Siwalik region occur. The debris flows commonly occur after landslide during heavy rainfall in the steep slope and such debris flows constrained in a narrow steep channel, therefore are considered gully-type debris flows, which are different from the hill slope debris flow (Vandine, 1985). The gully-type debris flows are triggered by flash flood during heavy rainfall (Kean et al., 2013). During flooding in the steep gully, the high-speed runoff causes erosion on the bank and washes away the eroded materials.

Various researchers have studied about the gully-type debris flow mechanism in the past (Hua-yong, 2015; Mei, 2018; Huang, 2019). Topography, geology and hydrology are three factors playing a major role in the formation of ordinary gully-type debris flow (Liu et al, 2009). The major responsible topographical factors include channel length, slope angle, slope curvature, form factors and elevation different (Lin et al., 2002; Lan et al., 2004; Ranjan et al., 2004; Catani et al., 2005; Chang and Chao 2006; Chang 2007; Lu et al., 2007; Lee and Pradhan 2007; Chang and Chien 2007; Tiranti et al., 2008; Tunusluoglu et al., 2008; Akgun et al., 2008). The formation mechanism of the triggered debris flows is the runoff-induced mechanism. Topography has influence on the formation of debris flows in gullies with almost identical hydrological and geological conditions (Li et al., 2015). Various factors are responsible for the occurrence of debris flow but this paper aims to relate debris flow occurrence due to topographic and geologic factors.

## STUDY AREA

The Malai River watershed is located in the west of Tulsipur, Dang District of Nepal, and flows 25 km SE to NW, almost parallel to the Babai River that falls in the Siwalik zone

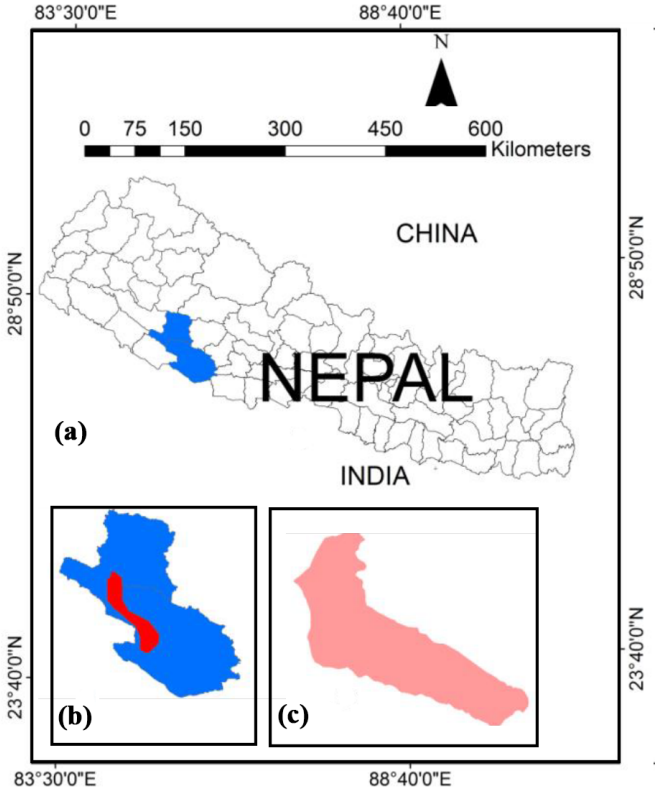


**Fig. 1: (a) Map of Nepal, (b) Dang and Salyan Districts showing study area, and (c) Map of the Malai catchment**

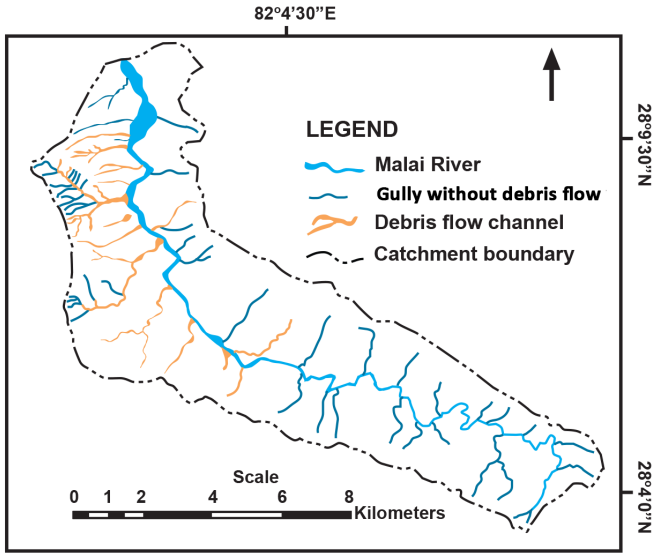


**Fig. 2 Drainage map with debris flow channel of the Malai River catchment**

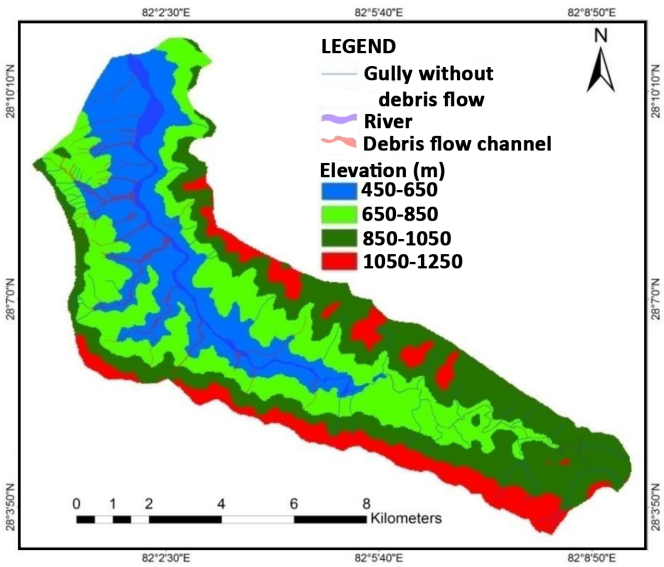


**Fig. 3: Elevation map of the Malai River Catchment**

of Nepal (Figs. 1 and 2). It is a tributary of the Babai River. The catchment size of the Malai River is 78 sq. km, having min. Elv. 484 m and max. Elv. 1210 m (Fig. 3). Altogether 67 gullies are present in the area, and 6 are sub catchment having area more than 4 sq. km. The gullies without debris flow are 31 and with debris flow are 36 (Fig. 2). The minimum area of debris flow channel is 1957 sq. m and maximum area is 242760 sq. m. The total area of debris channel is 1.178 sq. km and area of channel without debris flow is 0.56 sq. km. The total area of main channel of the Malai River is 1.81 sq. km. The maximum slope of study area is 58 degrees and maximum area is covered by the slope 10–30 degrees (Fig. 4).

The climate of study area is sub-tropical. The winter is very cold and summer is very hot. The rainfall is heavy and occasionally intense during rainy season. The average annual rainfall over the period 1986–2017 is in the range of 1400–3000 mm. More than 80 percent of rainfall occurs in rainy season. In the year 2015, the maximum 24 hours rainfall was recorded as 236.6 mm that was the highest rainfall within 24 hours since 2000. The total rainfall in three months (June, July and August) in 2015 was 1397.6 mm. The rainfall pattern in every part of study area is same.

## GEOLOGICAL SETTING

The Siwalik zone is located between two major Thrusts; Main Boundary Thrust (MBT) and Main Frontal Thrust (MFT), and is bounded by Indo-Gangetic Plain at South and the Lesser Himalayan zone at North. The Siwalik Group in the study area is lithologically divided into three units; Lower Siwalik, Middle Siwalik and Upper Siwalik in ascending order. The study area consists of two major thrusts; the Malai Thrust and the Babai Thrust. The Lower Siwalik consists of very fine to fine grained greenish grey sandstone interbedded with variegated mudstone where the proportion of mudstone dominates. The Middle Siwalik consists of medium to coarse grained thickly bedded sandstone with dark grey mudstone. The Upper Siwalik consists of well sorted pebble and cobble conglomerate with thin layer of mudstone and sandstone. The conglomerates beds are mostly clay bonded.

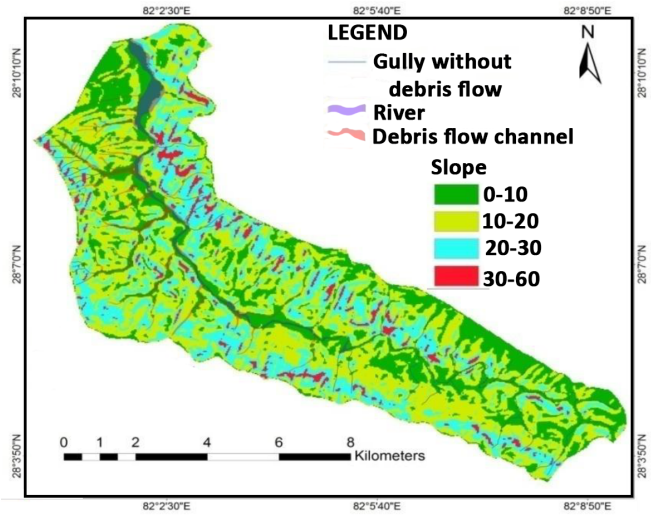


**Fig. 4: Slope map of the Malai River catchment**

## METHODS

DEM based data were used for analysis. The total length and area of debris flow were identified from the Google earth free online satellite image. Every gully with and without debris flow was traced out by polygon. The catchment area of each debris flow was measured by drawing polygon. Total area of gully and area of debris flow of each gully were identified. The debris flow inventory was prepared in the Google earth and verified in the field. Data that had been prepared in the Google earth were obtained in the Arc GIS and used to prepared a map. The origin of debris flow was studied in the field and the causative factors like slope geometry, curvature, geology and nature of gullies were studied in the field. The thrust zone was identified. Debris flow mechanism and occurrence were related with the hanging wall and foot wall of the thrust. The sub catchment of debris flow was sub divided in to source area such as transporting and depositional area. In the field, the major role of topographic factor for the debris flow occurrence was focused so that only the sensitive gully for debris flow occurrence could be selected. For the analysis of topographic factors, the certain topographical parameters, such as: watershed area, channel length, elevation different, average gradient of stream, form factor, percentage of basin area with slope angle as described by Li et al. (2015) were selected.

The form factor F was calculated using the equation developed by Li et al. (2015) as:

$$F = A / L2 \quad \text{.....(1)}$$

where, A is catchment size of each debris flow and L is the length of stream in the catchment. According to Chang (2007), under the same conditions, a watershed with a large form factor has a higher likelihood to generate debris flows.

The average gradient of a stream (J) was calculated as the ratio of the elevation difference between the slope of origin of the stream and the slope of outlet of the catchment to the stream length. For the calculation of the gradient, the stream can be divided into a number of sections, for each of which an average gradient of the stream is calculated (Eq. 2).

Average gradient of stream in the formation area of debris flow was calculated by using equation after Li et al. (2015) as:

$$J = [SUM(H_{i-1} + H_i)L_i - 2H_oL] / 1000L^2 \quad \text{.....(2)}$$

where, J is average gradient of stream, Hi is elevation of upper part of each section and H0 is elevation of lowest part of each stream. Li is the stream length of each section and L is the total length of debris flow channel.

The ratio of area of each catchment to area of potential slope (S) was measured by using DEM of 30 m resolution prepared by digitized topo map of 1:25,000 scales. The ratio of area of each slope class and area of catchment is denoted as 'S":

$$S = A/a \quad \text{.....(3)}$$

where, A = area of catchment and a = area of potential slope.

Gradient or slope of catchment plays vital role for the formation of debris flow. In general, Flow velocity of water is higher in the steep slope. Landslide and rock fall are very common phenomena in the slope >400. During heavy rainfall in the rainy season, the water having high velocity carries the deposited materials and slope cutting materials with it. So, slope is another important factor to occur debris flow.

Catchment size also determines the amount of debris flow sediment. Larger the catchment area, larger the sediments likely to be provided by landslide or any other mass movement (Li et al., 2015). The large catchment area collects large amount of water during heavy rainfall and flows with high speed towards downstream that causes higher discharge in the channel and debris flow.

Topographical factor (T) is the factor obtained from the combination of form factor, catchment size, average gradient of stream and ratio of slope class area and catchment area as after equation of Li et al. (2015):

$$T = FJS(A/a)^{0.2} \quad \text{.....(4)}$$

Every topographical factor was analysed by using linear regression. The relationship between each factor with debris flow occurrence was identified.

## RESULTS

Among the 67 gullies, debris flow event was present only in 36 gullies. But only 20 major gullies with debris flow were selected for study. The debris flow is found higher number in conglomerate bed in comparison with sandstone and mudstone (Fig. 5).

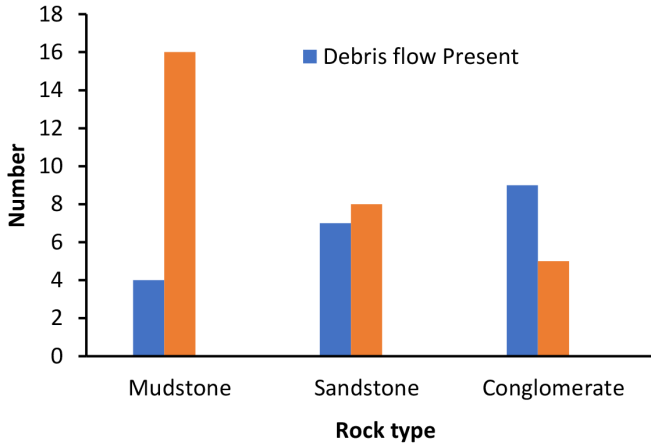


**Fig. 5: The bar diagram shows the debris flow present and absent in the associated rock type**

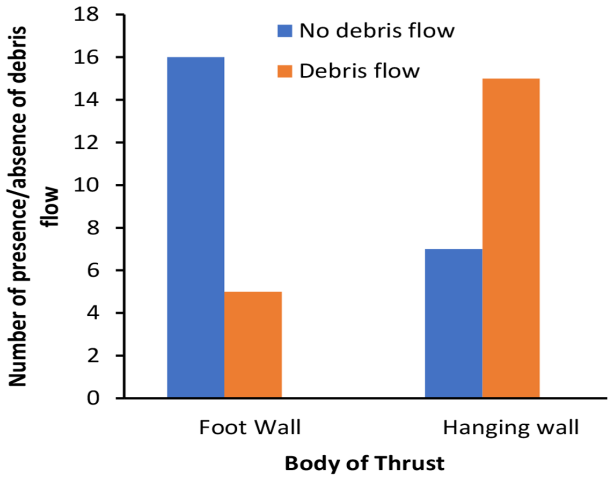


**Fig. 6: Number of debris flow present and absent in the foot wall and hanging wall of the Malai thrust**

Most of the landslides and debris flows (Fig. 3) are concentrated in the hanging wall of the Malai thrust (Fig. 6). The thrust separates the Middle and the Upper Siwaliks hanging wall from the Lower Siwalik foot wall.

Five major factors were considered for the debris flow analysis. Form factor (F), slope percentage (S), average gradient of stream (J) and topographical factor (T) (Table 1). It is considered that higher the form factor higher the discharge of water and higher the possibility of debris flow. Similarly, higher the catchment area, higher will be the flood possibility. The higher value of topographical factor is considered as the higher possibility of debris flow.

Relationship between different factors was identified by using general linear model. The relation between form factor and area slope percentage, form factor and catchment size, form factor and average gradient, average gradient and area percentage of each debris flow gullies were analysed.

It was assumed that there should be positive relation between each factor. But the relation was not satisfactory to conclude the result. Every debris flow occurred during the intense rainfall. The gullies of same topography without debris flow and with debris flow were compared. For the further verification and identification of gully-type debris flow mechanism, geological study was done.

**Table 1: Geological and topographical factors of debris flow channel, Malai Khola watershed**

| SN | Rock | Fr | A0 | A | L | F | J | S | T |
|---|---|---|---|---|---|---|---|---|---|
| 1 | Sandstone | MS | 0.020 | 0.690 | 2.17 | 0.15 | 0.110 | 0.4 | 0.006 |
| 2 | Sandstone | MS | 0.140 | 0.481 | 1.63 | 0.18 | 0.160 | 0.58 | 0.014 |
| 3 | Sandstone | MS | 0.027 | 0.356 | 1.84 | 0.11 | 0.100 | 0.55 | 0.005 |
| 4 | Sandstone | MS | 0.006 | 0.033 | 0.40 | 0.21 | 0.181 | 0.65 | 0.012 |
| 5 | Sandstone | MS | 0.063 | 0.641 | 5.64 | 0.02 | 0.360 | 0.63 | 0.004 |
| 6 | Mudstone | LS | 0.028 | 0.410 | 1.42 | 0.20 | 0.241 | 0.62 | 0.025 |
| 7 | Mudstone | Ls | 0.026 | 0.134 | 1.30 | 0.08 | 0.310 | 0.68 | 0.011 |
| 8 | Mudstone | LS | 0.242 | 2.220 | 6.90 | 0.05 | 0.420 | 0.7 | 0.016 |
| 9 | Mudstone | LS | 0.037 | 0.077 | 0.79 | 0.12 | 0.189 | 0.74 | 0.010 |
| 10 | Sandstone | MS | 0.060 | 0.280 | 2.00 | 0.07 | 0.287 | 0.72 | 0.011 |
| 11 | Sandstone | MS | 0.234 | 3.800 | 5.00 | 0.15 | 0.223 | 0.58 | 0.025 |
| 12 | Conglomerate | US | 0.107 | 2.900 | 4.45 | 0.15 | 0.123 | 0.64 | 0.006 |
| 13 | Conglomerate | US | 0.069 | 0.047 | 1.74 | 0.01 | 0.381 | 0.80 | 0.003 |
| 14 | Conglomerate | US | 0.028 | 0.068 | 0.70 | 0.14 | 0.221 | 0.82 | 0.015 |
| 15 | Conglomerate | US | 0.018 | 0.284 | 1.00 | 0.28 | 0.120 | 0.76 | 0.020 |
| 16 | Conglomerate | US | 0.026 | 0.250 | 1.50 | 0.11 | 0.090 | 0.74 | 0.006 |
| 17 | Conglomerate | US | 0.027 | 1.010 | 2.35 | 0.18 | 0.264 | 0.86 | 0.024 |
| 18 | Conglomerate | US | 0.022 | 0.220 | 1.60 | 0.09 | 0.368 | 0.76 | 0.018 |
| 19 | Conglomerate | US | 0.002 | 0.050 | 0.23 | 0.96 | 0.420 | 0.77 | 0.171 |
| 20 | Conglomerate | US | 0.032 | 0.140 | 1.13 | 0.12 | 0.112 | 0.55 | 0.005 |

Where, Fr: Formation, LS: Lower Siwaliks, MS: Middle Siwaliks, US: Upper Siwaliks, L: Length of debris flow channel, $A_0$: Area of debris flow channel, A: Area of catchment, F: Firm factor, J: Average gradient of debris channel, S: Slope area percentage, T: Topographical factor

To verify the T factors, the values of T factors of the gullies with and without debris flow were calculated and listed in Table 1. Gullies having larger debris flow event have T value greater than 0.01 and gullies having small debris flow event have T value less than 0.01. T values of gullies without debris flow were less than 0.001.

## DISCUSSION

Debris flow caused by long duration or short-term intense rainfall may be generated from landslide or several soil erosion. Takahashi (2000) studied about debris flow and concluded that landslide, bedrock erosion and natural dam destruction are three major causes to induce debris flow. In present study, slide-triggered debris flows were found negligible. Most of the debris flows occurred due to erosion of weathered bed rock and old colluvium during heavy runoff. The study area consists of weak and fragile Cenozoic, alternate layer of sedimentary rocks like mudstone, sandstone and conglomerate. The sandstone and conglomerate beds are found very weak and easily erodible in the study area.

It is found that most of the debris flow was occurred in 2015 AD. Maximum annual and 24-hour rainfall was recorded in the very same year. An earthquake of 7.8 ML was occurred in the same year. The debris flows are concentrated near and along the Malai Thrust. The earthquake may have loosened the slope material making them more unstable (Li et al., 1015).

Topographical factors were compared with geological factors. The form factor was found greater at the hanging wall than at the foot wall of the Malai Thrust. Most of the debris flows are at the hanging wall of thrust and those flows were occurred in the monsoon of 2015 after the Gorkha earthquake. The thrust can be one of major responsible factors for debris flow occurrence. Lithologically, the Middle and the Upper Siwaliks are found potential for debris flow occurrence. Mostly the gullies are formed due to continuous erosion. Erosion in the Upper Siwalik was found notable due to clay and loose cement binding conglomerate. Therefore, gully-type debris flow is common in the Upper Siwalik. The Middle Siwalik of study area consists of alternate beds of thick sandstone and thin mudstone (Bhandari and Dhakal, 2018). The weak and fragile mudstone erodes with flow of water mostly in steep slope, where sandstone beds get low support and detache from original beds generating landslides (Tamrakar and Yokota, 2008). The landslide mass flows through gully and converts in to debris flow at time of intense or continuous rainfall.

The topographical factor alone could not justify the occurrence of gully-type debris flow. If we see the result of debris flow occurrence and non-occurrence in the hanging wall and foot wall of the thrusts, debris flow occurrence in the hanging wall is higher than that in the foot wall, whereas opposite is true for non-occurrence of debris flow. The values of form factor, topographical factor, average gradient of gulley and area slope percentage are higher in hanging wall of thrust and these factors are higher in sandstone of the Middle Siwalik and Conglomerate of the Upper Siwalik.

## CONCLUSION

The rainfall conditions in the studied catchments were roughly identical during the large rainfall event. A topographic factor T is proposed as a single topographical indicator, which may be used as an indicator of the formation of gully-type debris flows. The major topographic factors related with the development of debris flows are the catchment form factor, the gradient of the stream channels, and the size of the catchments. The topographical factor T is a combination of these three factors and the area percentage of the catchment of terrain slopes between 100–600. Initiation of debris flow is also controlled by the local geological factor. Finally, the conclusion is made the Probability of debris flow to occur increases with increase of topographic factors in the thrust zone at weak sedimentary rocks. It can be concluded that the topographical and geological factors are mainly responsible for gully-type debris flow in the study area.

## REFERENCES

Akgun, A., Dag, S., and Bulut, F., 2008, Landslide susceptibility mapping for a landslide-prone area (Findikli, NE of Turkey) by likelihood frequency ratio and weighted linear combination models. Environ Geol., v. 54, pp. 1127–1143.

Bhandary, B.P. and Dhakal, S., 2018, Lithological Control on Landslide in the Babai Khola Watershed, Siwaliks Zone of Nepal. American Journal of Earth Sciences. Vol. 5, No. 3, pp. 54–6.

Catani, F., Casagli, N., Ermini, L., Righini, G., and Menduni, G., 2005, Landslide hazard and risk mapping at catchment scale in the Arno River basin. Landslides, v. 2, pp. 329–342.

Chang, T.C. and Chao, R.J., 2006, Application of back-propagation networks in debris flow prediction. Eng Geol., v. 85, pp. 270–280.

Chang, T.C., 2007, Risk degree of debris flow applying neural networks. Nat Hazards, v. 42, pp. 209–224.

Chang, T.C. and Chien, Y.H., 2007, The application of genetic algorithm in debris flows prediction, Environ Geol., v 53, pp. 339–347.

Huang, J., vanAsch, T.W.J., Wang, C., and Li, Q., 2019, Study on the combined threshold for gully-type debris ?ow early warning. Nat. Hazards Earth Syst. Sci., 19, pp. 41–51. https://doi.org/10.5194/nhess-19-41-2019

Hua-yong, N., 2015, Experimental study on initiation of gully-type debris flow based on artificial rainfall and channel runoff. AGRIS, Springer-Verlag, v. 73, no. 10, pp. 6213–6227.

Kean, J.W., McCoy, S.W., Tucker, G.E., Staley,. DM., and Coe, J.A., 2013, Runoff-generated debris flows: observations

and modeling of surge initiation, magnitude, and frequency. J Geophys Res Earth surf., v. 118, pp. 2190–2207.

Lan, H.X., Zhou, C.H., Wang, L.J., Zhang, HY., and Li, R.H., 2004, Landslide hazard spatial analysis and prediction using GIS in the Xiaojiang watershed, Yunnan, China. Eng Geol., v. 76, pp. 109–128.

Lee, S. and Pradhan, B., 2007, Landslide hazard mapping at Selangor, Malaysia using frequency ratio and logistic regression models. Landslides, v. 4, pp. 33–41.

Li, L., Yu B., Zhu, Y., Chu, S., and Wu, Y., 2015, Topographical factors in the formation of gully-type debris flows in Longxi River catchment, Sichuan, China. Environ Earth Sci, v. 73, pp. 4385–4398. DOI 10.1007/s12665-014-3722-7.

Lin, J.Y., Hung, J.C., and Yang, M.D., 2002, Assessing debris-flow hazard in a watershed in Taiwan. Eng Geol., v. 66, pp. 295–313.

Liu, C., Dong, J., Peng, Y., Huang, H., 2009, Effects of strong ground motion on the susceptibility of gully type debris flows. Eng Geol., v. 104, pp. 241–253.

Mei, H., Xiewen, H., and Kai, H., 2018, Comparative study between debris flow of wide-gentle and narrow-steep channel based on numerical simulation and prevention measures. Journal of Nepal Geological Society, 2018, vol. 55 (Sp. Issue), pp. 167–172

Ranjan, K.D., Shuichi, H., Atsuko, N., Minoru, Y., Takuro, M., and Katsuhiro, N., 2004, GIS-based weights-of-evidence modelling of rainfallinduced landslides in small catchments for landslide susceptibility mapping. Environ Geol., v. 54, pp. 311–324.

Stiny, J., 1910, Die Muren (Debris flows). Wagnerschen Univ., Buchhandlung, Innsbruck, Austria. English translation, EBA Consult., Vancouver, Canada, 199p.

Takahashi, T., 2007, Debris Flow Mechanics, Prediction and Countermeasures. Florence: Florence, KY, USA: CRC Press.

Takahashi, T., 2000, Initiation and flow of various types of debris flow. In: Wieczorek G.F. and Naeser N.D. (eds), Debris-flows hazard mitigation: mechanics prediction and assessment. Balkema, Rotterdam, pp. 15–25.

Tamrakar, N.K. and Yokota, S., 2008, Types and processes of slope movements along East-West Highway, Surai Khola area, Mid-Western Nepal Sub-Himalaya. Bulletin of the Department of Geology, Tribhuvan University, Kathmandu, Nepal, v. 11, pp. 1–4.

Tiranti, D., Bonetto, S., and Mandrone, G., 2008, Quantitative basin characterisation to refine debris-flow triggering criteria and processes: an example from the Italian Western Alps. Landslides, v. 5, pp. 45–57.

Tunusluoglu MC, Gokceoglu C, Nefeslioglu HA, Sonmez H (2008) Extraction of potential debris source areas by logistic regression technique: a case study from Barla, Besparmak and Kapi mountains (NW Taurids, Turkey). Environ Geol 54:9–22

Van Dine DF (1985). Debris flow and debris torrents in the Southern Canadian Cordillera. Can Geotech J 22:44–68

*Journal of Institute of Science and Technology*, *26*(1), 57-62 (2021)
*ISSN: 2469-9062 (print), 2467-9240 (e)*
https://doi.org/10.3126/jist.v26i1.37864


***Research Article***

# DECADAL EVOLUTION OF LANDSLIDES IN THE SIWALIK ZONE: A CASE STUDY OF BABAI WATERSHED, NEPAL

**Bharat Prasad Bhandari**[1], **Subodh Dhakal**[2*]

[1]*Central Department of Environmental Science, Tribhuvan University, Kirtipur, Nepal*
[2]*Department of Geology, Tri-Chandra Multiple Campus, Tribhuvan University, Kathmandu, Nepal*
[*]*Corresponding author: dhakalsubodh@gmail.com*

(***Received***: *January 31, 2021*; ***Revised***: *May 28, 2021*; ***Re-revised***: *June 07, 2021*; ***Accepted***: *June 08, 2021*)

## ABSTRACT

The Siwalik zone of the Nepal Himalaya is highly sensitive to landslides. The study of landslides in the catchment scale gives the basic concept of the overall landslides of the typical zone. In this study, the decadal evolution trend of the four largest landslides of the Babai River watershed was evaluated. The Landsat, Sentinel-2, and Google Earth imageries were used to obtain the physical data of the landslide from 2010 to 2019. The area, total length, and width of scar toe, and the body of landslides were obtained from the images. The rainfall data of two stations was used to evaluate the role of rainfall in the landslide development and evolution process. The trend of rainfall and area of landslides was not the same but the development process of all four landslides was more or less similar. The area of landslides fluctuated till 2014 but suddenly increased after 2015. The landslide area was highest in 2017 and moderately changed in 2018 and 2019. The landslides showed dynamic behavior in a decade with their typical expanding, widening, and reducing characters.

**Keywords:** Babai watershed, Image analysis, Landslide evolution, Siwalik, Temporal dynamics.

## INTRODUCTION

Landslide is a very common geological hazard in the Himalayas of Nepal that causes a long-term threat to the people, properties and vegetation (Devkota *et al*., 2013; Regmi *et al*., 2014; Acharya & Khadka, 2016; Gadtaula & Dhakal, 2019). Steep topography, dynamic geomorphology, inherently weak geological setting, and complex geological structures are the major contributing factors for the landslide evolution in the Himalayas of Nepal (Devkota *et al*. 2013; Regmi *et al*., 2014; Dhakal, 2015; Bhandari & Dhakal, 2021). After 2000, the torrential rainfall caused soil erosion and land degradation in the southern face of the Siwalik Hills (Bhattarai, 2015); and it has exacerbated the flood and sedimentation in the Terai (Dhakal, 2013; Pathak, 2017).

To reduce the future threat and risk, the evolution mechanism of the landslide should be identified. The Babai River catchment of the Siwalik group of Nepal has been selected for the present study. The study area lies in the western part of Nepal and a geologically small part of the Siwalik group. Politically, the area extends into three districts of Western Nepal as Bardia, Dang, and Salyan.

Previous researchers divided the Siwalik zone into the three geological divisions based on mapable lithological similarity as the Lower Siwalik, Middle Siwalik, and Upper Siwalik from bottom to top respectively (Auden, 1935). The rock found in the present study area was also divided into three geological units namely the Lower Siwalik, Middle Siwalik, and Upper Siwalik (Bhandari & Dhakal, 2018). The geological map is shown in Fig. 1.

Interbedding of fine to very fine-grained sandstone and red-purple, brown mudstone are a composition of the Lower Siwalik. The sandstone beds are weak and erodible. The mudstone along with shale is highly fractured and easily breakable. During the Monsoon period, the mudstone erodes out after the continuous effect of rainwater. The characteristics feature of the Middle Siwalik is medium to coarse-grained, thickly-bedded as pebbly-sandstone and variegated mudstone. The thin layers of mudstones are present alternatively with thickly-bedded sandstone. After the continuous interaction with water, the thin layer of mudstone undergoes physical weathering.

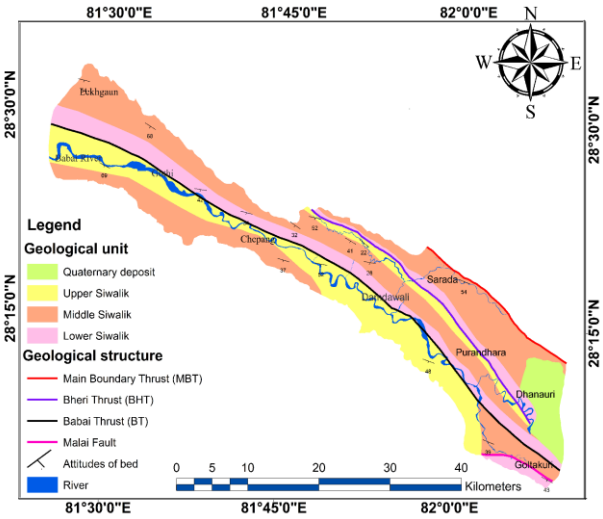


**Fig. 1. Geological map of the Babai River watershed**

After eroding the mudstone, the thickly bedded sandstone loses its support. Ultimately, the landslide (rockfall) occurs in the Middle Siwalik (Bhandari & Dhakal, 2020a). The Upper Siwalik consists of the cobble and pebble-bearing conglomerate. The conglomerates' beds are cemented with clay and mostly calcite. The cementing clay loses cohesion in the saturated state. Similarly, the calcite undergoes chemical weathering. The detached boulder, cobble, and pebble along with clay particles move down on the slope in the saturated state.

Numerous researchers (Ghimire, 2011; Devkota *et al*., 2013; Regmi *et al*., 2014; Gyawali & Tamrakar, 2018; CDES, 2016; Tamrakar *et al*., 2002; Thapa & Bhandari 2019) studied the landslide susceptibility and dynamics however, the studies lacked the evolution process of landslides. The landslides of the Babai River catchment are not inherent by road construction and human disturbance where most of the landslides naturally occurred (Bhandari & Dhakal, 2021). Studying the natural process of landslide development in the Siwalik Hills is paramount important. This research was conducted to identify the decadal evolution process and temporal mechanism of landslides on the catchment scale at the Babai watershed of Nepal. The study will be useful for the policymakers, different stakeholders of the Siwalik region, and researchers to understand the landslide and to manage for a safe settlement.

## MATERIALS AND METHODS

### Methods

As this study focused on the formation of the landslide, a series of landslide events were selected. The four largest landslides of the study area were selected for the study of evolution trends. The four largest among all landslides were selected randomly by managing the spatial variation (Fig. 2). Satellite images of those landslides were studied in the temporal series from 2010 to 2019 using Sentinel-2, Landsat-8, and Google Earth imageries. The area of each year was obtained by drawing a polygon on each image of different years. The slide surfaces, too length, scar length, the width of landslide body, and geology of four selected landslides were studied in the field. Physical characteristics of landslides, including landslide description and the other parameters contributing to the initiation of landslides were studied.

## RESULTS

Major 4 largest landslides were selected for the case study in the Siwalik group of Babai watershed. Typical features and evolution trends of each landslide are described separately.

### Case 1

This landslide (Landslide 1 in Fig. 2) lies about 2.15 km downstream from Mathillo Bharyang ridge of Bardia district. This particular area is the contact between the Lower Siwalik and the Middle Siwalik. This landslide was initiated in 2000 AD but the area of the landslide varied till the end of 2019. The slope varies from $20^0$ to $30^0$ in the total landslide area. The area has SE to SW aspect, elevation ranges from 350-372 m. The mean annual rainfall in 2014, 2015, and 2016 was similar (2446-2678 mm). The decadal physical measurement is shown in Table 1. The landslide images are shown in Fig. 3.

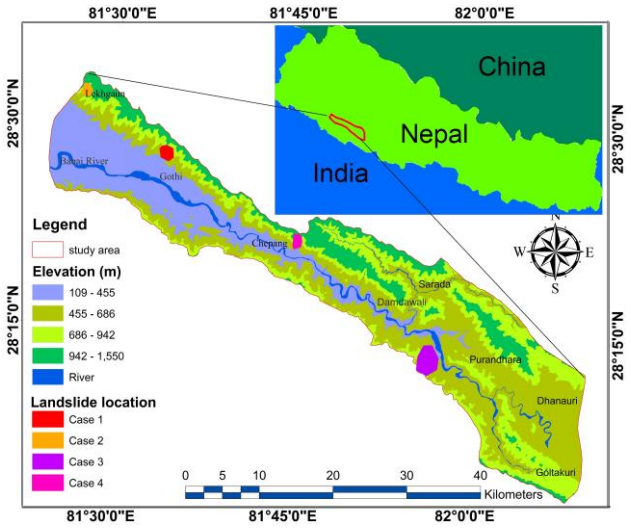


**Fig. 2. Location map of the Babai River watershed with the selected four landslides for case study**

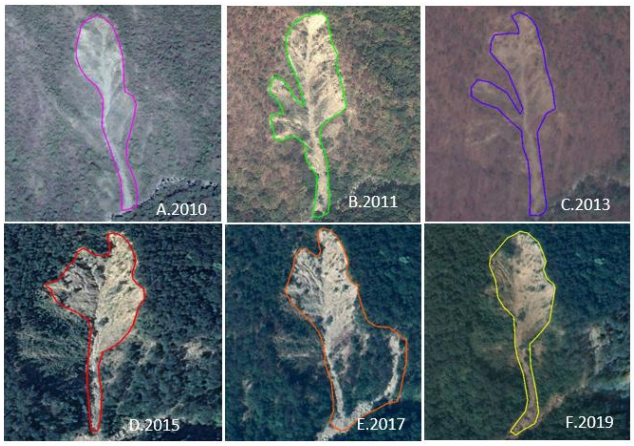


**Fig. 3. The temporal series of Google earth images show the dynamic nature of landslide (Source: Google Earth)**

### Case 2

This landslide (Landslide 2 in Fig. 2) is located 2.1 km downstream from Jumlibas hill of Bardiya district. Geologically, the area lies in the Lower Siwalik. The temporal images from 2010 to 2019 were used for landslide analysis. The annual rainfall pattern of this particular region is the same. Topographically, the slope angle varies from 25° to 40°, the aspect is the southwest,

and the elevation difference is 400 m. The landslide masses were dumped in the valley and flows down with a high discharge of water during heavy rainfall. The same landslides became active every year and no new landslides were formed before 2015 (Fig. 4). The area distribution of landslides from 2010 to 2019 is shown in Table 2.

**Table 1. The physical measurement of a landslide along with maximum rainfall within 24 hrs in the six different years**

| Year | Landslide area ($m^2$) | Length (m) | Scar length (m) | Body width (m) | Maximum rainfall within 24 hrs (mm) | Change in the area (%) |
|---|---|---|---|---|---|---|
| 2010 | 16052 | 343 | 117 | 72.5 | 112.5 | 0 |
| 2011 | 21017 | 339 | 89.3 | 82.7 | 124.5 | 30.9 |
| 2013 | 15353 | 363 | 63 | 61.2 | 187.5 | -26.9 |
| 2015 | 13846 | 368 | 132 | 114 | 263.3 | - 9.8 |
| 2017 | 31746 | 338 | 135 | 133 | 220.4 | 129.2 |
| 2019 | 18558 | 315 | 126 | 98 | 224.4 | -41.5 |

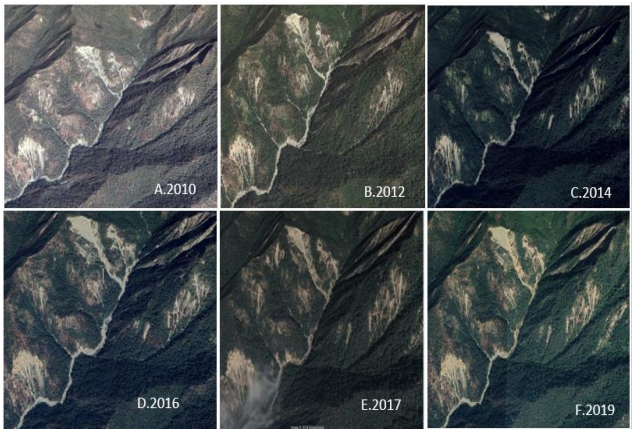


**Fig. 4. Temporal dynamics of Jumlibas landslide of Bardia from 2010 to 2019 (Source: Google Earth)**

**Table 2. Area distribution of Jumlibas landslide from 2010 to 2019**

| Year | Landslide area ($m^2$) | Change in area (%) |
|---|---|---|
| 2010 | 152790 | 0 |
| 2012 | 243517 | 59.38 |
| 2013 | 136021 | 44.41 |
| 2014 | 139241 | 2.36 |
| 2015 | 305725 | 119.5 |
| 2016 | 363195 | 18.79 |
| 2017 | 371512 | 2.28 |
| 2018 | 388199 | 4.49 |
| 2019 | 394051 | 1.5 |

### Case 3

This landslide (Landslide 3 in Fig. 2) is located in the forest of the Bangaun area of Babai valley. Geologically, the landslide lies in the Middle Siwalik. The temporal evolution of the Bangaun landslide is given in Fig. 5. The landslide was active in 2010. The area of landslide subsequently decreased in 2012. Then, the landslide advanced and widened in 2014. The area increased in 2018 but decreased in 2019. Here, the landslide showed dynamic nature during the development process. The area distribution and physical measurement of landslides are shown in Table 3.


**Fig. 5. The images of the landslide from 2010 to 2019** (Source: Google Earth)

### Case 4

This particular landslide (Landslide 4 in Fig. 2) is called the Gidde landslide and is located at the boundary of the Salyan and Bardia district. This huge catastrophic landslide occurred on 7-28-1992 at midnight. The Babai thrust passes through it (black line in Fig. 6). The Gidde landslide is located at the hanging wall of the Thrust. The sliding surface has a slope greater than 45°, elevation 1340 m, aspect S, SW, and geologically at Middle Siwalik (Fig. 6). The landslide started with a huge rockfall, then slided to the downslope, and finally converted into a debris flow. The huge amount of debris deposited at the

toe of landslides was carried out by flowing water through the narrow valley and finally deposited at the bottom of the slope in terms of talus cone and alluvial fan.

**Table 3. Year-wise area distribution of Bangaun landslide**

| Year | Area ($m^2$) | Area changed (%) | Length (m) | Toe width (m) | Scar width (m) | Body width (m) |
|---|---|---|---|---|---|---|
| 2010 | 37896 | 0 | 256 | 262 | 229 | 201 |
| 2012 | 26988 | 28.78 | 151 | 196 | 196 | 104 |
| 2014 | 35517 | 31.6 | 143 | 170 | 170 | 119 |
| 2015 | 37384 | 5.2 | 189 | 164 | 164 | 114 |
| 2017 | 34457 | 8.5 | 224 | 191 | 191 | 153 |
| 2019 | 31751 | 7.8 | 215 | 153 | 153 | 142 |

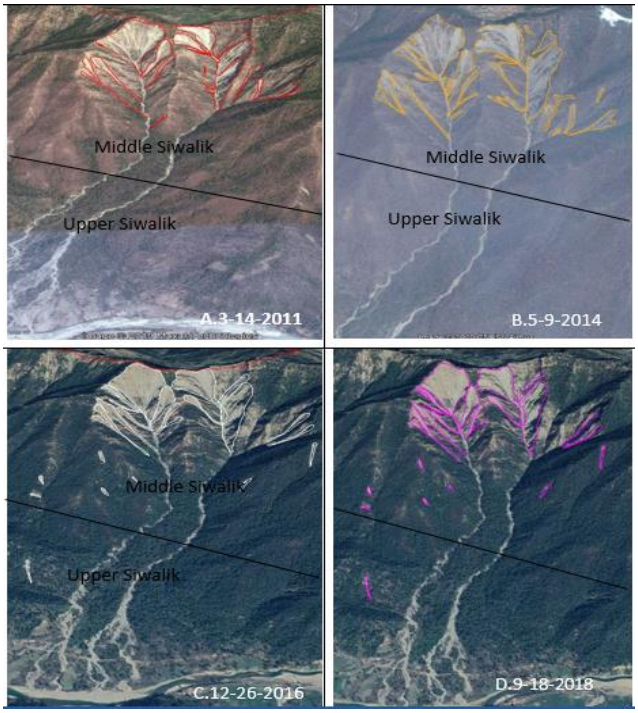


**Fig. 6. The evolution of landslide of Gidde Khola from 2011 to 2018, black lines in the figure represent the Babai thrust**

The landslide showed both active and inactive nature but the area of the total landslide was the highest in 2015. The slope surface consists only of bedrock predominantly sandstone. But there exists a thin layer of mudstones between thick layers of sandstone. The area of the landslide from the year 2011 to 2019 is presented in Table 4.

## DISCUSSION

In the year 2010, the area of landslide 1 was 16052 $m^2$ but in 2011 the landslide widened towards the west though the total distance between toe and scar was similar. The area of landslide in March 2015 was only 13846 $m^2$ but in September 2016 the area was 31746 $m^2$. The landslides widened towards the east but there was no change in scar and toe length. The area increased by 2.29 times in 2016 compared to in 2015, whereas the area was 31746 $m^2$ in 2017. The landslide reactivated and some new landslides were generated nearby the major landslide. But the total area of landslides in August 2019 was 18588 $m^2$. The area decreased by 0.58 times in 2019. The mean annual rainfall in 2014, 2015, and 2016 was similar (2446-2678 mm) but the area of the landslide changed simultaneously. This landslide is located at the boundary between the Lower Siwalik and Middle Siwalik. In the Siwalik Hills, the contact between two geological units is weak and fragile due to which the landslide may occur even in the situation of less amount of rainfall if it is continuous.

**Table 4. The area and rainfall dynamics of the Babai River catchment**

| Year | Area ($km^2$) | Change in the area (%) | Maximum rainfall within 24 hrs (mm) |
|---|---|---|---|
| 2010 | 0.34 | 0 | 46 |
| 2012 | 0.42 | 23.52 | 65 |
| 2014 | 0.38 | -9.5 | 112 |
| 2015 | 0.48 | 26.31 | 136 |
| 2017 | 0.43 | -10.41 | 118 |
| 2019 | 0.35 | -18.6 | 106 |

In the case of landslide 2, the landslides became active every year and no new landslides were formed before 2015. From 2010 to 2014, the area of the landslides slightly fluctuated but there was a sudden increase in the total area in 2015. The new landslides originated in 2015, 2016, 2017 & 2018. On 14$^{th}$ February 2015, the total area of landslides was 192321 $m^2$ but on 19 December 2015, the total area of landslides was 305725 $m^2$. Similarly, in 2016 the area became 363198 and further increased in 2019 and reached 388199 $m^2$. The landslides became more active after 2015. Landslide 3 was active in 2010. The area of landslide subsequently decreased in 2012. Then, the landslide advanced and widened in 2014. The area increased in 2018 but decreased in 2019. Here the

landslide showed dynamic nature during the development process. Landslide 1 and landslide 4 lies in the boundary between Lower and Middle Siwalik. Similarly, landslide 2 and landslide 4 are located on the thrust zone. According to Bhandari and Dhakal (2021), the thrust zone mainly hanging wall is more sensitive for the landslide in the Siwalik Hills.

Bhandari and Dhakal (2018) signified the geological control on the landslides in the same study area. The long-term rainfall in the monsoon period makes the soil saturated. After the higher saturation, the soil loses cohesion, and ultimately, it begins to slide down (Bhandari & Dhakal, 2020b). The soil composition also plays a major role on landslides in the rainy season. The proportions of sand, silt, and clay compositions are highly responsible for landslides during the saturation stage (Yalcin, 2011; Bicocchi, 2019; Bhandari & Dhakal, 2020b). The result shows that the mechanism of landslide does not depend upon the amount of rainfall but depends on the long-term rainfall. Bhandari & Dhakal, (2020a) concluded that long-term rainfall is more sensitive for landslides in the Siwalik Hills. The overall trend of landslide development in the four landslides shows that the landslide development process is dynamic in the study area.

## CONCLUSION

The evolution trend of four landslides selected for this case study of the Babai River watershed was analyzed in detail. The data from 2010 to 2019 was obtained from satellite imageries of Google Earth, Sentinel-2, and Landsat. The evolution trends of four landslides were similar. The result showed that the landslides of the Siwalik zone are quite dynamic in nature that changes the geometry and area for a time. A favorable relationship exists between the slope and geology along with the sliding surface. Among the four case studies, landslides did not evolve directly due to the effect of intense rainfall. The initiation and development of the landslide process were similar for all four landslides. The area of landslides increased after 2015 and fluctuated till 2019. A sudden increment of the area of a landslide after 2015 could be due to the impact of the 7.8 ML Gorkha earthquake. The study concluded that the large-sized landslide occurred in the Siwalik hill without significant instance rainfall. A small but continuous rainfall in the rainy season also caused a large size landslide.

## REFERENCES


Acharya, S., & Khadka, U. (2016). Loss of tree biomass in Jure landslide, Sindhupalchowk, Nepal. *Journal of Institute of Science and Technology*, 21(1), 65-70.

Auden, J. B. (1935). Traverses in the Himalayas. *Geological Survey of India*, *69*, 123-167.

Bhandari, B. P., & Dhakal S. (2020a). Compositional analysis and phase relationship of soil mass from the active landslides of Babai River watershed, Siwalik zone of Nepal. *Engineering Geology*, https://doi.org/10.1016/j.enggeo.2020.105851

Bhandari, B. P., & Dhakal S. (2020b). Spatiotemporal dynamics of landslide in the sedimentary terrain: A case of Siwalik zone of Babai watershed, Nepal. *SN Applied Sciences*, *2*, 854. https://doi.org/10.1007/s42452-020-2628-0

Bhandari, B. P., & Dhakal, S. (2018). Lithological control on landslide in the Babai Khola watershed, Siwaliks zone of Nepal. *American Journal of Earth Sciences*, *5*, 54-64.

Bhandari, B. P., & Dhakal, S. (2021). A multidisciplinary approach of landslide characterization: a case of the Siwalik zone of Nepal Himalaya. *Journal of Asian Earth Sciences: X*, *5*, 100061. https://doi.org/10.1016/j.jaesx.2021.100061

Bhattarai, T. N. (2015). Flood events in Gangapur village, Banke district: an example of climate change-induced disaster in Nepal. *Journal of Institute of Science and Technology*, 19(1), 79-85.

Bicocchi, G., Tofani, V., D'Ambrosio, M., Tacconi-Stefanelli, C., Vannocci, P., Casagli, N., Lavorini, G., & Catani, F. (2019) Geotechnical and hydrological characterization of hillslope deposits for regional landslide prediction modeling. *Bulletin of Engineering Geology and Environment*, *78*, 4875-4891.

CDES. (2016). *Landslide inventory characterization and engineering design for mitigation works of Chure area in ten districts*. Central Department of Environmental Science, Tribhuvan University and Government of Nepal, Chure-Tarai Madhesh Conservation Development Board, Kathmandu.

Devkota, K. C., Regmi, A. D., Pourghasemi, H. R., Yoshida, K., Pradhan, B., Ryu, I. C., Dhital, M. R., & Althuwaynee, O. F. (2013). Landslide susceptibility mapping using certainty factor, index of entropy, and logistic regression models in GIS and their comparison at Mugling-Narayanghat road section in Nepal Himalaya. *Natural Hazards*, *65*, 135-165 (2013).

Dhakal, S. (2015). Evolution of geomorphologic hazards in Hindu Kush Himalaya, In Shaw, R. & Nibanupudi, H. K. (Eds.), *Mountain Hazards and Disaster Risk Reduction* (pp. 53-72), Japan: Springer. https://doi.org/10.1007/978-4-431-55242-0_4

Dhakal, S. (2013). Flood hazard in Nepal and new approach of risk reduction. *International Journal of Landslide and Environment*, *1*, 13-14.

Gadtaula, A., & Dhakal, S. (2019). Landslide susceptibility mapping using weight of evidence method in Haku, Rasuwa district, Nepal. *Journal of Nepal Geological Society*, *58*, 163-172.

Ghimire, M. (2011). Landslide occurrence and its relation with terrain factors in the Siwalik hills, Nepal: a case study of susceptibility assessment in three basins. *Natural Hazards*, *56*(1), 299-320.

Gyawali, P., & Tamrakar, N. (2018). Landslide susceptibility assessment of the Chure Khola Catchment area of the Siwalik region, Central Nepal. *Journal of Nepal Geological Society*, *56*(1), 19-30.

Pathak, D. (2017). Delineation of groundwater potential zone in the Indo-Gangetic plain through GIS analysis. *Journal of Institute of Science and Technology*, *22* (1), 104-109.

Regmi, A. D., Devkota, K. C., Yoshida, K., Pradhan, B., Pourghasem, H. R., Kumamoto, T., & Akgun, A. (2014). Application of frequency ratio, statistical index, and weights-of-evidence models and their comparison in landslide susceptibility mapping in central Nepal Himalaya. *Arab Journal of Geosciences*, *7*, 725-742.

Tamrakar, N. K., Yokota, S., & Osaka, O. (2002). A toppled structure with sliding in the Siwalik hills, midwestern Nepal. *Engineering Geology*, *64*(4), 339-350.

Thapa, D., & Bhandari, B. (2019). GIS-Based frequency ratio method for identification of potential landslide susceptible area in the Siwalik zone of Chatara-Barahakshetra section, Nepal. *Open Journal of Geology*, *9*, 873-896.

Yalcin, A. (2011). A geotechnical study on landslides in the Trabon Province, NE Turkey. *Applied Clay Science*, *52*, 11-19.

# Lithological Control on Landslide in the Babai Khola Watershed, Siwaliks Zone of Nepal

**Article** · January 2018

CITATIONS
21

READS
1,111

**2 authors:**

Bharat Prasad Bhandari
Tribhuvan University
**15** PUBLICATIONS **84** CITATIONS
SEE PROFILE

Subodh Dhakal
Tribhuvan University, Department of Geology
**53** PUBLICATIONS **255** CITATIONS
SEE PROFILE

**American Journal of Earth Sciences**
2018; 5(3): 54-64
http://www.openscienceonline.com/journal/ajes
ISSN: 2381-4624 (Print); ISSN: 2381-4632 (Online)

Open Science

# Lithological Control on Landslide in the Babai Khola Watershed, Siwaliks Zone of Nepal

Bharat Prasad Bhandari[1, *], Subodh Dhakal[2]

[1]Central Department of Environmental Science, Tribhuvan University, Kathmandu, Nepal

[2]Department of Geology, Tri-Chandra Campus, Tribhuvan University, Kathmandu, Nepal

## Email address

bbhandari@cdes.edu.np (B. P. Bhandari)

[*]Corresponding author

## To cite this article

Bharat Prasad Bhandari, Subodh Dhakal. Lithological Control on Landslide in the Babai Khola Watershed, Siwaliks Zone of Nepal. *American Journal of Earth Sciences.* Vol. 5, No. 3, 2018, pp. 54-64.

**Received**: May 5, 2018; **Accepted**: June 18, 2018; **Published**: July 24, 2018

## Abstract

Sub-Himalayan zone also called Siwalik is located between the Main Boundary Thrust (MBT) at north and the Main Frontal Thrust (MFT) at south. As a consequence of lithospheric plate dynamic between the Indian and Tibetan plate, the young and fragile sedimentary rock of the Siwaliks area are highly weathered and highly deformed. The Siwaliks range is made up of geologically very young sedimentary rocks such as mudstones, shale, sandstones, siltstones and conglomerates, due to such young and weak geological condition, trend of occurring different types of landslide is higher in the Siwaliks zone. Present study was conducted in Babai Khola watershed of Mid-Western Nepal to find the landslide distribution in different geological formations and to identify the lithistratigraphic control for landslide occurrence. Landslide inventory map was prepared by using Google Earth pro, 2017 and Arc. GIS 10.3, and it was verified by several field survey. Geological map was prepared in the field by detailed study of Lithostratigraphy and geological structures. Loosening of cementing materials in conglomerate is found the major cause of debris fall; block slide and gulley erosion in the Upper Siwaliks. Red clay cementing materials of conglomerates undergoes weathering and makes the gravel loose and fragile. Highly weathered and easily erodible mudstone beds between thick sandstone beds are responsible for landslide in the Middle Siwaliks. The mudstones in the Lower Siwaliks are highly to completely weathered, which are in the form of residual soil in the surface at many places. These are less permeable but can be easily eroded by rain action due to soft nature. The eroded masses are soluble with water and moved through erosional gullies. So that, several gully erosion, erosion induced landslide, mud flow and mud slide were occurred in Lower Siwaliks. Total 867 landslides are identified in the study area. Among them 101 landslides are observed in Lower Siwaliks, 575 in Middle Siwaliks and 191 in Upper Siwaliks. Landslide density is found higher in Middle Siwaliks. Landslides are found majorly controlled by lithology in the study area.

## Keywords

Siwaliks, Lithology, Landslide

## 1. Introduction

Landslides are natural hazards which occur due to different triggering factors like rainfall, slope, geological conditions, earthquake etc. Landslides are amongst the most damaging natural hazards in Nepal. Nepal is facing the several problems of landslide each year during monsoon period with huge loss of life and properties. Many people become homeless and lose their lives every year due to landslides. Landslides are common natural hazard for all the continents due to that there social and economic impacts can be tremendous and widespread. Each year the death caused by landslide is increasing in many countries. In Nepal, between 1971 to 2016 landslides have caused 3246 casualties, comprising 4980 deaths, 174 missing and 1871 injured [1]. It represents an average of 112 deaths or missing parsons each year. This value is greater than the death caused by flood and other disasters in Nepal. In Nepal since 2015 -2016 the direct and indirect cost of the damages caused by landslides is Rs.811,084,600.

Analyzing the data of 2015-2016, landslides have caused 290 casualties, 276 deaths, 42 missing and 226 injured.

There are various factors which are responsible for landslide occurrence. Different variables (intrinsic and extrinsic) are responsible for landslide including elevation, geomorphology, bedrock geology, engineering properties of soil, soil thickness, slope aspect and so on. Probability of landslide occurrence is higher in to the highly weathered, highly fractured and weak rocks. The mechanism of landslide is widely studied topic but the major factors for landslide occurrence are concluded that the amount of rain fall, nature of slope materials, discontinuities and weathering [2-7]. Weathering and slope materials are depend on the lithology and lithostratigraphy. Water infiltration is a significant triggering factor for slope failures around the world. Intense rainfall can trigger landslides, floods and secondary floods (stagnancy of rain on low permeability surfaces) that could result in damage and fatalities [8]. Lithostratigraphical analysis depends on the lithological (compositional) analysis of rock body and stratigraphical sequence of strata. Some minerals like feldspar and mica undergoes chemical weathering and may cause the landslide. The stability of rock on the slope depends on the mineral present, bonding mechanism of the mineral, chemical properties of mineral, weathering behaviors of mineral. Due to variable strength and weathering behaviors, different rock types behave differently with respect to the landslide occurrence [9, 10].

The Sub Himalayan zone also called Siwaliksis youngest Himalaya of the Himalayan series. This zone is located between Lesser Himalaya in north and indo-Gangetic plain in South. Tectonically, the Siwaliks zone is bounded by Main Frontal Thrust (MFT) in the south and Main Boundary Thrust (MBT) in the north. Siwaliks comprised of fluvial sediments, which were deposited as a result of Neogene tectonics of the Himalaya [11-14]. It is the youngest Himalaya of the Himalayan series which is made up of geologically very young sedimentary rocks such as mudstones, shale, sandstones, siltstones and conglomerates due to such young and weak geological condition, trend of occurring different types of landslide is higher in Siwaliks zone [15]. Due to weak geological condition and adverse lithostratigraphic situation, problem of landslide occurring is increasing day by day in Siwaliks region. Situated entirely in the Himalaya, Nepal suffers from tremendous landslide disaster problems every year, and a great number of people are affected by large- and small-scale landslides throughout the country, especially during monsoon periods [7]. The landslide occurs and reactivates with the starting of monsoon in the Nepal Himalaya.

The rocks of Siwaliks zone are majorly sandstone, mudstone and conglomerate. On the basis of lithology and dominancy of rock type, the Siwaliks are divided into different lithological units. Each type of rocks are very weak and fragile [16-25, 11, 14, 10]. Possibility of landslide hazard is more in to the tectonically weak and fragile Siwaliks [15, 26, 27]. The main objective of this study is to identify the lithological control for landslide occurrence in the Siwaliks region through inventory based analysis. Lithostratigraphic controls on Landslide occurrence is new topic to relate the previous studies and to know the role of lithology for landslide mechanism. The main purpose of the study is to establish the relation between lithostratigraphy and landslide in the Siwaliks region of Nepal.

## 2. Materials and Methods

### 2.1. Study Area

The study area falls in four districts of Mid Western Development region (Figure 1a & 1b). The Babai River is east-west trending river originated from Siwaliks and located between $27^0$57'59.03"N, $82^0$33'42.80"E at east, $28^0$28'30.14" N, $81^0$28'30.14"E at west, $28^0$12'47.90"N, $82^0$15'46.08" at north and $28^0$01'03.89"N, $82^0$12'39.61"E at south. Total area covered is 1952 $m^2$ and perimeter is 316636 m. The study area is highly prone to landslide.


a)

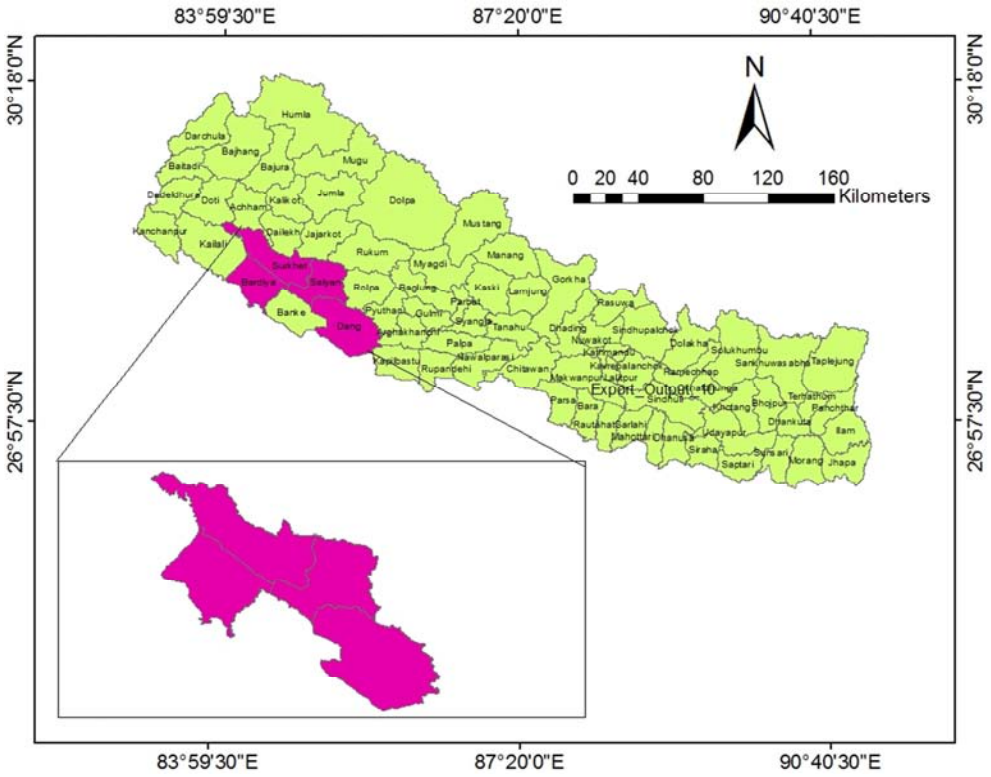


b)

***Figure 1.*** *a) Study area in Google map b) Study area in Physiographic map.*

The study area contains one intermountain valley called Dang (Dun) valley. It is an oval shaped valley with the length of about 50 km and width of about 17 km and is filled up by the Quaternary fluvial sediments deposited essentially by the north-south flowing rivers [10]. The Siwaliks have altitudes ranging from 500 m to 1500 m and exhibit a very rugged topography with highly dissected gullies and steep slopes. Most of the mountain ridges in the study area extend in the east-west direction, parallel to the main geological structures. The landforms of the study area are mainly controlled by the tectonic processes and subordinately by mass wasting and weathering. The erosional landforms predominate over the depositional ones. There are rugged hills, numerous deep gorges, steep slopes, cliffs, and active gullies representing the erosional landforms, whereas river terraces, alluvial fans, and talus cones are the examples of depositional landforms.

### 2.2. Methods

Landslide inventory map was prepared by using Google earth pro 2017. Inventory was prepared by drawing polygon on the past landslides. Polygons were drawn from scar to toe. The scar area and deposit area are separated. The landslide database of different types of landslide was prepared. The size and area of landslide was calculated. The inventory map was verified in the field. The major bodies of landslides were measured manually in the field. Major causes of landslide occurrence, landslide materials, groundwater condition, slope condition, vegetation status, rock and soil type and soil thickness were studied in the field. The thickness of bed, condition of joints, and orientation of bed rock with respect to slope were studied in the field. The longitude, latitude of each landslide was measured for further verification of inventory map. Way of landslide distribution, effects of thrust, effect of geological contact, and mechanism of cluster landslide were analyzed in field. Geological study was conducted together with the study of lithology, stratigraphy, genetic classification of soil, geological structures and rock weathering. Lithological study was carried out in the field by direct observation and using magnifying lens. Geological formations were separated on the basis of three fold classification adopted by previous researchers. Landslide characterization was done on the basis of shape, size, type, geology and material. Stratigraphy of area is separated by preparing geological map in 1:25,000 scales. Landslide mechanism was studied on the basis of lithology and stratigraphical sequence. Landslides are classified according to existing classification system [28]. Total length, area and perimeter of the landslides are measured in Arc. GIS.

## 3. Results

### 3.1. Lithostratigraphy of the Study Area

Lithostratigraphic study was carried out by detail study of rock unit, lithology and rock strata. Taking the reference of previous literatures, the rocks of study area is divided in to three Formations [16, 18, 19]. From bottom to top they are Lower Siwaliks, Middle Siwaliks and Upper Siwaliks respectively.

*Lower Siwaliks*

Lower Siwaliks consists of interbedding of fine to very fine grained grey green sandstone and red purple brown mudstone (Figure 2). Mudstone bed is medium to thick, highly fractured and highly weathered. Sandstone bed is of thinly bedded and spheroidically weathered (Figure 3). The minerals present in sandstone are Quartz, Muscovite, Biotite and Feldspar but presence of Muscovite is higher. The rocks of Lower Siwaliks are well exposed in to Phulbari area of Tui Khola section, Upper part of Malai Khola section and Babai valley section.

***Figure 2.*** *Varigated mudstone bed of Lower Siwaliks exposed in to Fulbari of Tuikhola Valley, dang.*

***Figure 3.*** *Spheroidally weathered sandstone interbedded with mudstone from Lower Siwaliks on the Dang-Nepalgunj road section.*

*Middle Siwaliks*

Middle Siwaliks consists of medium to course grained thickly bedded salt and pepper as well as pebbly sandstone and variegated mudstone (Figure 4). Sandstone beds are massive, less compact and weathered due to poor intergranular bonding. The sandstone of Middle Siwaliks consist Quartz, Feldspar, Muscovite and Biotite. The bed of Sandstone is thicker than Mudstone. The thickness of Sandstone bed varies from 30 cm to 2.4 m whereas thickness of mudstone bed varies from 7 cm to 32 cm.

***Figure 4.*** *Exposure of Middle Siwaliks at Harre of Surkhet, along the road section.*

*Upper Siwaliks*

Upper Siwaliks consists of cobble and pebble bearing conglomerate (Figure 5) interbedded with yellow to brown mudstone. The cementing material of conglomerate is calcite and mostly clay. The size of clast in conglomerate varies from 5 mm to 10 cm.

***Figure 5.*** *Conglomerate with cementing material Calcite observed at Salghari Gaun of Salyan.*

## 3.2. Landslide Number and Area-Frequency

The study area is divided into four different sections (Dang section, Salyan section, Surkhet section and Bardiya section). Dang valley has excluded in this study. All together 867 landslides has identified with total 893 $Km^2$ area (Figure 6). The area of total catchment of Babai Khola is 1722 $Km^2$ among them 829 $Km^2$ has occupied by Dang valley. The area of landslides varies from 52.479 $m^2$ to 517601.94 $m^2$. Total area covered by landslides is 4.378 $Km^2$. The overall landslide density of study area is 0.49%. The landslides density has increased towards western part of study area due to double thrusting effect of Babai Thrust and Bheri Thrust. The effect of stress accumulated due to both thrust (trending north and extended east-west) has seen clearly due to that the area is fragile and very weak. The concentration of landslide

has not observed in particular rock unit though they are dispersed in different rock unit. But the number and landslide density are varied in to different rock units. Mostly the landslide density is higher in sandstone, stratigraphically in Middle Siwaliks. Among the 867 landslides, Lower Siwaliks consist of 101, Middle Siwaliks consist of 575 and Upper Siwaliks consist of 191 landslides (Figure 7).

The abundance of stiff slope is one of the main factors that influence landslide activity. In the study area stiff slopes are associated with thick and weak sandstone bed alternate with thin mudstone beds of Middle Siwaliks. So, area covered by landslide is higher in Middle Siwaliks.

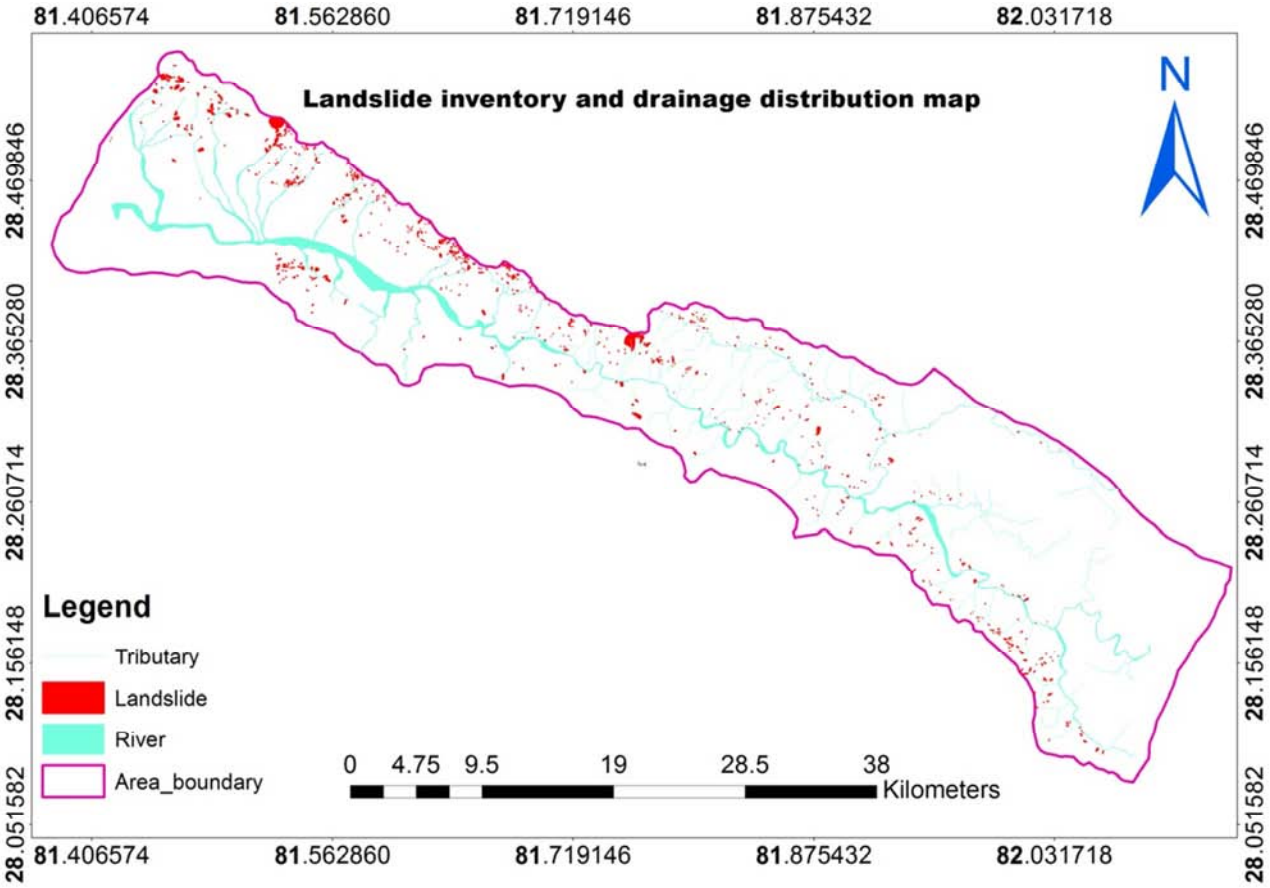


***Figure 6.*** *Landslide inventory map of study area.*

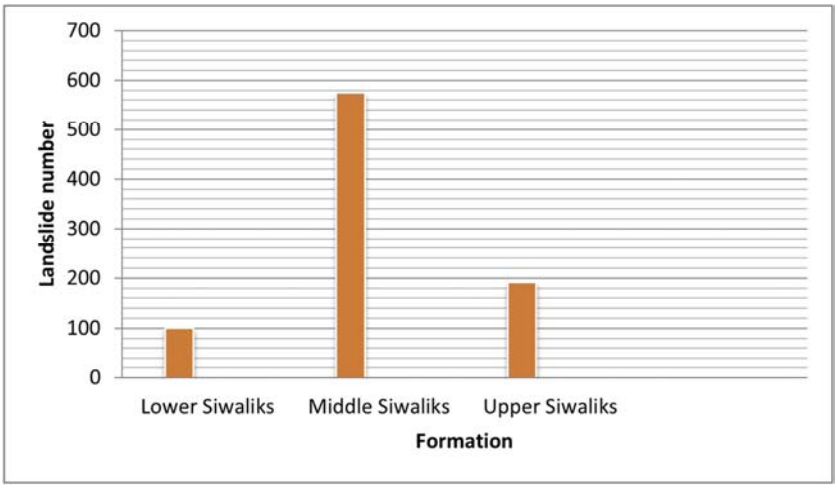


***Figure 7.*** *Landslide distribution in different formations.*

## 3.3. Landslides in Different Siwaliks Section

In lower Siwaliks, the rocks are mainly mudstone and sandstone. Thin layer of sandstones are interbedded with thick bed of mudstone. In the study area, most of the mudstone beds are highly weathered and decomposed.

Sandstones are weak and spheroidically weathered. Due to that those weathered and weakly composited rocks undergoes mud slide, debris flow, rock slide and erosion induced landslide (Figure 8). In Middle Siwaliks, sandstone beds are of course grained, less compacted and massive. There is very weak intergranular bonding in sandstone beds. The permeability of sandstone is high. Due to that the rain water can easily penetrate the weak and permeable sandstone. It causes the low friction angle and makes easy to slide. Similarly, the sandstone consists of feldspar, mica and quartz. The feldspar undergoes chemical weathering which is another major cause of landslide in Middle Siwaliks. There exist thin layer of weak mudstone between thick sandstone beds. When mudstone beds undergoes weathering and eroded out, the sandstone beds are unable to bears their own load and slide down. The major landslide types of the Middle Siwaliks are rock fall, debris fall, debris slide and complex (Figure 9). There exist thin layer of weak and loose mudstone between conglomerate beds in Upper Siwaliks. The weak and loose mudstone erodes out in heavy rain. After eroding the mudstone, the conglomerate beds separate and sliding down which causes block slide, block fall and debris fall (Figure 10). Similarly, the cementing material is very weak in conglomerates. In most of the study area, the cementing material in conglomerate is clay. In rainy season, the clay becomes soft and erodes by water which causes the separating of pebbles and clasts from conglomerates (Figure 11).

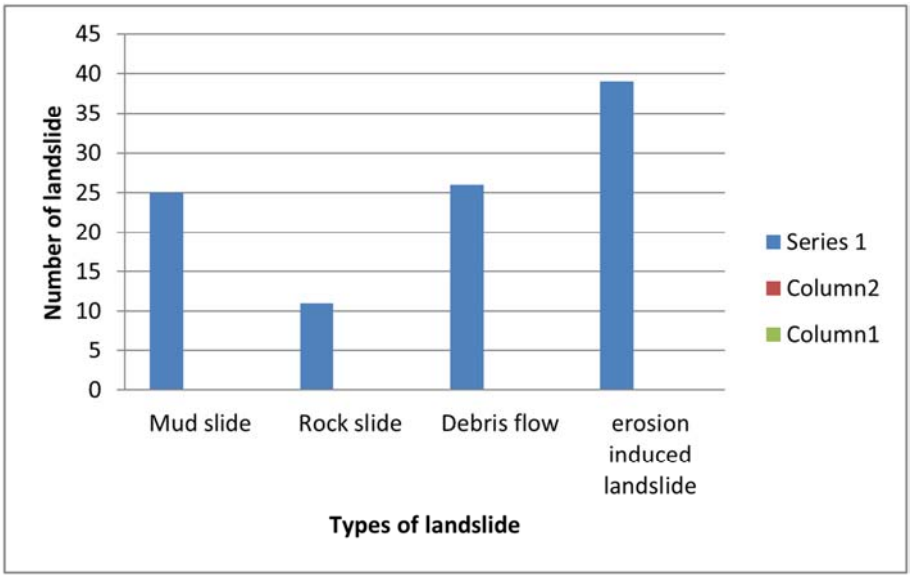


***Figure 8.*** *Landslide type distribution in Lower Siwaliks.*

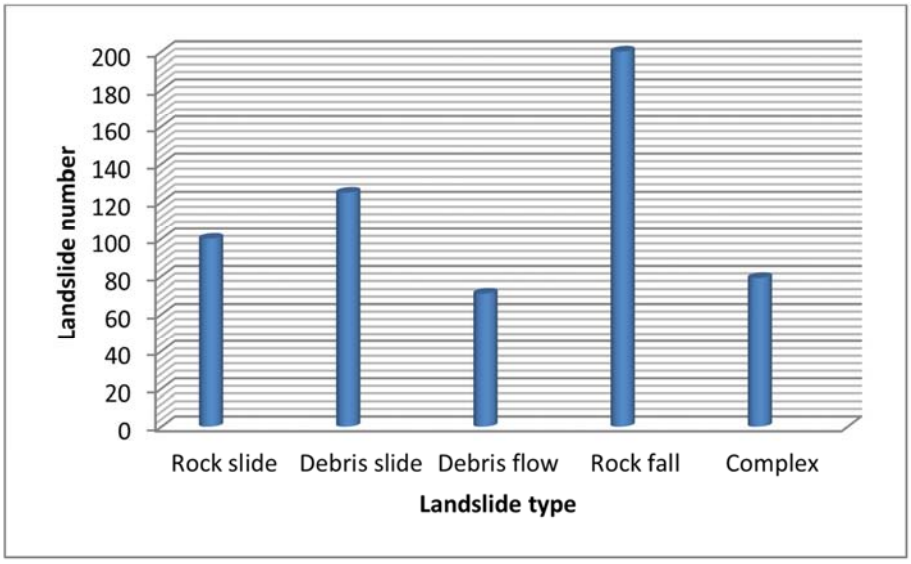


***Figure 9.*** *Landslide type distribution in Middle Siwaliks.*

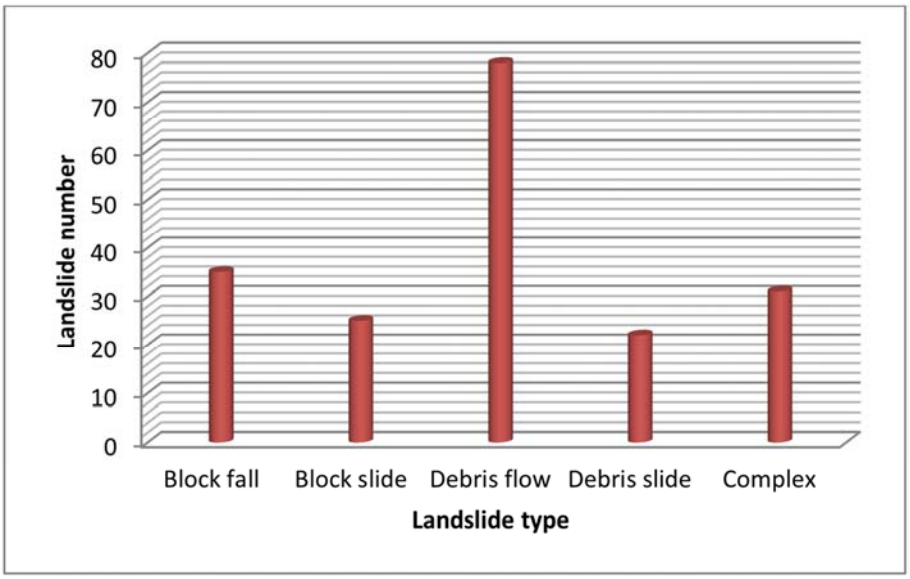


***Figure 10.*** *Type distribution of Landslide in Upper Siwaliks.*

***Figure 11.*** *Landslide in conglomerate observed near BabaiBridge at Babai Valley, Surkhet.*

## 3.4. Landslide Frequency Area Distribution

The overall distribution of landslide shows that the mean area of landslide is 5050 $m^2$ and maximum frequency of landslide size varies between1000 $m^2$ to 10000 $m^2$ (Figure 12). However there are lithostratigraphic differences: size frequency of landslide for Lower Siwaliks and Upper Siwaliks is maximum between 100 $m^2$ to 1000 $m^2$ while those in Middle Siwaliks is between 1000 $m^2$ to 10000 $m^2$ (Figure 13). The cumulative frequency curve (Figure 14) shows that the slope of middle is stiffer up to 550 and became slightly gentle beyond 550.

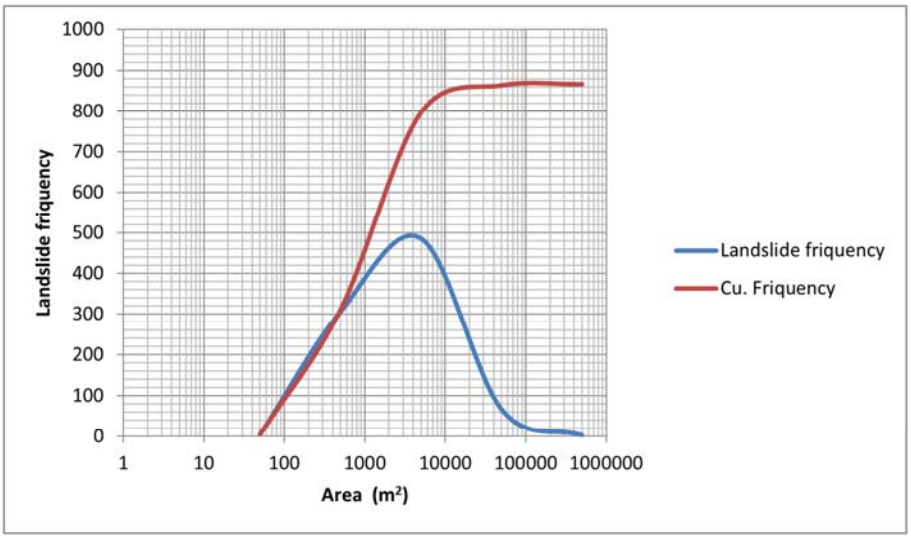


***Figure 12.*** *Landslide area- frequency distribution of study area.*

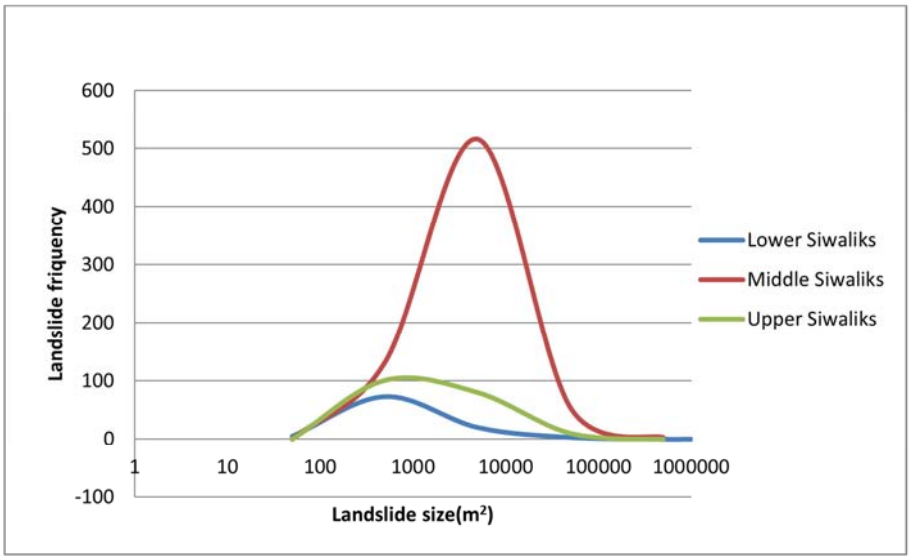


***Figure 13.*** *Landslide area- frequency distribution in different geological formations.*

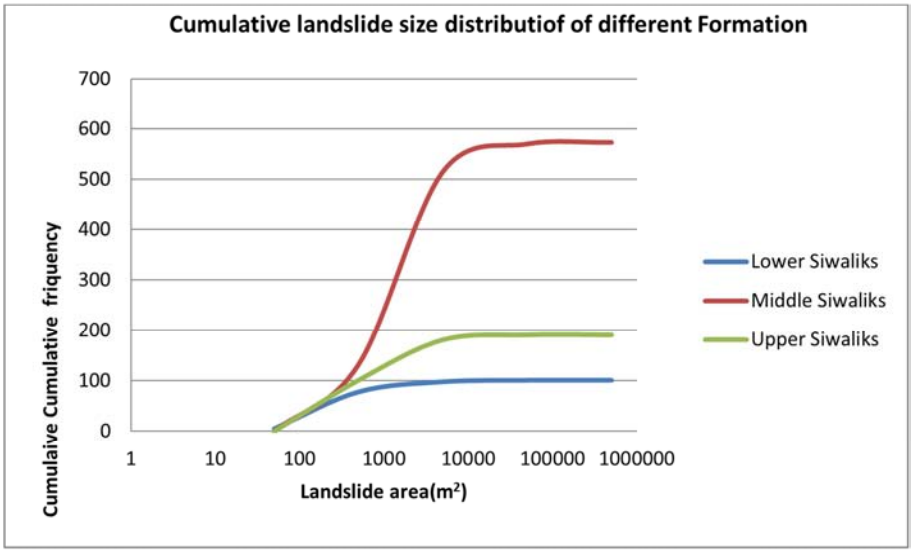


***Figure 14.*** *Cumulative landslide size distribution in different geological formation.*

As per the result of landslide distribution in the different rock units, number of landslides is higher in Middle Siwaliks. Both landslide frequency and landslide size frequency are greater in Middle Siwaliks. Rock avalanche (fall) is highest in number at Sandstone (Middle Siwaliks) beds. The maximum size distribution of landside is ranges between 1000 $m^2$ to 10000 $m^2$ which belongs to the Middle Siwaliks. Lithological condition of Middle Siwaliks is supporting for landslide occurrence. The thin layer of mudstone between thick sandstone beds is highly erodible due to its fragile and weak nature. The mudstone beds undergo physical and chemical weathering and erode easily during heavy rain. After the erosion of mudstone beds, the thick sandstone beds loose support and slide or fall down due to gravity action and reduction of friction at higher elevation. The mechanism results the rock avalanche (fall and slide) in Middle Siwaliks. Erosion induced landslides are dominated in the Lower Siwaliks. Lithologically, the Lower Siwaliks consists of variegated mudstone and thin layer of sandstones. The mudstone beds are highly weathered and easily erodible. The soil thickness is more in Lower Siwaliks. During heavy rain, the sandstone beds erode out. The land sliding process begins from erosion and induces to shallow landslides. Thus, the landslides are named as erosional induced landslide. The conglomerates beds of Upper Siwaliks are cemented by calcite and fine clay. The clasts of conglomerate cemented by clay are weakly bonded and weakly connected to each other. After getting contact with water for long time, the cemented clay loses the cohesion and separates the particles from each other. The separated fragments and clay particles flow with water during heavy rain and causes debris flow.

## 4. Conclusions

The study area is divided in to three formations (Lower Siwaliks, Middle Siwaliks and Upper Siwaliks) on the basis of lithology. Landslide inventory was prepared in detailed on the basis of geological formation and rock unit. Alltogether 867 landslides were identified in the study area. The area distribution, frequency distribution and lithological distribution of landslides indicate that Middle Siwaliks is prone area for landslide occurrence. The several field study and observation brought to know that very weak, highly fractured mudstone and highly eroded (spheroidal) sandstone of Lower Siwaliks causes erosion induced landslide, mudslide and debris slide. Medium to course grained, loose intergranular bonding, loose compacted sandstone and thin layer of weathered and weak mudstone between sandstone beds cause Rock fall, rock slide, debris slide and complex landslide in Middle Siwaliks. Weathered and weak cementing material (clay and calcite) in conglomerate and thin layer of soft mudstone between conglomerate beds causes debris slide, debris flow, block fall and gulley erosion in Upper Siwaliks. Number of Landslide is higher in Middle Siwaliks i.e. in sandstone, then in Middle Siwaliks (Conglomerate) and in Lower Siwaliks (mudstone). Loose and highly weathered cementing materials in Conglomerate, soft and weathered mudstone, weak intergranular bonded, less compacted sandstone plays main role for the occurrence of landslide in study area. The types, size and mechanism of landslides in study area are found as directly controlled by Lithostratigraphy.

## References

[1] Nepal Disaster Report 2017 (The road to Sendai), Ministry of Home Affair, Nepal Government.

[2] Inverson RM. (2000) Landslide triggering by rain infiltration. Water Resour Res 36 (7): 1897–1910.

[3] Msilimba G, Holmes P. (2010) Landslides in the rumphi district of northern Malawi: characteristics and mechanisms of generation. Nat Hazards 54 (3): 657–677.

[4] Wang FW, Sassa K, Wang G. (2002) Mechanism of a long-runout landslide triggered by the August 1998 heavy rainfall in Fukushima prefecture, Japan. EngGeol 63 (1–2): 169–185.

[5] Sassa K, Wang G, Fukuoka H, Wang FW, Ochiai T, Sugiyama ST. (2004) Landslide risk evaluation and hazard mapping for rapid and long-travel landslides in urban development areas. Landslides 1 (3): 221–235.

[6] Guzzetti F, Brunetti M. T, Peruccacci S. Rossi M, Luciani S, Valigi D. (2010) Rainfall thresholds for the possible occurrence of landslides in Italy. Natural Hazard and Earth System Science 10, 447–458.

[7] Dahal R. K., Hasegawa S. (2008) Representative rainfall thresholds for landslides in the Nepal Himalaya. Geomorphology 100, 429-443.

[8] Petrucci O, Polemio M. (2009) The role of meteorological and climatic conditions in the occurrence of damaging hydrogeologic events in Southern Italy, Natural Hazards and Earth System Sciences, 2009.

[9] Vlastelica and Miscevic (2014). Impact of weathering on slope stability in soft rock mass. Journal of Rock Mechanics and Geotechnical Engineering, vol. 6 (3), 240-250.

[10] Regmi A. D, Dhital M. R, Gadtaula R, Tamrakar N. K, Yoshida K (2011) Lithostratigraphy and Structure of the Siwaliks rocks in the Southern parts of Dang and its surrounding Area, South eastern Nepal. J. FAC.SCI.SHISHNU UNIVERSITY, vol. 43, pp 1-41.

[11] Ulak, P. D. and Nakayama, K., 1998. Lithosratigraphy and evolution of the fluvial style in the Siwalik Group in the Hetauda-Bakiya Khola area, Central Nepal. Bull. Dept. Geol., v. 6, pp. 1–14.

[12] Ulak, P. D. and Nakayama, K. (2001) Neogene fluvial systems in the Siwalik Group along the Tinau Khola section, west-central Nepal Himalaya. Jour. Nepal Geol. Soc. v. 25, pp. 111–122.

[13] Ulak, P. D., (2004) Evolution of fluvial system in Siwalik Group of Chatara- Barahakshetra area, East Nepal Himalaya. Jour. Nepal Geol. Soc., v. 30, pp. 67–74.

[14] Ulak P. D. (2009). Lithostratigraphy and late Cenozoic fluvial styles of Siwalik Group along Kankai River section, East Nepal Himalaya. Bull. Dept. Geol. V. 12, pp 63-74.

[15] Dahal R. K., Hasegawa S., Bhandary N. P., Poudel P. P., Nonomura A., Yatabe R., 2012, A replication of landslide hazard mapping at catchment scale, Geomatics, Natural Hazards and Risk, First version DOI: 10.1080/19475705.2011.629007.

[16] Auden, J. B. (1935) Traverses in the Himalaya. Rec. Geol. Surv. India, 69, 123-167.

[17] Glennie, K. W. and Ziegler, M. A. (1964) The Siwlaik Formation in Nepal. International Geol. Cong., Sess. Rep. Pt. 25, 82-95.

[18] Hagen, T. (1969) Report on the geological survey on Nepal. v. 1, Denschr. Schweiz. Naturf. Gesell., 86, 1-185.

[19] Chaudhari, R. S. (1982) Petrology of the Siwalik Group of Nepal Himalaya. Recent Researches in Himalaya, 8, 424-466.

[20] West, R. M. and Munthe, J. (1981) Cenozoic vertebrate paleontology and stratigraphy of Nepal. Himalayan Geology, 11, 18-27.

[21] Tokuoka, T., Takayasu, K., Yoshida, M., and Hisatomi, K. (1986) The Chur (Siwalik) Group of the Arung Khola area, West Central Nepal. Mem. Fac. Sci. Shimane Univ., 20, 135-210.

[22] Harrison, T. M., Copeland, P., Hall, S. A., Quade, J., Burner, S., Ojha, T. P., and Kidd, W. S. F. (1993) Isotopic preservation of Himalayan/Tibetian uplift, denudation, and climatic histories in the two molasses deposits. Jour. Geol., 101, 157-175.

[23] Corvinus, G. (1988) The Mio-Plio- Pliestocene litho and biostratigraphy of the Surai Khola Siwaliks in West Nepal: first result. C. R. Acad. Sci., Pais, 306, 1471-1477.

[24] Dhital, M. R., Gajurel, A. P., Pathak, D., Paudel, L. P. and Kizaki, K. (1995) Geology and structure of the Siwaliks and Lesser Himalaya in the SuraiKhola- Bardanda area, Mid – Western Nepal. Bull. Dept. Geology, Tribhuvan University., 4, Special issue, 1-70.

[25] Mugnier, J. L. (1995) Structural and Thermal Evolution of the Siwaliks of Western Nepal. Jour. Nepal Geol. Soc., 11, 171-178.

[26] Pokhrel K. P (2013) Chure Forestry Conservation and Management Plan: A case study of Arghakhanchi District, Nepal. Journal of Geography and Regional Planing, vol. 6 (5). pp. 172-183.

[27] TU-CDES (2016) Landslide Inventory Characterization and Engineering Design for Mitigation Works of Chure Area in Ten Districts. Central Department of Environmental Science, Tribhuvan University and Government of Nepal, President. Chure-Tarai Madhesh Conservation Development Board, Kathmandu.

[28] Varnes, D. J (1978) Slope movement types and processes, landslide analysis and control, Special Report 176, Transportation Research Board, National Academy of Sciences, pp. 11-33.